Spatial and temporal analyses of catchment and in-stream nitrate dynamics

Insights derived from fully distributed, process-based modeling and high-frequency monitoring

---

Kumulative Dissertation

zur Erlangung des akademischen Grades

"doctor rerum naturalium"

(Dr. rer. nat.)

in der Wissenschaftsdisziplin "Geoökologie"

eingereicht an der

Mathematisch-Naturwissenschaftlichen Fakultät

der Universität Potsdam

von

Xiaoqiang Yang

Hauptbetreuer:	Prof. Dr. Michael Rode, Universität Potsdam/Helmholtz-Zentrum für Umweltforschung – UFZ, Deutschland
Betreuer:	Prof. Dr. Gunnar Lischeid, Universität Potsdam/Leibniz-Zentrum für Agrarlandsforschung – ZALF, Deutschland
Gutachter:	Prof. Dr. Martyn N. Futter, Swedish University of Agricultural Sciences, Sweden

Potsdam, den 01.09.2019

Published online on the
Publication Server of the University of Potsdam:
https://doi.org/10.25932/publishup-47702
https://nbn-resolving.org/urn:nbn:de:kobv:517-opus4-477029

Preface

This dissertation is prepared and submitted in accordance with the guidelines for the degree of Doctor of Philosophy in Faculty of Science (Discipline Geoecology) at the University of Potsdam, Germany. The Ph.D. study was under the supervision of Prof. Dr. Michael Rode (Helmholtz Centre for Environmental Research – UFZ) and Prof. Dr. Gunnar Lischeid (University of Potsdam/Leibniz Centre for Agricultural Landscape Research – ZALF). The study was carried out at UFZ.

The study was mainly funded by the Chinese Scholarship Council (CSC) for a period of four years (No. 201506710068) and partially supported by the Department of Aquatic Ecosystem Analysis and Management (ASAM), UFZ.

The dissertation is presented as an accumulation of three peer-reviewed publications, including a general Introduction and a general Discussion as Chapter 1 and Chapter 5, respectively. Chapters 2 – 4 present the three peer-reviewed manuscripts and are slightly modified from the three original publications as detailed below:

Chapter 2 **Yang, X.,** Jomaa, S., Zink, M., Fleckenstein, J. H., Borchardt, D., & Rode, M. (2018), A new fully distributed model of nitrate transport and removal at catchment scale, *Water Resources Research*, 54(8), 5856-5877. https://doi.org/10.1029/2017WR022380.

Chapter 3 **Yang, X.,** Jomaa, S., Büttner, O., & Rode, M. (2019), Autotrophic nitrate uptake in river networks: A modeling approach using continuous high-frequency data, *Water Research*, *157*, 258-268. https://doi.org/10.1016/j.watres.2019.02.059.

Chapter 4 **Yang, X.,** Jomaa, S., & Rode, M. (2019), Sensitivity analysis of fully distributed parameterization reveals insights into heterogeneous catchment responses for catchment water quality modeling, *Water Resources Research*, 55, 10935-10953. https://doi.org/10.1029/2019WR025575.

The catchment nitrate model (mHM-Nitrate) developed from this study is an open-source software, following the GNU General Public License. The source code of the mHM-Nitrate model (v2.0) is publically accessible (Yang, X., & Rode, M. (2020), A Fully Distributed Catchment Nitrate Model - mHM-Nitrate v2.0. Zenodo. https://doi.org/10.5281/zenodo.3891629).

Declaration

I, *Xiaoqiang Yang*, hereby declare that this dissertation entitled “Spatial and temporal analyses of catchment and in-stream nitrate dynamics--Insights derived from fully distributed, process-based modeling and high-frequency monitoring” represents my own work. This dissertation has not been submitted to any other institution of higher education.

Xiaoiqang Yang

Magdeburg, September 1st 2019

Acknowledgement

It would never be possible to reach this point without being surrounded by a group of friendly people. I would like to express my sincere thanks to those people who have supported and encouraged me during the journey of pursuing a PhD degree.

Most importantly, I would like to thank my supervisor, Prof. Michael Rode, who brought me here in Germany and continuously encourages and trusts me in the following four years. I very much appreciate his guidance both scientifically and emotionally. His patience and encouragement at the beginning strengthened my confidence on commencing the tough task of the new model development. I am deeply thankful to Michael for always being there for my problems and questions and always being able to clarify them and provide the most potential directions to go on. I enjoyed a lot the relaxed chatting during the weekday lunch-time.

A special thanks to Prof. Gunnar Lischeid for his co-supervision of the PhD project and for all the constructive and enjoyable discussions. I would like to thank Prof. Martyn Futter for his review of this dissertation and for the interesting discussions in several scientific conferences.

At this point, I would like to thank all my friends and UFZ colleagues. There are many more names than these I can name here. Firstly, my great gratitude goes to Dr. Seifeddine Jomaa, who guided me step-by-step with tremendous patience at the very beginning and gave me endless emotional support which helped me pass through the difficult times. I very much appreciate his support and trust just like my elder brother! I will never forget all the happy time together with the research group of Hydrological and Water Quality Modeling in *Haus 11*: Julia Vanessa Kunz, Jiangshui Huang, Salman Ghaffar, Xiangqian Zhou, Ghulam Abbas and Xiaolin Zhang. Thank you all! I shall not forget all the administrative support and help received from Dr. Christiane Katterfeld and Mrs. Martina Klapputh. Notably, I would like to express my great appreciation to Prof. Dietrich Borchardt, the head of Department ASAM, for his constructive contribution to my first paper and for always being supportive in my attendance of international conferences.

Last but not least, my enormous gratitude goes to my family, my beloved grandparents, parents and sisters, for their forever love and endless trust. I enjoy the happy time together with them, being surrounded by the cute next generation of our big family. Especially, I would like to thank my beloved Xiaolin, who appears right on time and lights up my life, for her understanding, tolerance and support.

Contents

Abstract

Water quality in river systems is of growing concern due to rising anthropogenic pressures and climate change. Mitigation efforts have been placed under the guidelines of different governance conventions during last decades (e.g., the Water Framework Directive in Europe). Despite significant improvement through relatively straightforward measures, the environmental status has likely reached a plateau. A higher spatiotemporal accuracy of catchment nitrate modeling is, therefore, needed to identify critical source areas of diffuse nutrient pollution (especially for nitrate) and to further guide implementation of spatially differentiated, cost-effective mitigation measures. On the other hand, the emerging high-frequency sensor monitoring upgrades the monitoring resolution to the time scales of biogeochemical processes and enables more flexible monitoring deployments under varying conditions. The newly available information offers new prospects in understanding nitrate spatiotemporal dynamics. Formulating such advanced process understanding into catchment models is critical for model further development and environmental status evaluation. This dissertation is targeting on a comprehensive analysis of catchment and in-stream nitrate dynamics and is aiming to derive new insights into their spatial and temporal variabilities through the new fully distributed model development and the new high-frequency data.

Firstly, a new fully distributed, process-based catchment nitrate model (the mHM-Nitrate model) is developed based on the mesoscale Hydrological Model (mHM) platform. Nitrate process descriptions are adopted from the Hydrological Predictions for the Environment (HYPE), with considerable improved implementations. With the multiscale grid-based discretization, mHM-Nitrate balances the spatial representation and the modeling complexity. The model has been thoughtfully evaluated in the Selke catchment (456 km^2), central Germany, which is characterized by heterogeneous physiographic conditions. Results show that the model captures well the long-term discharge and nitrate dynamics at three nested gauging stations. Using daily nitrate-N observations, the model is also validated in capturing short-term fluctuations due to changes in runoff partitioning and spatial contribution during flooding events. By comparing the model simulations with the values reported in the literature, the model is capable of providing detailed and reliable spatial information of nitrate concentrations and fluxes. Therefore, the model can be taken as a promising tool for environmental scientists in advancing environmental modeling research, as well as for stakeholders in supporting their decision-making, especially for spatially differentiated mitigation measures.

Secondly, a parsimonious approach of regionalizing the in-stream autotrophic nitrate uptake is proposed using high-frequency data and further integrated into the new mHM-Nitrate model. The new regionalization approach considers the potential uptake rate (as a general parameter) and effects of above-canopy light and riparian shading (represented by global radiation and leaf area index data, respectively). Multi-parameter sensors have been continuously deployed in a forest upstream reach and an agricultural downstream reach of the Selke River. Using the continuous high-frequency data in both streams, daily autotrophic uptake rates (2011-2015) are calculated and used to validate the regionalization approach. The performance and spatial transferability of the approach is validated in terms of well-capturing the distinct seasonal patterns and value ranges in both forest and agricultural streams. Integrating the approach into the mHM-Nitrate model allows spatiotemporal variability of in-stream nitrate transport and uptake to be investigated throughout the river network.

Thirdly, to further assess the spatial variability of catchment nitrate dynamics, for the first time the fully distributed parameterization is investigated through sensitivity analysis. Sensitivity results show that parameters of soil denitrification, in-stream denitrification and in-stream uptake processes are the most sensitive parameters throughout the Selke catchment, while they all show high spatial variability, where hot-spots of parameter sensitivity can be explicitly identified. The Spearman rank correlation is further analyzed between sensitivity indices and multiple catchment factors. The correlation identifies that the controlling factors vary spatially, reflecting heterogeneous catchment responses in the Selke catchment. These insights are, therefore, informative in informing future parameter regionalization schemes for catchment water quality models. In addition, the spatial distributions of parameter sensitivity are also influenced by the gauging information that is being used for sensitivity evaluation. Therefore, an appropriate monitoring scheme is highly recommended to truly reflect the catchment responses.

Chapter 1: Introduction

1.1. Problem statement

Water quality in river systems is of growing concern due to rising anthropogenic pressures and climate change. Among others, diffuse source (mainly from agriculture) has become one of the main causes blaming for eutrophication in fresh and coastal waters, especially for nitrogen pollution. In the European Union (EU), agriculture contributes 50-80% of the total nitrogen load and is the main pollution source in most regions and catchments (EEA, 2005). For instance, agricultural diffuse source affects 79% of water bodies in Germany (the Water Information System for Europe – WISE, last accessed on June 13th, 2019). After implementation of multiple directives (e.g., the Nitrate Directive and the Urban Waste Water Treatment Directive in 1991, and Water Framework Directive – WFD in 2000), considerable management efforts have been in place and significant improvement has been achieved. However, large proportion of surface waters (ca. 60%) has not yet reached the environmental "good status", and diffuse sources have likely remained at a constant level (EEA, 2005, 2018). Such bottleneck problem has likely been encountered after the implementation of relatively straightforward measures; further improvement will only be possible by much more costly actions (Reusch et al., 2018). This gives a rise to the need for cost-effective, on-farm mitigation measures, which intend to target on critical source areas (CSAs) of diffuse pollution (EEA, 2005; Collins et al., 2014; Refsgaard et al., 2019). Therefore, to further mitigate the fresh water eutrophication and to achieve the environmental objectives of governance conventions (e.g., the WFD in EU), advanced scientific knowledge should be formulated and be available for different governance levels (EEA, 2012; Collins et al., 2014; Reusch et al., 2018).

Catchment-scale nutrient models, as decision supporting tools, have gained wide acceptance from scientists and managers, specifically in assessing current and further environmental status and in evaluating effectiveness of candidate mitigation measures (Rode et al., 2009). Currently, most of the widely used models are semi-distributed, which hierarchically disaggregate a catchment into several subcatchments and further into homogenous classes (e.g., hydrological response unit) (Wellen et al., 2015). The semi-distributed structure largely reduces the model complexity, but overlooks spatial information within the catchment/subcatchments (e.g., nutrient states and fluxes at specific locations). Such detailed information, however, is increasingly asked for to identify CSAs and guide corresponding mitigation measures in those areas (Arnold et al., 2010; Refsgaard et al., 2014; Bieger et al., 2017). Therefore, fully distributed catchment models (i.e., grid-based model structure) are needed to balance the accurate spatial representation and the model complexity (Clark et al., 2017).

In addition, the development of sensor techniques enables monitoring of in-stream ecosystem processes at much higher temporal and spatial resolutions (Rode et al., 2016b; Wollschläger et al., 2016). Advances of process understanding have been increasingly gained based on high-frequency monitoring. As a step beyond, the advanced process understanding offers new opportunities on process-based environmental modeling in terms of, e.g., developing new process descriptions and new parameterization schemes (Rode et al., 2016b). Studies have shown that high-frequency data can help to identify nutrient sources and dominant transport pathways (Mellander et al., 2013; Bowes et al., 2015) and to quantify the coupled nutrient processing and metabolism (Heffernan & Cohen, 2010; Dupas et al., 2016). However, on the one hand, such process insights are mostly site-specific but the biogeochemical processes are spatiotemporally heterogeneous; on the other hand, few models are capable of compromising between reach/plot scale and network/catchment scale. To date, modeling activities at larger scales have not yet made full use of high-frequency data.

Nitrate has been intensively investigated due to its mobility and environmental abundances and effects (Meybeck, 1982; Grant et al., 2018). Moreover, nitrate optical sensors, among others, are widely deployed and robust. Therefore, in this dissertation I exclusively focus on spatiotemporal analysis of nitrate dynamics based on fully distributed catchment modeling and its integration with the information provided by the emerging high-frequency sensor data.

1.2. Background and state-of-the-art

1.2.1. Hydrological and nitrate modeling at catchment scale

Process-based understanding of hydrological and nitrate dynamics

Mineral fertilizers and manure have long been applied to agricultural lands to increase the food production all over the world. Excess nutrients are stored in the soil and transported following hydrological processes, resulting in serious water pollutions in fresh and coastal waters (Smith et al., 1987; Davis et al., 2018; Yu et al., 2019). Hydrologists and environmental scientists have advocated tremendous efforts in understanding hydrological and biogeochemical processes of water and nutrient transports in both terrestrial and in-stream phases. Since 1960s, different types of hydrological and water quality models have been developed in serving scientific and societal concerns. Process-based models have gained the highest attraction (Beven, 1989; Fatichi et al., 2016; Clark et al., 2017).

Numbers of high-reputational reservoirs-based catchment hydrological models have been proposed, including the HBV model in Europe (Bergström, 1976, 1995), the Sacramento Soil Moisture Accounting

Model (SAC-SMA) in the US (Burnash et al., 1973; Burnash, 1995) and the Xinanjiang model in China (Zhao et al., 1980; Zhao, 1992). Despite differences in process descriptions, they all consider major processes of the hydrological cycle. Tremendous model versions that embed newly emerged data have been developed since 1970s, but the basic principles of model structure have been remained. Rainfall and snow are firstly intercepted by plant canopy and then received by pervious and impervious areas. Direct runoff generates directly from the impervious areas (e.g., urban paved areas and water body surface). In pervious areas, precipitation infiltrates into deeper soil layers and supplements the soil water therein. Depending on soil water content, water fluxes can be calculated (i.e., evapotranspiration, deep groundwater percolation and runoff generation). The generated runoff is routed from headwaters to the outlet/receiving water bodies. Multiple soil layers are usually defined to represent variant soil properties along the depth below surface and to consider their impacts on soil moisture constants (i.e., wiling point, field capacity and saturation capacity), which directly determine the calculation of water fluxes. Conceptual reservoirs are defined to represent the water storages and dynamics in different phases of the hydrological cycle.

Nutrient dynamics at catchment scale are predominantly driven by hydrological dynamics (Rode et al., 2010; Jiang et al., 2014; Dupas et al., 2016; Dupas et al., 2017). Moreover, under current anthropogenic impacts, significant external nitrogen has been added into the catchment through agricultural fertilizer application and atmospheric deposition (Bergström & Jansson, 2006; Schlesinger, 2009). Especifically for nitrate, sources from atmospheric wet deposition are added into catchment simultaneously with rainfall. Together with applied fertilizer on agricultural land, external nitrate sources infiltrate into soils and integrate with water dynamics. In addition to the physical mixing and dynamics, biogeochemical transformations are also considered in the soil (**Figure 1.1**). Important biogeochemical processes in the terrestrial phase include plant/crop uptake, denitrification and transformations related to solid organic nitrogen (e.g., mineralization and degradation) (Lindström et al., 2010); for the in-stream phase, denitrification and assimilatory uptake are the most important transformation processes. These processes are normally conceptualized as a function of scaling factors (i.e., reaction rates as model parameters), available pool size of initial nitrogen status and other known factors (e.g., soil temperature, soil moisture, etc.). All transformations are considered at each time step to calculate nitrate concentration in soil water and to update pool sizes of each nitrogen forms (**Figure 1.1**). Following hydrological dynamics, nitrate fluxes are calculated based on the water fluxes and the concentration of respective water storage.

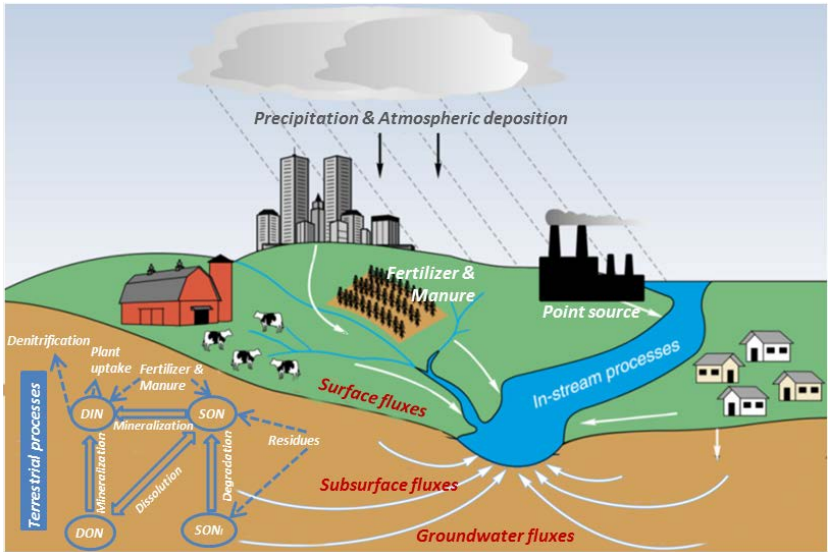

Figure 1.1. hydrological and nutrient dynamics at catchment scale (Modified from Phillips et al. (1999)). Four different nitrogen forms are normally defined: dissolved inorganic nitrogen (DIN) and dissolved organic nitrogen (DON), active solid organic nitrogen (SON) and inactive solid organic nitrogen (SON_I).

Spatial discretization of catchment water quality models

Based on above process understandings, numbers of catchment water quality models have been developed. Spatially distributed catchment models are highly recommended to represent the high heterogeneity of catchment characteristics and anthropogenic impacts (Refsgaard, 1997; Beven, 2001; Borah & Bera, 2003; Wellen et al., 2015). According to the review by Wellen et al. (2015), the top five spatially distributed, process-based models are the Soil Water Assessment Tool (SWAT) (Arnold et al., 1998), the Integrated Catchment Model (INCA) (Whitehead et al., 1998; Futter et al., 2014), the Agricultural Nonpoint Source Pollution Model (AGNPS) (Young et al., 1989), the Hydrological Simulation Program-Fortran (HSPF) (Bicknell et al., 1997) and the HBV-NP model (now revised as Hydrological Predictions for the Environment - HYPE) (Lindström et al., 2010). Most of them follow similar philosophy of describing flow and nutrient processes, while the way how they disaggregate the catchment into multiple units can be divided into two categories: semi-distributed and fully distributed (or grid-based) models.

Most of the models developed and applied adopt the semi-distributed structure (Wellen et al., 2015). Semi-distributed models firstly disaggregate the whole catchment into multiple subcatchments based on surface topography and then further divide each subcatchment into multiple homogenous units (e.g., the hydrological response unit for SWAT and the soil and landuse class for HYPE). Due to the

topographic division, meteorological inputs are specified differently for each subcatchment. The homogenous unit is usually defined by overlapping multiple geographic data (e.g., land use and soil type), so that similar hydrological and nutrient responses can be assumed. Such hierarchical structure largely reduces the model complexity, while maintains certain degree of representation of the spatial variability of parameters and inputs (Krysanova et al., 1998). However, one of the main disadvantages of the semi-distributed structure is the lack of detailed information at specific location and its interaction with surrounding areas (Arnold et al., 2010). Moreover, the river network of semi-distributed models is usually conceptualized by the total length of each subcatchment and the linkage between all subcatchments. This sets a structural barrier for detailed in-stream process investigations, e.g., the mitigation effect of buffer strip implementation (Stutter et al., 2012) and the assessment of geomorphological impacts on in-stream nutrient retention (Gomez-Velez et al., 2015).

Fully distributed models discretize the whole catchment into square grids, where terrestrial hydrological and nutrient dynamics are calculated. All grid cells are linked according to the topographic information (e.g., flow direction based on digital elevation model - DEM). Therefore, detailed spatial information of flow and nutrient fluxes can be derived explicitly and it can be easily linked to potential driving factors. However, the other side of the coin is that all meteorological and geographic inputs should be extracted and model parameters should be specified for each grid cell. Studies have emphasized the need for finer resolution of basic input data (Chaubey et al., 2005; Shrestha et al., 2006). For instance, Chaubey et al. (2005) evaluated the effect of DEM resolution on SWAT performance and argued that DEM resolution needed for nutrient simulation is higher than that for discharge simulation. This will increase the model complexity largely (Rathjens et al., 2015) and arise the scaling issues (Refsgaard et al., 2016), especially for large catchments (e.g., catchment with size greater than 300 km^2). Therefore, a novel design of multiscale discretization is needed to balance the spatial representation and model complexity (Samaniego et al., 2010).

Advanced multiscale discretization of the mHM model

Samaniego et al. (2010) developed the process-based mesoscale Hydrological Model (mHM) and the multiscale parameter regionalization technique (MPR), which allow multiple resolutions of input data according their respect availability and can automatically integrated into the modeling level (**Figure 1.2**). Model parameters (e.g., soil moisture constants) and state variables (e.g., soil moisture in different soil layers) are firstly defined at the basic geographic level (level 0) with higher resolution (e.g., 100 m). This implementation ensures sufficient spatial representation of the model parameters because the

resolution is compatible with the driving factors (the geographic information, such as land-use and soil types). As the second step of the MPR, the parameter and geographic information are upscaled to the modeling level (i.e., level 1, with user-specified resolution), where the lumped HBV model is applied. Therefore, each grid cell at level 1 acts as a combined role of subcatchment and homogenous unit. In addition, basic stream morphological information (e.g., stream length and flow direction) is also calculated at level 0 and scaled up to the modeling level, where an additional routing resolution can be specified (Thober et al., 2019). Such multiscale implementation balances well the spatial representation and the model complexity, in terms of largely reduced computational load and explicit spatial information at specific locations, respectively.

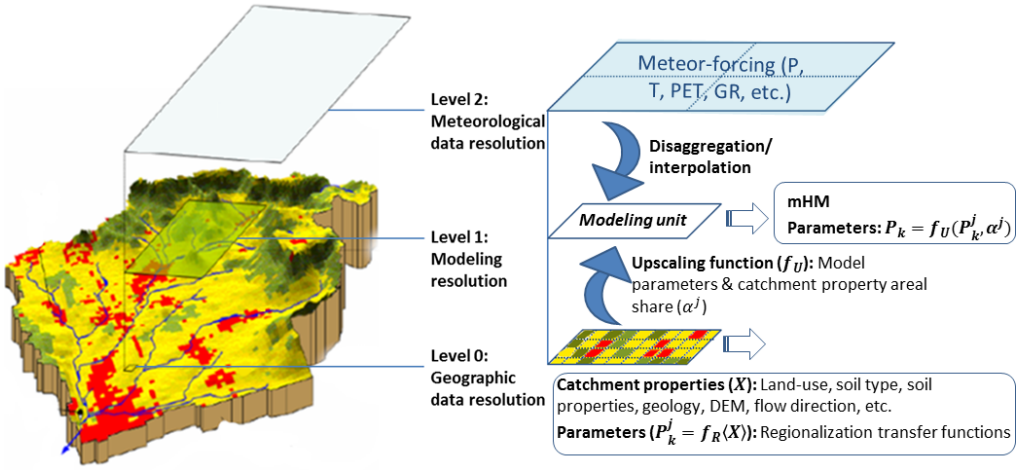

Figure 1.2. Spatial discretization and multi-resolution structures of the mHM model, and the parameterization and upscaling technique (MPR).

As mentioned above, nitrate processes are predominated by hydrological processes, but their dynamics are likely more spatially heterogeneous due to additional impacts of human activities on the biogeochemical transformations (Hansen et al., 2014). Sufficient spatial representation of nitrate modeling is, therefore, needed to represent the higher spatial variability and to provide scientific guides for different mitigation measures, especially for the more cost-effective, spatially differentiated measures (Refsgaard et al., 2019). Due to its advanced implementation, the mHM provides a promising platform for further water quality model development.

1.2.2. In-stream nitrate uptake at river network scale

Streams and rivers act as important sinks for nitrate due to their intrinsic connections with terrestrial systems and high rate of biological activities in both water column and hyporheic zone (Mulholland et al.,

2008; Trauth et al., 2015; Dodds & Smith, 2016; Grant et al., 2018). Biogeochemical transformations are greatly influenced by hydrological, morphological and biochemical conditions, resulting in high spatiotemporal variability throughout the river network (Bernhardt et al., 2005). Headwater streams (i.e., 1st and 2nd order streams) play a disproportionate role (Gomez-Velez & Harvey, 2014; Wohl, 2017); meanwhile higher order streams can also exert considerable influence on nutrient transport (Ensign & Doyle, 2006; Wollheim et al., 2006). Therefore, thoughtful investigations of in-stream nutrient transport and removal should be carried out for the whole river network.

Nutrient spiraling concept

The term nutrient "spiraling" was firstly named by Webster (1975) describing the intimate spatiotemporal coupling of waterborne nutrient cycling in fluvial environments (streams and rivers). The nutrient spiraling concept describes the cycling of nutrients being (1) assimilated from the water column into benthic biomass, (2) temporarily retained, and (3) re-mineralized back into the water column. The mathematical framework was formalized by Newbold et al. (1981). In his model, spiraling length (S) is introduced as an integrated measure of water velocity and the influence of biochemical demand and sorption by sediment. Nutrient addition approaches (by injecting isotopic tracers or bulk addition of N and P to streams) are commonly used to gain the information of the whole-stream nutrient cycling (Stream Solute Workshop, 1990).

Nutrient uptake metrics are, therefore, developed to quantify impacts of biochemical factors (e.g., bacteria, algae and macrophytes) and geomorphic factors (stream physical properties, e.g., channel size and transient storage) (Ensign & Doyle, 2006). The spiraling length of the inorganic form in water column ($S_w, length\ time^{-1}$), which is the dominant part of the total length S, can be directly calculated by regression of the injection experiment measurements. Considering the impact of advection, the uptake rate ($U, mass\ length^{-2}\ time^{-1}$) can be calculated from S_w, stream water nutrient flux and stream morphological information. Pursuing a more effective comparison between streams, the uptake velocity ($V_f = U/C, length\ time^{-1}$) is recommended to be independent from concentration (C) and hydrological conditions. For a systematic review of the nutrient spiraling concept and metrics, please refer to Stream Solute Workshop (1990) and Ensign and Doyle (2006).

Direct measuring of nitrate uptake by traditional reach scale experiments

Nutrient spiraling experiments were firstly conducted in 1983 using ^{32}P as isotopic tracer (Newbold et al., 1983). Due to the difficulties in using radioactive P in surface waters, most experiments shifted to use ^{15}N as isotopic tracer. The Lotic Intersite Nitrogen eXpermient (LINX) project and the subsequent LINX II

project provide the most information on whole-stream N cycling (Webster et al., 2003; Mulholland et al., 2008). The project conducted ^{15}N injection experiments in numbers of streams across varying climatic and anthropogenic characteristics. Using standard experimental protocols, the project investigated the controlling hydrodynamic, chemical and metabolic characteristics for stream N uptake, retention and cycling. Advanced understandings on in-stream N cycling have been achieved (Mulholland et al., 2008; Covino et al., 2010).

However, theoretical limitations of such stream tracer experiments are also well documented:

- Nutrient additions likely alter the natural biochemical nutrient uptake, which can potentially affect measurements and the subsequent calculations of spiraling metrics (Mulholland et al., 2002).
- The majority of experiments were conducted in short periods of time and mostly during low flow conditions, which hampered the use of the gained knowledge in long-term investigation of nutrient dynamics (Doyle, 2005).
- Despite the large variations in stream conditions, most of them are small headwater streams (e.g., the LINX streams); while empirical experiments in large rivers are still lagging behind, but are needed to understand the role of entire river systems (Tank et al., 2008).

Nitrate uptake and stream metabolism using high-frequency sensors

Geomorphic factors do explain certain variation in nutrient uptake, while they only indirectly affect the stream biota taking up nutrients. Stream metabolism is intrinsically related to in-stream nutrient cycling. Evidence has shown that gross primary production (GPP) controls autotrophic assimilatory N uptake; while ecosystem respiration (ER) is more important to heterotrophic N uptake/removal (Tank et al., 2017). Hall and Tank (2003) found GPP and ER together explained 82% of variation in ammonium uptake, while GPP alone explained 75% of variation in nitrate uptake. In other words, stream metabolism rates are more predictive of nutrient uptake than physical variables (Roberts & Mulholland, 2007). Instead of conducting logistically heavy injection experiments, stream metabolism rates can be easily calculated from direct measurements of dissolved oxygen concentration (DO) using high-frequency sensors. For instance, Roberts et al. (2007) and Roberts and Mulholland (2007) measured 15min DO for a two-year period, and conducted intensive campaigns of nutrient sampling (2-3 time per week for a 18-month period, plus hourly sampling over 24 hours on 13 dates) in a first-order forest stream. Such intensive

campaigns allow temporal variability to be examined in a more comprehensive way (Hoellein et al., 2007).

As sensor techniques develop further, increasing number of solutes can be measured automatically at high temporal resolution (Rode et al., 2016b), which opens new perspectives for in-stream nutrient investigation in large rivers. Heffernan and Cohen (2010) found a strong correlation between measured autotrophic nitrate uptake ($U_{a-NO_3^-}, mg\ N\ m^{-2}\ d^{-1}$; derived from diel amplitudes of nitrate concentration measurements) and calculated values (based on daily GPP and the stoichiometric C: N ratio). Rode et al. (2016a) confirmed the robust relationship both in forest and agricultural streams (4th order). Jarvie et al. (2018) combined the above $U_{a-NO_3^-}$ calculations with mass balance measurements based on high-frequency measurements, so that net nitrification and denitrification can also be estimated. Therefore, benefiting from sensor technology, information of in-stream nitrate uptake can be directly obtained at different stream conditions (especially large, higher-order rivers) at high temporal resolution.

Networked modeling of the in-stream nitrate uptake

Networked modeling of in-stream nitrate dynamics is usually accomplished through two aspects: (1) advanced process understandings gained from reach-scale studies, and (2) a network modeling platform that can capture the spatiotemporal variability of stream characteristics.

Results of reach-scale studies are used to identify the most influential factors for nitrate uptake; measurements across stream conditions are used to quantify (or regionalize) the impacts of those factors on nitrate uptake through empirical relationships (Helton et al., 2011; Ye et al., 2012). Mulholland et al. (2008) demonstrated that uptake velocity decreases with increasing nitrate concentration, based on which, a simple power-law function and further a stream network model were developed. Their empirical parameters were derived separately from experimental stream segments within each region. Alexander et al. (2009) estimated denitrification by nonlinear regressions between measured denitrification rate and influential factors (e.g., nitrate concentration, stream flow and temperature) based on more than 300 published measurements. Hall et al. (2013) collected in total 969 separate nutrient uptake experiments and examined the impacts of stream size (indicated by specific discharge), nitrate concentration and the distance from the headwaters for different solutes. Since the majority of experiments were conducted in small rivers, Ye et al. (2017) extended the dataset with new measurements from 15 large rivers and compared the differences of modeled nutrient uptake across

river networks. However, most of the experiments are conducted in summer, low-flow periods with a few number of measurements (Hall et al., 2016). Wollheim et al. (2008) considered the seasonality of the maximum N uptake using a Q_{10} approach to extrapolate the value derived from LINX to the course of the year, while they also argued that such scaling approach would be one of the main sources of uncertainty. As aforementioned, the emerging high-frequency sensor monitoring could open a door for sufficient representations of both spatial variability (e.g., be deployed in small streams and large rivers) and temporal dynamics (e.g., long-term continuous deployment).

Measurements (either traditional experiments or high-frequency sensor monitoring) are only a snapshot of time and space. It is not possible to measure contiguously across river networks (Helton et al., 2011). A comprehensive numerical framework is needed to represent the biogeochemical processes and to accommodate the impacts of hydrological, biochemical and geomorphological controls (Ye et al., 2012). Several network models have been proposed to overcome the monitoring limitations, such as SPARROW (Alexander et al., 2009), RivR-N (Seitzinger et al., 2002), FrAMES (Wollheim et al., 2008) and NEXSS (Gomez-Velez & Harvey, 2014). However, current modeling limitations and future directions are also highlighted in literature (e.g., oversimplified catchment hydrology and river hydrogeomophology, insufficient consideration of stoichiometric relationship between nitrogen and other elements (Helton et al., 2011)). To tackle those limitations requires the melding of concepts and approaches from both terrestrial and in-stream modeling.

1.2.3. Parameterization of catchment water quality models

Complexity of high-dimensional parameterization

The incorporation of our increasing understandings of earth and environmental systems and their feedback mechanisms leads to progressively complex and computationally intensive model formulations (Sheikholeslami et al., 2019). In modeling design, basic physical principles of hydrological and nutrient dynamics are formulated by mathematical equations with considerable simplifications and assumptions (Beven, 1989), particularly for the process-based models. The applicability under different natural and anthropogenic conditions is, therefore, determined mainly by input configurations and model parameters. Despite the aforementioned advantages, the fully distributed modeling provides both opportunities and challenges for model parameterization. Spatially differentiated parameter configuration allows parameters to be directly linked to multiple spatial information and, therefore, to achieve a better represent of spatial heterogeneity of natural processes (Bronstert & Bárdossy, 1999;

Güntner & Bronstert, 2004; Clark et al., 2017). However, the costs of that is the largely increased complexity:

- The total number of model parameters can range from hundreds to thousands depending on the modeling resolution and the number of substances interested (Tang et al., 2007).
- The high risk of over-parameterization and the consequent "equifinality" effect (Beven, 1989).
- The difficulty of estimating appropriate parameter sets in the high-dimensional, nonlinear parametric spaces.
- The rapid increase of the dimension of parameter spaces lead to an exponentially increase of model runs for parameter analysis (e.g., the sensitivity analysis) (Sheikholeslami et al., 2019).

To tackle above parameterization challenges, efforts have been placed to reduce the dimensionality of the problem in mainly two aspects: parameter sensitivity analysis (SA) and parameter regionalization.

SA has long been taken as a foundational diagnostic approach in characterizing the impact and significance of input factors on model responses, among which model parameter is the most intensively focused topic. Numbers of global SA techniques have been proposed by analyzing partial derivatives (e.g., the Morris method (Morris, 1991)) or variances (e.g., the Sobol' method (Sobol', 2001)). See, e.g., Song et al. (2015) and Pianosi et al. (2016) for systematic methodological introduction and review. All methods have pros and cons, and the method selection depends on specific objectives and available computational budget (see Figure 3 in Pianosi et al. (2016) for an overview). It is still challenge to generate accurate estimates of the sensitivity indices (Gupta & Razavi, 2018). Therefore, sensitivity ranking and screening, aiming at generating the ranking of parameters based on their relative importance and identifying parameters that have negligible influences, respectively, are more targeted in the context of spatially distributed parameter configuration. Moreover, parameter SA has become a standard procedure, and also usually the first step, for earth and environmental modeling studies. Catchment modelers usually focus only on relatively influential parameters due to the complexity of the problem and the insufficiency of observations.

Parameters that introduced in the process-based models normally have relatively clear physical meanings. This provides the foundation of parameter regionalization, i.e., parameter values can be determined by catchment characteristics and therefore be spatially transferable (Wagener & Wheater, 2006). In hydrological modeling, the most common regionalization approach is based on statistical regressions among a large number of catchments (Merz & Blöschl, 2004; Oudin et al., 2008) or several

archetypes of hydrological dynamics (Wagener & Wheater, 2006), assuming the uniqueness of each catchment can be covered by a group of catchment characteristics. However, many, if not most, of such regionalization studies observed significant decrease in model performance and considerable increase in uncertainty, presumably due to the failure of the uniqueness assumption (Beven, 2000). Therefore, cautious thinking in reducing regionalization uncertainty should be in place on (1) selection of catchment properties in both local and regional modeling steps, (2) selection of the local model structure and identification of the local parameters, (3) identification of the regional model structure and its parameters, and (4) selection of the regionalization procedures.

Spatially distributed parameter sensitivity

Despite the heavy computational load needed, several studies have investigated the parameter sensitivity of hydrological modeling at a full spatial range. Tang et al. (2007) set up a full-spatial parameter configuration using the grid-based SAC-SMA model and showed high spatial variability of parameter sensitivity during two flood events. Based on the sensitivity results, parameter- and cell-based screening strategies reduced 75% of computational load, while explained ca. 70% of the model output variance. Herman et al. (2013a) tested the efficiency of the Morris method in the fully spatial domain, and compared its effectiveness with the Sobol' method which is considered as the most accurate and robust global sensitivity method (Yang, 2011). They demonstrated that the Morris sensitive indices with the lowest sample size (N=20) are spatially and statistically comparable to those calculated by the Sobol' with the highest sample size (N= 6000 and consumed ca. 50 000 computing hours in the high-performance cluster). Sheikholeslami et al. (2019) proposed a new grouping strategy for high-dimensional parametric problems (e.g., the number of parameters > 40) to reduce computational cost but maintain the stability and convergence. Therefore, by screening and ranking the whole set of parameters, the parametric dimension can be reduced significantly without scarifying model performance; by careful selection of available SA methods, the computational load can be further reduced to a manageable level.

Studies have shown that spatially explicit SA offers new modeling perspectives to further diagnose the model responses and advance our understanding of model structures. The study of Tang et al. (2007) revealed that storage variation, spatial distribution of forcing and cell proximity to the outlet are primary factors for model response. van Werkhoven et al. (2008a) further evaluated the significant impacts of rainfall distribution on sensitivity distribution using virtual mathematical experiments. To tackle the potential diagnostic biases due to the priori selection of events, Herman et al. (2013b) investigated

parameter distribution at full spatial and temporal ranges. They explicitly demonstrated that the relative importance of different hydrological processes varied at different locations under different hydrological condition. Wagener et al. (2009) assessed the impacts of multiple objective functions on parameter spatial distributions. In a similar study, van Werkhoven et al. (2008b) analyzed the correlations between parameter sensitivity and catchment properties across a hydroclimatic gradient. They suggested that such correlations could help to extend the number of identifiable parameters than usually assumed.

For catchment water quality modeling, parameters are usually grouped into several categories of broad landscape characteristics that are spatially available (e.g., land-use and soil types). However, such broad information can probably underestimate the spatial heterogeneity that observed in nature (Clark et al., 2017). Moreover, biogeochemical reactions are most likely influenced by multiple factors/pressures (Tockner et al., 2010). To date, much less have been done on parameters of catchment water quality models.

1.3. Objectives

The main goal of this dissertation is to gain advanced insights into the spatiotemporal nitrate dynamics at catchment and river network scale by integrating the fully distributed model and the emerging high-frequency sensor data. To this end, (1) a new fully distributed catchment nitrate model (mHM-Nitrate), that is capable of providing detailed and reliable spatial information of nitrate dynamics, is developed and validated in the Selke catchment (456 km^2), central Germany (Chapter 2); (2) advanced understanding of in-stream autotrophic nitrate uptake process is gained using continuous high-frequency data and further upscaled to the river network scale using the mHM-Nitrate model (Chapter 3), and (3) spatially distributed parameterization of the nitrate submodel is analyzed through sensitivity analysis to further evaluate the relative importance of nitrate biogeochemical processes at a full spatial range (Chapter 4).

Chapter 2: A new fully distributed model of nitrate transport and removal at catchment scale

Key points

- New grid-based catchment nitrate model (mHM-Nitrate) with a flexible multi-resolution structure
- Spatiotemporal validation with uncertainty analysis is conducted in a nested heterogeneous catchment using multi-frequency observations
- The mHM-Nitrate model provides detailed and reliable catchment-wide spatial information of nitrate concentrations and flux

2.1. Abstract

Hydrological water quality models have gained wide acceptance from environmental scientists and water managers to address deterioration of surface water quality. Higher spatiotemporal accuracy of such models is increasingly required for better understanding the functional heterogeneity of catchments and improving management decisions at different governance levels. However, balancing spatial representation and model complexity remains challenging. We present a new flexibly designed, fully distributed nitrate transport and removal model (mHM-Nitrate) at catchment scale. The model was developed mainly based on the mesoscale Hydrological Model (mHM) and the Hydrological Predictions for the Environment (HYPE) model. The mHM-Nitrate model was tested in the Selke catchment (Central Germany), which is characterized by heterogeneous physiographic and land-use conditions, using adequate observed hydrological and nitrate data at three nested gauging stations. Long term (1997-2015) daily simulations showed that the model well reproduced the seasonal dynamics of biweekly nitrate observations in forested, agricultural and urban areas. High-frequency measurements (2010-2015) were additionally used to validate model performance of simulating short-term changes in stream-water concentrations that reflect changes in runoff partitioning and event-based dilution effects. Uncertainty analysis confirmed the model's robustness. Moreover, model calculations showed that mean terrestrial nitrate input/output (in total 105 kg ha^{-1} yr^{-1}) and in-stream removal (8% of mean nitrate load) were in comparable ranges with literature, respectively. The new mHM-Nitrate model is capable of providing detailed spatial information on nitrate concentrations and fluxes, which can

motivate more specific catchment investigations on nitrate transport processes and provide guidance on spatially differentiated agricultural practices and measures.

2.2. Introduction

Water quality in river systems is of growing concern due to rising anthropogenic pressures and climate change. Current understanding of the mechanisms and dynamics of nutrient leaching and transport from in-situ monitoring has significantly improved (Rode et al., 2016b; Rozemeijer et al., 2016). Mathematical modeling is one way to formalize this knowledge (Jackson-Blake et al., 2016) and transfer it to sub-areas that are not covered by monitoring schemes. Models can enhance our understanding of the natural behavior of environmental systems (Kirchner, 2006); for instance, they can test alternative explanations of observed phenomena to suggest the most plausible ones. Catchment models can also scientifically support decision-making (e.g., guide optimization of monitoring strategies and analyze different future climate and agricultural scenarios (Rode et al., 2016b)).

Spatially distributed, process-based models are recommended to adequately represent the heterogeneity of catchment characteristics. Wellen et al. (2015) evaluated the current state of distributed catchment water quality models and summarized the five models mostly used worldwide: Soil Water Assessment Tool (SWAT) (Arnold et al., 1998), Integrated Catchment model (INCA) (Whitehead et al., 1998a) , Agricultural Nonpoint Source Pollution Model (AGNPS/AnnAGNPS) (Young et al., 1989), Hydrological Simulation Program-Fortran (HSPF) (Bicknell et al., 1997) and HBV-NP (now revised as Hydrological Predictions for the Environment (HYPE) (Lindström et al., 2010)). Four of them, except AGNPS/AnnAGNPS, are semi-distributed and most studies use this type of model (e.g., SWAT, INCA, HSPF and HYPE account for more than 70% of 257 studies investigated by Wellen et al. (2015)). These models usually disaggregate a catchment into sub-catchments based on surface topography and then define homogenous classes (e.g., Hydrological Response Units (HRUs) in SWAT and Soil and Land-use Classes in HYPE) within each sub-catchment based on land-use and soil type combinations. Consequently, information on class locations and interactions with neighboring classes is lost (Rathjens & Oppelt, 2012). Although these models simulate terrestrial processes for each class, they aggregate outputs from each class to the whole sub-catchment. Detailed spatial information, such as nutrient status (e.g., soil moisture concentration) and dynamics (e.g., leaching and percolation) in specific locations is missing (Rathjens et al., 2015). This kind of information, however, is increasingly asked for by researchers and stakeholders. For instance, the information can help to identify critical source areas of non-point source pollution and to place agricultural mitigation measures at the field scale (Bieger et al.,

2017). Moreover, in-stream processes in such semi-distributed models are usually simulated in a river network represented by the total length of rivers within each sub-catchment and the connections between all sub-catchments. Terrestrial outputs are routed along this conceptual river network, neglecting the variability of nutrient transport processes within sub-catchments. However, the river network must be represented in detail to reflect the variability of in-stream residence time and stream morphological characteristics, which are essential factors driving in-stream processes (Alexander et al., 2000). Additionally, locations where point-source inputs may enter the river network can significantly influence in-stream processes and corresponding spatial distribution of stream water quality.

Efforts are in place to improve the spatial representation of semi-distributed models. For instance, the landscape unit (LSU) version of SWAT was developed to increase its description of connections between spatial objects (i.e., HRUs, LSUs and sub-catchments) (Arnold et al., 2010); however, detailed connection information for each object (e.g., accurate proportions of runoff assigned to receiving objects) is difficult to determine. Ultimately, a grid-based model structure, with high spatial representation of catchment heterogeneity (Rathjens et al., 2015), facilitates mechanistic analyses of variable flow and matter flux processes (Schulz et al., 2006). Some grid-based water quality models have been developed. One of them is AGNPS/AnnAGNPS (for event-based modeling of sediment bound compounds (Rode & Frede, 1997; Young et al., 1989)) and for continuous simulations (Yuan et al., 2001), respectively). Studies have verified advantages of the grid-based structure of AGNPS (Emili & Greene, 2013; Liu et al., 2008), but among other limits (Edsel et al., 2011), most of the studies are limited to catchments smaller than 200 km^2 (see arguments by Krysanova et al. (1998)) and the grid size normally does not exceed 1 km^2. Similar scale limitations have also been observed in other grid-based water quality modeling studies, such as the integrations of physically based Water Flow and Balance Simulation Model (WaSiM-ETH) with nutrient routines (Rode & Lindenschmidt, 2001; Shrestha et al., 2007), the STREAM-N model (Dunn et al., 2013) and a nitrate transport model development based on the J2000 model (Hesser et al., 2010). This is probably due to the imbalance between spatial representation and model complexity, resulting in high computational demand as catchment size increases. This dilemma can be reflected in the development of the grid-based version of SWAT (Rathjens & Oppelt, 2012; Rathjens et al., 2015), which takes each Digital Elevation Model (DEM) cell as a sub-catchment with one HRU defined. Meanwhile, a high DEM resolution (e.g., 100 m) is strongly recommended to minimize uncertainties (Chaubey et al., 2005). This leads to long run-times of the code in larger catchments (e.g., nearly 1 hour per simulated year for Rathjens et al. (2015) in a 334 km^2 catchment) and practically limits applications of the model to relative small catchments (Pignotti et al., 2017). Overall, grid-based catchment water quality model

developments need to find a compromise between accurate spatial representation and a flexible and manageable structure.

In addition to catchment discretization, adequate descriptions of flow and matter flux processes along different flow paths is one of the core challenges in water quality modeling. Most process-based catchment models focus on describing processes at the surface and in the shallow subsurface (i.e., the upper 2 m of soil depth) because they are the most active response zones for stream flow and nutrient concentrations. The dynamics of deeper groundwater are largely simplified or even excluded in some models. However, groundwater and its nutrient dynamics become more essential during low-flow conditions, when baseflow contributes most to total stream flow. Studies have been conducted to couple catchment models with groundwater models (e.g., MODFLOW) (Bailey et al., 2016; Wriedt & Rode, 2006); but doing so greatly increases model complexity and data requirements, which constrains applicability of the coupled models, although such complexity is needed in many cases (Fatichi et al., 2016). It is believed that hydrological processes are only sensitive to the dynamic part of groundwater storage (Kirchner, 2009), thus deep groundwater storage in hydrological models is typically considered to be of minor importance for stream flow simulation. In contrast, the dynamics of deep groundwater storage are much more important for nutrient models, due to the long residence time of groundwater and the associated impacts on nutrient concentrations (Benettin et al., 2015; Wriedt & Rode, 2006). This subject still needs further consideration in process-based catchment water quality models.

A model's capability to support decision-making is largely based on how it represents anthropogenic pressures, such as impacts of agricultural practices and of point-source pollution. Non-point sources from agricultural land are identified to be a major cause of high nutrient concentrations in surface water (EEA, 2005). Effects of agricultural management practices and mitigation measures on improving water quality have been intensively evaluated (Hashemi et al., 2016; Rode et al., 2009). However, studies targeting effects of spatially differentiated agricultural management are still not well covered (Hansen et al., 2017; Hashemi et al., 2016), partly due to the few models that can do this at catchment scale and their inability to provide the necessary cropping information at the field scale. For instance, current catchment models insufficiently represent crop rotations since cropping patterns are difficult to be identified from commonly used land-use map, where agricultural fields are always classified as one "arable land" type. Similarly, model limitations exist in studying effects of spatially distributed point sources on water quality in river networks.

Overall, the need exists to develop a flexibly structured catchment water quality model with comprehensive descriptions of flow and matter flux dynamics and greater ability to simulate changing anthropogenic conditions. In this study, we present a new grid-based nitrate model (mHM-Nitrate) at catchment scale, which is able to balance model complexity and representation of nitrate transport and removal processes. The model is mainly based on the advanced implementations of the mesoscale Hydrological Model (mHM) (Samaniego et al., 2010) and the HYPE model (Lindström et al., 2010). Since mHM has been evaluated in catchments with a wide range of sizes (Kumar et al., 2013), it is a promising hydrological platform to further extend to a water quality model. The main objectives of this study are 1) to develop the new mHM-Nitrate model, 2) to validate the model's ability to reproduce dynamics of long-term and high-frequency observations in a heterogeneous catchment at nested locations, 3) to evaluate model parameter sensitivity and model uncertainty, and 4) to provide detailed spatial information on nitrate concentrations and fluxes.

2.3. Methodology

2.3.1. Model description

Hydrological submodel

The mHM model (www.ufz.de/mhm) has a flexible reservoirs based structure, in which users can specify multiple spatial resolutions: From input data perspective, resolutions of geographic and meteorological data levels can be defined independently; According to specific research objectives, resolutions of modeling levels (i.e., terrestrial hydrological process and in-stream routing levels) can be specified individually. Cell size of all specified resolutions must be multiples of each other. All geographic and meteorological information is aggregated or disaggregated to the modeling levels and the scaling issues are done automatically according to the resolutions specified by users. For each cell of the terrestrial modeling level, the conceptual HBV model (Bergström, 1995) is used to represent the most important hydrological processes: evapotranspiration, canopy interception, snowpack and snowmelt, soil moisture dynamics and percolation, and runoff generation (**Figure 2.1**). Three conceptual reservoirs are defined to represent water storage in impervious areas, the unsaturated soil zone and the deep saturated subsurface zone, which generate direct flow, interflow (fast near surface flow and slow interflow) and baseflow, respectively. Total runoff from each terrestrial modeling cell is disaggregated or aggregated to the routing level and then routed along the river network. The river network is generated according to the main flow direction of each cell of routing level, which is upscaled from flow direction data at geographic data level.

The mHM model also integrates the multiscale parameter regionalization (MPR) technique for hydrological parameters (Samaniego et al., 2010), which overcomes common parameterization problems in distributed models while maintaining spatial variability in hydrological parameters and state variables (Samaniego et al., 2010). Unlike a standard regionalization scheme (Pokhrel & Gupta, 2010), MPR uses different transfer functions to regionalize most hydrological model parameters at geographic data level. For instance, using pedotransfer functions, soil moisture contents are calculated from soil properties provided by the soil map at geographic data level. Parameters introduced in these transfer functions, along with parameters that have not been regionalized (e.g., baseflow recession rate which varies by geological unit), must be upscaled (the second phase of MPR) to model levels and calibrated against observations. Noticeably, the parameters of transfer functions are denoted as "global parameters", indicating greater transferability across locations and scales (Rakovec et al., 2016; Zink et al., 2017). Detailed descriptions of the technique and mHM model parameters are given by Samaniego et al. (2010) and Kumar et al. (2013).

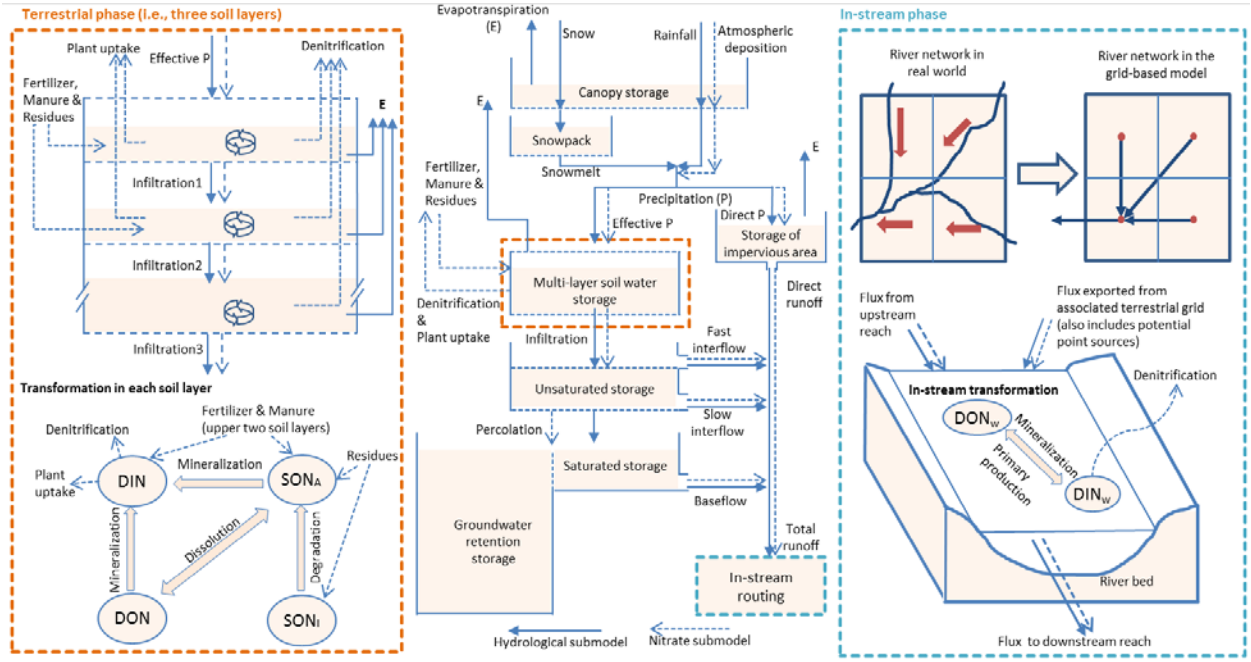

Figure 2.1. Structure of the mHM-Nitrate model, adapted from mHM and HYPE concepts (Lindström et al., 2010; Samaniego et al., 2010). In the terrestrial phase, four different nitrogen forms are defined (i.e., dissolved inorganic (DIN) and organic (DON) nitrogen, active (SON_A) and inactive (SON_I) solid organic nitrogen); in the in-stream phase, two forms are defined (i.e., dissolved inorganic (DIN_w) and organic (DON_w) nitrogen in stream water).

Nitrate submodel

We considered nitrate-nitrogen ($N - NO_3^-$) as equivalent to dissolved inorganic nitrogen (DIN). Other forms of DIN, namely ammonium (NH_4^+) and nitrite, typically account for less than 15% and 1%, respectively, at natural levels (Meybeck, 1982), and both compounds are rapidly transformed into NO_3^- during their transport downstream. Moreover, improved waste water treatment has substantially decreased NH_4^+ concentrations (EEA, 2012), which remain at a low level as in natural rivers (Meybeck, 1982). It is theoretically possible to calculate dissolved organic nitrogen (DON) concentrations, but they are generally low and rarely measured.

The nitrogen mass balance and transformation equations were mainly adopted and modified from HYPE, which is revised from HBV-NP (Andersson et al., 2005; Lindström et al., 2010) and widely verified in many catchment water quality modeling studies (Arheimer et al., 2012; Jiang et al., 2014; Jomaa et al., 2016). In the terrestrial phase (**Figure 2.1**), four different nitrogen pools (i.e., active solid organic nitrogen (SON_A), inactive solid organic nitrogen (SON_I), DON and DIN) were defined in each soil layer for each cell of terrestrial modeling level. Sources (i.e., atmospheric deposition, fertilizer and manure application and plant residues), sinks (i.e., denitrification and plant uptake) and transformations between the pools (i.e., degradation, dissolution and mineralization) for nitrogen mass balance and dynamics were included. DIN and DON fluxes (i.e., infiltration into deeper soil layers, percolation into groundwater and leaching into the stream) were calculated with flow dynamics, with the assumption of full mixing in each reservoir. In the in-stream phase (**Figure 2.1**), dissolved inorganic (DIN_w) and organic (DON_w) pools were defined in each reach at the routing level. We assumed that all inputs (i.e., transport from upstream, exports from associated terrestrial grids and potential point-source inputs) of each reach fully mixed with the pre-stored volume in the reach. For in-stream processes, we considered denitrification and transformations between the DIN_w and DON_w pools (inverse processes of primary production and mineralization). Initial pool sizes and transformation parameters were mainly land use dependent. More detailed descriptions of nitrate-related processes can be found in **Supporting Information** (**Text S2.1**) and Lindström et al. (2010).

Additional implementations

In order to further improve the model representation of nitrate dynamics and model ability of considering anthropogenic impacts, we added three major improvements in the mHM-Nitrate model development.

First, we divided deep groundwater storage into two parts. The hydrological submodel considers only a relatively small storage, which actively contributes to baseflow generation. Additional retention groundwater storage, which can be as large as tens of meters, was added to the nitrate submodel. The mass conservative equation for calculating baseflow $N-NO_3^-$ concentration was modified from the INCA-N model (Wade et al., 2002; Whitehead et al., 1998a):

$$\frac{dC_{bf}}{dt} = \frac{1}{V_r + V_h}\left(M_{perc} - M_{bf}\right), \tag{2.1}$$

where C_{bf} denotes baseflow $N-NO_3^-$ concentration ($mg\ l^{-1}$); V_r and V_h denote retention storage and hydrologically active storage of deep groundwater, respectively (mm); and M_{perc} and M_{bf} denote percolated mass per unit area and baseflow export load, respectively ($mg\ N\ m^{-2}$). This ordinary differential equation was solved using the fourth order Runge-Kutta technique. Initial values of C_{bf} and V_r were set as land-use type dependent (**Supporting Information**, **Table S2.1**).

Second, we added an input map of "crop rotation" to provide the spatial distribution of crop rotation types and a corresponding look-up table to define the crop sequence of each rotation type. Technically, the crop rotation map can be easily modified from the land-use map by separating arable land into different rotation regions. Forest and pasture can be treated as individual rotation types in this map, so that their nitrogen supply (e.g., plant/grass residues and animal wastes) and uptake can be defined in the look-up table to estimate the terrestrial nitrogen mass balance.

Third, we added the ability to consider time series inputs of waste water treatment plants (WWTPs) based on their exact geographic locations. Therefore, point sources can be added to nearby streams and be routed along the spatially explicit river network. In other words, the model facilitates the assessment of impacts of spatially differentiated point-source pollution. Furthermore, time-series data of point source inputs enabled long-term continuous simulations under changing point-source conditions.

2.3.2. Model parameters and sensitivity analysis

We parsimoniously parameterized the nitrate submodel using only six parameters for rates of soil denitrification (*denis*), degradation (*degdr*), dissolution (*dislr*), mineralization (*minlr*), in-stream denitrification (*deniw*) and in-stream primary production (*pprt*). All parameters represent individual or combined biogeochemical reaction(s) in nitrate transport and removal processes. These reactions, which depend greatly on specific physical, chemical and biological characteristics, have not been fully

understood and conceptualized in catchment modeling. Therefore, parameters were defined as land-use dependent at the geographic data level, except for in-stream denitrification rate (*deniw*) which is a general parameter. These parameters, along with state variables in the nitrate sub-model, were upscaled to the terrestrial and in-stream modeling levels, following the second phase of MPR. Among the upscaling operators that can be chosen to maintain spatial variability (Samaniego et al., 2010), we chose the area-weighted mean method in this study.

Although some of mHM parameters are potentially transferable (Kumar et al., 2013) and hydrological simulations are insensitive to some parameters (Cuntz et al., 2015), the total number of mHM-Nitrate parameters is still too large to be calibrated directly. Therefore, parameter sensitivity analysis is needed. We used the SAFE (Sensitivity Analysis For Everybody) tool developed by Pianosi et al. (2015).The Elementary Effects (EE) (Morris, 1991) method was selected for the sensitivity analysis, based on the screening and ranking purpose (Pianosi et al., 2016). It is a multiple-starts perturbation method and each trajectory allows for evaluating one EE per factor. The elementary effect of the i^{th} parameter (EE_i) is based on a sample generated from the radial one-factor-at-a-time sampling strategy (Campolongo et al., 2011). The EE_i and absolute mean (μ_i^*) and standard deviation (σ_i) of EE_i in r trajectories are calculated:

$$EE_i = \frac{f(p_i+\Delta_i)-f(p_i)}{\Delta_i}, \tag{2.2}$$

$$\mu_i^* = \frac{1}{r}\sum_{j=1}^{r}\left|EE_i^j\right|, \sigma_i = \sqrt{\frac{1}{r-1}\sum_{j=1}^{r}\left(EE_i^j - \mu^*\right)^2}, \tag{2.3}$$

Where f denotes the objective function used for sensitivity analysis (here we selected the Root-Mean-Square-Error, RMSE); p_i denotes the value of the i^{th} parameter; Δ_i denotes the sampling step; EE_i^j denotes EE_i in the j^{th} trajectory; and r denotes the number of sampled trajectories. By plotting μ_i^* versus σ_i of all parameters, the sensitivity ranking is obtained, with the more to the right-up section the point, the more influential and interdependent, respectively, the parameter becomes.

We first separately analyzed sensitivity ranking of hydrological and nitrate submodel parameters for discharge and nitrate simulation, respectively. Then we simultaneously analyzed all parameter sensitivities for nitrate simulation, to take account interactions between hydrological and nitrate processes.

2.3.3. Model calibration and uncertainty analysis

Based on sensitivity analysis, the most sensitive parameters have to be carefully calibrated against observations. Due to the complexity of grid-based parameterization approach, it is necessary to use an effective and efficient automatic optimization method. We used the Dynamically Dimensioned Search (DDS) method (Tolson & Shoemaker, 2007), which is developed for identifying approximation of global optimal solutions of computationally demanding models in limited evaluations (Behrangi et al., 2008).

Apart from a powerful optimization method, selection and construction of an objective function, which reflects the goodness-of-fit between observations and simulated results, is also critical for successful model calibration. We used a multi-objective calibration approach with multi-criteria, multi-site and multi-variable.

First, we used the Nash-Sutcliffe Efficiency (NSE) coefficient (Nash & Sutcliffe, 1970) as one of the criteria. Given the equivalent importance of high- and low-value periods in nitrate simulations, we also combined the logarithmic transformation of NSE ($\ln NSE$), which flattens high values to a comparable level with low values (Krause et al., 2005). Thus, the multi-criteria objective function was:

$$OF_{multi-c} = min\left\{\sqrt[6]{(1-NSE)^6 + (1-\ln NSE)^6}\right\}, \tag{2.4}$$

$$NSE = 1 - \frac{\sum_{i=1}^{n}(VAR_{sim}^{i} - VAR_{obs}^{i})^2}{\sum_{i=1}^{n}(VAR_{obs}^{i} - \overline{VAR_{obs}})^2}, \tag{2.5}$$

$$\ln NSE = 1 - \frac{\sum_{i=1}^{n}(\ln VAR_{sim}^{i} - \ln VAR_{obs}^{i})^2}{\sum_{i=1}^{n}(\ln VAR_{obs}^{i} - \overline{\ln VAR_{obs}})^2}, \tag{2.6}$$

where VAR_{sim}^{i} and VAR_{obs}^{i} denote simulated and observed variables (discharge or $N-NO_3^-$ concentration), respectively, at time step i; $\overline{VAR_{obs}}$ and $\overline{\ln VAR_{obs}}$ denote the mean of observed values and of their log-transformation, respectively; n denotes the number of time steps. Second, multi-site calibration has been proofed outperforming single-site approaches in heterogeneously characterized catchments (Jiang et al., 2015; Li et al., 2010). Thus, the multi-site objective function (for both discharge and $N-NO_3^-$ concentration) was adapted as follows:

$$OF_{multi-s} = min\left\{\sum_{k=1}^{m} OF_{multi-c}^{k}\right\}, \tag{2.7}$$

where $k = 1,2,\cdots m$ and m denotes the number of gauging stations. Third, nitrate transport processes are mostly driven by hydrological processes. While in model calibration, nitrate observations can help to constrain hydrological processes (e.g., indicating runoff partitioning which cannot be reflected in discharge observations (Zhang et al., 2016)). Thus a weight-aggregated multi-variable function was constructed as follows:

$$OF_{multi-v} = min\{w_q \cdot OF^q_{multi-s} + w_n \cdot OF^n_{multi-s}\}, \tag{2.8}$$

where $w_q = 0.9$ and $w_n = 0.1$ denote weights for discharge and $N - NO_3^-$ concentration objectives, respectively. The weight for each variable can be optimized, or using Pareto multi-objective optimization, but it is not within the scope of this study.

After model calibration, we used three evaluation criteria, namely NSE, RMSE and percent bias (PBIAS), to evaluate the model performance in discharge and $N - NO_3^-$ concentration simulations.

We also integrated a widely used Markov Chain Monte Carlo (MCMC) approach - $DREAM_{ZS}$ (Differential Evolution Adaptive Metropolis algorithm) (ter Braak & Vrugt, 2008; Vrugt et al., 2009; Wilusz et al., 2017) to evaluate model uncertainties. Model parameter inferences were based on the log-likelihood function:

$$logL = \frac{M+N}{2}\log(2\pi) - \sum_{i=1}^{M+N} log\sigma_i - \sum_{i=1}^{M+N} \frac{\varepsilon_i^2}{2\sigma_i^2} \tag{2.9}$$

where $i = 1,2,\cdots M, M+1, \cdots M+N$ and M, N denote the number of discharge and nitrate measurements, respectively; ε_i denotes the model error at ith measurement; and σ_i denotes the error standard deviation. Following the work of Vrugt et al. (2005), the discharge σ was tested as heteroscedastic ($\sigma_i = 0.09 \times discharge$), while nitrate σ was homoscedastic ($\sigma = 0.32\ mg/l$, see details in **Supporting Information**, **Figure S2.1**). We also assumed the errors independently follow the Gaussian distribution. The 95% confidence band of parameter uncertainty was generated from 10,000 MCMC evaluations in this study, and that of total uncertainty was calculated from model simulations with random errors (normal distribution$\sim N(0,\ \sigma_i)$).

2.4. Test catchment and data analysis

2.4.1. Catchment description

The mHM-Nitrate model was tested in the Selke catchment, a sub-catchment of the Bode catchment in Central Germany (the TERENO Harz/Central German Lowland Observatory (Wollschläger et al., 2016)).

The drainage area of the Selke catchment is approximately 456 km^2. Mean annual precipitation is 660 mm, ranging from 792 mm in the upper mountainous areas to 450 mm in the lower agricultural lands. Mean monthly temperature is 9°C (ranging from -1.8°C in winter to 15.5°C in summer) and a considerable amount of snowmelt from the upper mountains contributes to stream discharge according to our field experience. Three nested gauging stations (Silberhütte, Meisdorf and Hausneindorf, with area of 99, 184 and 456 km^2, respectively) and five WWTPs were considered in this study (**Figure 2.2a**). The station Meisdorf, above which 72% of the area is occupied by forest, measures discharge and nutrient exports from the upper forest area. Agricultural land dominates the lower part of the catchment (almost 80% of the area between the station Meisdorf and the outlet station Hausneindorf), with considerable urban areas (**Figure 2.2b**). The main crops planted on agricultural land are winter wheat, winter barley, triticale, rye, rapeseed, maize and sugar beet. The amount of fertilizer applied each year ranges from 130 to 190 kg N ha^{-1} (Kistner, 2007). Soil and geological characteristics also differ in areas upstream and downstream of the station Meisdorf. Upstream of the station Meisdorf, cambisols and schist/claystone form the soils and geology, respectively, while chernozems and tertiary sediments with loess dominate the lower parts of the catchment (**Figure 2.2c and d**). Due to this heterogeneity of physiographic condition, the Selke catchment was selected to test the new mHM-Nitrate model.

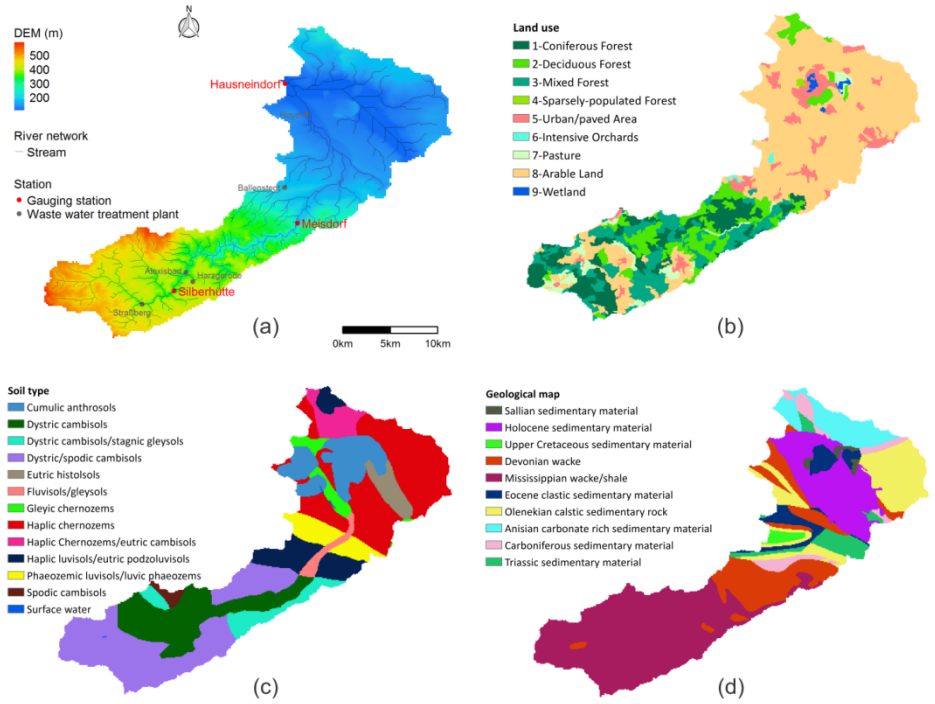

Figure 1.2. Geographic data of the Selke catchment, Central Germany: (a) Digital Elevation Model (DEM), river network and station locations, (b) land use types, (c) soil types, and (d) geological map.

Geographic data were resampled from original sources into a user-defined resolution (100 m in this study, **Table 2.1**). Resolution of the crop rotation map was set equal to that of the land-use map for technical simplification since it is modified from the land-use map and unique rotation type was assigned in all arable lands in this study. Meteorological data were collected from the German Weather Service. The number of precipitation stations within and around the Selke catchment has decreased from 16 to 8 after 2004 and another station was dismantled in 2013. There is no reservoir constructed in the catchment. Evaluation data (discharge and concentration observations) were collected from the State Agency for Flood Protection and Water Management of Saxony-Anhalt -LHW (daily discharge data for 1993-2015 and biweekly $N-NO_3^-$ concentration data for 1997-2009, with a one-year gap) and the Helmholtz Center for Environmental Research - UFZ (biweekly and 15-minute $N-NO_3^-$ concentrations for 2010-2015). In the years 1998-2004, about 18% of annual stream flow was abstracted from the downstream part for flooding of a mining pit. Resolutions of terrestrial modeling and in-stream routing levels were set as 1km and 8 km, respectively. Daily discharge and nitrate data were averaged values from high-frequency measurements, and biweekly nitrate data were grab sample measurements.

Table 2.1. Data used to set-up and evaluate the mHM-Nitrate model in the Selke catchment, Germany. Data source: BGR - Federal Institute for Geosciences and Natural Resources, Germany; DWD - German Weather Service; LHW - State Agency for Flood Protection and Water Management of Saxony-Anhalt; UFZ - Helmholtz Center for Environmental Research. SR: spatial resolution.

Data catalog	Data type	Resolution	Period	Source
Geographic data	Digital Elevation Model	SR (All resampled to 100 m): 30 m,	--	State Survey Office/ BGR
	Land-use	30m,		
	Soil-type	1:1 000 000,		
	Geological map	1:1 000 000		
Agricultural practices	Application of fertilizer/manure	--	--	Field survey/ interview
	Dates of farming practices			
	Map & look-up table of crop rotations	SR: 100 m (based on the land-use map)	--	
Point source	Discharge and water	Daily	2002-2010	Five waste water

data	quality			treatment plants
Meteorological data	Precipitation Temperature Potential evapotranspiration	Daily SR: 1 km	1993-2015 (warming period: 1993-1996)	DWD
	Atmospheric nitrogen deposition	9-15 kg ha^{-1} yr^{-1}		State agricultural authority
Evaluation data (three gauging stations)	Discharge	Daily	1997-2015	LHW
	Nitrate concentration	Biweekly	1997-2015	LHW/UFZ
		Daily	2010-2015	UFZ

2.4.2. Time-series data analysis and pre-processing

Long-term dynamics of observed biweekly $N - NO_3^-$ concentrations showed notable differences between dominant land-use types. Mean concentration at the outlet (3.61 $mg\ l^{-1}$ at Hausneindorf) was much higher than that from the upper forest-dominant area (1.60 $mg\ l^{-1}$ at Meisdorf). Seasonal Mann-Kendall Test (Hirsch et al., 1982) for 1997-2015 (results not shown) indicated no significant trend at Silberhütte, while at Meisdorf, a negative trend was only observed in July (p value equaled to 0.019) when the lowest flow occurred. At Hausneindorf, however, a strong negative trend was detected throughout the year, except in February and March which are the main high flow months. Seasonal patterns of concentration also differed largely. At the two upper stations (Silberhütte and Meisdorf), the pattern was clear and consistent with the discharge pattern, showing high concentrations (ca. 4 $mg\ l^{-1}$) in high-flow periods and low concentrations (as low as 0.5 $mg\ l^{-1}$) in low-flow periods. However, the pattern at Hausneindorf changed during the periods studied. After 2007, concentrations in high-flow periods were higher than those in low-flow periods, but amplitudes of seasonal variability were much lower than those of the two upper stations, primarily due to much higher minimum values (ca. 2 $mg\ l^{-1}$). In the previous period (1997-2006), concentrations slightly decreased (from ca. 4 to 2 $mg\ l^{-1}$) in the recession phases of the main high-flow period of the year, but greatly increased during subsequent low-flow periods (up to 8 $mg\ l^{-1}$).

Five WWTPs have been constructed since 2002, but they only started to properly operate in 2007, identified by annual mean outflow discharge (**Figure S2.2** to **S2.4**). We assumed that the unrecorded waste water was put directly into streams at the plant sites. Therefore, we estimated the unknown point-source inputs before 2007 according to available measurements (WWTP Harzgerode, for which inflow measurements were collected) and urban populations (WWTPs Ballenstedt and Hoym, for which inflow measurements were missing). The estimation of daily point-source data were given in **Supporting**

Information (**Figure S2.2** to **S2.4**). We excluded WWTPs Straßberg and Alexisbad in this study since the outflow discharge and city population were much less than the other ones.

As a part of the TERENO Harz/central German lowland observatory, high-frequency monitoring has been performed in the Selke catchment since 2010. We aggregated daily mean $N-NO_3^-$ concentrations from newly available 15-minute sensor data at the three gauging stations. Given the quantity and quality of $N-NO_3^-$ observations, daily discharge and biweekly concentration data in the period 2010-2015 were used for daily model calibration and data in the period 1997-2009 were used for long-term model validation. Also, daily concentration observations in the period 2010-2015 were used for additional high-resolution validation. The period 1993-1996 was used as a spin-up period for hydrological simulation and the initial conditions for the nitrate simulation are provided in the **Supporting Information** (**Table S2.1**).

2.5. Results

2.5.1. Parameter analysis

We identified nine land use types and ten geological units in the Selke catchment (**Figure 2.2b** and **d**). Consequently, the total number of parameters reached up to 99, (53 and 46 in hydrological and nitrate submodels, respectively), making a parameter sensitivity analysis necessary.

Separate parameter sensitivity ranking (PSR) results showed that parameters related to soil moisture (*soil*) influenced hydrological simulations the most, followed by those related to evapotranspiration (*pet*) and interflow generation (*intfl*) (**Figure 2.3a**), which highlights the importance of soil moisture dynamics, evapotranspiration and interflow generation processes in simulating discharge. Results also showed that denitrification rates in stream water (*deniw*) and for land-use types (*denis*) influenced nitrate simulation the most (**Figure 2.3b**). Simultaneous sensitivity results showed that hydrological parameters dominated the upper-right section, with one nitrate parameter ranked in the third place (**Figure 2.3c**), demonstrating that nitrate simulation was mainly driven by hydrological processes. Specifically, the most influential processes were also soil moisture dynamics, interflow generation and evapotranspiration. Comparing the separate and simultaneous analyses of nitrate submodel parameters **(Figure 2.3b** and **c**), the top ten parameters differed in both rank and number, with a decrease in denitrification process parameters and an increase in in-stream primary production process parameters (*pprt*). This indicates that hydrological processes also influenced the sensitivity of nitrate sub-model parameters.

Results of simultaneous analysis also showed large variance in sensitivity among all parameters (i.e., wide range and dramatic decrease in values of μ^* and σ) (**Figure 2.3c**). We selected the top ten and top six hydrological and nitrate submodel parameters, respectively, for model calibration and uncertainty analysis. We further grouped the land-use dependent nitrate parameters into an agricultural group (parameters in intensive orchard, pasture and arable lands) and a non-agricultural group. The DDS calibration method was used and 50,000 iterations were set as the terminal criterion. The calibrated optimal values are given in **Table 2.2**.

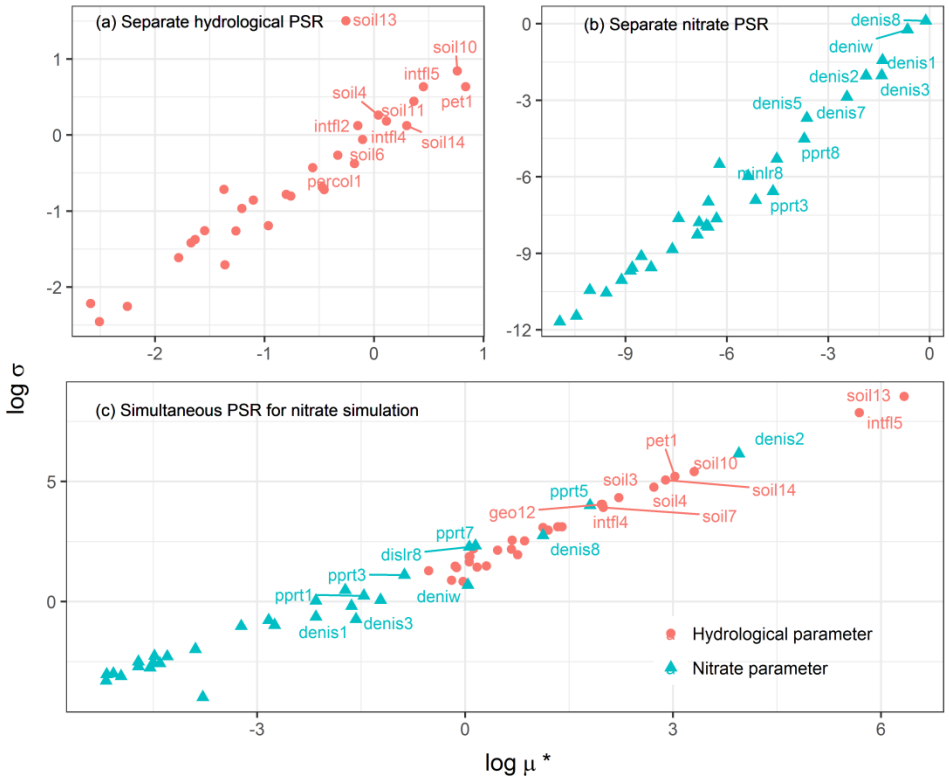

Figure 2.3. mHM-Nitrate parameter sensitivity ranking (PSR) using the Elementary Effect method. Graphs (a) and (b) show the top 30 parameters, with the top 10 labeled; graph (c) shows the top 60 parameters, with 20 labeled (the top 10 of hydrological and nitrate parameters, respectively). Labeled parameters are related to soil moisture (soil), evapotranspiration (pet), interflow generation (infl), geological units (geo), soil denitrification rates (denis), dissolution rate (dislr), mineralization rate (minlr), in-stream denitrification rates (deniw) and in-stream primary production rate (pprt). Numbers after nitrate parameter refer to land-use types numbered in Figure 2b. The more to the right-up section the point, the more influential and interdependent, respectively, the parameter becomes. Note the log-log scales.

Table 2.2. Description of the calibrated model parameters. More detailed descriptions of hydrological submodel parameters are given by Samaniego *et al.* (2010). Shaded rows indicate nitrate submodel parameters, with subscripts "na" and "a" denote non-agricultural group and agricultural group, respectively.

Parameter	Brief description	Parameter range	Optimal value
soil3	Correction factor of hydraulic conductivity considering organic matter content	[0.00E+0;4.00E+0]	3.99E+0
soil4	Pedotransfer function parameter for calculating soil moisture content (Zacharias & Wessolek, 2007)	[6.46E-1; 9.51E-1]	9.50E-1
soil7	Pedotransfer function parameter for calculating soil moisture content (Zacharias & Wessolek, 2007)	[5.36E-1; 1.12E+0]	9.21E-1
soil10	Transfer function parameter for calculating saturated hydraulic conductivity (Cosby et al., 1984)	[-1.20E+0; -2.85E-1]	-9.02E-1
soil13	Transfer function parameter for calculating saturated hydraulic conductivity (Cosby et al., 1984)	[1.00E+0; 1.50E+2]	6.23E+1
soil14	Fraction of roots for calculating actual evapotranspiration in forest areas	[9.00E-1; 9.99E-1]	9.62E-1
intfl4	Transfer function parameter for recession rate in slow interflow generation process	[1.00E+0; 3.00E+1]	1.42E+1
intfl5	Transfer function parameter for exponent coefficient (alpha) in slow interflow generation process	[5.00E-2; 3.00E-1]	1.20E-1
pet1	Parameter for aspect correction of input potential evapotranspiration data	[7.00E-1; 1.30E+0]	1.02E+0
geo12	Baseflow recession rate under geological unit number 12	[1.00E+0; 1.00E+3]	2.10E+2
$denis_{na}$	Soil denitrification rate in non-agricultural land (d^{-1})	[1.00E-4; 1.00E-1]	1.87E-2
$denis_{a}$	Soil denitrification rate in agricultural land (d^{-1})	[1.00E-4; 1.00E-1]	3.98E-3
deniw	In-stream denitrification rate (kg m^{-2} d^{-1})	[1.00E-8; 5.00E-2]	3.94E-4
$pprt_{na}$	Primary production rate in non-agricultural stream (kg m^{-3} d^{-1})	[1.00E-8; 1.00E+0]	6.73E-2
$pprt_{a}$	Primary production rate in agricultural stream (kg m^{-3} d^{-1})	[1.00E-8; 1.00E+0]	5.40E-4
$dislr_{a}$	Soil dissolution rate in agricultural land (d^{-1})	[1.00E-1; 2.00E+2]	2.00E+2

2.5.2. Model performance

Long-term discharge simulation results (**Figure 2.4**) and corresponding evaluation criteria (**Table 2.3**) showed that the model performed well for both calibration (2010-2015) and validation (1997-2009) periods. For the two upper stations, Silberhütte and Meisdorf, the model adequately captured seasonal dynamics of discharge, covering both the high- and low-flow periods. NSE values were above 0.81 and 0.76 for discharge simulations in the calibration and validation periods, respectively. NSE values at Meisdorf (0.81 and 0.76 for calibration and validation, respectively) were slightly lower than those at Silberhütte (0.85 and 0.82, respectively). This could be attributed to the underestimation of several flow peaks at Meisdorf after 2006, since NSE is strongly influenced by high values. The amount of precipitation recorded during these events seems to be too low to generate such high flows compared to those of previous flood events (**Figure 2.4a** and **b**). This insufficient precipitation is probably due to the reduced number of precipitation stations in the Selke catchment after 2004 (see **section 2.4.1**). However, the water balance at Meisdorf (discharge PBIAS within ±10%) was better than that at Silberhütte (discharge PBIAS exceeded -10% in the validation period). Underestimation of the discharge balance in mountainous areas (e.g., station Silberhütte) is frequently reported in hydrological modeling studies. This is probably due to the large uncertainties in meteorological input data in these areas. Weather conditions change rapidly due to the high geographic heterogeneity, which leads to decreased spatial representation of weather stations. Moreover, simplifying snowmelt processes likely worsened model performance in the mountainous areas.

For discharge simulation at station Hausneindorf, the model had a somewhat worse performance than that for the upper stations, but still reproduced the observed discharge reasonably well (NSEs were 0.68 and 0.65 in calibration and validation periods, respectively, **Table 2.3**). Underestimation of peak flows probably propagated from the upper part of the catchment where most of the flow is generated. The lower spatial density of precipitation stations in the lower catchment probably exacerbated the problem of insufficient precipitation data. The water balance in the model was most accurate in the calibration period (PBIAS was -4.6%), and least accurate in the validation period (PBIAS reached up to 24.4%). Jiang *et al.* (2014) reported that approximately 18% of mean annual stream flow was abstracted in the downstream part of the Selke catchment during 1998-2004. However, water balance was still slightly overestimated after considering the abstraction. A similar slight overestimation also occurred at Meisdorf (10%) in the validation period. Due to the sparser precipitation stations in the calibration period, the model was likely forced to increase the runoff generation to fit the observed discharge more accurately. Consequently, during the validation period when precipitation data differed, water balance

(PBIAS) was slightly overestimated. Additionally, the RMSE for all stations (not exceeding 0.02) indicated reasonable simulation of discharge (**Table 2.3**).

For nitrate simulations at the two upper stations, the model adequately reproduced the observed concentrations covering both high and low values (**Figure 2.4a** and **b**). NSE values of $N - NO_3^-$ concentration at Silberhütte were even higher than 0.70, presumably due to the clear seasonal concentration pattern. $N - NO_3^-$ concentrations under low-flow conditions were slightly higher at Meisdorf than Silberhütte in the validation period, probably due to unknown point sources from the city of Harzgerode. By estimating the unknown point-source inputs, the model adequately simulated the increased concentration in low flow conditions (NSE was 0.47). Biweekly RMSE and PBIAS values also indicated adequate nitrate simulations at the two upper stations (**Table 2.3)**. At Hausneindorf, $N - NO_3^-$ concentrations were obviously higher than those

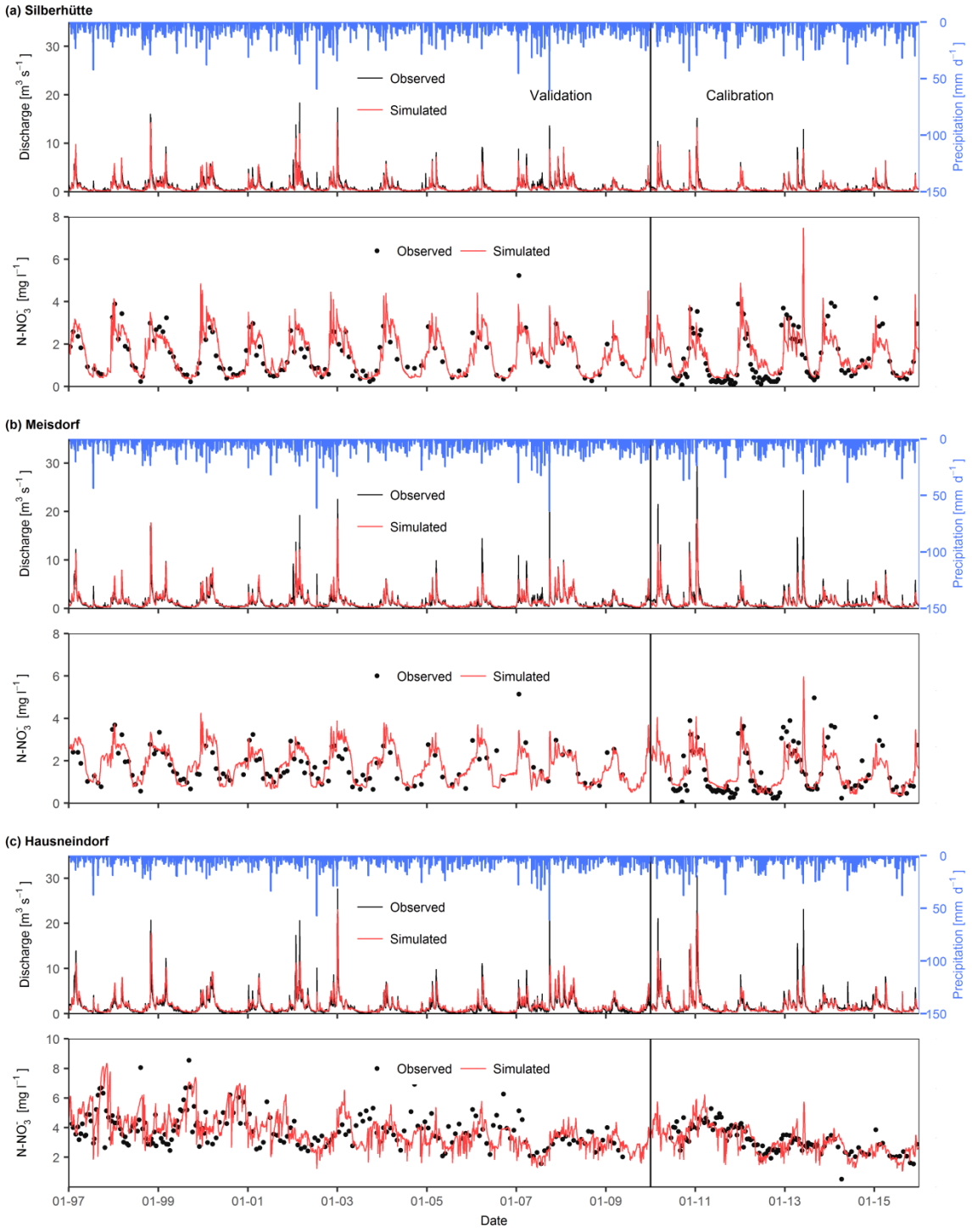

Figure 2.4. Model performances of discharge and $N - NO_3^-$ concentrations in calibration (2010-2015) and long-term validation (1997-2009) periods at the three gauging stations.

at the two upper stations (**Figure 2.4c**), due to strong impacts from intensive agricultural activities on arable lands and from point sources in urban areas. The model simulated nitrate concentration well in the calibration period, when point sources were clearly controlled by two large WWTPs in the lower part (plants Hoym and Ballenstedt, **Figure 2.2a**). Statistical performance in the calibration period illustrated a good simulation accuracy (NSE = 0.37, RMSE = 0.07 and PBIAS = -3.38%). In the validation period, long-term nitrate dynamics were acceptably reproduced by estimating the changing unknown point sources in lower urban areas, although the NSE value was slightly less than zero (-0.07). The largely increased concentrations in low-flow conditions were not captured well. RMSE (0.07) and PBIAS (3.34%) were similar with that in the calibration period, and were acceptable. The Quantile-Quantile plots of observations vesus simulations were shown in **Supporting Information** (**Figure S2.8**).

Regarding the additional validation using daily observations of $N-NO_3^-$ concentration (2010-2015), the model adequately reproduced seasonal patterns and fluctuations during high value periods at the two upper stations (**Figure 2.5a** and **b**). NSE values were both 0.66 and RMSE were below as low as 0.02 and 0.01, respectively (**Table 2.3**). The complex dynamics of concentration at Hausneindorf were reproduced well. Peaks and drops in simulated results were reasonably validated by daily observations (**Figure 2.5c**). Statistically, NSE was high and RMSE and PBIAS values were relatively low, confirming the model performance of daily validation (**Table 2.3**).

We used the daily discharge and biweekly $N-NO_3^-$ concentration data (2010-2015) for the uncertainty analysis. The discharge uncertainty results showed that the uncertainty in high-flow periods was much higher than that in low-flow periods and differences between total uncertainty and parameter uncertainty in high-flow periods were also larger than those in low-flow periods (**Figure 2.6a** and **Figures S2.4 to S2.6**), demonstrating that higher uncertainty from input data and model structure occurs in high-flow periods. This, to some extent, corroborates the above explanations for reduced model performance of the flow peaks. The 95% total uncertainty band of $N-NO_3^-$ concentration covered most of grab-sampling observations (ca. 98%) and most of them were also within or around the parameter uncertainty band (**Figure 2.6b** and **Figures S2.4 to S2.6**).

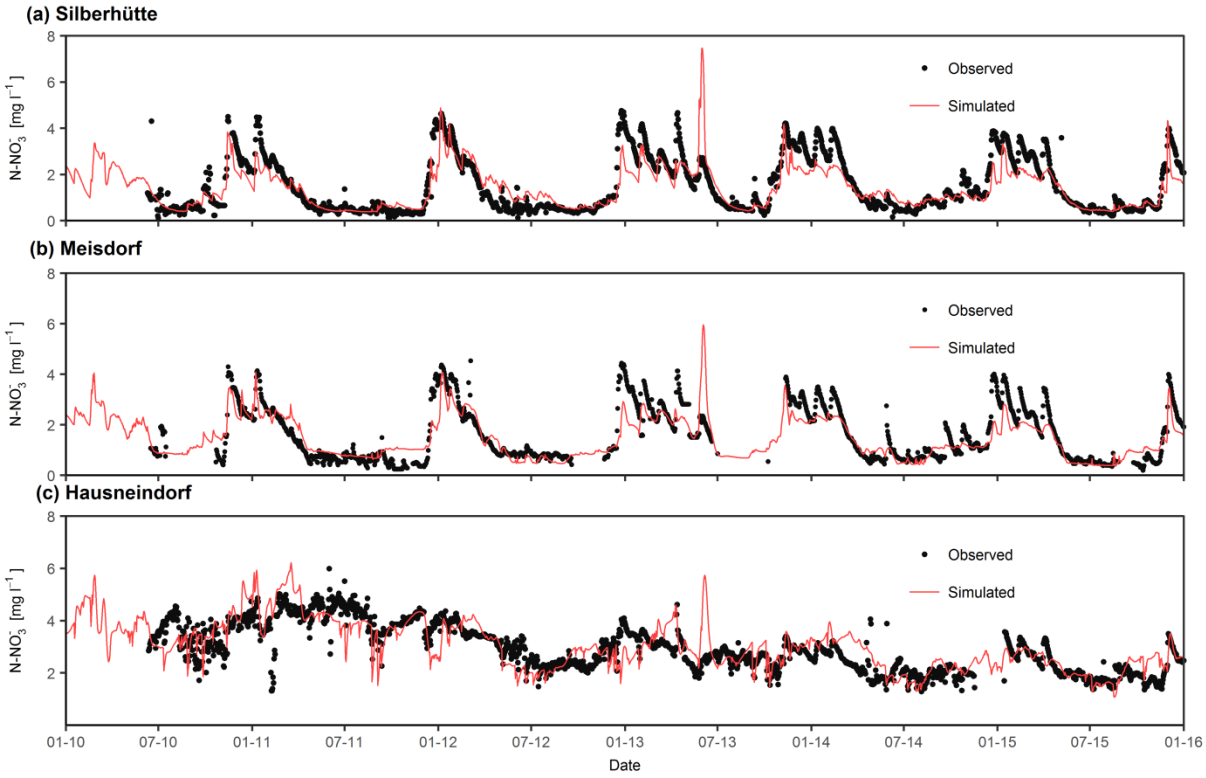

Figure 2.5. Model validation using daily $\boldsymbol{N-NO_3^-}$ concentration observations at the three gauging stations.

Table 2.3. Statistical criteria (Nash-Sutcliffe Efficiency – NSE, Root-mean-square Error –RMSE and Percent Bias - PBIAS) of model calibration and validation for Hausneindorf (Haus), Meisdorf (Meis) and Silberhütte (Silber) in the Selke catchment, Germany.

Variable	Criterion	Calibration 2010-2015			Validation 1997-2009			2010-2015		
		Haus	Meis	Silber	Haus	Meis	Silber	Haus	Meis	Silber
Discharge	NSE	0.68	0.81	0.85	0.65	0.76	0.82	--	--	--
	RMSE	0.02	0.02	0.01	0.01	0.01	0.01	--	--	--
	PBIAS (%)	-4.61	-9.02	-8.86	24.36	10.63	-17.50	--	--	--
	Frequency	Bi-weekly			Bi-weekly			Daily		
$N-NO_3^-$ concentration	NSE	0.37	0.59	0.70	-0.07	0.47	0.72	0.43	0.66	0.66
	RMSE	0.07	0.07	0.07	0.07	0.07	0.06	0.02	0.02	0.01
	PBIAS (%)	-3.38	-2.88	2.48	3.34	-3.35	-0.45	2.75	-7.38	-8.83

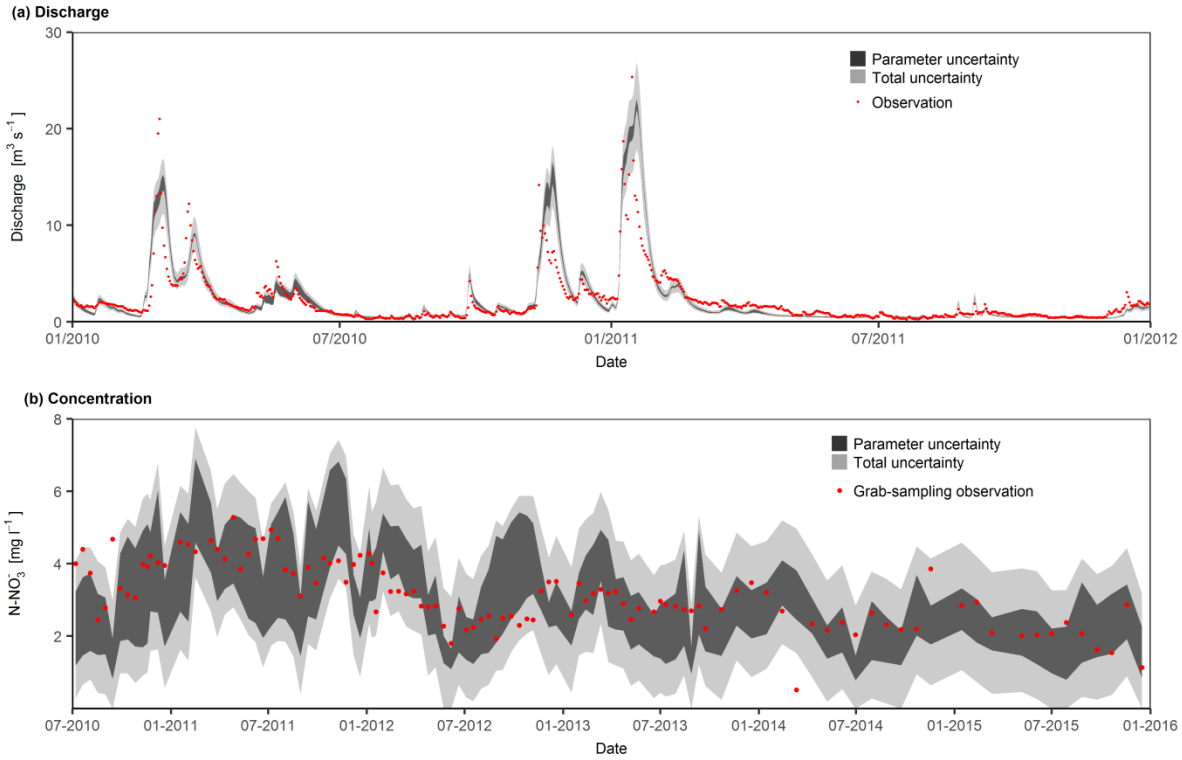

Figure 2.6. The 95% confidence bands of (a) discharge and (b) $\boldsymbol{N-NO_3^-}$ concentration at station Hausneindorf using DREAM$_{ZS}$. Graph (a) shows only results of two-year period (2010-2011) for a better visibility. Complete results of uncertainty analysis at all three gauging stations were provided in Supporting Information (Figures S5 to S7).

2.5.3. Spatial information

We calculated the spatial distributions of mean interflow and baseflow $N-NO_3^-$ concentrations for the period of 2010-2015 (**Figure 2.7**), representing nitrate statuses in soil moisture and groundwater, respectively. Interflow concentrations of agricultural land were much higher than those in forested areas (**Figure 2.7a**), which reflects the strong environmental impacts of agricultural practices (e.g., fertilizer and manure applications). Also, variability for agricultural land was high and most critical source areas were located near the catchment outlet. Baseflow concentrations of the lower agricultural land were higher than interflow concentrations (**Figure 2.7b**), indicating the impacts of long-term agricultural fertilizer application on groundwater nitrate concentration (Musolff et al., 2016).

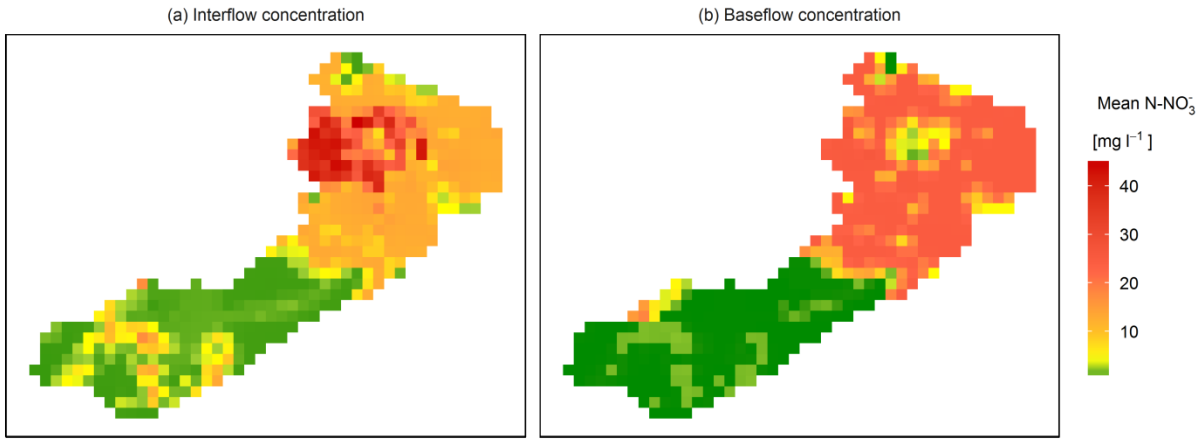

Figure 2.7. Spatial distributions of nitrate concentration ((a) interflow and (b) baseflow concentrations, representing nitrate statuses in soil moisture and groundwater, respectively) provided by the mHM-Nitrate model (cell size: 1 km × 1 km) in period 2010-2015.

Nitrate terrestrial inputs/outputs and internal transformation processes can also be provided by the model spatially. All results (**Figure 2.8**) were averaged from model calculations in period 2010-2015. Main transformation processes (i.e., mineralization, uptake and denitrification) showed high spatial variability across the heterogeneous landscapes in the Selke catchment (**Figure 2.8b**, **d** and **e**). Compared to results in forested areas, these processes were generally more active in agricultural areas. The variability within agricultural areas was also higher than that within forested areas, especially for the denitrification process which is strongly influenced by soil moisture. The calculated terrestrial export loads, which are predominated by annual runoff generation, showed even higher variability in agricultural lands (annual load ranges from 0.1 to 18 $kg\ N\ ha^{-1}\ yr^{-1}$, **Figure 2.8f**). Nitrate external supply through fertilizer and manure application and nitrate soil uptake by crops and plants, accounted for the largest fractions of nitrate input and output, respectively (**Figure 2.8a** and **d**). The overall terrestrial mean balance was nearly closed in the Selke catchment, with a mean total input amount of 106 $kg\ N\ ha^{-1}\ yr^{-1}$ (the sum of nitrate external supply, mineralization and atmospheric wet deposition) equivalent to a mean total output amount of 105 $kg\ N\ ha^{-1}\ yr^{-1}$ (the sum of crop/plant uptake, denitrification and terrestrial export).

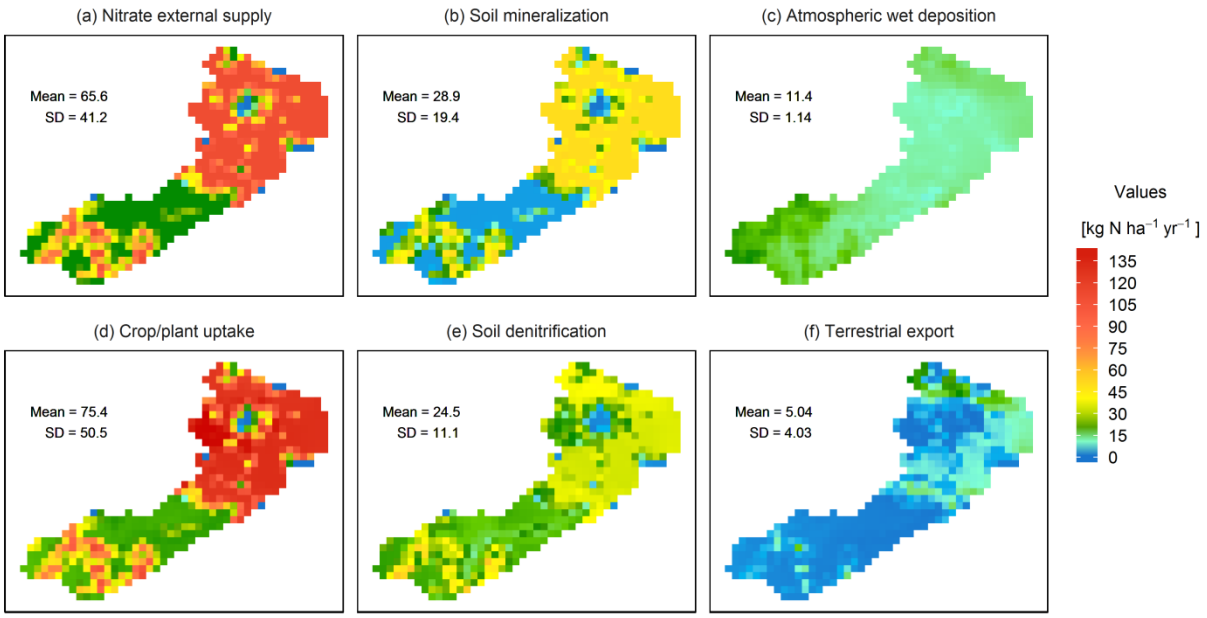

Figure 2.8. Spatial distributions of terrestrial nitrate inputs/outputs and internal transformation processes provided by the mHM-Nitrate model (cell size: 1 km × 1 km) in period 2010-2015.

Information of in-stream removal (i.e., net removal by primary production and denitrification processes) showed high variability both temporally and spatially (**Table 2.4**). Nitrate loads were much higher in wet-winter seasons than in dry-summer seasons due to the hydrological seasonal pattern. Loads at Meisdorf accounted for 35% and 59% of the loads at the outlet (station Hausneindorf) in summer and winter, respectively. Nitrate removal was highest in summer and lowest in winter. Removal in the upper forested reaches was 26-54% of the amount removed from the whole river network. Generally, more nitrates were removed from the lower agricultural reaches than the upper reaches, except spring when they were equivalent. The proportion of nitrate removal to load (percentage) showed high seasonal variability. The highest percentage occurred in summer (e.g., 76% and 54% in the upper forested reaches and the whole river network, respectively, in July) and the lowest removal occurred in winter (e.g., only ca. 0.1% and 0.3%, respectively, in February). Spatial variability of the percentage was not pronounced throughout the whole year, except in summer when nitrate load at Meisdorf was very low (with 83.4 $kg\ N\ d^{-1}$ vs. 234 $kg\ N\ d^{-1}$ at the outlet).

Table 2.4. Seasonal and annual mean values of the in-stream balance at station Meisdorf and Hausneindorf. The loads were calculated based on model simulated discharge and concentrations at two

stations and the removal (primary production and denitrification) values were amount from all reaches above each station.

Mean	Spring		Summer		Autumn		Winter		Annual	
(kg N d^{-1})	Meis	Haus	Meis	Haus	Meis	Haus	Meis	Haus	Meis	Haus
Load	279	555	83.4	234	144	332	487	826	248	486
Removal	28.3	52.5	36.3	79.4	9.60	27.9	1.77	6.73	19.0	41.6
Percentage (%)	10.1	9.46	43.5	33.9	6.67	8.40	0.36	0.81	7.64	8.55

2.6. Discussion

2.6.1. Model evaluation

Dynamics of $N - NO_3^-$ concentrations depend largely on the spatial distribution of non-point sources (Musolff et al., 2017). Due to heterogeneous land-use types, soil types and geological characteristics in the contributing areas upstream of the three nested gauging stations, the validation results demonstrates that the model can represent different nitrate behaviors well. Seasonal variability in $N - NO_3^-$ concentrations at the two upper stations represents mainly the nitrate behavior in natural forest-dominated areas, which has high interflow concentrations and extremely low baseflow concentrations. Due to the impermeable geological property, a shallow and flashier flow pathway is developed in the upper Selke (Dupas et al., 2017). The fertilizers and plant residues added to the upper arable lands and forests, respectively, increased $N - NO_3^-$ concentrations of soil moisture, but not of deeper groundwater. The model reasonably captured the processes under these conditions and performed well throughout the whole simulation period. At the catchment outlet, $N - NO_3^-$ concentrations combine exports from the upper natural forested areas and intensive agricultural and considerable urban areas in the lower parts of the catchment. The lowland agricultural area is dominated by sedimentary materials and loess, which leads to a deeper and slower groundwater dominant hydrological behavior (Musolff et al., 2016). Due to long-term fertilizer application, concentrations were much higher in soil moisture and also in deeper groundwater (ca. 25 $mg\ l^{-1}$, from field measurements). Point sources from lower urban areas were clearly controlled by WWTPs in the calibration period (2010-2015), and exports from upper areas were captured well at Meisdorf. Therefore, model performance at Hausneindorf can reflect the model ability to simulate agricultural exports. The adequate results validate the applicability of mHM-Nitrate in typical intensive agricultural areas.

Although point sources contributed to a small proportion of nitrate load, they strongly influenced the pattern of observed concentrations. For instance, in the validation period (1997-2009), the change

points of observed $N - NO_3^-$ concentration pattern at Hausneindorf (i.e., the years 2002 and 2007, **Figure 2.4c**) were correspondent to the change points of waste water treatments (see **Section 2.4.2** and **Supporting Information**). Therefore, we reconstructed the point-source time series according to WWTP measurements. The changes of seasonal patterns were reasonably captured by simulations, although the NSE was slightly less than zero. This is probably due to large uncertainties which might be involved in estimating unknown point-source inputs in the validation period. Overall, by considering the exact locations of WWTPs and time series of point source inputs, mHM-Nitrate facilitates the use for long-term continuous simulation under changing anthropogenic conditions.

Benefiting from currently available high-frequency monitoring, the daily data (2010-2015) were used to validate short-term nitrate behavior that is rarely observed in regular grab sampling. At the two upper stations, the fluctuations of $N - NO_3^-$ concentrations in high-flow periods are presumably due to shifting runoff partitioning among runoff components (surface direct flow with relatively low concentrations, interflow with high concentrations and baseflow with extremely low concentrations). Outlet concentrations frequently decreased during small storm events in low-flow periods, reflecting dilution by small events from upper forested areas or direct runoff from paved urban areas. The model captures general dynamics accurately and mimics peaks and drops reasonably well. Even though the daily model was calibrated using biweekly nitrate data, simulations reasonably captured the short-term dynamics (i.e., the concentration fluctuations, peaks and drops) that can only be observed in higher frequency observations. Moreover, during spring and summer in 2011, the discharge contribution from the lower part (below the station Meisdorf) was abnormally higher than in other years. The model successfully captured the discharge and concentration changes, indicating its ability to represent variable spatial contributions of runoff and nitrate.

The uncertainty results were consistent with above model calibration and validations, although the evaluation criteria are different (log-likelihood function and multi-objective function, respectively). This indicated the model's robustness and reduced the risk of over-optimization. The mHM-Nitrate model can be a suitable tool to explicitly present spatial distributions of catchment nitrate concentrations and fluxes. Nitrate statuses of soil moisture and groundwater were represented by nitrate concentrations in interflow and baseflow, respectively, due to the basic fully mixing assumption and the lack of precise information of soil DIN pool size, of which initial value was also assigned in form of concentration. The nitrate concentration appeared to be generally stable in different seasons, consistently with the almost closed mean terrestrial balance in the catchment. Moreover, the spatial variabilities of soil nitrate

concentrations and fluxes were also correspondent. For instance, in the north-west part of the Selke catchment, the relatively lower nitrate outputs (i.e., soil denitrification and terrestrial exports, **Figure 2.8e** and **f**) resulted in nitrate enrichment in the soil moisture and $N - NO_3^-$ concentration reached up to 45 mg l^{-1} in recent years (**Figure 2.7a**).

Although the model was validated at the three gauging stations, nitrate distributions of concentrations and fluxes were in reasonable ranges that suggested by literature (Hofstra & Bouwman, 2005; Wade et al., 2002; Whitehead et al., 1998b) and field measurements. Hofstra and Bouwman (2005) summarized 336 denitrification experiments in agricultural soils and reported mean values ranged 8-51 $kg\ N\ ha^{-1}\ yr^{-1}$, comparing with our modeling mean value 24.5 $kg\ N\ ha^{-1}\ yr^{-1}$. Wade et al. (2002) reported INCA-N model results of crop/plant uptake, denitrification, mineralization and N-leaching (i.e., terrestrial export in this study) in an England catchment and provided literature ranges respectively. Calculations from local authority (LLFG, 2012) showed that N mineralization is 30-45 $kg\ N\ ha^{-1}\ yr^{-1}$ in the arable lands of the study area. Jiang et al. (2014) calculated the N terrestrial export (0-10.6 $kg\ N\ ha^{-1}\ yr^{-1}$) of the Selke catchment using the HYPE model. These findings are compatible with our results. This rationalizes the use of spatial information provided in each model cell to support spatially differentiated N balance investigations. We recognized that a more theoretical and comprehensive scale analysis should be conducted to assess the predictive capability at model grid scale. The representative elementary scale concept, suggested by Refsgaard et al. (2016), can be a potential approach for further study. Calculated in-stream nitrate removal reflected high seasonal variability of the in-stream processes. The annual mean percentage of nitrate removal was about 8%. This value is comparable to values from other in-stream nitrate retention studies, given a wide range of values that has been reported (Alexander et al., 2009; Covino et al., 2010). Rode et al. (2016a) calculated the in-stream assimilatory uptake based on high-frequency sensor measurements in the Selke catchment. They reported nitrate gross assimilatory uptake of 12.4 and 45.2 $kg\ N\ d^{-1}$ in upper forest reaches and lower agricultural reaches, respectively. The order of magnitude is in line with our modeling results of net removal (**Table 2.4**). Given model uncertainty and "equifinality" effects, internal terrestrial and in-stream information provided by mHM-Nitrate only gives a coarse estimation on catchment-wide nitrate status. For a more comprehensive simulation, more in-situ knowledge benefiting from newly available monitoring data should be integrated in future catchment model development (Rode et al., 2016b).

2.6.2. Remarks on model representation

Balancing accurate representation and complexity remains a major challenge in model development (Clark et al., 2017). The grid-based mHM-Nitrate model was developed to address issues related to model representation.

Representing spatial variability

Most current hydrological water quality models adopt the semi-distributed structure, mainly because 1) sub-catchments and basic modeling units are delineated based on natural geographic information (topography, land use and soil types) that, to some extent, ensures a close relationship between model parameters and catchment characteristics, and 2) the hierarchical structure greatly decreases the number of basic units and increases computing efficiency (Krysanova et al., 1998). However, the spatial representation of these models has been criticized for their lack of location and connecting information for spatial objects (Bieger et al., 2017). In mHM-Nitrate, catchment characteristics and model parameters are assigned at the basic input-data level and then upscaled to model levels, for which users can specify the resolutions. Representation of variability in catchment characteristics and model parameters becomes more accurate if a finer model resolution is specified; however, the computational demand will increase accordingly. By simply changing settings in the model configuration file, users can test different modeling resolutions to obtain the optimal catchment discretization scheme.

Representing subsurface water storage and nitrate concentration

Studies have shown the significance of nitrate retention in subsurface water (Højberg et al., 2017; Wriedt & Rode, 2006). However, there are different options on how to conceptualize the subsurface water storage (e.g., the general “groundwater” storage or separated “soil moisture” and “deep groundwater” storages), and how to estimate nitrate concentration therein considering its vertical distribution (Dupas et al., 2016; Musolff et al., 2016). In the reservoirs based mHM-Nitrate model, subsurface storage is represented by a sequence of conceptual reservoirs (i.e., multi-layer soil moisture and beneath deep groundwater). Regarding water storage, the active water volumes for hydrological and nutrient calculations need to be different because the retention storage is critical only for chemical response in the catchment (Benettin et al., 2015). This difference is more pronounced in lower deep groundwater, where the hydrologically active volume only accounts for a small proportion of total storage. Therefore, groundwater storage was subdivided in the new model and relatively large retention storage was assigned. Water and nitrate dynamics are considered separately and interactively between each reservoir to represent the vertical variability. Currently, nitrate retention (e.g., denitrification and

transformation) is considered only in soil layers, not in deep groundwater (**Figure 2.1**). First, potential denitrification in groundwater is somehow considered in soil layer (with a depth of around 2 m), part of which can be below groundwater table. Second, denitrification in deeper groundwater is not pronounced in the study region, especially given the large storage assigned in the model. For aquifers where nitrate reduction is significant, an additional reaction term and corresponding parameter have to be added to the Eq. (1). Due to the vertical variability of nitrate concentration in deep groundwater, the assumption of full mixing is probably not appropriate. Therefore, we modified the equation from the INCA-N model (Wade et al., 2002), which still follows the full mixing assumption but avoids calculating the nitrate concentration in the retention storage. Based on the equation, the initial baseflow concentration reflects long-term N percolation from upper soil layers and the large retention storage (e.g., tens of meters) keeps baseflow concentration stable to represent the long-delayed deep groundwater nitrate transport.

Representing crop rotation and point source pollution

In most existing models, crop rotation, if being considered, is represented by assigning crop sequences to homogeneous units (e.g., HYPE) or to land-use/cover types (e.g., SWAT). However, the former usually lacks spatial information, while the latter ignores other influential factors (e.g., climate conditions, soil types and choices of farmers). In mHM-Nitrate, spatial variability in agricultural crop rotations is explicitly defined using crop rotation maps, which also ensures an easy setup for further analysis of agricultural scenarios.

Catchment water quality models are mainly oriented to address environmental problems from non-point sources, but point sources strongly and directly influence stream water quality. Due to the relatively long residence time for natural nutrient transport processes, especially in lowland areas (Wriedt & Rode, 2006), it can take years to decades to observe the impacts of agricultural practices on stream water concentrations. Thus, modelers prefer to have long-term monitoring data and conduct continuous modeling. However, changes in point sources (e.g., new pollution sources or improved waste water treatments) require careful consideration before using long-term stream water observations to calibrate catchment model for natural processes. In mHM-Nitrate, time-series point-source input is allowed and can be added in the exact location within the river network. This feature enables the model to assess their impacts on nutrient transport more reasonably and can provide a better evaluation of changing point sources within the river network (e.g., in the context of restoration measures).

2.7. Conclusions

The new grid-based mHM-Nitrate model was developed mainly based on implementations of the mHM and HYPE models. Benefiting from a multi-resolution discretization scheme, spatial representation of catchment characteristics and model parameters were flexibly designed based on the user-specified modeling resolution. Major improvements were added to represent more accurately nitrate dynamics in deep groundwater, crop rotation practices in agricultural land and point-source impacts. The mHM-Nitrate model successfully simulated nitrate transport and removal processes in the highly heterogeneous Selke catchment, Germany. It well reproduced seasonal dynamics of biweekly $N - NO_3^-$ observations in forested and agricultural areas. Additionally, daily observations from high-frequency monitoring confirmed its general ability to reproduce short-term changes that reflect runoff partitioning changes and event-based dilution effects. Moreover, uncertainty analysis results confirmed the model robustness and reduced the risk of over-optimization.

The mHM-Nitrate model provided detailed spatial information (e.g., spatially resolved nitrate terrestrial concentrations and fluxes) that is within reasonable ranges. Therefore, it offers promising opportunities for further evaluation of nutrient transport and removal processes spatiotemporally, for instance, to support future studies that target spatial agricultural mitigation measures (Hashemi et al., 2016)and interactions between terrestrial and in-stream processes (Dupas et al., 2017). Further validation of the new model needs to be done by cross validating for catchments that differ in natural conditions and scales. An internal scale analysis also can help to assess the model predictive capability at grid scale (Refsgaard et al., 2016). Furthermore, we consider the model as a starting point and new platform for investigations of new parameter regionalization and upscaling procedures, and for further model development to consider other water quality compounds (e.g., phosphorus, organic carbon), and their interactions.

Acknowledgement

Xiaoqiang Yang is funded by the Chinese Scholarship Council (CSC). We would like to thank Dr. Luis Samaniego, Dr. Andreas Musolff and Prof. Sabine Attinger for their constructive comments. We highly appreciate the comments from the Editor Martyn Clark, Riccardo Rigon and three anonymous Reviewers, which helped us to improve the manuscript significantly. The high-frequency data are provided by TERENO (Terrestrial Environment Observatories) project. We thank the German Weather Service (DWD), Federal Institute for Geosciences and Natural Resources (BGR), State Agency for Flood Protection and

Water Management of Saxony-Anhalt (LHW) for providing meteorological, geological and discharge and water quality data, respectively. The data used are presented in the tables, figures and supplements. The model is developed based on the GNU General Public License. Source codes and relevant data to rebuild the work are available under request to X. Yang and M. Rode, and are on-line accessible under https://git.ufz.de/yangx/mHM-Nitrate (also find the ***Appendix A*** in the CD that accompanied this dissertation).

2.8. References

Alexander, R. B., Smith, R. A., & Schwarz, G. E. (2000), Effect of stream channel size on the delivery of nitrogen to the Gulf of Mexico, *Nature*, *403*(6771), 758-761. https://doi.org/10.1038/35001562

Alexander, R. B., Böhlke, J. K., Boyer, E. W., David, M. B., Harvey, J. W., Mulholland, P. J., Seitzinger, S. P., et al. (2009), Dynamic modeling of nitrogen losses in river networks unravels the coupled effects of hydrological and biogeochemical processes, *Biogeochemistry*, *93*(1), 91-116. https://doi.org/10.1007/s10533-008-9274-8

Andersson, L., Rosberg, J., Pers, B. C., Olsson, J., & Arheimer, B. (2005), Estimating catchment nutrient flow with the HBV-NP model: sensitivity to input data, *AMBIO*, *34*(7), 521-532. https://doi.org/10.1579/0044-7447-34.7.521

Arheimer, B., Dahné, J., & Donnelly, C. (2012), Climate Change Impact on Riverine Nutrient Load and Land-Based Remedial Measures of the Baltic Sea Action Plan, *AMBIO*, *41*(6), 600-612. https://doi.org/10.1007/s13280-012-0323-0

Arnold, J. G., Srinivasan, R., Muttiah, R. S., & Williams, J. R. (1998), Large area hydrologic modeling and assessment part I: Model development *J. Am. Water Resour. Assoc.*, *34*(1), 73-89. https://doi.org/10.1111/j.1752-1688.1998.tb05961.x

Arnold, J. G., Allen, P. M., Volk, M., Williams, J. R., & Bosch, D. D. (2010), Assessment of different representations of spatial variability on SWAT model performance, *Trans. ASABE*, *53*(5), 1433-1443. https://doi.org/10.13031/2013.34913

Bailey, R. T., Wible, T. C., Arabi, M., Records, R. M., & Ditty, J. (2016), Assessing regional-scale spatio-temporal patterns of groundwater–surface water interactions using a coupled SWAT-MODFLOW model, *Hydrol. Process.*, *30*(23), 4420-4433. https://doi.org/10.1002/hyp.10933

Behrangi, A., Khakbaz, B., Vrugt, J. A., Duan, Q., & Sorooshian, S. (2008), Comment on "Dynamically dimensioned search algorithm for computationally efficient watershed model calibration" by Bryan A. Tolson and Christine A. Shoemaker, *Water Resour. Res.*, *44*(12). https://doi.org/10.1029/2007WR006429

Benettin, P., Kirchner, J. W., Rinaldo, A., & Botter, G. (2015), Modeling chloride transport using travel time distributions at Plynlimon, Wales, *Water Resour. Res.*, *51*(5). https://doi.org/10.1002/2014WR016600

Bergström, S. (1995), The HBV model, in *Computer Models of Watershed Hydrology*, edited by V. P. Singh, pp. 443-476, Water Resour. Publ., Highlands Ranch, Colorado, USA.

Bicknell, B. R., Imhoff, J. C., Kittle, J. L., Jr., Donigian, A. S., Jr., & Johanson, R. C. (1997), *Hydrological Simulation Program--Fortran, User's manual for version 11: U.S. Environmental Protection Agency*, National Exposure Research Laboratory, Athens, Georgia.

Bieger, K., Arnold, J. G., Rathjens, H., White, M. J., Bosch, D. D., Allen, P. M., Volk, M., et al. (2017), Introduction to SWAT+, A Completely Restructured Version of the Soil and Water Assessment Tool, *J. Am. Water Resour. Assoc.*, *53*(1), 115-130. https://doi.org/10.1111/1752-1688.12482

Campolongo, F., Saltelli, A., & Cariboni, J. (2011), From screening to quantitative sensitivity analysis. A unified approach, *Comput. Phys. Commun.*, *182*(4), 978-988. https://doi.org/10.1016/j.cpc.2010.12.039

Chaubey, I., Cotter, A. S., Costello, T. A., & Soerens, T. S. (2005), Effect of DEM data resolution on SWAT output uncertainty, *Hydrol. Process.*, *19*(3), 621-628. https://doi.org/10.1002/hyp.5607

Clark, M. P., Bierkens, M. F. P., Samaniego, L., Woods, R. A., Uijlenhoet, R., Bennett, K. E., Pauwels, V. R. N., et al. (2017), The evolution of process-based hydrologic models: historical challenges and the collective quest for physical realism, *Hydrol. Earth Syst. Sci.*, *21*(7), 3427-3440. https://doi.org/10.5194/hess-21-3427-2017

Cosby, B. J., Hornberger, G. M., Clapp, R. B., & Ginn, T. R. (1984), A Statistical Exploration of the Relationships of Soil Moisture Characteristics to the Physical Properties of Soils, *Water Resour. Res.*, *20*(6). https://doi.org/10.1029/WR020i006p00682

Covino, T., McGlynn, B., & Baker, M. (2010), Separating physical and biological nutrient retention and quantifying uptake kinetics from ambient to saturation in successive mountain stream reaches, *J. Geophys. Res. Biogeosci.*, *115*(G4). https://doi.org/10.1029/2009JG001263

Cuntz, M., Mai, J., Zink, M., Thober, S., Kumar, R., Schäfer, D., Schrön, M., et al. (2015), Computationally inexpensive identification of noninformative model parameters by sequential screening, *Water Resour. Res.*, *51*(8). https://doi.org/10.1002/2015WR016907

Dunn, S. M., Johnston, L., Taylor, C., Watson, H., Cook, Y., & Langan, S. J. (2013), Capability and limitations of a simple grid-based model for simulating land use influences on stream nitrate concentrations, *J. Hydrol.*, *507*(Supplement C), 110-123. https://doi.org/10.1016/j.jhydrol.2013.10.016

Dupas, R., Jomaa, S., Musolff, A., Borchardt, D., & Rode, M. (2016), Disentangling the influence of hydroclimatic patterns and agricultural management on river nitrate dynamics from sub-hourly to decadal time scales, *Sci. Tot. Environ.*, *571*, 791-800. https://doi.org/10.1016/j.scitotenv.2016.07.053

Dupas, R., Musolff, A., Jawitz, J. W., Rao, P. S. C., Jäger, C. G., Fleckenstein, J. H., Rode, M., et al. (2017), Carbon and nutrient export regimes from headwater catchments to downstream reaches, *Biogeosciences*, *14*(18), 4391-4407. https://doi.org/10.5194/bg-14-4391-2017

Edsel, B. D., Camp, J. V., LeBoeuf, E. J., Penrod, J. R., Dobbins, J. P., & Abkowitz, M. D. (2011), Watershed modeling and its applications: a state-of-the-art review, *The Open Hydrology Journal*, *5*, 26-50. https://doi.org/10.2174/1874378101105010026

EEA (2005), Source apportionment of nitrogen and phosphorus inputs into the aquatic environment, *Rep. No 7/2005*, European Environment Agency, Copenhagen, Denmark.

EEA (2012), European waters — current status and future challenges, *Rep. No 9/2012*, European Environment Agency, Copenhagen, Denmark.

Emili, L. A., & Greene, R. P. (2013), Modeling agricultural nonpoint source pollution using a geographic information system approach, *Environ. Manage.*, *51*(1), 70-95. https://doi.org/10.1007/s00267-012-9940-4

Fatichi, S., Vivoni, E. R., Ogden, F. L., Ivanov, V. Y., Mirus, B., Gochis, D., Downer, C. W., et al. (2016), An overview of current applications, challenges, and future trends in distributed process-based models in hydrology, *J. Hydrol.*, *537*(Supplement C), 45-60. https://doi.org/10.1016/j.jhydrol.2016.03.026

Hansen, A. L., Refsgaard, J. C., Olesen, J. E., & Børgesen, C. D. (2017), Potential benefits of a spatially targeted regulation based on detailed N-reduction maps to decrease N-load from agriculture in a small groundwater dominated catchment, *Sci. Tot. Environ.*, *595*, 325-336. https://doi.org/10.1016/j.scitotenv.2017.03.114

Hashemi, F., Olesen, J. E., Dalgaard, T., & Børgesen, C. D. (2016), Review of scenario analyses to reduce agricultural nitrogen and phosphorus loading to the aquatic environment, *Sci. Tot. Environ.*, *573*, 608-626. https://doi.org/10.1016/j.scitotenv.2016.08.141

Hesser, F. B., Franko, U., & Rode, M. (2010), Spatially distributed lateral nitrate transport at the catchment scale, *J. Environ. Qual.*, *39*(1), 193-203. https://doi.org/10.2134/jeq2009.0031

Hirsch, R. M., Slack, J. R., & Smith, R. A. (1982), Techniques of trend analysis for monthly water quality data, *Water Resour. Res.*, *18*(1). https://doi.org/10.1029/WR018i001p00107

Hofstra, N., & Bouwman, A. F. (2005), Denitrification in Agricultural Soils: Summarizing Published Data and Estimating Global Annual Rates, *Nutr. Cycl. Agroecosys.*, *72*(3), 267-278. https://doi.org/10.1007/s10705-005-3109-y

Højberg, A. L., Hansen, A. L., Wachniew, P., Żurek, A. J., Virtanen, S., Arustiene, J., Strömqvist, J., et al. (2017), Review and assessment of nitrate reduction in groundwater in the Baltic Sea Basin, *J. Hydrol.: Regional Studies*, *12*, 50-68. https://doi.org/10.1016/j.ejrh.2017.04.001

Jackson-Blake, L. A., Wade, A. J., Futter, M. N., Butterfield, D., Couture, R. M., Cox, B. A., Crossman, J., et al. (2016), The INtegrated CAtchment model of phosphorus dynamics (INCA-P): Description and demonstration of new model structure and equations, *Environ. Model. Software*, *83*, 356-386. https://doi.org/10.1016/j.envsoft.2016.05.022

Jiang, S., Jomaa, S., & Rode, M. (2014), Modelling inorganic nitrogen leaching in nested mesoscale catchments in central Germany, *Ecohydrology*, *7*(5), 1345-1362. https://doi.org/10.1002/eco.1462

Jiang, S., Jomaa, S., Büttner, O., Meon, G., & Rode, M. (2015), Multi-site identification of a distributed hydrological nitrogen model using Bayesian uncertainty analysis, *J. Hydrol.*, *529, Part 3*, 940-950. https://doi.org/10.1016/j.jhydrol.2015.09.009

Jomaa, S., Jiang, S., Thraen, D., & Rode, M. (2016), Modelling the effect of different agricultural practices on stream nitrogen load in central Germany, *Energy Sustain. Soc.*, *6*(1), 1-16. https://doi.org/10.1186/s13705-016-0077-9

Kirchner, J. W. (2006), Getting the right answers for the right reasons: Linking measurements, analyses, and models to advance the science of hydrology, *Water Resour. Res.*, *42*(3). https://doi.org/10.1029/2005WR004362

Kirchner, J. W. (2009), Catchments as simple dynamical systems: Catchment characterization, rainfall-runoff modeling, and doing hydrology backward, *Water Resour. Res.*, *45*(2). https://doi.org/10.1029/2008WR006912

Kistner, I. (2007), Anwendung des Modells ANIMO zur Simulation des gelösten Phosphors im Oberflächenabfluss auf der Feldskala und der Phosphorverfügbarkeit im Oberboden auf der Einzugsgebietsskala, Ph.D thesis, Helmholtz-Zentrum für Umweltforschung GmbH - UFZ. Leipzig, Germany.

Krause, P., Boyle, D., & Bäse, F. (2005), Comparison of different efficiency criteria for hydrological model assessment, *Adv. Geosci.*, *5*, 89-97. https://doi.org/10.5194/adgeo-5-89-2005

Krysanova, V., Müller-Wohlfeil, D.-I., & Becker, A. (1998), Development and test of a spatially distributed hydrological/water quality model for mesoscale watersheds, *Ecol. Model.*, *106*(2–3), 261-289. https://doi.org/10.1016/S0304-3800(97)00204-4

Kumar, R., Samaniego, L., & Attinger, S. (2013), Implications of distributed hydrologic model parameterization on water fluxes at multiple scales and locations, *Water Resour. Res.*, *49*(1). https://doi.org/10.1029/2012WR012195

Li, X., Weller, D. E., & Jordan, T. E. (2010), Watershed model calibration using multi-objective optimization and multi-site averaging, *J. Hydrol.*, *380*(3–4), 277-288. https://doi.org/10.1016/j.jhydrol.2009.11.003

Lindström, G., Pers, C., Rosberg, J., Strömqvist, J., & Arheimer, B. (2010), Development and testing of the HYPE (Hydrological Predictions for the Environment) water quality model for different spatial scales, *Hydrol. Res.*, *41*(3-4), 295-319. https://doi.org/10.2166/nh.2010.007

Liu, J., Zhang, L., Zhang, Y., Hong, H., & Deng, H. (2008), Validation of an agricultural non-point source (AGNPS) pollution model for a catchment in the Jiulong River watershed, China, *J. Environ. Sci.*, *20*(5), 599-606. https://doi.org/10.1016/S1001-0742(08)62100-2

LLFG (2012), Werkzeug zur Modellierung der diffusen N- und P-Emissionen in Sachsen-Anhalt zur Umsetzung des Nährstoffkonzepts 2010-2013, Landesanstalt für Landwirtschaft, Forsten und Gartenbau des Landes Sachsen-Anhalt, Bernburg, Germany.

Meybeck, M. (1982), Carbon, nitrogen, and phosphorus transport by world rivers, *Am. J. Sci*, *282*(4), 401-450. https://doi.org/10.2475/ajs.282.4.401

Morris, M. D. (1991), Factorial sampling plans for preliminary computational experiments, *Technometrics*, *33*(2), 161-174. https://doi.org/10.2307/1269043

Musolff, A., Fleckenstein, J. H., Rao, P. S. C., & Jawitz, J. W. (2017), Emergent archetype patterns of coupled hydrologic and biogeochemical responses in catchments, *Geophys. Res. Lett.*, *44*(9), 4143-4151. https://doi.org/10.1002/2017GL072630

Musolff, A., Schmidt, C., Rode, M., Lischeid, G., Weise, S. M., & Fleckenstein, J. H. (2016), Groundwater head controls nitrate export from an agricultural lowland catchment, *Adv. Water Resour.*, *96*, 95-107. https://doi.org/10.1016/j.advwatres.2016.07.003

Nash, J. E., & Sutcliffe, J. V. (1970), River flow forecasting through conceptual models part I — A discussion of principles, *J. Hydrol.*, *10*(3), 282-290. https://doi.org/10.1016/0022-1694(70)90255-6

Pianosi, F., Sarrazin, F., & Wagener, T. (2015), A matlab toolbox for global sensitivity analysis, *Environ. Model. Software*, *70*, 80-85. https://doi.org/10.1016/j.envsoft.2015.04.009

Pianosi, F., Beven, K., Freer, J., Hall, J. W., Rougier, J., Stephenson, D. B., & Wagener, T. (2016), Sensitivity analysis of environmental models: A systematic review with practical workflow, *Environ. Model. Software*, *79*, 214-232. https://doi.org/10.1016/j.envsoft.2016.02.008

Pignotti, G., Rathjens, H., Cibin, R., Chaubey, I., & Crawford, M. (2017), Comparative Analysis of HRU and Grid-Based SWAT Models, *Water*, *9*(4), 272. https://doi.org/10.3390/w9040272

Pokhrel, P., & Gupta, H. V. (2010), On the use of spatial regularization strategies to improve calibration of distributed watershed models, *Water Resour. Res.*, *46*(1). https://doi.org/10.1029/2009WR008066

Rakovec, O., Kumar, R., Mai, J., Cuntz, M., Thober, S., Zink, M., Attinger, S., et al. (2016), Multiscale and multivariate evaluation of water fluxes and states over European river basins, *J. Hydrometeorol.*, *17*(1), 287-307. https://doi.org/10.1175/JHM-D-15-0054.1

Rathjens, H., & Oppelt, N. (2012), SWATgrid: An interface for setting up SWAT in a grid-based discretization scheme, *Comput. Geosci.*, *45*, 161-167. https://doi.org/10.1016/j.cageo.2011.11.004

Rathjens, H., Oppelt, N., Bosch, D. D., Arnold, J. G., & Volk, M. (2015), Development of a grid-based version of the SWAT landscape model, *Hydrol. Process.*, *29*(6), 900-914. https://doi.org/10.1002/hyp.10197

Refsgaard, J. C., Højberg, A. L., He, X., Hansen, A. L., Rasmussen, S. H., & Stisen, S. (2016), Where are the limits of model predictive capabilities?, *Hydrol. Process.*, *30*(26), 4956-4965. https://doi.org/10.1002/hyp.11029

Rode, M., & Frede, H.-G. (1997), Modification of AGNPS for agricultural land and climate conditions in central Germany, *J. Environ. Qual.*, *26*(1), 165-172. https://doi.org/10.2134/jeq1997.00472425002600010024x

Rode, M., & Lindenschmidt, K.-E. (2001), Distributed sediment and phosporus transport modeling on a medium sized catchment in central germany, *Phys. Chem. Earth Part B*, *26*(7), 635-640. https://doi.org/10.1016/S1464-1909(01)00061-2

Rode, M., Thiel, E., Franko, U., Wenk, G., & Hesser, F. (2009), Impact of selected agricultural management options on the reduction of nitrogen loads in three representative meso scale catchments in Central Germany, *Sci. Tot. Environ.*, *407*(11), 3459-3472. https://doi.org/10.1016/j.scitotenv.2009.01.053

Rode, M., Halbedel née Angelstein, S., Anis, M. R., Borchardt, D., & Weitere, M. (2016a), Continuous in-stream assimilatory nitrate uptake from high-frequency sensor measurements, *Environ. Sci. Technol.*, *50*(11), 5685-5694. https://doi.org/10.1021/acs.est.6b00943

Rode, M., Wade, A. J., Cohen, M. J., Hensley, R. T., Bowes, M. J., Kirchner, J. W., Arhonditsis, G. B., et al. (2016b), Sensors in the stream: The high-frequency wave of the present, *Environ. Sci. Technol.*, *50*(19), 10297-10307. https://doi.org/10.1021/acs.est.6b02155

Rozemeijer, J. C., Visser, A., Borren, W., Winegram, M., van der Velde, Y., Klein, J., & Broers, H. P. (2016), High-frequency monitoring of water fluxes and nutrient loads to assess the effects of controlled drainage on water storage and nutrient transport, *Hydrol. Earth Syst. Sci.*, *20*(1), 347-358. https://doi.org/10.5194/hess-20-347-2016

Samaniego, L., Kumar, R., & Attinger, S. (2010), Multiscale parameter regionalization of a grid-based hydrologic model at the mesoscale, *Water Resour. Res.*, *46*(5). https://doi.org/10.1029/2008WR007327

Schulz, K., Seppelt, R., Zehe, E., Vogel, H. J., & Attinger, S. (2006), Importance of spatial structures in advancing hydrological sciences, *Water Resour. Res.*, *42*(3). https://doi.org/10.1029/2005WR004301

Shrestha, R. R., Bárdossy, A., & Rode, M. (2007), A hybrid deterministic–fuzzy rule based model for catchment scale nitrate dynamics, *J. Hydrol.*, *342*(1–2), 143-156. https://doi.org/10.1016/j.jhydrol.2007.05.020

ter Braak, C. J. F., & Vrugt, J. A. (2008), Differential Evolution Markov Chain with snooker updater and fewer chains, *Stat. Comput.*, *18*(4), 435-446. https://doi.org/10.1007/s11222-008-9104-9

Tolson, B. A., & Shoemaker, C. A. (2007), Dynamically dimensioned search algorithm for computationally efficient watershed model calibration, *Water Resour. Res.*, *43*(1). https://doi.org/10.1029/2005WR004723

Vrugt, J. A., Diks, C. G. H., Gupta, H. V., Bouten, W., & Verstraten, J. M. (2005), Improved treatment of uncertainty in hydrologic modeling: Combining the strengths of global optimization and data assimilation, *Water Resour. Res.*, *41*(1). https://doi.org/10.1029/2004WR003059

Vrugt, J. A., ter Braak, C. J. F., Diks, C. G. H., Robinson, B. A., Hyman, J. M., & Higdon, D. (2009), Accelerating Markov Chain Monte Carlo Simulation by Differential Evolution with Self-Adaptive Randomized Subspace Sampling, *Int. J. Nonlin. Sci. Num.*, *10*(3), 273. https://doi.org/10.1515/IJNSNS.2009.10.3.273

Wade, A. J., Durand, P., Beaujouan, V., Wessel, W. W., Raat, K. J., Whitehead, P. G., Butterfield, D., et al. (2002), A nitrogen model for European catchments: INCA, new model structure and equations, *Hydrol. Earth Syst. Sci.*, *6*(3), 559-582. https://doi.org/10.5194/hess-6-559-2002

Wellen, C., Kamran-Disfani, A.-R., & Arhonditsis, G. B. (2015), Evaluation of the Current State of Distributed Watershed Nutrient Water Quality Modeling, *Environ. Sci. Technol.*, *49*(6), 3278-3290. https://doi.org/10.1021/es5049557

Whitehead, P. G., Wilson, E. J., & Butterfield, D. (1998a), A semi-distributed Integrated Nitrogen model for multiple source assessment in Catchments (INCA): Part I — model structure and process equations, *Sci. Tot. Environ.*, *210–211*, 547-558. https://doi.org/10.1016/S0048-9697(98)00037-0

Whitehead, P. G., Wilson, E. J., Butterfield, D., & Seed, K. (1998b), A semi-distributed integrated flow and nitrogen model for multiple source assessment in catchments (INCA): Part II — application to large river basins in south Wales and eastern England, *Sci. Tot. Environ.*, *210-211*, 559-583. https://doi.org/10.1016/S0048-9697(98)00038-2

Wilusz, D. C., Harman, C. J., & Ball, W. P. (2017), Sensitivity of Catchment Transit Times to Rainfall Variability Under Present and Future Climates, *Water Resour. Res.*, *53*(12). https://doi.org/10.1002/2017WR020894

Wollschläger, U., Attinger, S., Borchardt, D., Brauns, M., Cuntz, M., Dietrich, P., Fleckenstein, J. H., et al. (2016), The Bode hydrological observatory: a platform for integrated, interdisciplinary hydro-ecological research within the TERENO Harz/Central German Lowland Observatory, *Environ. Earth Sci.*, *76*(1), 29. https://doi.org/10.1007/s12665-016-6327-5

Wriedt, G., & Rode, M. (2006), Modelling nitrate transport and turnover in a lowland catchment system, *J. Hydrol.*, *328*(1–2), 157-176. https://doi.org/10.1016/j.jhydrol.2005.12.017

Young, R., Onstad, C., Bosch, D., & Anderson, W. (1989), AGNPS: A nonpoint-source pollution model for evaluating agricultural watersheds, *J. Soil Water Conserv.*, *44*(2), 168-173.

Yuan, Y., L. Bingner, R., & A. Rebich, R. (2001), Evaluation of AnnAGNPS on Mississippi Delta MSEA watersheds, *Trans. ASAE*, *44*(5), 1183. https://doi.org/10.13031/2013.6448

Zacharias, S., & Wessolek, G. (2007), Excluding Organic Matter Content from Pedotransfer Predictors of Soil Water Retention *Soil Sci. Soc. Am. J.*, *71*, 43-50. https://doi.org/10.2136/sssaj2006.0098

Zhang, Y., Shao, Q., & Taylor, J. A. (2016), A balanced calibration of water quantity and quality by multi-objective optimization for integrated water system model, *J. Hydrol.*, *538*, 802-816. https://doi.org/10.1016/j.jhydrol.2016.05.001

Zink, M., Kumar, R., Cuntz, M., & Samaniego, L. (2017), A high-resolution dataset of water fluxes and states for Germany accounting for parametric uncertainty, *Hydrol. Earth Syst. Sci.*, *21*(3), 1769-1790. https://doi.org/10.5194/hess-21-1769-2017

2.9. Supplementary Materials

Text S2.1. Governing equations of nitrogen processes in the mHM-Nitrate model

1. Common functions for impacts of well-known factors. These common functions are used for calculating different nitrogen transformations.

(i) Impact of soil temperature ($soil\_temp$, ℃):

$$f_{temp} = \begin{cases} 0, & soil\_temp < 0 \\ 2^{(soil\_temp-20)/10}, & 0 < soil\_temp < 5 \\ \frac{soil\_temp}{5} \cdot 2^{(soil\_temp-20)/10}, & soil\_temp > 5 \end{cases}$$

Soil temperature is calculated from the soil temperature in previous time step, air temperature (air_temp) and deep soil temperature (fixed as 5 ℃) and aggregated as:

$$soil\_temp = (1 - weight - 0.001) \cdot soil\_temp + weight \cdot air\_temp + 0.001 \cdot 5$$

where $weight = \frac{1}{30+10 \cdot snowdepth}$ and the $snowdepth$ is the snow depth that is updated at each time step of the model simulation.

(ii) Impact of soil moisture (SM):

$$f_{sm} = \begin{cases} 0, & SM < 0.3 \\ (\frac{\frac{SM}{SM\_SAT} - 0.3}{1 - 0.3})^{2.5}, & 0.3 < SM < 1 \end{cases}$$

where SM_SAT denotes the saturated soil moisture content.

(iii) Impact of nitrate concentration in soil water (SMC):

$$f_{conc} = \frac{SMC}{SMC + 1.0}$$

For more information on those empirical equations, please refer to the source code of mHM-Nitrate (https://git.ufz.de/yangx/mHM-Nitrate) or the HYPE model description document (http://www.smhi.net/hype/wiki/doku.php?id=start:hype_model_description, last accessed on September 1st 2019).

2. Nitrogen processes in each soil layer (terrestrial phase)

(1) Degradation from inactive solid organic nitrogen pool (SON_I) to active solid organic nitrogen pool (SON_A)

$$TRANS = degdr \cdot f_{temp} \cdot f_{sm} \cdot SON_I \cdot DT$$
$$SON_A = SON_A + TRANS$$
$$SON_I = SON_I - TRANS$$

(2) Mineralization from SON_A and dissolved organic nitrogen pool (DON), respectively, to dissolved inorganic nitrogen pool (DIN)

$$TRANS1 = minlr \cdot f_{temp} \cdot f_{sm} \cdot SON_A \cdot DT$$

$$TRANS2 = minlr \cdot f_{temp} \cdot f_{sm} \cdot DON \cdot DT$$
$$SON_A = SON_A - TRANS1$$
$$DON = DON - TRANS2$$
$$DIN = DIN + TRANS1 + TRANS2$$

(3) Dissolution from SON_A to DON

$$TRANS = dislr \cdot f_{temp} \cdot f_{sm} \cdot SON_A \cdot DT$$
$$SON_A = SON_A - TRANS$$
$$DON = DON + TRANS$$

where $TRANS$ denotes transferred amount ($mg\ N\ m^{-2}$); $degdr$, $minlr$ and $dislr$ denote land-use dependent degradation rate, mineralization rate and dissolution rate, respectively (d^{-1}); f_{temp} and f_{sm} denote common functions that represent impacts of soil temperature and soil moisture, respectively (details in Lindström et al. (2010)); $DT = model\ timestep\ (h)/\ 24$.

(4) Soil denitrification

$$DENI = denis \cdot f_{temp} \cdot f_{sm} \cdot f_{conc} \cdot DIN \cdot DT$$
$$DIN = DIN - DENI$$

where $DENI$ denotes denitrified nitrate amount ($mg\ N\ m^{-2}$), $denis$ denotes soil denitrification rate (d^{-1}); f_{conc}denote function that represent impacts of soil moisture concentration on denitrification (details in Lindström et al. (2010)).

(5) Plant/crop uptake

Potential uptake ($UPTK_{max}$) is based on the logistic plant/crop growth function from SOILN model in HYPE (Lindström et al., 2010).

$$UPTK = \min(UPTK_{max}, (1 - \frac{wilting\ point}{soil\ moisture}) \cdot DIN)$$
$$DIN = DIN - UPTK$$

where $UPTK$ denotes the uptake amount ($mg\ N\ m^{-2}$).

3. Nitrogen processes in each reach (in-stream phase)

(1) In-stream denitrification

$$DENIw = deniw \cdot f_{tempw} \cdot f_{concw} \cdot A \cdot DT$$
$$DINw = DINw - DENIw$$

where $DENIw$ denotes denitrified nitrate amount in stream water; $deniw$ denotes in-stream denitrification rate ($mg\ m^{-2}\ d^{-1}$); f_{tempw} and f_{concw} denote functions that represent impacts of stream water temperature and nitrate concentration, respectively (Lindström et al., 2010) (the functions are in the same formats as for above soil phase, but stream water temperature is calculated as 20-day's moving average of air temperature); A denotes beneath area of reach; $DINw$ denotes dissolved inorganic nitrogen pool in stream water.

(2) In-stream primary production and mineralization are inverse transformation between DINw and dissolved organic nitrogen pool in stream water (DONw)

$$TRANSw = pprt \cdot f_{tempw} \cdot f_{tp} \cdot A \cdot H \cdot DT$$

where $TRANSw$ denotes in-stream transformation between DINw and DONw, $pprt$ denotes in-stream primary production rate ($mg\ m^{-3}\ d^{-1}$), $f_{tp} = 0.091$ representing the mean impact of total phosphorus concentration (simplified from (Lindström et al., 2010) since the phosphorus simulation is not considered in this work), H denotes the water depth.

$if\ 10 - day's\ mean\ water\ temperature > 20 - day's\ mean\ water\ temperature$
$then\ assimilatory\ uptake\ process\ dominates$

$$DONw = DONw + TRANSw$$
$$DINw = DINw - TRANSw$$

$else\ mineralization\ process\ dominates$

$$DONw = DONw - TRANSw$$
$$DINw = DINw + TRANSw$$

end if

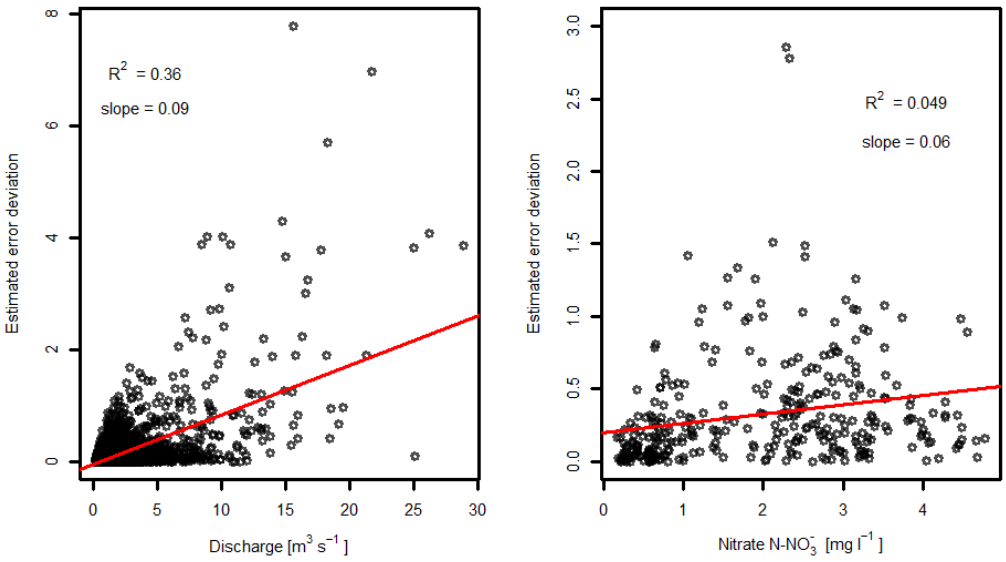

Figure S2.1. The heteroscedasticities of discharge (left panel) and nitrate concentration (right panel) observations. According to the values of R^2 and slope, error deviation of discharge was detected as heteroscedastic, while of concentration was detected as homoscedastic.

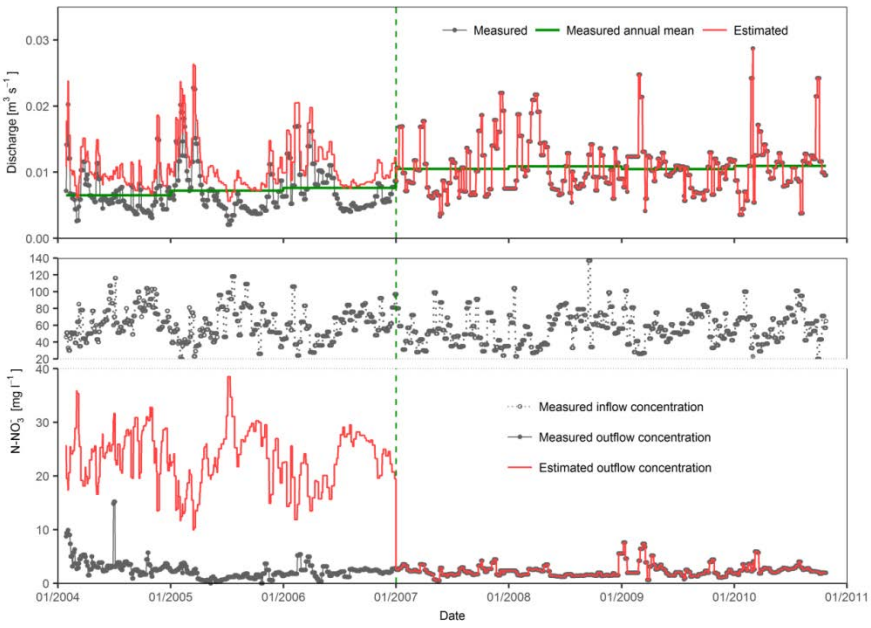

Figure S2.2. Point-source measurements (2004-2010) at the waste water treatment plant (WWTP) Harzgerode and the estimated outflow discharge and concentrations. Point-source concentrations before 2004 and after 2010 were set as 50 mg l^{-1} and 2.4 mg l^{-1}, respectively, which are the means of measured inflow and outflow concentration, respectively. Point-source discharge was set as the mean discharge after 2007 (0.011 m^3 s^{-1}).

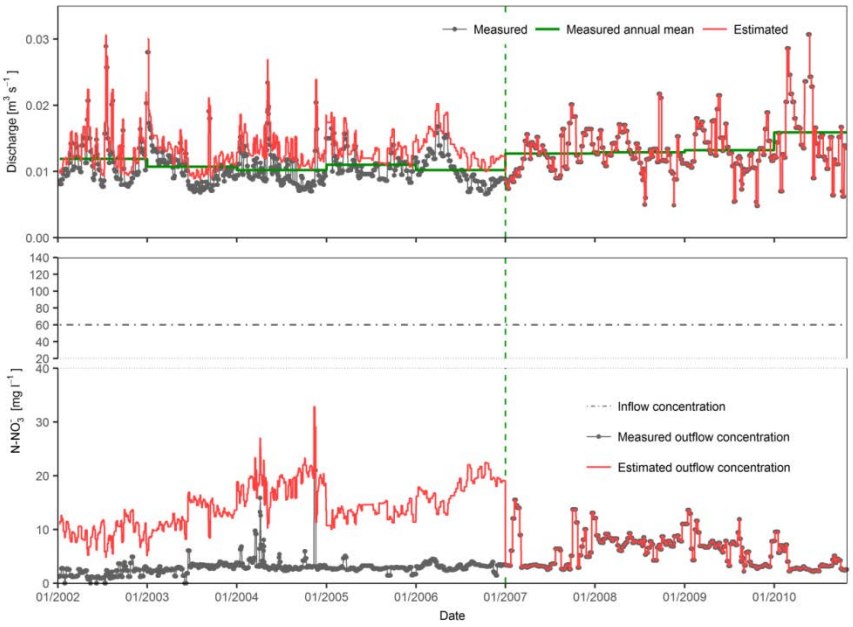

Figure S2.3. Point-source measurements (2002-2010) at the WWTP Ballenstedt and the estimated outflow discharge and concentrations. Inflow concentrations were missing and thus were set as 60 mg l^{-1}, which was estimated based on inflow measurements at plant Harzgerode. After 2010, concentrations were set as the mean outflow concentration (4.2 mg l^{-1}). Point-source discharge in those two periods was set as the mean discharge after 2007 (0.013 m^3 s^{-1}).

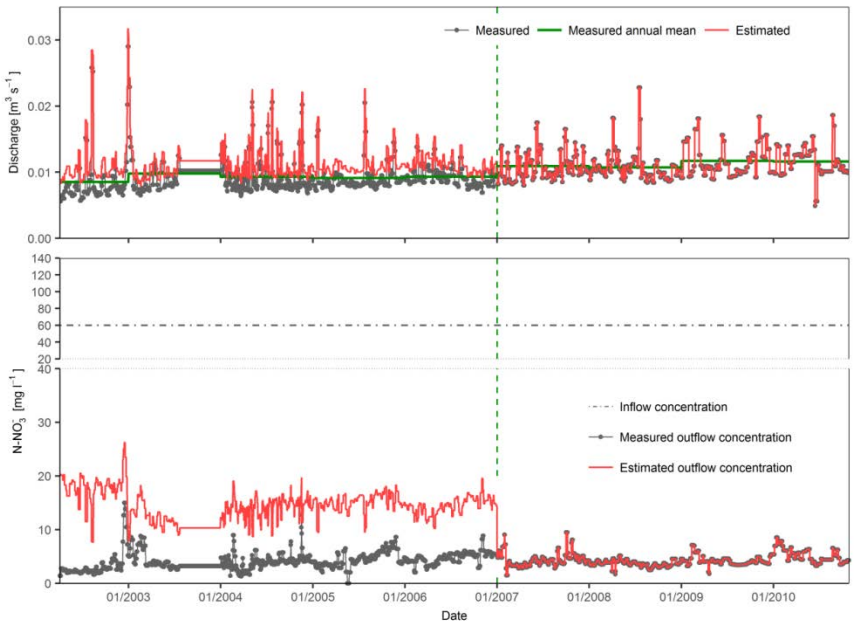

Figure S2.4. Point-source measurements (2002-2010) at the WWTP Hoym and the estimated outflow discharge and concentrations. Inflow concentrations were missing and thus were set as 60 mg l^{-1}, which was estimated based on inflow measurements at plant Harzgerode. After 2010, concentrations were set as the mean outflow concentration (4.3 mg l^{-1}). Point-source discharge in those two periods was set as the mean discharge after 2007 (0.011 m^3 s^{-1}).

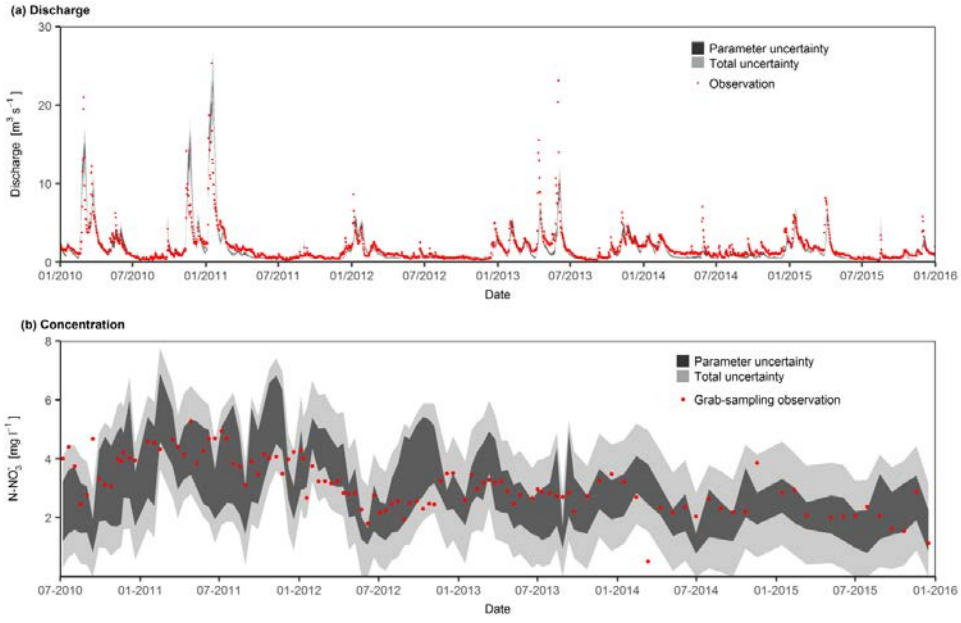

Figure S2.5. 95% confidence bands of (a) discharge and (b) $\mathrm{N-NO_3^-}$ concentration at station Hausneindorf using DREAMZS in period 2010-2015.

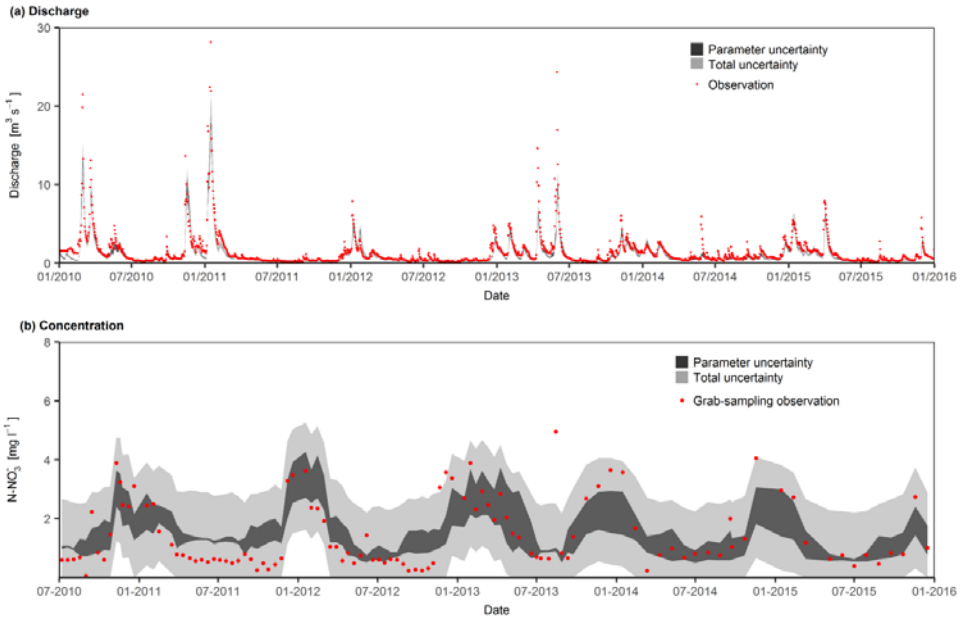

Figure S2.6. 95% confidence bands of (a) discharge and (b) $\mathbf{N-NO_3^-}$ concentration at station Meisdorf using DREAM$_{ZS}$ in period 2010-2015.

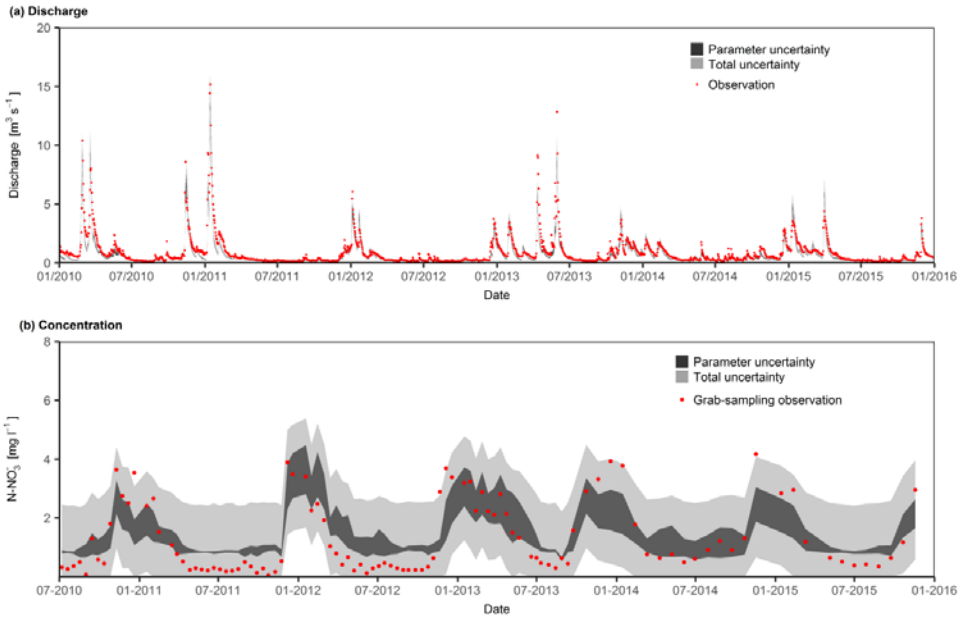

Figure S2.7. 95% confidence bands of (a) discharge and (b) $\mathbf{N-NO_3^-}$ concentration at station Silberhuette using DREAM$_{ZS}$ in period 2010-2015.

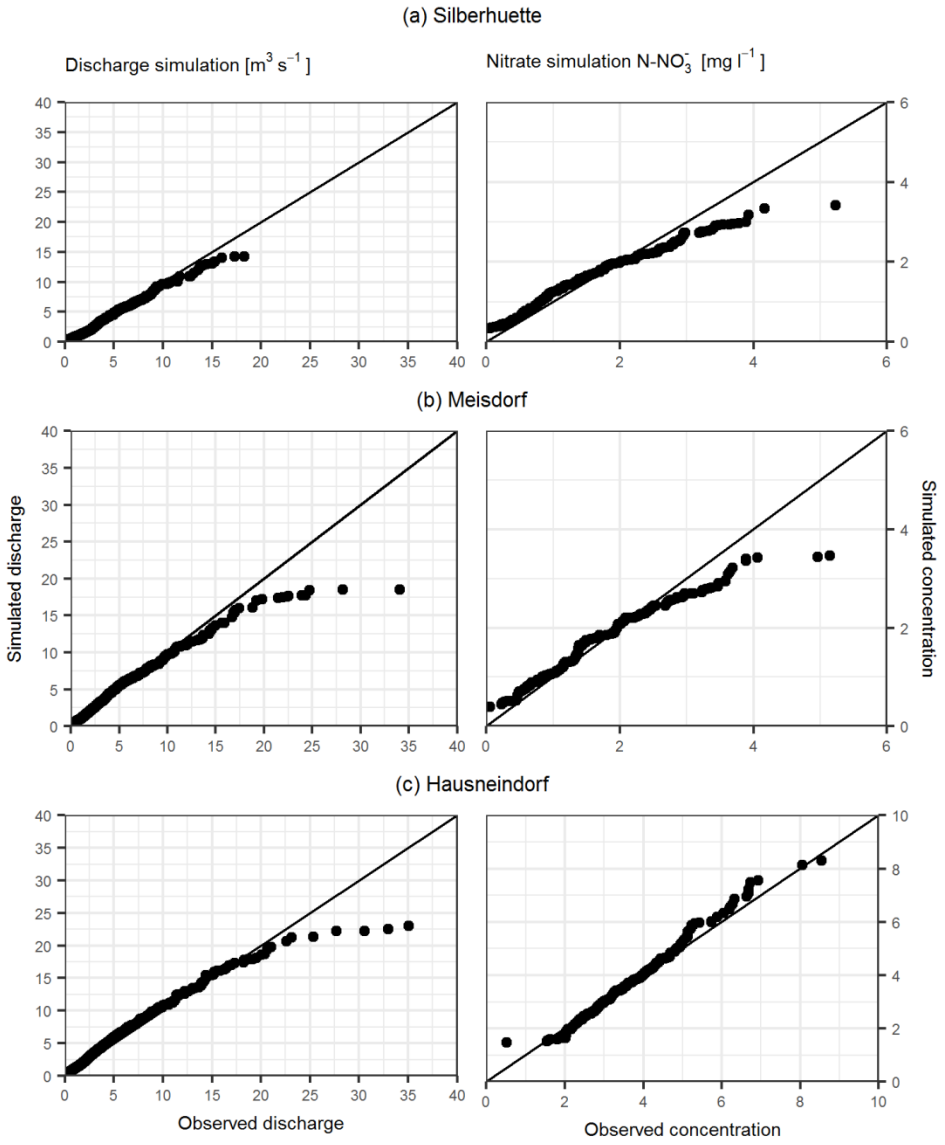

Figure S2.8. The Quantile- Quantile plot of discharge and concentration simulations at three gauging stations in the Selke catchment.

Table S2.1. Initial conditions of soil nitrogen forms (DIN, DON, SON_A and SON_I) at the Selke catchment. All forms were defined as land-use dependent, with DIN and DON forms given as concentrations (IN_conc and ON_conc, respectively)**.** DIN and DON were set as the same values for all soil layers, respectively, while SON_A and SON_I exponentially decreased along the depth with parameter "onhalf" (Lindström et al., 2010; Jiang et al., 2014). $initC_{bf}$ and $initV_r$ are initial values of baseflow concentration and retention storage of deep groundwater, respectively.

Land-use ID	Land-use type	IN_conc	ON_conc	SON_A	SON_I	onhalf	$initC_{bf}$ (mg/l)	$initV_r$ (10^3 mm)
1	Coniferous forest	0.5	0.1	20	8032.98	1.65	0.5	5
2	Deciduous forest	0.5	0.1	300	8032.98	0.4013	0.5	5
3	Mixed forest	0.5	0.1	80	8032.98	0.4	0.5	5
4	Sparse forest	0.5	0.1	162	8032.98	0.1515	0.5	5
5	Urban area	5	0.1	414	8032.98	0.1425	5	10
6	Intensive Orchards	25	0.1	153	8032.98	0.1177	25	10
7	Pasture	0.5	0.1	260	8032.98	0.0553	0.5	10
8	Arable land	25	0.1	200	8032.98	0.338	25	10
9	Wetland	0.5	0.1	223	8032.98	0.0373	0.5	10

Chapter 3: Autotrophic nitrate uptake in river networks: A modeling approach using continuous high-frequency data

Key points:

- Stream metabolism differs significantly under different riparian conditions
- Continuous $U_{a-NO_3^-}$ can newly be obtained based on its robust correlation with GPP
- A parsimonious approach for regionalizing $U_{a-NO_3^-}$ is validated using the new data
- Networked upscale modeling reveals high spatiotemporal variability of nitrate uptake
- Uptake efficiency varies depending on riparian shading and hydrochemical conditions

3.1. Abstract

High-frequency sensor measurements enable calculation of continuous autotrophic nitrate uptake rate based on its intrinsic relationship with gross primary production (GPP). The spatiotemporally available data offer prospects to advance process understandings across scales. We used continuous 15-min data (2011-2015) from a forest upstream reach and an agricultural downstream reach of the Selke River, Germany. Based on the high-frequency data, we developed a parsimonious approach for regionalizing the autotrophic uptake rate, considering effects of global radiation and riparian shading. For networked modeling, we integrated this approach into the fully distributed mesoscale hydrological nitrate model (mHM-Nitrate). Daily GPP-based uptake rate calculations showed distinct seasonal patterns and ranges in the agricultural and forest streams (mean values were 80.9 and 15.5 $mg\ N\ m^{-2}d^{-1}$, respectively). Validation in the two streams showed acceptable performance (R^2 = 0.47and 0.45, respectively) and spatial transferability of the regionalization approach, given its parsimony. Networked modeling results showed high spatiotemporal variability in nitrate transport and uptake throughout the river network. The magnitude of gross uptake increased, whereas uptake efficiency decreased significantly along stream order. Longitudinal analysis in the main stem of the Selke River revealed that riparian shading and inter-annual hydrochemical variations strongly influenced daily dynamics of the uptake efficiency. This study provides a parsimonious and transferable procedure for regionalizing in-stream autotrophic nitrate uptake based on high-frequency data at reach scale. Integrating this approach in the mHM-Nitrate model allows detailed nitrate transport and in-stream uptake processes to be investigated throughout river networks.

3.2. Introduction

Streams deliver nutrients to catchment outlets and estuaries, and also transform and remove nutrients as traveling through the river network (Alexander et al. 2009). Hydrological, morphological and biogeochemical characteristics influence in-stream nutrient processing greatly, resulting in high spatiotemporal variability throughout the river network (Bernhardt et al. 2005). The in-stream processing is also influenced by factors resulting from terrestrial processes, such as nutrient availability and hydrological conditions (Mulholland et al. 2008). With such a high level of complexity, investigating nutrient dynamics at the river network scale remains challenging (Helton et al. 2011).

Following the nutrient spiraling concept (i.e., the cycling of nutrient being assimilated, temporarily retained and mineralized (Ensign and Doyle 2006)), reach-scale studies have provided much information on influential factors and in-stream uptake quantifications (Mulholland et al. 2008). Due to experimental constraints, traditional tracer studies are mostly conducted in headwater streams rather than in large streams and rivers. Networked nutrient spiraling metrics (e.g., uptake rate constant k) have been correlated with influential factors (e.g., water depth or nutrient concentrations) (Mulholland et al. 2008, Ye et al. 2017) using empirical functions. Selections of these functions (e.g., first-order kinetics) and their corresponding parameters are based on measurements across experimental sites/reaches (Alexander et al. 2009, Helton et al. 2011). However, the limitations of regionalizing and upscaling procedures are reflected in (1) dubious representativeness of measurements in small headwater streams for large streams with diverse natural characteristics and anthropogenic impacts, (2) inadequate quantification of distal factors (Helton et al. 2011), e.g., riparian vegetation and land cover conditions that influence stream light availability, and (3) insufficient coverage of spatiotemporal variations in in-stream processes and terrestrial allochthonous inputs.

Nitrate (NO_3^-) has been intensively investigated due to its mobility and environmental impacts (Grant et al. 2018). The in-stream fate of NO_3^- is strongly correlated with ecosystem metabolism in lotic systems due to biotic demand in benthic biofilms and hyporheic zones (Bernhardt et al. 2018, Gomez-Velez et al. 2015, Rode et al. 2016a). Measurements in small headwaters demonstrate a strong relationship between total NO_3^- uptake and ecosystem metabolism rates, and a significant linear regression between NO_3^- diel amplitude (due to autotrophic uptake) and gross primary production (GPP) (Roberts and Mulholland 2007). However, traditional sampling campaigns are mostly conducted in streams where and when stream conditions are optimum (Bernhardt et al. 2018). Consequently, they are not sufficient

for estimating temporal dynamics (Heffernan and Cohen 2010), nor for transferal to different stream conditions.

The development of sensor techniques allows continuous monitoring under a much wider range of stream conditions and therefore improves understanding of ecosystem processes (Rode et al. 2016b). Among others, NO_3^- sensors are widely available and the autotrophic NO_3^- uptake rate ($U_{a-NO_3^-}, mg\ N\ m^{-2}\ d^{-1}$) can be measured directly from high-frequency NO_3^- concentration measurements, i.e., the diel amplitude. Based on high-frequency monitoring, Heffernan and Cohen (2010) found a strong correlation between measured $U_{a-NO_3^-}$ and calculations based on measured GPP and the stoichiometric ratio in a subtropical spring-fed river in the USA. Rode et al. (2016a) related measured $U_{a-NO_3^-}$ to GPP based on high-frequency data in forest and agricultural streams in Germany, and demonstrated the agreement between regression and stoichiometric methods. Therefore, high-frequency monitoring facilitates reliable in-stream measurements, which can stimulate new insights into NO_3^- uptake processing across stream conditions.

Given abundant NO_3^- availability, stream metabolism is usually controlled by physical factors, such as light, temperature and flow disturbance (O'Connor et al. 2012, Uehlinger 2006). Among proximal factors, light (i.e., photosynthetically active radiation - PAR) dominates the variation in GPP (Mulholland et al. 2001, Roberts et al. 2007). Meanwhile, distal factors (e.g., land cover and riparian vegetation) largely impact the stream surface light availability (Bernot et al. 2010). However, the surface light regime and its impact on GPP have not been quantified adequately, most likely due to the difficulty in relating the light regimes to widely available data (Bernhardt et al. 2018). Based on continuous high-frequency sensor deployment, Rode et al. (2016a) explicitly showed different seasonal patterns of GPP in closed- and open-canopy streams. Interestingly, the patterns are highly consistent with those of PAR measured above forested stream surface and above forest canopy, respectively (measurements in Roberts et al. (2007)). Therefore, information derived from continuous high-frequency monitoring can be used for relating in-stream autotrophic NO_3^- uptake to its driving factors, especially under diverse light regimes.

One main challenge in modeling networked NO_3^- uptake, especially uptake efficiency (i.e., the percentage of the uptake amount to the load), is covering the spatiotemporal heterogeneity of terrestrial exports (e.g., NO_3^- load). Most network models emphasize in-stream processes and simplify greatly representations of terrestrial processes. They either statistically relate terrestrial exports to catchment characteristics (e.g., the SPARROW model) (Wollheim et al. 2008) or define one or more flow

components as end-members. Those simplifications restrict the ability to model river networks that have heterogeneous conditions, and in which allochthonous terrestrial inputs are likely more diverse (Dupas et al. 2017). Alternatively, mechanistic catchment water quality models describe catchment characteristics thoroughly (Rode et al. 2010); Among them, grid-based models are preferable due to their inherent higher degree of spatial representation (Yang et al. 2018). Moreover, the grid-based routing structure provides detailed reach-scale information (e.g., stream geomorphological features) for analyzing in-stream processes. To our knowledge, mechanistic catchment models that provide detailed terrestrial exports have rarely been used to upscale reach-scale advances to the network scale.

In this study, we propose a parsimonious regionalization approach for $U_{a-NO_3^-}$ based on continuous high-frequency NO_3^- concentration and stream metabolic data (2011-2015) in a forest and an agricultural stream reach of the Selke River, Germany. We upscale the findings to the river network scale based on the fully distributed catchment NO_3^- model (mHM-Nitrate) (Yang et al. 2018). Influential factors of global radiation (GR) and riparian shading are chosen to quantify the stream surface light availability. The new data and the modeling approach allow us to (1) obtain continuous daily $U_{a-NO_3^-}$ data from the high-frequency measurements and the intrinsic relationship between $U_{a-NO_3^-}$ and GPP, (2) validate the performance of the $U_{a-NO_3^-}$ regionalization approach and test the spatial transferability for deviating stream riparian conditions, and (3) upscale the approach to the whole Selke river network based on the mHM-Nitrate model and provide detailed spatiotemporal information on NO_3^- transport and uptake at the river network scale.

3.3. Materials and Methods

3.3.1. Study site and high-frequency data collection

The Selke River, central Germany, has a drainage area of 456 km^2. It is part of the TERENO (TERrestrial ENvironmental Observatories) project (http://www.tereno.net/overview-de, last accessed October 31, 2018). The elevation ranges from 605 m in the upper mountains to 53 m in the lowlands. The two study reaches are located upstream of the gauging stations Meisdorf and Hausneindorf, representing the dominant forested and agricultural land, respectively (**Figure 3.1**). Due to gradients of meteorological and geomorphological conditions, the catchment is characterized by high hydrological heterogeneity (**Table S3.1**). Due to highly fertile soils, the agricultural land is dominated by arable land cropped mainly with winter wheat, winter barley and maize. Pasture accounts only for 3.5% of total catchment area and is exclusively located in the upper part of the catchment. Agricultural streams are mostly characterized

by open canopy. This is confirmed by a detailed survey from the State Agency for Flood Protection and Water Management of Saxony-Anhalt (LHW) on riparian vegetation using 100 m stream segment. At the two largest agricultural tributaries of the Selke River (i.e., the Getel and the Hauptseegraben, **Figure S3.1**), only 6% of the surveyed stream segments have gallery trees (80% of them occur only on one side of the stream). Most of the agricultural streams have no high riparian vegetation. Only the main stem of the lowland Selke River (4th and 5th order) is partly shaded by bushes and riparian gallery trees. The open canopy allows high irradiance at the water surface and the subsequent development of large mats of periphyton and macrophytes (Rode et al. 2016a).

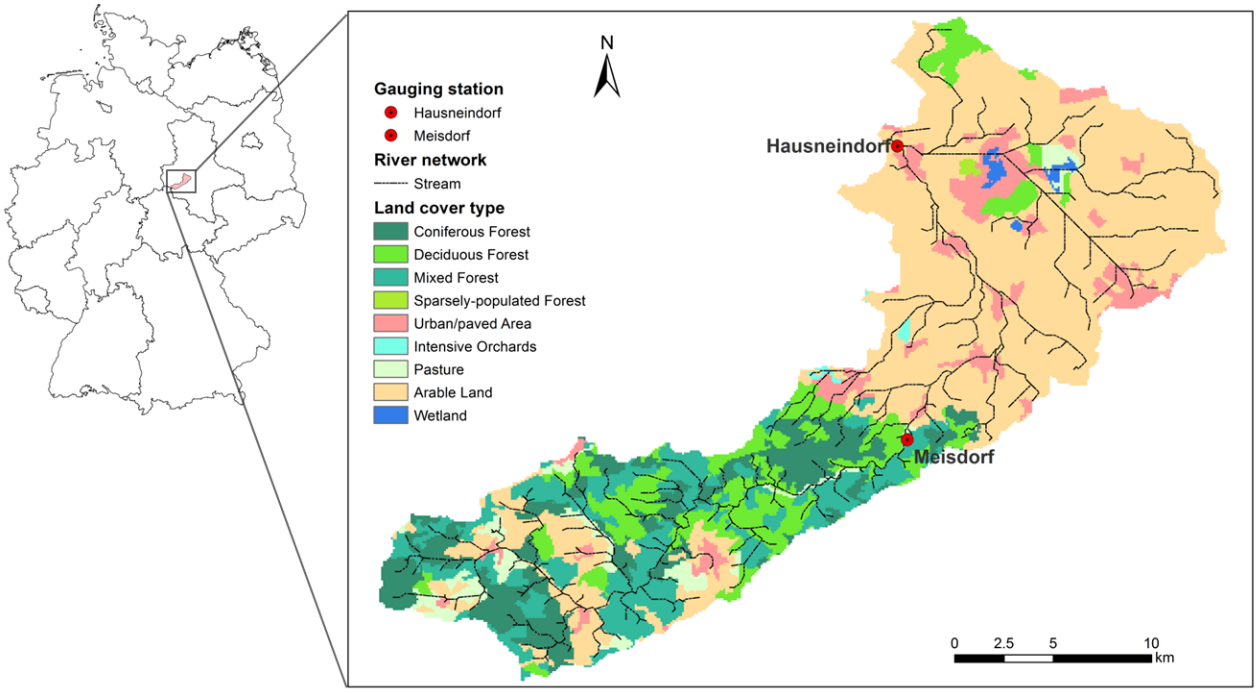

Figure 3.1. The Selke catchment, river network and land cover types. Multi-parameter sensors were deployed at station Hausneindorf and station Meisdorf, representing agricultural and forest streams, respectively.

The outlet station Hausneindorf measures flow and NO_3^- dynamics of the entire catchment. Reaches upstream of this station represent open or very-sparse canopy agricultural streams. Upstream reaches of the station Meisdorf are mostly forest streams, of which riparian zones are dominated by trees with a closed-canopy during the vegetation period. In the lowland streams, NO_3^- concentrations are much higher than those in the upper streams (values of biweekly grab samples 1997-2015 at the two stations

are 3.61 ± 1.09 and 1.60 ± 1.00 $mg\ l^{-1}$, respectively) due to long-term agricultural activities. Concentrations of soluble reactive phosphorus (SRP) are similarly high (0.040 ± 0.022 $mg\ l^{-1}$) at both stations.

Multi-parameter sensors (YSI 610 and TRIOS ProPS-UV) were deployed at the two stations. We continuously measured dissolved oxygen (DO), water temperature, pH, turbidity (only available in 2015) and NO_3^- concentration at a 15-min interval. The quality of high-frequency sensor NO_3^- measurements was validated using parallel grab samples (linear regression R^2=0.93, see Rode et al. (2016a)). We collected five years of data (from January 1, 2011 to December 31, 2015) from the two stations. High-frequency discharge and air pressure data were collected from the state agency (LHW) and the German Weather Service, respectively. For more details on the high-frequency monitoring and maintenance, refer to Rode et al. (2016a).

3.3.2. Calculation of metabolism rates and NO_3^- uptake rate

Daily GPP ($g\ O_2\ m^{-2}\ d^{-1}$) and ecosystem respiration (ER, $g\ O_2\ m^{-2}\ d^{-1}$) from 15-min DO measurements were calculated based on the single-station method (Odum 1956). The determination of the reaeration coefficient is one of the key issues in metabolic calculation (Raymond et al. 2012). The energy dissipation method (Bott et al. 2006, Tsivoglou and Neal 1976) was used in this study, which has been evaluated with a propan tracer test in the study site (Rode et al. 2016a). DO saturation percentage was determined from the measured DO concentration, water temperature and barometric pressure. Rates of GPP and ER were calculated using the measured DO differences between consecutive 15-min records, considering the effects of DO saturation deficit and reaeration. Day-time ER was assumed to be equal to the night-time ER. Daily net ecosystem production (NEP) was calculated as daily $GPP - ER$. For more details on the calculation, please refer to the Supplementary Materials. Values during over-bank flow periods (discharge > 7 $m^3 s^{-1}$) were not considered, and unrealistic negative GPP and ER values were omitted (11% and 14% for Meisdorf and Hausneindorf, respectively). For detailed quality control of metabolism rate calculation, refer to Rode et al. (2016a).

Theoretically, $U_{a-NO_3^-}$ ($mg\ N\ m^{-2}\ d^{-1}$) can be obtained directly from the diel amplitude of NO_3^- concentration (i.e., measured $U_{a-NO_3^-}$, modified from Heffernan and Cohen (2010)):

$$U_{a-NO_3^-} = \frac{1}{A}\sum_{t=0}^{n}[Q_t \cdot ([NO_3^{-1}]_{\max(0)} - [NO_3^{-1}]_t)] \quad (3.1)$$

where $[NO_3^-]_{\max(0)}$ and $[NO_3^-]_t$ ($mg\ l^{-1}$) denote the preceding predawn peak of NO_3^- concentration and NO_3^- concentration at time step t, respectively; Q_t ($l\ s^{-1}$) denotes discharge at time step t; A denotes benthic area (m^2), which is estimated from the reaeration coefficient and flow velocity measured upstream of each gauging station (Rode et al. 2016a); and n denotes the number of measurements per diel change.

As mentioned by Hensley and Cohen (2016) and Rode et al. (2016a), upstream effects propagate over a longer distance for NO_3^- than for DO and the diel change of NO_3^- can be disturbed rapidly by additional upstream inputs. Therefore, the measured $U_{a-NO_3^-}$ from diel amplitudes of NO_3^- concentration can only be obtained during steady low-flow conditions. Based on the five years of measurements, we defined the regression between measured $U_{a-NO_3^-}$ and GPP to obtain continuous daily $U_{a-NO_3^-}$ calculations (i.e., GPP-based $U_{a-NO_3^-}$ calculations).

3.3.3. Stream surface light availability and the $U_{a-NO_3^-}$ regionalization approach

Light availability near the stream surface is increased by PAR above the canopy and decreased by shading of riparian vegetation. We collected daily sunshine duration data from the Ummendorf weather station (35 km north of the Hausneindorf station) and calculated the theoretical daily GR (Allen et al. 1998) from 2011-2015. For details on the GR calculation, please refer to the Supplementary Materials. Since the daily series of GR fluctuated greatly, we smoothed the data using a 5-day moving average method and obtained averaged daily global radiation $GR_{\bar{t}}$ ($MJ\ m^{-2}d^{-1}$). The time window of 5 days was arbitrarily chosen to balance the trends and fluctuations. The impact of GR on light availability was calculated by min-max normalization of the smoothed GR data (feature scaling):

$$f_{GR,t} = \frac{GR_{\bar{t}} - \min\left(GR_{\bar{t}\in[1,n]}\right)}{\max\left(GR_{\bar{t}\in[1,n]}\right) - \min\left(GR_{\bar{t}\in[1,n]}\right)} \tag{3.2}$$

where $f_{GR,t} \in [0,1]$ denotes the GR coefficient at time t; $\max\left(GR_{\bar{t}\in[1,n]}\right)$ and $\min\left(GR_{\bar{t}\in[1,n]}\right)$ denote the maximum and minimum $GR_{\bar{t}}$ values, respectively; and n denotes the day number of the time series. Field measurements of GR and PAR in a nearby weather station (Wulferstädt station, 2013-2015) showed a strong linear relationship between GR and PAR ($PAR = 0.64 \times GR$, $R^2 = 0.98$) and agreement between calculated GR at Ummendorf and measured GR at Wulferstädt ($R^2 = 0.96$, **Figure S3.2**). Normalization also eliminated the scale effect. Therefore, we used GR directly, instead of PAR.

We assumed that riparian vegetation is the same as that in the surrounding landscape. Therefore, the condition of the riparian vegetation was represented by land cover type. Leaf area index (LAI) was chosen to represent spatiotemporal distribution of the riparian canopy. The negative impact of riparian shading on light availability was calculated by min-max normalization of LAI among all land cover types (i.e., the riparian shading coefficient). To simplify preparation of LAI data, we calculated generic daily LAI values for each land cover type using the mean monthly values and applied each annual pattern for all five years. When year-to-year LAI changes significantly, the measured values or remote sensing data are recommended.

The overall stream surface light availability was calculated as:

$$f_{L,t}^{j} = f_{GR,t} \cdot (1 - \sum_{i=1}^{k} \alpha_j^i \cdot f_{LAI,t}^i) \quad (3.3)$$

where $f_{L,t}^{j} \in [0,1]$ denotes the overall coefficient of near surface light availability of stream segment j at time t; $f_{LAI,t}^{i} \in [0,1]$ denotes the riparian shading coefficient of land cover type i; and α_j^i denotes the areal proportion of each land cover type i surrounding stream segment j. From grid-based modeling perspective, one stream segment was defined for each modeling grid cell. Therefore, α_j^i was equivalent to the length proportion of each riparian vegetation type. We further assumed that no significant shading for streams surrounded by non-forest types (e.g., agricultural streams) and set $f_{LAI,t}^{i}$ values of these stream segments to zero.

The light availability coefficient ($f_{L,t}^{j}$) provides a spatiotemporal estimate of the combined impact of GR and riparian shading. Therefore, $U_{a-NO_3^-}$ was simply quantified as:

$$U_{a-NO_3^-,t}^{j} = U_{a,max} \cdot f_{L,t}^{j} \quad (3.4)$$

where $U_{a-NO_3^-,t}^{j}$ denotes $U_{a-NO_3^-}$ of stream j at time t, and $U_{a,max}$ denotes the general parameter (i.e., the potential uptake rate). This parameter can be explained physically as the $U_{a-NO_3^-}$ value under optimal GR conditions (e.g., on clear-sky dates with the longest sunshine duration of the year). Based on this parsimonious approach, $U_{a-NO_3^-}$ and its spatiotemporal variability can be easily obtained based on commonly available data (i.e., GR, LAI and land cover information).

3.3.4. The grid-based mHM-Nitrate model and networked upscaling

The mHM-Nitrate model is a fully distributed catchment nitrate model (Yang et al. 2018). The model is developed on the multi-scale platform of the mHM model (Samaniego et al. 2010). The mHM-Nitrate model provides reliable spatial simulations of hydrological and nitrate fluxes, as well as spatial details of physical and environmental characteristics of the catchment. These characteristics are upscaled from basic geographical data levels to the modeling level using the multi-scale parameter regionalization procedure (Samaniego et al. 2010). Each stream segment contains a complete set of flow routing and nitrate processing (i.e., assimilatory uptake, mineralization and denitrification). Therefore, stream morphological information can be linked directly to simulating NO_3^- transport and uptake processes.

The new approach of $U_{a-NO_3^-}$ regionalization (**Eqs. 3.2 – 3.4**) was integrated into the mHM-Nitrate model. Since assimilated nitrogen can be remineralized and return to the in-stream nitrate pool, mineralization was refined to equal a proportion of autotrophic NO_3^- uptake, while denitrification remained as that of the original mHM-Nitrate. The model was set up in the Selke catchment using a 1 km^2 cell size for both terrestrial and in-stream phases, and was calibrated against observations of the two gauging stations. Daily discharge and NO_3^- concentration were simulated and provided for each stream. The proportion of each land cover type in the area of each model cell was calculated using the basic land cover map (100 m resolution). Morphological characteristics were calculated for each stream, as follows: Stream length was calculated as the distance to the adjacent or diagonal cell based on the Digital Elevation Model (DEM, 100 m resolution) and summed up to the modeling level (1 km resolution); Stream width was estimated from simulated discharge, based on the empirical equation by Rode et al. (2016a). GR data from the Ummendorf station were used for the entire catchment. We matched the modeled river network to the real network that generated from the DEM and modified according to topographical maps (source from the State Agency for Survey and Geoinformation of Sachsen-Anhalt, Germany). We assigned model simulations to corresponding streams in the real network. The main stem of the Selke River from the modeled network was used for the daily longitudinal analysis (**Figure S3.1**).

3.3.5. Approach validation at reach scale and statistical analysis methods

The approach was firstly validated using the daily GPP-based $U_{a-NO_3^-}$ calculations from the agricultural stream (station Hausneindorf). Potential outliers in the calculations were detected using the interquartile range (IQR) method, and the $U_{a,max}$ value was assigned as 1.5 IQR of the upper quartile (ca. 99.65%). This parameter value was then applied directly to the forest stream (station Meisdorf), whose

daily $U_{a-NO_3^-}$ calculations were used to validate the performance of the approach and the transferability of the parameter under different riparian conditions.

To evaluate the spatial pattern and seasonality of modeled autotrophic NO_3^- uptake, each stream was identified by three attributes: stream order, riparian vegetation type and mean uptake values of each season. We summarized three types of vegetation at the modeling level: agriculture (streams surrounded by > 80% of agricultural land), forest (streams surrounded by > 80% of forest) and mixture (all other streams). Analysis of variance (ANOVA) was conducted using *R software* (Team 2017). Normality of the data was ensured using log-transformation, and homogeneity of variance was tested using the Levene's test (results not shown). Significant ANOVA results ($p < 0.01$) were examined further using post-hoc test (Tukey's Test) for pairwise comparisons. The *beta* coefficient (*lm.beta* package in *R*) was calculated to identify the most descriptive attributes (higher absolute *beta* value indicates a stronger effect).

3.4. Results and Discussion

3.4.1. Metabolism rates and GPP-based $U_{a-NO_3^-}$ calculations

In the agricultural stream (**Figure 3.2**), GPP (mean ± standard deviation (SD) = 2.10 ± 1.78 $g\ O_2\ m^{-2}d^{-1}$) was moderately correlated with GR ($R^2 = 0.42, p < 0.01$) and therefore generally peaked in summer. ER (mean ± SD = 3.28 ± 1.75 $g\ O_2\ m^{-2}d^{-1}$) was slightly higher than GPP but within the same order of magnitude. It was also correlated with global radiation ($R^2 = 0.33, p < 0.01$), but the correlation was sometimes influenced by flooding events. NEP was generally close to zero (mean = - 1.10 ± 1.83 $g\ O_2\ m^{-2}d^{-1}$), with slightly positive values in spring (0.50 ± 2.03 $g\ O_2\ m^{-2}d^{-1}$) and mostly negative values in late autumn (-2.38 ± 1.10 $g\ O_2\ m^{-2}d^{-1}$). Results generally agreed with the first two-year calculation by Rode et al. (2016a). However, seasonal patterns of metabolism rates in the last three years were more diverse. For instance, during the months of June-October, GPP was significantly lower in 2014-2015 than in 2011-2013 (mean = 1.66 vs. 2.74 $g\ O_2\ m^{-2}d^{-1}$, respectively; ANOVA, $p < 0.01$). In 2014, comparable degree of reductions in GPP and ER were observed and mean NEP (- 0.97 $g\ O_2\ m^{-2}d^{-1}$) was similar to the annual mean value. The reductions may be attributed to higher discharge during the dry months (mean = 1.26 vs. 0.62 m^3s^{-1} for other years) which increases bottom shear stress, possibly resulting in moderate removal of benthic communities. Biofilm aging and algal sloughing may also contribute to the reduction in both GPP and ER during moderate flow (Uehlinger 2006). In 2015, GPP decreased more than ER, resulting in higher negative NEP (mean = - 2.04 vs. -

1.22 $g\ O_2\ m^{-2}d^{-1}$ for other years). Turbidity is the most likely cause of this stronger decrease in GPP than in ER (**Figure S3.3**). Increased turbidity reduces the amount of light that penetrates from the surface to the riverbed, while the fine sediments being transported stimulate respiration due to their high concentrations of labile organic carbon (O'Connor et al. 2012, Roberts et al. 2007).

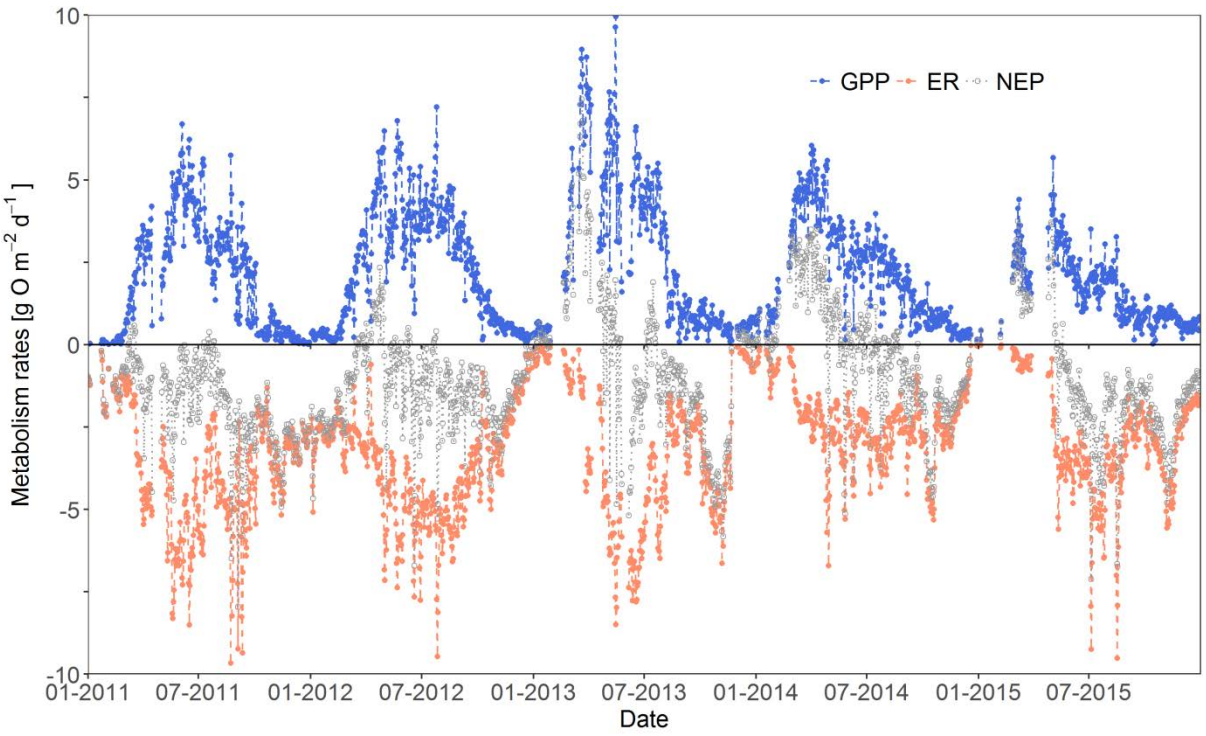

Figure 3.2. Daily metabolism rates (i.e., gross primary production-GPP, ecosystem respiration-ER and net ecosystem production-NEP) at Hausneindorf, representing typical agricultural streams. ER was shown as negative values for better visibility.

Metabolism rates in the forest stream (**Figure S3.4**) had distinctly different behavior than those in the agricultural stream. GPP (mean ± SD = 0.54 ± 0.62 $g\ O_2\ m^{-2}d^{-1}$) was significantly lower (ANOVA, $p < 0.01$), and the seasonal pattern differed completely. It increased in spring due to the increase in GR and peaked (mean = 2.85 $g\ O_2\ m^{-2}d^{-1}$) at the beginning of May, when significant shading from riparian vegetation occurred. In the following month, GPP decreased dramatically to a low level (mean = 0.25 $g\ O_2\ m^{-2}d^{-1}$) and remained low until late autumn. After litterfall, GPP increased slightly (e.g., in 2013-2015), but the increase was low due to the already reduced GR in late autumn (Roberts et al. 2007). ER (mean ± SD = 4.65 ± 5.61 $g\ O_2\ m^{-2}d^{-1}$) was generally much higher than GPP, indicating strong net heterotrophic behavior in the forest stream ($NEP < 0$ throughout the year). The seasonal ER pattern was more diverse, with generally higher values in winter and spring and high variability

throughout the year. ER was correlated with stream flow ($R^2 = 0.60, p < 0.01$), most likely because ER can be stimulated by hydrological events which provide more allochthonous labile organic inputs (Mulholland et al. 2001).

Linear regressions between measured $U_{a-NO_3^-}$ and GPP at stations Hausneindorf and Meisdorf (n = 90 and 67, respectively, **Figure 3.3**) were similar to those of a former study using the first two years of data (2011-2012) (Rode et al. 2016a). This demonstrated that the correlation was robust in the Selke catchment.

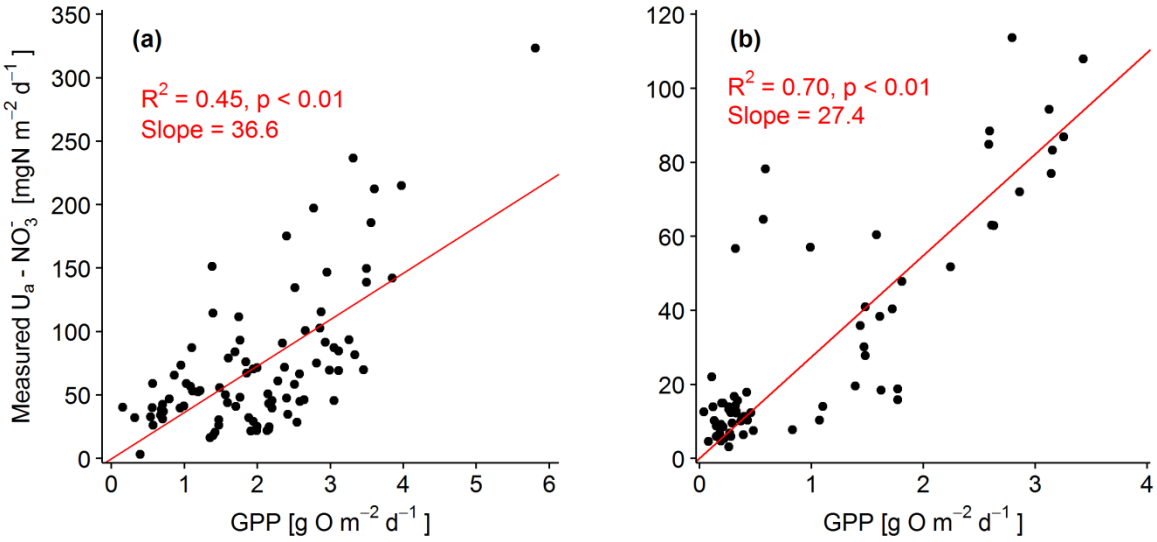

Figure 3.3. Linear regressions between measured autotrophic NO_3^- uptake ($U_{a-NO_3^-}$) and GPP at (a) Hausneindorf and (b) Meisdorf, representing the agricultural and forest streams, respectively, during low flow conditions (discharge$< 0.8\ m^3\ s^{-1}$). The standard errors of linear predictions were 41.58 and 16.07 $mg\ N\ m^{-2}d^{-1}$ for Hausneindorf and Meisdorf, respectively.

3.4.2. Performance of the $U_{a-NO_3^-}$ regionalization approach

The GR coefficient (**Figure S3.5a**) showed a clear seasonal pattern with considerable differences among years (e.g., unimodal or multimodal). The shading coefficient based on LAI (**Figure S3.5b**) demonstrated clear differences in shading among forest types: deciduous trees provided the highest shading in July-August and almost no shading before leaf-out and after litterfall; conifers provided constant high shading throughout the year; and the other forest types in the Selke catchment provided intermediate levels of shading. Based on our assumptions, non-forest shading was set to zero. The overall light

coefficient (Eq. 3) for each stream depended on the proportions of each land cover type (see an example in **Figure S3.5c**).

Daily GPP-based $U_{a-NO_3^-}$ calculations for agricultural and forest streams (Hausneindorf and Meisdorf, respectively, **Figure 3.4**) were estimated based on continuous daily GPP and correlations between measured $U_{a-NO_3^-}$ and GPP, respectively. The potential uptake rate ($U_{a,max}$) was determined as 283 $mg\ N\ m^{-2}d^{-1}$ based on the dataset from Hausneindorf (n = 1563, **Figure S3.6**). For the open-canopy agricultural stream, simulations from the regionalization approach reproduced the seasonal pattern of the calculated $U_{a-NO_3^-}$ relatively well (**Figure 3.4a**), especially in the first two years, when discharge in low-flow periods was relatively low and stable. In 2013, GPP-based $U_{a-NO_3^-}$ calculations were extremely high (≥ 300 $mg\ N\ m^{-2}d^{-1}$) during March-June (i.e., the off-set and in-between periods of two extreme flooding events). Simulations underestimated by more than 50%. The higher discharge (mean = 2.50 $m^3\ s^{-1}$) and lower temperature (ca. 4 °C lower than the daily mean) during these periods might have introduced high uncertainty in metabolism rate calculations (Riley and Dodds 2012). Similarly, in March 2014 and 2015, measured $U_{a-NO_3^-}$ (mean = 66.6 $mg\ N\ m^{-2}d^{-1}$, n=12) were similar to the simulations (mean = 76.1 $mg\ N\ m^{-2}d^{-1}$, n=62), but much lower than the GPP-based calculations (mean = 131.5 $mg\ N\ m^{-2}d^{-1}$, n=59). This further suggests that uncertainty in calculated metabolism rate may increase with increased discharge.

We determined the proportion (α) of each land cover type in a 1 km^2 area surrounding Meisdorf, i.e., coniferous forest (0.00), deciduous forest (0.52), mixed forest (0.25) and pasture (0.23). The simulated $U_{a-NO_3^-}$ reproduced the range and seasonal pattern of GPP-based calculations remarkably well (**Figure 3.4b**). Although we observed discrepancies for the agricultural stream and transferred the potential uptake rate directly to the forest stream, the approach clearly captured the large differences of calculated $U_{a-NO_3^-}$ between the two riparian conditions. Slight overestimates occurred from May-June, most likely due to aspect shading from the steep valley alongside the stream (Bernhardt et al. 2018). The approach missed several observed spikes, which likely correspond to pulses of discharge and turbidity. The dramatic decrease in calculated $U_{a-NO_3^-}$ in 2012 is probably due to the sharp decrease in water temperature (Rode et al. 2016a).

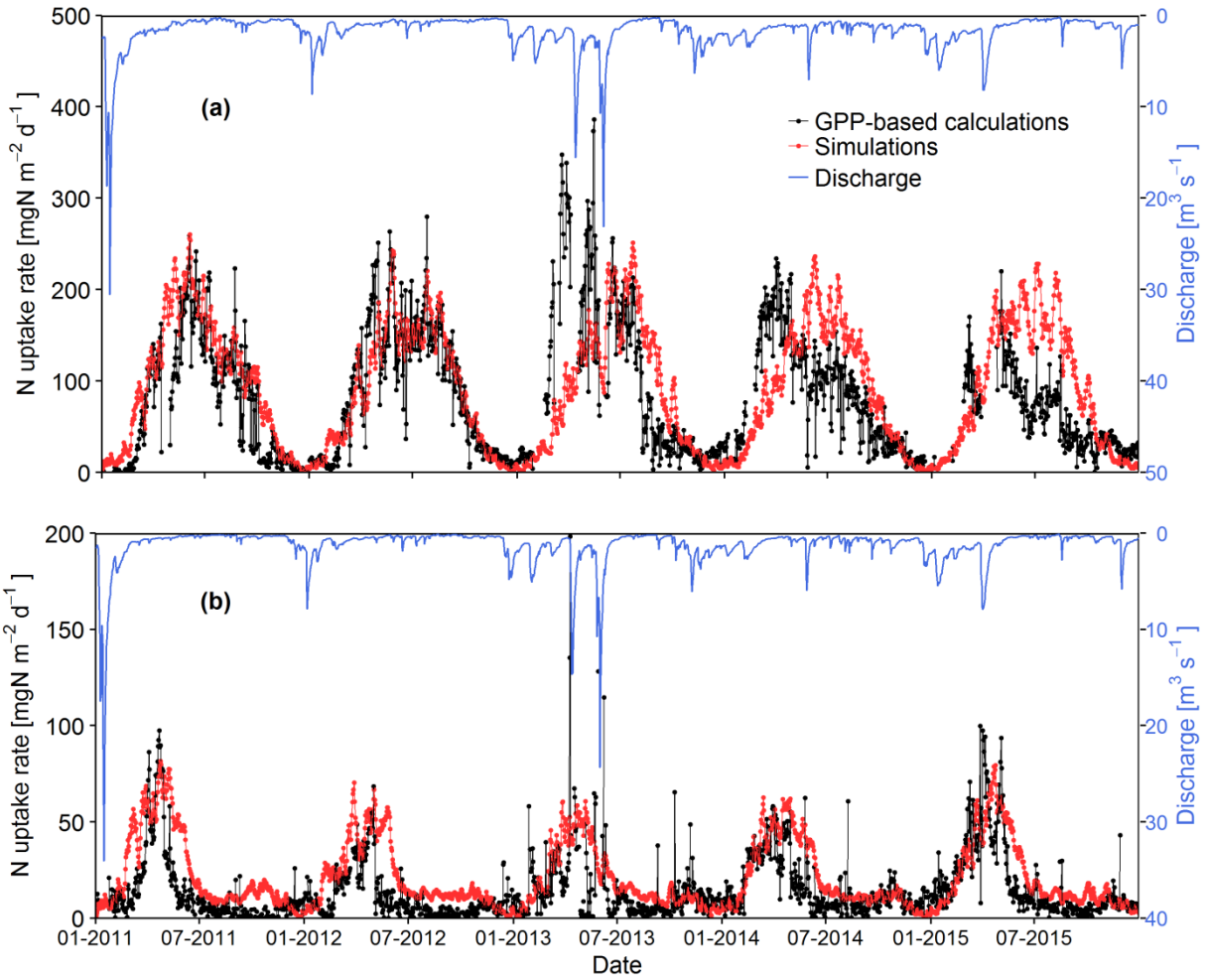

Figure 3.4. GPP-based calculations and approach simulations of the N uptake rate (i.e., $U_{a-NO_3^-}$) at (a) Hausneindorf and (b) Meisdorf, representing the agricultural and forest streams, respectively.

In addition to the visual consistency in seasonal patterns, the simulations correlated reasonably with the GPP-based $U_{a-NO_3^-}$ calculations ($R^2 = 0.47$ and 0.45 for Hausneindorf and Meisdorf, respectively), given the parsimony of the approach and the distinct uptake behaviors at the two sites. Therefore, light can be identified as the main factor influencing the seasonal autotrophic NO_3^- uptake in the Selke River. Other influential factors were similar at the two sites. The C/N ratios of benthic biofilm were similar (8.7 and 8.5 for the agricultural and forest streams, respectively) (Kamjunke et al. 2015). From June-October, water temperature was 14.2 ± 4.3 and 12.0 ± 4.2 °C, respectively, which is sufficient in supporting high growth rates of diatoms (Anderson 2000).

We assumed that riparian vegetation is the same as the surrounding landscape. This assumption is validated by the LHW survey data in the catchment. Although the lowland main stem of the Selke is

dominated by sparse gallery trees, GPP values at Hausneindorf are comparable with values reported in other agricultural streams (e.g., Beaulieu et al. (2013) and Griffiths et al. (2013)) and the approach performed well. This indicates that the gallery trees do not provide sufficient shading on the stream surface, presumably due to the relatively large side-to-side distance and less shading density of the trees. Still, the assumptions might not completely valid for agricultural or urban streams with a significant buffer of trees planted along the stream corridor. However, such information is rarely available at river network scale (e.g., resolution mismatching of satellite data and expensive to survey all tributaries) and extrapolating the shading effect from on-site measurements remains challenging (Davies-Colley and Rutherford 2005).

Our regionalization approach focuses on quantifying stream surface light availability. Other factors are not included in its design. Water temperature is not explicitly considered because it is not available network wide, and spatiotemporal estimates of water temperature can be quite uncertain. The impact of water temperature is partly considered by light and is more relevant for ER than for GPP (Demars et al. 2011). Turbidity decreases the amount of light that penetrates to benthic areas (Julian et al. 2008), which likely resulted in the overestimation of the simulated $U_{a-NO_3^-}$ in the summer/autumn periods of 2014-2015. Based on the continuous measurements in 2015 (**Figure S3.3**), we observed a plausible correspondence between the increase in turbidity and the decrease in GPP, but the relationship is quantitatively unclear, let alone linking turbidity to widely available discharge data for regionalization purposes. Flow disturbance likely has significant episodic impact on stream metabolism, following a threshold behavior (O'Connor et al. 2012, Uehlinger 2006). The resilience of GPP to flow disturbance is suspected to be relatively quick, especially in high PAR seasons, except for highly complicated cases in which successive disturbances occur (O'Connor et al. 2012). The impact of flow disturbance is mechanistically controlled by turbulence and sediment interactions (O'Connor et al. 2012), which are challenging to determine and require adequate descriptions of hydraulics and sediment properties. Therefore, flow disturbance is excluded from the approach. Nutrient limitation may constraint the autotrophic uptake in certain cases. However, the relationship between nutrient supply and GPP increase is also reported as weak (Bernot et al. 2010), most likely due to the already high nutrient levels in anthropogenically impacted streams.

3.4.3. Network upscaling and spatiotemporal variability of NO_3^- uptake

Integrating the approach into mHM-Nitrate model predicted a strong spatial variability of seasonal mean $U_{a-NO_3^-}$ (**Figure S3.7**). Agricultural streams had much higher uptake rates than forest streams (mean ±

SD = 86.4 ± 1.9 vs. 18.8 ± 6.2 $mgNm^{-2}d^{-1}$, respectively) due to less riparian shading. The differences between the two main riparian vegetation types were much smaller in winter (10.1 ± 0.42 vs. 4.6 ± 2.2 $mg\ N\ m^{-2}d^{-1}$) probably due to the universally low winter GR. The higher SD for forest streams indicated more diverse uptake patterns due to different shading patterns (represented by different LAI patterns) in different forest types. We used only basic information (i.e., global radiation, LAI and land cover information), but did provide the varied seasonality of $U_{a-NO_3^-}$ under different light regimes.

By multiplying modeled stream benthic areas, seasonal mean gross NO_3^- uptake ($U_{ass}, kg\ N\ d^{-1}$) was calculated for each stream in the network (**Figure 3.5**). The coefficient of variance (CV) of U_{ass} was much higher than that of $U_{a-NO_3^-}$ (CVs of annual mean = 1.51 and 0.57, respectively), indicating a higher overall spatial variability. Due to variations in stream morphological properties, U_{ass} varied among areas with the same shading condition. Two-way ANOVA showed that U_{ass} varied significantly among different stream orders and vegetation types in all seasons. A post-hoc test (Tukey's test) identified that the U_{ass} of 1st (annual mean = 0.27 $kg\ N\ d^{-1}$) and 2nd (0.51 $kg\ N\ d^{-1}$) order streams was significantly lower than that of higher orders (1.77 $kg\ N\ d^{-1}$ for all 3rd -5th order streams) due to flow accumulation in higher order streams. The U_{ass} of forest streams differed significantly from those of agricultural and mixed streams, except in winter, when all values were low. U_{ass} also showed significant seasonal variability in all streams (ANOVA, $p < 0.01$). However, Post-hoc test revealed that mean values in spring and summer differed significantly only in forest streams. The differences in agricultural and mixed streams (p = 0.50 and 0.93, respectively) attenuated due to the larger benthic area in spring, albeit generally higher $U_{a-NO_3^-}$ in summer. The *beta* coefficients indicated that season and stream order had the greatest effect on U_{ass}, whereas season and vegetation type had the greatest effect on $U_{a-NO_3^-}$.

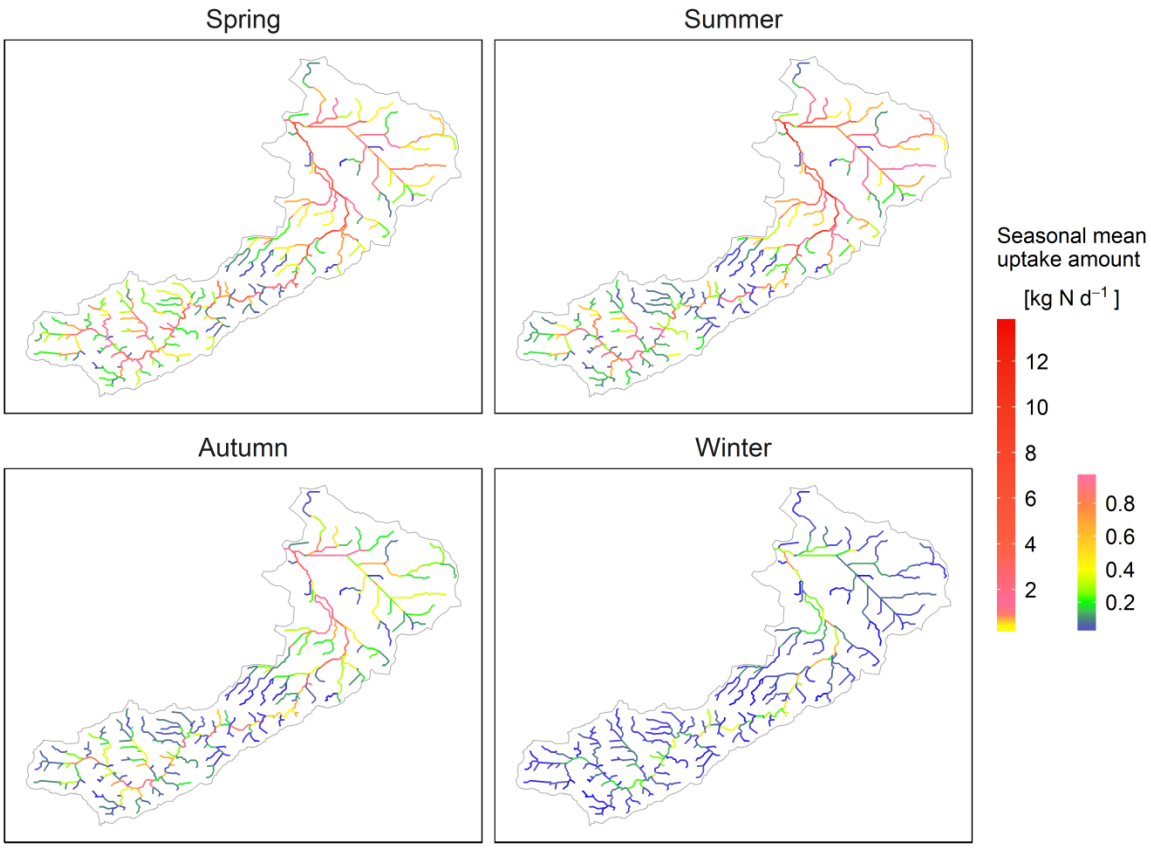

Figure 3.5. Seasonal mean gross NO_3^- uptake amount (U_{ass}) at the Selke river network. The color ramp of the legend within the range of [0,1] $kg\ N\ d^{-1}$ was zoomed in on the right side.

We used the detailed spatial simulations of nitrate loads ($L_{NO_3^-}, kg\ N\ d^{-1}$) from the mHM-Nitrate model (**Figure S3.8**) to calculate the uptake efficiency (i.e., the uptake percentage, $U_P = U_{ass}/L_{NO_3^-} \times 100$) for each stream in the network. U_P peaked in summer (mean ± SD = 21.4 ± 17.8%), when the highest U_{ass} encountered the lowest $L_{NO_3^-}$ (**Table S3.2**), whereas in winter, U_P values were extremely low throughout the river network (1.0 ± 1.7%) due to the high $L_{NO_3^-}$ and low U_{ass}. U_P was consistently lower in higher order streams (e.g., annual means were ca. 14% and 4% in 1st and 4th order streams, respectively), mainly due to the greater increase in $L_{NO_3^-}$ than in U_{ass} with increasing stream order. However, all pairs of adjacent stream orders (i.e., 1st-2nd, 2nd-3rd and 3rd-4th) did not differ significantly ($p > 0.01$) in summer. This can be attributed to the consistently low $L_{NO_3^-}$ from 1st to 4th order streams in summer (mean = 5 to 55 $kg\ N\ d^{-1}$, respectively).

Longitudinal daily U_P in the main stem of the Selke clearly showed the strong impact of riparian vegetation on U_P seasonal dynamics and its inter-annual variation (**Figure 3.6**). Critical locations and

periods of high NO_3^- uptake percentage (e.g., $>$ 40%) could be explicitly identified. The critical period was longer in upper agricultural streams (≥ 23 km from the outlet) than in lower agricultural streams (≤ 11 km from the outlet). The shallow impermeable bedrock in the upper Selke catchment results in a preference of flashier flow path, which prevents NO_3^- accumulation in the soil (Dupas et al. 2017). Whereas loess sediments dominate the lower agricultural part of the catchment and NO_3^- concentration in the soil can reach up to ca. 40 $mg\ l^{-1}$ due to agricultural activities (Yang et al. 2018). Therefore, $L_{NO_3^-}$ was much lower in the upstream of the Selke River than in the downstream, especially during baseflow dominant periods. This presumably prolonged the periods of high uptake percentage in the upper agricultural streams. U_P in forest streams (ca. 12-22 km from the outlet) generally increased from winter to spring and peaked in May or June, then sharply decreased to a low level (mean = 3%). Seasonal dynamics of U_P differed among years, depending on the spatiotemporal combination of $L_{NO_3^-}$ and U_{ass}. The spatial distributions and temporal dynamics of $L_{NO_3^-}$ had more influence on U_P due to its higher order of magnitude, compare to those of U_{ass}. In lowland agricultural streams, the period of high uptake percentage in 2011 was much more pronounced in streams upstream of the confluence than downstream, where the Getel stream joins the main Selke (**Figure 3.6**). This is due to much lower $L_{NO_3^-}$ from the upper Selke stream in June-October of 2011 (mean load = 41.6 vs. 107.3 $kg\ N\ d^{-1}$ for the five-year mean of this dry period) and higher relative contribution of $L_{NO_3^-}$ from the Getel stream (32% vs. 15% for the five-year mean).

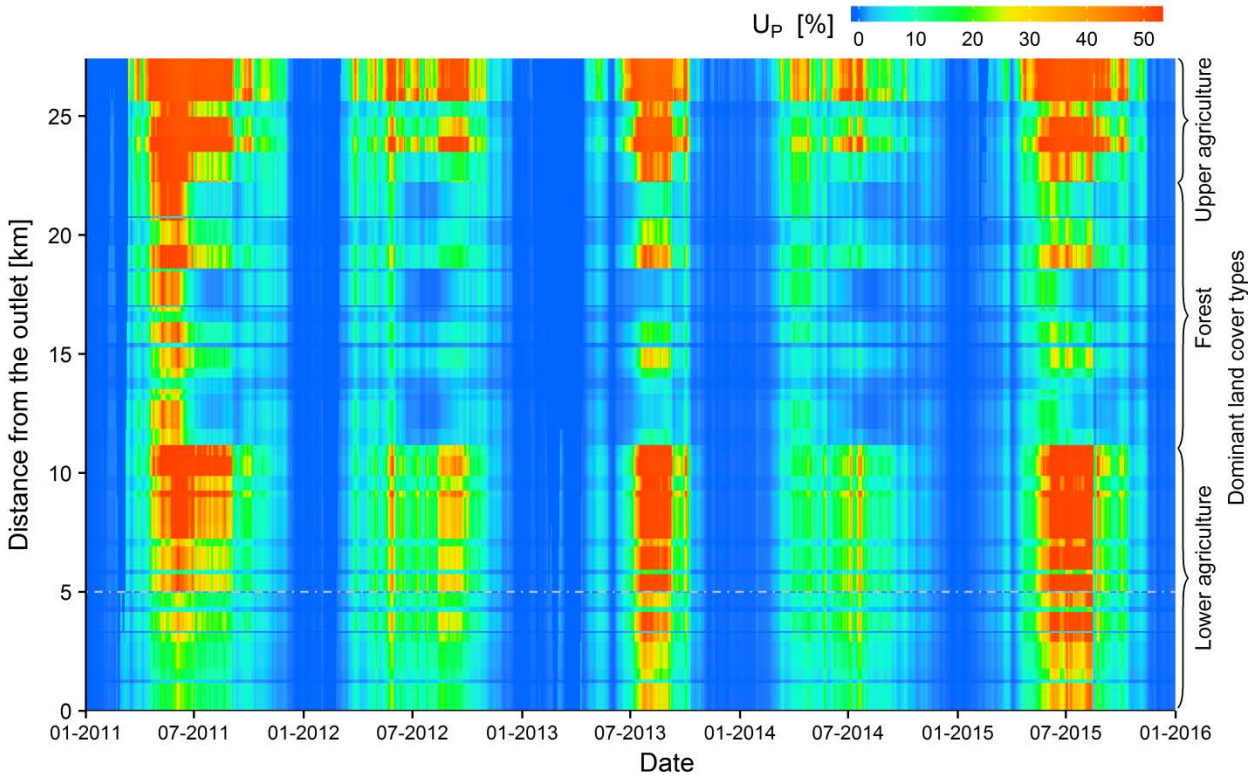

Figure 3.6. Longitudinal daily dynamics of the uptake percentage (U_P) in the main stem of the Selke (marked in Figure S2). The width of each horizontal band indicates the length of each stream. The gray dashed line identifies the location where stream Getel joins the main Selke.

3.4.4. Implications

An increasing number of water quality parameters, such as pH, DO, turbidity, NO_3^- and SRP, can be measured at high temporal resolution by sensors. The new data thus provide potential insights of in-stream processes at reach scale (Rode et al. 2016b). However, regionalizing those processes remains challenging, because in-stream processes (e.g., NO_3^- assimilation and remineralization) always interact intensively, and only a few can be individually linked to observations (e.g., the autotrophic NO_3^- uptake in this study). Therefore, novel reach-scale experimental designs are needed in current/future research to provide direct measurements of individual processes. e.g., A new reach scale mass balance approach by Kunz et al. (2017) can potentially be used to regionalize the in-stream denitrification process.

In the regionalization procedure, the selection of key environmental factors is critical at both reach and network scales. There is a high risk of over-parameterizing approaches based on reach-scale understandings. We are unable to consider certain influential factors due to data limitations, and catchment-scale behavior might be simpler than that expected from detailed process understanding (Jackson-Blake et al. 2017). Therefore, a parsimonious approach can be an appropriate initial step for

upscaling issues (Kirchner 2006). Specifically, the parsimony of an approach is reflected, in our opinion, in two perspectives: (1) input data requirements (i.e., the applicability of an approach depends largely on the input data it requires and the accessibility of these data) and (2) the parameterization (i.e., the introduced parameter should be easily identifiable and transferable with clear physical meaning). The proposed regionalization of $U_{a-NO_3^-}$ used only GR, LAI and land cover data, which are widely available for entire catchment, but quantified spatiotemporal variations in stream surface light regimes well. The physical meaning of the parameter $U_{a,max}$ indicates that it can be measured directly by traditional field experiments and be transferred to regions with similar radiation condition.

3.5. Conclusions

- Five-year continuous high-frequency measurements revealed strong correlations between in-stream autotrophic NO_3^- uptake and ecosystem metabolism (specifically GPP), and distinct seasonal behaviors in forest and agricultural streams were observed in this study.
- A parsimonious approach was proposed to quantify stream surface light availability (i.e., using basic GR, LAI and land cover information) and to regionalize $U_{a-NO_3^-}$. The approach performed well in terms of capturing seasonal variations and improving spatial transferability to different riparian shading conditions.
- The parsimonies of data requirements and parameterization suggest that the approach has a strong upscaling capability. By integrating the approach into the fully distributed mHM-Nitrate model, more detailed spatiotemporal variability of NO_3^- transport and uptake could be investigated at river network scale, which is informative in guiding water quality management.
- This study provides a working procedure for regionalizing in-stream process understandings inspired from new high-frequency data and upscaling such reach-scale findings to river network scale using fully distributed catchment models.

Acknowledgements

Xiaoqiang Yang is funded by the Chinese Scholarship Council (CSC). We would like to thank Dr. Daniel Graeber and Dr. Robert Hensley for their constructive comments and discussions. We highly appreciate the comments from the Editor and the anonymous Reviewers, which helped us to improve the manuscript significantly. This research is supported by the TERENO (TERrestrial ENvironmental Observatories) project. We thank the German Weather Service (DWD) for providing meteorological data, State Agency for Flood Protection and Water Management of Saxony-Anhalt (LHW) for providing discharge and riparian vegetation survey data, State Agency for Survey and Geoinforamtion of Saxony-

Anhalt for providing topographic maps, and Dr. Corinna Rebmann (Helmholtz Centre for Environmental Research - UFZ) for sharing the radiation measurements (photosynthetically active radiation and global radiation) at station Wulferstädt.

3.6. References

Alexander, R.B., Böhlke, J.K., Boyer, E.W., David, M.B., Harvey, J.W., Mulholland, P.J., Seitzinger, S.P., Tobias, C.R., Tonitto, C. and Wollheim, W.M. (2009) Dynamic modeling of nitrogen losses in river networks unravels the coupled effects of hydrological and biogeochemical processes. Biogeochemistry 93(1), 91-116, https://doi.org/10.1007/s10533-008-9274-8.

Allen, R.G., Pereira, L.S., Raes, D. and Smith, M. (1998) Crop evapotranspiration - Guidelines for computing crop water requirements, FAO - Food and Agriculture Organization of the United Nations, Rome, Italy.

Anderson, N.J. (2000) Miniview: Diatoms, temperature and climatic change. European Journal of Phycology 35(4), 307-314, https://doi.org/10.1080/09670260010001735911.

Beaulieu, J.J., Arango, C.P., Balz, D.A. and Shuster, W.D. (2013) Continuous monitoring reveals multiple controls on ecosystem metabolism in a suburban stream. Freshwater Biology 58(5), 918-937, https://doi.org/10.1111/fwb.12097.

Bernhardt, E.S., Heffernan, J.B., Grimm, N.B., Stanley, E.H., Harvey, J.W., Arroita, M., Appling, A.P., Cohen, M.J., McDowell, W.H., Hall, R.O., Read, J.S., Roberts, B.J., Stets, E.G. and Yackulic, C.B. (2018) The metabolic regimes of flowing waters. Limnology and Oceanography 63(S1), S99-S118, https://doi.org/10.1002/lno.10726.

Bernhardt, E.S., Likens, G.E., Hall, R.O., Buso, D.C., Fisher, S.G., Burton, T.M., Meyer, J.L., McDowell, W.H., Mayer, M.S., Bowden, W.B., Findlay, S.E.G., Macneale, K.H., Stelzer, R.S. and Lowe, W.H. (2005) Can't See the Forest for the Stream? In-stream Processing and Terrestrial Nitrogen Exports. BioScience 55(3), 219-230, https://doi.org/10.1641/0006-3568(2005)055[0219:ACSTFF]2.0.CO;2.

Bernot, M.J., Sobota, D.J., Hall, R.O., Mulholland, P.J., Dodds, W.K., Webster, J.R., Tank, J.L., Ashkenas, L.R., Cooper, L.W., Dahm, C.N., Gregory, S.V., Grimm, N.B., Hamilton, S.K., Johnson, S.L., Mcdowell, W.H., Meyer, J.L., Peterson, B., Poole, G.C., Valett, H.M., Arango, C., Beaulieu, J.J., Burgin, A.J., Crenshaw, C., Helton, A.M., Johnson, L., Merriam, J., Niederlehner, B.R., O'Brien, J.M., Potter, J.D., Sheibley, R.W., Thomas, S.M. and Wilson, K. (2010) Inter-regional comparison of land-use effects on stream metabolism. Freshwater Biology 55(9), 1874-1890, https://doi.org/10.1111/j.1365-2427.2010.02422.x.

Bott, T.L., Montgomery, D.S., Newbold, J.D., Arscott, D.B., Dow, C.L., Aufdenkampe, A.K., Jackson, J.K. and Kaplan, L.A. (2006) Ecosystem metabolism in streams of the Catskill Mountains (Delaware and Hudson River watersheds) and Lower Hudson Valley. Journal of the North American Benthological Society 25(4), 1018-1044, https://doi.org/10.1899/0887-3593(2006)025[1018:Emisot]2.0.Co;2.

Davies-Colley, R.J. and Rutherford, J.C. (2005) Some approaches for measuring and modelling riparian shade. Ecological Engineering 24(5), 525-530, https://doi.org/10.1016/j.ecoleng.2004.01.006.

Demars, B.O.L., Russell, M.J., Ólafsson, J.S., Gíslason, G.M., Gudmundsdóttir, R., Woodward, G., Reiss, J., Pichler, D.E., Rasmussen, J.J. and Friberg, N. (2011) Temperature and the metabolic balance of

streams. Freshwater Biology 56(6), 1106-1121, https://doi.org/10.1111/j.1365-2427.2010.02554.x.

Dupas, R., Musolff, A., Jawitz, J.W., Rao, P.S.C., Jäger, C.G., Fleckenstein, J.H., Rode, M. and Borchardt, D. (2017) Carbon and nutrient export regimes from headwater catchments to downstream reaches. Biogeosciences 14(18), 4391-4407, https://doi.org/10.5194/bg-14-4391-2017.

Ensign, S.H. and Doyle, M.W. (2006) Nutrient spiraling in streams and river networks. Journal of Geophysical Research: Biogeosciences 111(G4), https://doi.org/10.1029/2005JG000114.

Gomez-Velez, J.D., Harvey, J.W., Cardenas, M.B. and Kiel, B. (2015) Denitrification in the Mississippi River network controlled by flow through river bedforms. Nature Geoscience 8, 941-945, https://doi.org/10.1038/ngeo2567.

Grant, S.B., Azizian, M., Cook, P., Boano, F. and Rippy, M.A. (2018) Factoring stream turbulence into global assessments of nitrogen pollution. Science 359(6381), 1266-1269, https://doi.org/10.1126/science.aap8074.

Griffiths, N.A., Tank, J.L., Royer, T.V., Roley, S.S., Rosi-Marshall, E.J., Whiles, M.R., Beaulieu, J.J. and Johnson, L.T. (2013) Agricultural land use alters the seasonality and magnitude of stream metabolism. Limnology and Oceanography 58(4), 1513-1529, https://doi.org/10.4319/lo.2013.58.4.1513.

Heffernan, J.B. and Cohen, M.J. (2010) Direct and indirect coupling of primary production and diel nitrate dynamics in a subtropical spring-fed river. Limnology and Oceanography 55(2), 677-688, https://doi.org/10.4319/lo.2010.55.2.0677.

Helton, A.M., Poole, G.C., Meyer, J.L., Wollheim, W.M., Peterson, B.J., Mulholland, P.J., Bernhardt, E.S., Stanford, J.A., Arango, C., Ashkenas, L.R., Cooper, L.W., Dodds, W.K., Gregory, S.V., Hall, R.O., Hamilton, S.K., Johnson, S.L., McDowell, W.H., Potter, J.D., Tank, J.L., Thomas, S.M., Valett, H.M., Webster, J.R. and Zeglin, L. (2011) Thinking outside the channel: modeling nitrogen cycling in networked river ecosystems. Frontiers in Ecology and the Environment 9(4), 229-238, https://doi.org/10.1890/080211.

Hensley, R.T. and Cohen, M.J. (2016) On the emergence of diel solute signals in flowing waters. Water Resources Research 52(2), 759-772, https://doi.org/10.1002/2015WR017895.

Jackson-Blake, L.A., Sample, J.E., Wade, A.J., Helliwell, R.C. and Skeffington, R.A. (2017) Are our dynamic water quality models too complex? A comparison of a new parsimonious phosphorus model, SimplyP, and INCA-P. Water Resources Research 53(7), 5382-5399, https://doi.org/10.1002/2016WR020132.

Julian, J.P., Doyle, M.W. and Stanley, E.H. (2008) Empirical modeling of light availability in rivers. Journal of Geophysical Research: Biogeosciences 113(G3), https://doi.org/10.1029/2007JG000601.

Kamjunke, N., Mages, M., Büttner, O., Marcus, H. and Weitere, M. (2015) Relationship between the elemental composition of stream biofilms and water chemistry—a catchment approach. Environmental Monitoring and Assessment 187(7), 432, https://doi.org/10.1007/s10661-015-4664-6.

Kirchner, J.W. (2006) Getting the right answers for the right reasons: Linking measurements, analyses, and models to advance the science of hydrology. Water Resources Research 42(3), https://doi.org/10.1029/2005WR004362.

Kunz, J.V., Hensley, R., Brase, L., Borchardt, D. and Rode, M. (2017) High frequency measurements of reach scale nitrogen uptake in a fourth order river with contrasting hydromorphology and variable water chemistry (Weiße Elster, Germany). Water Resources Research 53(1), 328-343, https://doi.org/10.1002/2016WR019355.

Mulholland, P.J., Fellows, C.S., Tank, J.L., Grimm, N.B., Webster, J.R., Hamilton, S.K., Martí, E., Ashkenas, L., Bowden, W.B., Dodds, W.K., Mcdowell, W.H., Paul, M.J. and Peterson, B.J. (2001) Inter-biome comparison of factors controlling stream metabolism. Freshwater Biology 46(11), 1503-1517, https://doi.org/10.1046/j.1365-2427.2001.00773.x.

Mulholland, P.J., Helton, A.M., Poole, G.C., Hall, R.O., Hamilton, S.K., Peterson, B.J., Tank, J.L., Ashkenas, L.R., Cooper, L.W., Dahm, C.N., Dodds, W.K., Findlay, S.E.G., Gregory, S.V., Grimm, N.B., Johnson, S.L., McDowell, W.H., Meyer, J.L., Valett, H.M., Webster, J.R., Arango, C.P., Beaulieu, J.J., Bernot, M.J., Burgin, A.J., Crenshaw, C.L., Johnson, L.T., Niederlehner, B.R., O'Brien, J.M., Potter, J.D., Sheibley, R.W., Sobota, D.J. and Thomas, S.M. (2008) Stream denitrification across biomes and its response to anthropogenic nitrate loading. Nature 452, 202-205, https://doi.org/10.1038/nature06686.

O'Connor, B.L., Harvey, J.W. and McPhillips, L.E. (2012) Thresholds of flow-induced bed disturbances and their effects on stream metabolism in an agricultural river. Water Resources Research 48(8), https://doi.org/10.1029/2011WR011488.

Odum, H.T. (1956) Primary Production in Flowing Waters. Limnology and Oceanography 1(2), 102-117, https://doi.org/10.4319/lo.1956.1.2.0102.

Raymond, P.A., Zappa, C.J., Butman, D., Bott, T.L., Potter, J., Mulholland, P., Laursen, A.E., McDowell, W.H. and Newbold, D. (2012) Scaling the gas transfer velocity and hydraulic geometry in streams and small rivers. Limnology and Oceanography: Fluids and Environments 2(1), 41-53, https://doi.org/10.1215/21573689-1597669.

Riley, A.J. and Dodds, W.K. (2012) Whole-stream metabolism: strategies for measuring and modeling diel trends of dissolved oxygen. Freshwater Science 32(1), 56-69, https://doi.org/10.1899/12-058.1.

Roberts, B.J. and Mulholland, P.J. (2007) In-stream biotic control on nutrient biogeochemistry in a forested stream, West Fork of Walker Branch. Journal of Geophysical Research: Biogeosciences 112(G4), https://doi.org/10.1029/2007JG000422.

Roberts, B.J., Mulholland, P.J. and Hill, W.R. (2007) Multiple Scales of Temporal Variability in Ecosystem Metabolism Rates: Results from 2 Years of Continuous Monitoring in a Forested Headwater Stream. Ecosystems 10(4), 588-606, https://doi.org/10.1007/s10021-007-9059-2.

Rode, M., Arhonditsis, G., Balin, D., Kebede, T., Krysanova, V., van Griensven, A. and van der Zee, S.E.A.T.M. (2010) New challenges in integrated water quality modelling. Hydrological Processes 24(24), 3447-3461, https://doi.org/10.1002/hyp.7766.

Rode, M., Halbedel née Angelstein, S., Anis, M.R., Borchardt, D. and Weitere, M. (2016a) Continuous In-Stream Assimilatory Nitrate Uptake from High-Frequency Sensor Measurements. Environmental Science & Technology 50(11), 5685-5694, https://doi.org/10.1021/acs.est.6b00943.

Rode, M., Wade, A.J., Cohen, M.J., Hensley, R.T., Bowes, M.J., Kirchner, J.W., Arhonditsis, G.B., Jordan, P., Kronvang, B., Halliday, S.J., Skeffington, R.A., Rozemeijer, J.C., Aubert, A.H., Rinke, K. and Jomaa,

S. (2016b) Sensors in the Stream: The High-Frequency Wave of the Present. Environmental Science & Technology 50(19), 10297-10307, https://doi.org/10.1021/acs.est.6b02155.
Samaniego, L., Kumar, R. and Attinger, S. (2010) Multiscale parameter regionalization of a grid-based hydrologic model at the mesoscale. Water Resources Research 46(5), https://doi.org/10.1029/2008WR007327.
Team, R.C. (2017) R: A Language and Environment for Statistical Computing, R Foundation for Statistical Computing, Vienna, Austria.
Tsivoglou, E.C. and Neal, L.A. (1976) Tracer Measurement of Reaeration: III. Predicting the Reaeration Capacity of Inland Streams. Journal (Water Pollution Control Federation) 48(12), 2669-2689, http://www.jstor.org/stable/25040082
Uehlinger, U. (2006) Annual cycle and inter-annual variability of gross primary production and ecosystem respiration in a floodprone river during a 15-year period. Freshwater Biology 51(5), 938-950, https://doi.org/10.1111/j.1365-2427.2006.01551.x.
Wollheim, W.M., Peterson, B.J., Thomas, S.M., Hopkinson, C.H. and Vörösmarty, C.J. (2008) Dynamics of N removal over annual time periods in a suburban river network. Journal of Geophysical Research: Biogeosciences 113(G3), https://doi.org/10.1029/2007JG000660.
Yang, X., Jomaa, S., Zink, M., Fleckenstein, J.H., Borchardt, D. and Rode, M. (2018) A new fully distributed model of nitrate transport and removal at catchment scale. Water Resources Research 54(8), 5856-5877, https://doi.org/10.1029/2017WR022380.
Ye, S., Reisinger, A.J., Tank, J.L., Baker, M.A., Hall Jr., R.O., Rosi, E.J. and Sivapalan, M. (2017) Scaling Dissolved Nutrient Removal in River Networks: A Comparative Modeling Investigation. Water Resources Research 53(11), 9623-9641, https://doi.org/10.1002/2017WR020858.

3.7. Supplementary Materials

Text S3.1. Metabolic rates calculations (single-station method by Odum (1956).

(1) The gas transfer coefficient K

The gas transfer coefficient at 20 ℃ (K_2) was calculated based on the energy dissipation method originally from Tsivoglou and Neal (1976).

$$K_2 = \begin{cases} 0.177\left(\frac{\Delta h}{t_f}\right) = 15300\ (s\,m^{-1}d^{-1}), Q > 0.56\,m^3s^{-1} \\ 0.25\left(\frac{\Delta h}{t_f}\right) = 21300\ (s\,m^{-1}d^{-1}), 0.28\ < Q < 0.56\,m^3s^{-1} \\ 0.36\left(\frac{\Delta h}{t_f}\right) = 28300\ (s\,m^{-1}d^{-1}), Q < 0.28\,m^3s^{-1} \end{cases} \quad \text{(S3.1)}$$

Where hydraulic properties: Δh is the change in elevation head and t_f is the time of flow. Dupas et al. (2016) corrected K_2 with slope(S), flow velocity (V) and temperature (T) and obtained the coefficient (K) at given water temperature (Bott et al., 2006):

$$K = K_2 SV \times 1.024^{(T-20)}/(24 \times 60) \quad \text{(S3.2)}$$

Since our sensor data were 15min, all the calculation were performed at 15min resolution. Therefore the unit of K is (min^{-1}).

(2) The DO deficit D

$$D = DO_{100\%sat} - DO_{meas} \quad \text{(S3.3)}$$

$$DO_{100\%sat} = (-0.04884853 + 0.019158425 * P_{air} - 0.0008395 * T - 0.00057798 * T^2)/(1 - 0.0000076485 * P_{air} + 0.028348446 * T + 0.0000652821 * T^2 - 0.0000018179 * T^3) \quad \text{(S3.4)}$$

Where P_{air} is the air pressure (mm Hg).

(3) Reaeration flux EX ($g\ O_2\ m^{-3}\ min^{-1}$)

$$EX = K \times D \quad \text{(S3.5)}$$

(4) The night-time respiration rate per time interval (15min) ER_n ($mg\ O_2\ m^{-2}\ 15min^{-1}$)

$$ER_{ni} = (\Delta DO_i - EX_i) \times Depth \quad \text{(S3.6)}$$

$$\overline{ER_n} = \frac{1}{M}\sum_{i=1}^{M}(ER_{ni}) \quad \text{(S3.7)}$$

Where $\overline{ER_n}$ is the averaged ER per time interval. M is the number of the night-time increments, $Depth$ is the water depth. We assumed that the day-time respiration (ER_d) is the same as the night-time respiration ($\overline{ER_n}$). Therefore,

(5) The daily gross primary production GPP ($mg\ O_2\ m^{-2}\ d^{-1}$)

$$GPP = \sum_{i=1}^{96-M}((\Delta DO_i - EX_i) \times Depth) + ER_d \times (96 - M) \quad \text{(S3.8)}$$

Where $\sum_{i=1}^{96-M}((\Delta DO_i - EX_i) \times Depth)$ is the sum of DO changes at the day time period and the $ER_d \times (96 - M)$ is the sum of ER flux at the day time period. $96 - M$ is the number of the day-time increments. Note that $96 = 24 \times \frac{60}{15}$ is the total number of increments in 24 hours.

(6) The daily ecosystem respiration ER ($mg\ O_2\ m^{-2}\ d^{-1}$)

$$ER = M \times \overline{ER_n} + ER_d \times (96 - M) \quad \text{(S3.9)}$$

(7) The net ecosystem production NEP ($mg\ O_2\ m^{-2}\ d^{-1}$)

$$NEP = GPP - ER \quad \text{(S3.10)}$$

Text S3.2. Theoretical Global radiation calculations (Allen et al., 1998).

(1) Extraterrestrial radiation (R_a), the solar radiation received at the top of the earth's atmosphere on a horizontal surface. It can be estimated for each day of the year and for different latitudes from the solar constant (G_{sc}), the solar declination (δ) and the time of the year.

$$R_a = \frac{24\times60}{\pi} G_{sc} d_r [\omega_s \sin(\varphi) \sin(\delta) + \cos(\varphi)\cos(\delta)\sin(\omega_s)] \quad \text{(S3.11)}$$

Where

R_a extraterrestrial radiation $[MJm^{-2}d^{-1}]$,

$G_{sc} = 0.0820[MJm^{-2}min^{-1}]$ solar constant,

$d_r = 1 + 0.033\cos(\frac{2\pi}{365}k)$ inverse relative distance Earth-Sun,

$\omega_s = arccos[-\tan(\varphi)\tan(\delta)]$ sunset hour angle,

φ latitude,

$\delta = 0.409\sin(\frac{2\pi}{365}k - 1.39)$ solar declination,

and k is the number of the day in the year between 1 and 365 (366).

(2) Daylight hours (N)

$N = \frac{24}{\pi}\omega_s$

(3) Global radiation (GR)

$$GR = R_a(a + b\frac{n}{N}) \quad \text{(S3.12)}$$

Where n is the actual duration of sunshine, a is the fraction of extraterrestrial radiation reaching the earth on overcast days ($n = 0$), and $a + b$ is the fraction of extraterrestrial radiation reaching the earth on clear days ($n = N$). Here the parameters were determined as 0.20 and 0.57, respectively, based on values of stations Braunschweig, Seehausen and Braunlage, Germany.

Table S3.1. Geographical and meteorological comparison between upper and lower Selke subcatchments. Mean discharge and nutrient concentrations are the values observed at the two stations. $N - NO_3^-$ and SRP represent nitrate-N and soluble reactive phosphorus, respectively.

Attributes	Upper Selke subcatchment	Lower Selke subcatchment
Area (km^2)	184	272
Mean elevation (m)	410	140
Mean annual precipitation (mm)	790	450
Mean temperature (°C)	6.7	9.8
Mean discharge (m^3/s)	1.52 (Meisdorf)	1.75 (Hausneindorf)
Mean $N - NO_3^-$ concentration (mg l^{-1})	1.60 (Meisdorf)	3.61 (Hausneindorf)
Mean SRP concentration (mg l^{-1})	0.039 (Meisdorf)	0.040 (Hausneindorf)
Dominant land use	Forest (72%)	Agricultural land (80%)
Dominant soil type	Cambisols	Chernozems
Dominant geology	Schist/Claystone	Tertiary sediments/Loess

Table S3.2. Seasonal mean uptake percentage at the Selke river network. Based on ANOVA analysis, the vegetation types were catagoried because its interaction terms with season and order were both significant, while the interaction term of season and order was not significant. *There was only one 5th order stream at the outlet.

Vegetation	Season	Order					*Beta*
		1st	2nd	3rd	4th	5th *	
Forest streams (n=124)	Spring	22.45	17.48	4.91	2.69	--	--
	Summer	24.10	16.49	8.80	3.17	--	*0.04*
	Autumn	11.48	8.36	2.56	1.12	--	*-0.17*
	Winter	2.63	1.74	0.25	0.20	--	*-0.59*
	Beta	--	*-0.04*	*-0.12*	*-0.50*	--	
agricultural streams (n=91)	Spring	13.89	7.98	5.12	3.01	0.61	--
	Summer	25.56	16.47	8.41	9.91	1.76	*0.19*
	Autumn	6.21	3.56	1.83	1.91	0.37	*-0.21*
	Winter	0.84	0.45	0.35	0.17	0.04	*-0.70*
	Beta	--	*-0.13*	*-0.32*	*-0.31*	*-0.15*	
mixed streams (n=138)	Spring	15.63	10.92	6.13	5.72	--	--
	Summer	38.09	28.38	19.61	14.28	--	*0.22*
	Autumn	10.05	6.47	4.35	3.15	--	*-0.12*
	Winter	0.88	0.60	0.27	0.47	--	*-0.67*
	Beta	--	*-0.11*	*-0.25*	*-0.21*	--	

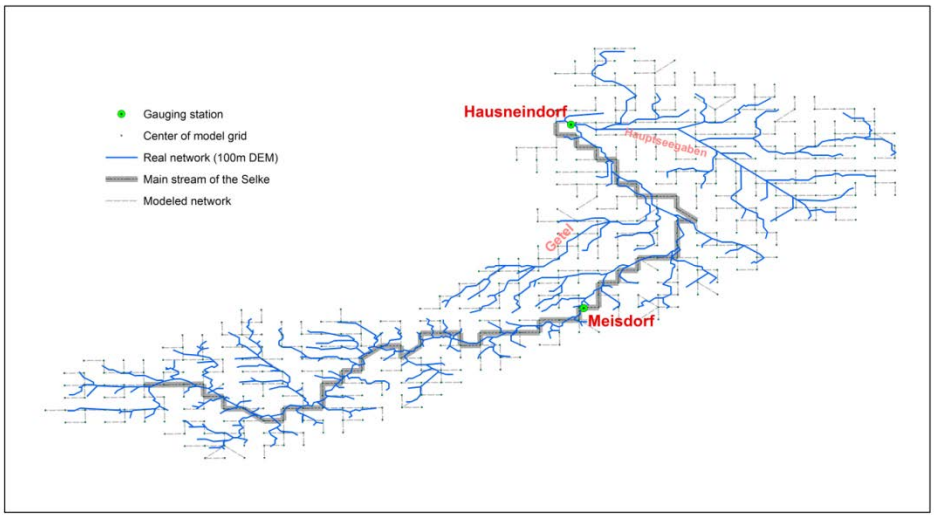

Figure S3.1. The Selke river networks. Blue lines represent the real river network generated from the 100 m DEM (digital elevation model) and topographic maps (source from the State Agency of Survey and Geoinforamtion of Saxony-Anhalt, Germany). Gray dashed lines represent the modeled river network in the mHM-Nitrate model. Bold shaded line represents the main stem of the Selke River from the model that involved in the longitudinal analysis.

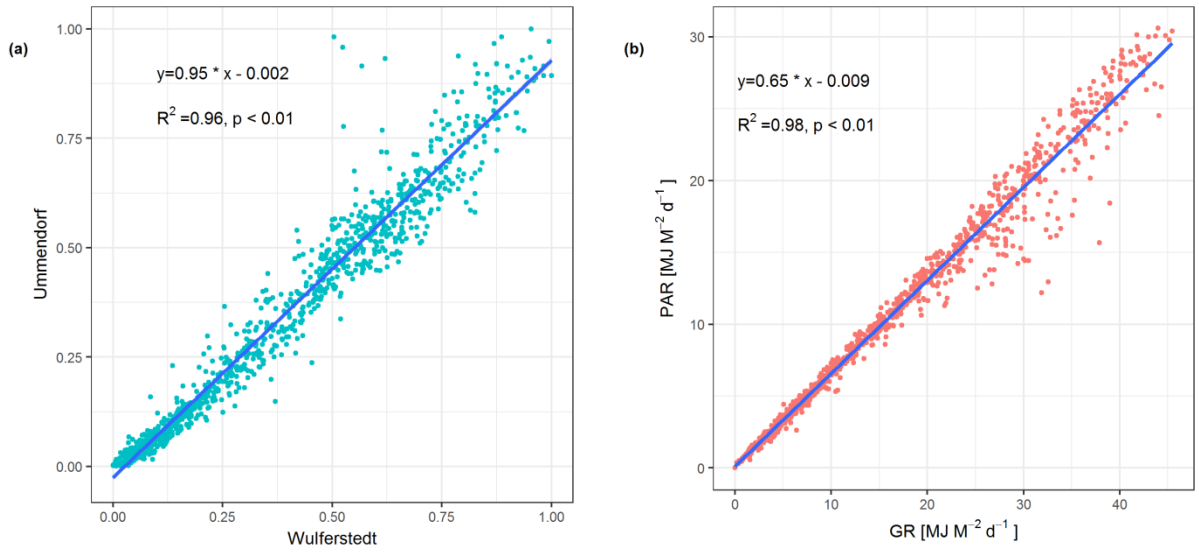

Figure S3.2. (a) The correlation between calculated global radiation (GR) at Ummendorf and measured GR at Wulferstädt (ca. 20 km north of station Hausneindorf). The data were smoothed and normalized as described in Equation 2 and 3. (b) The correlation between measured photosynthetically active radiation (PAR) and global radiation (GR) at station Wulferstädt (2013-2015).

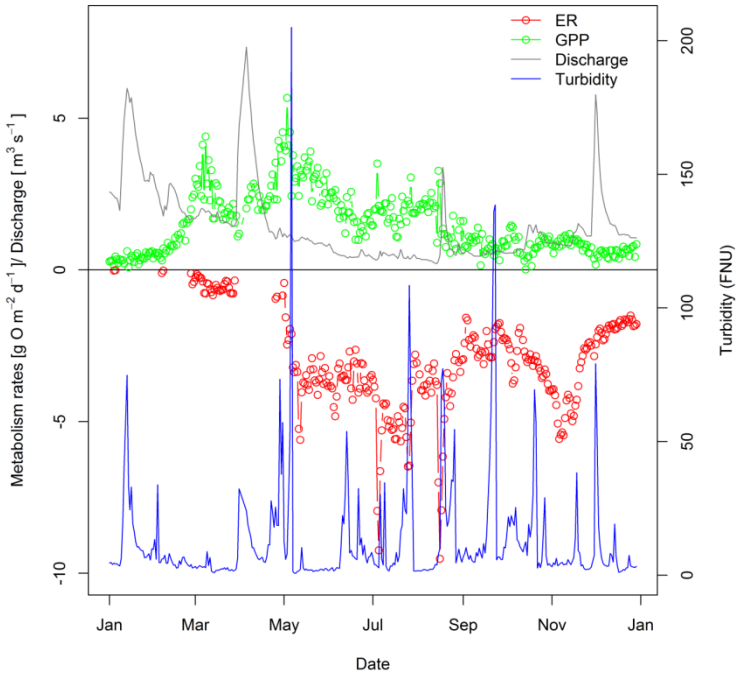

Figure S3.3. The dynamics of turbidity, discharge, GPP and ER in 2015 based on high frequency sensor data. GPP - Gross primary production and ER - ecosystem respiration.

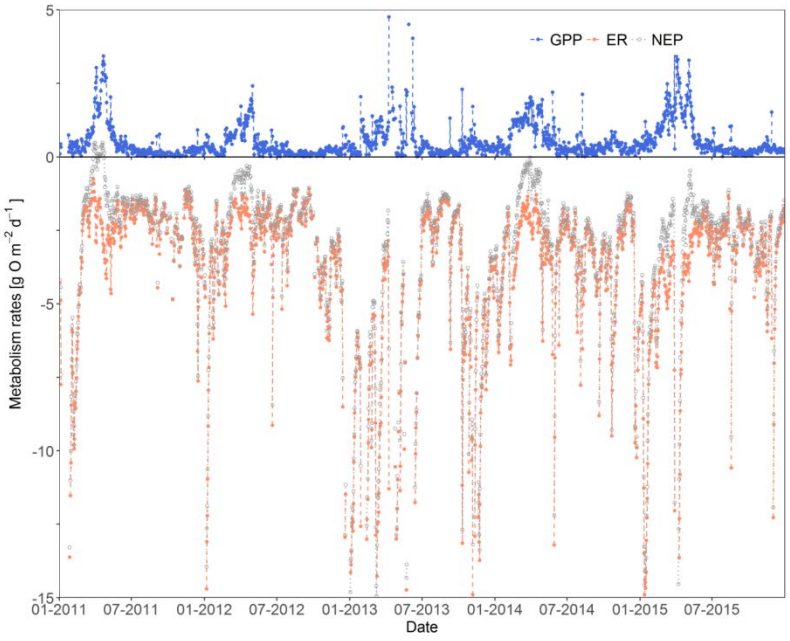

Figure S3.4. Daily metabolism rates (GPP: green line; ER: gray line; and net ecosystem production-NEP: orange line) at Meisdorf, representing typical forest streams. ER was shown as negative values for better visibility.

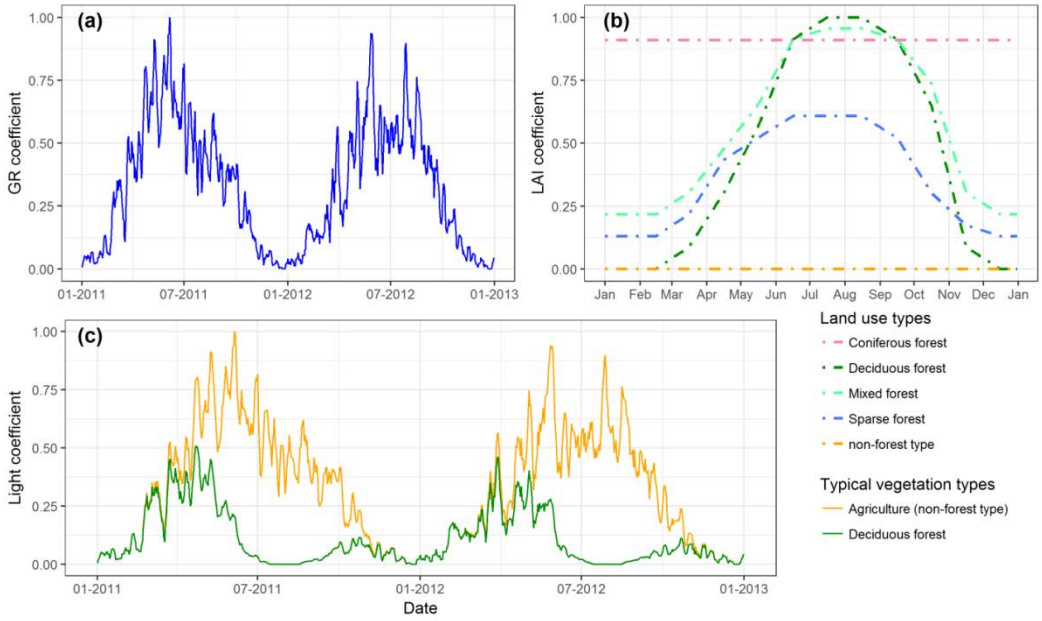

Figure S3.5. Coefficients of (a) global radiation impact (GR, only shown the first two years), (b) riparian shading (leaf area index - LAI) and (c) examples of overall coefficients of stream surface light availability in the purely agricultural stream and the purely deciduous forest stream, respectively.

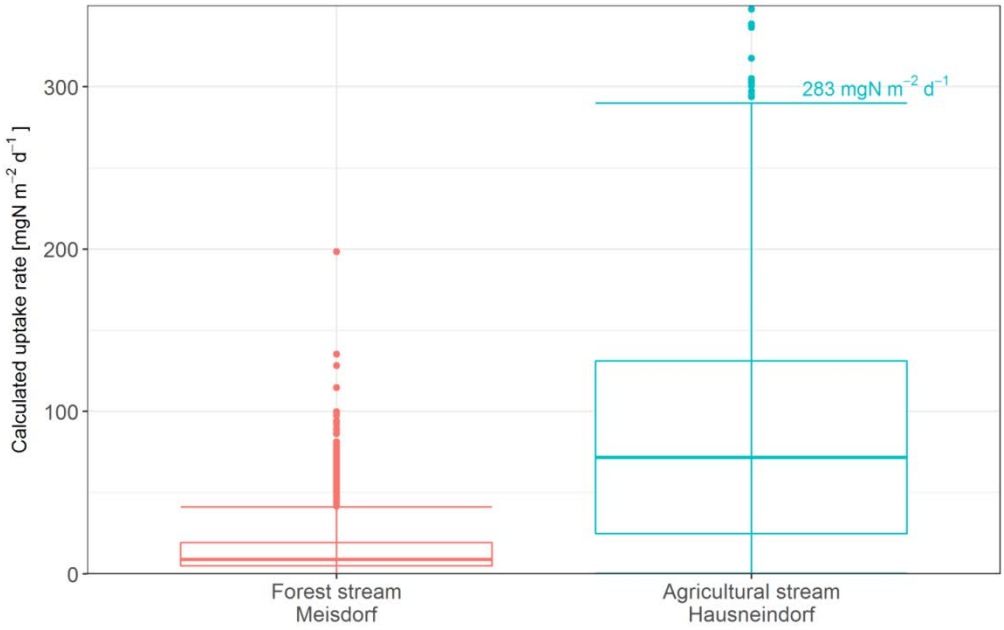

Figure S3.6. Boxplots of the GPP-based calculations of uptake rate at the two stations (Meisdorf and Hausneindorf). The upper whisker value was set to 1.5 interquartile ranges (IQR) of the upper quartile.

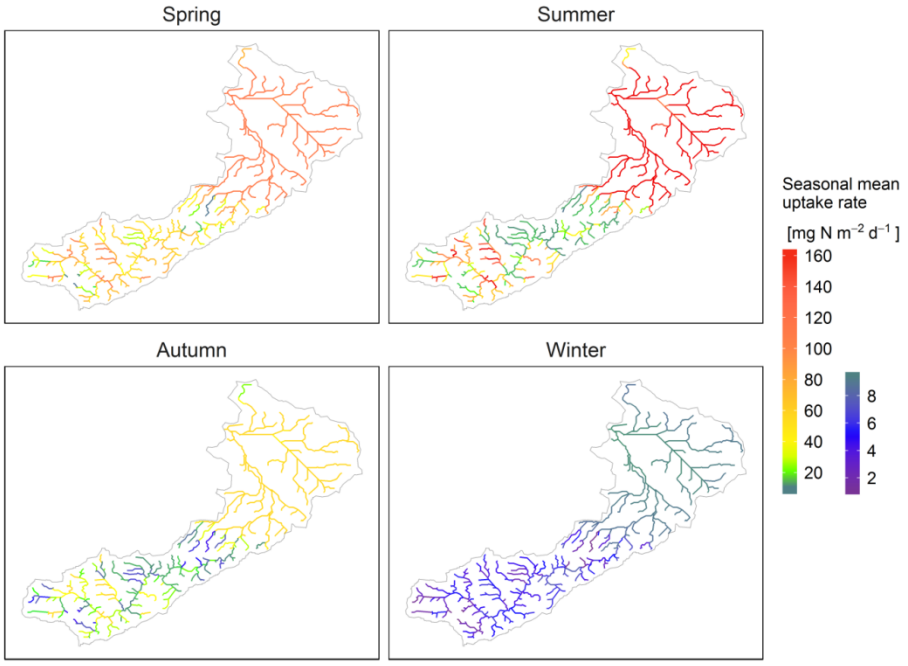

Figure S3.7. Seasonal mean autotrophic NO_3^- uptake rate ($U_{a-NO_3^{-1}}$) at the Selke river network.

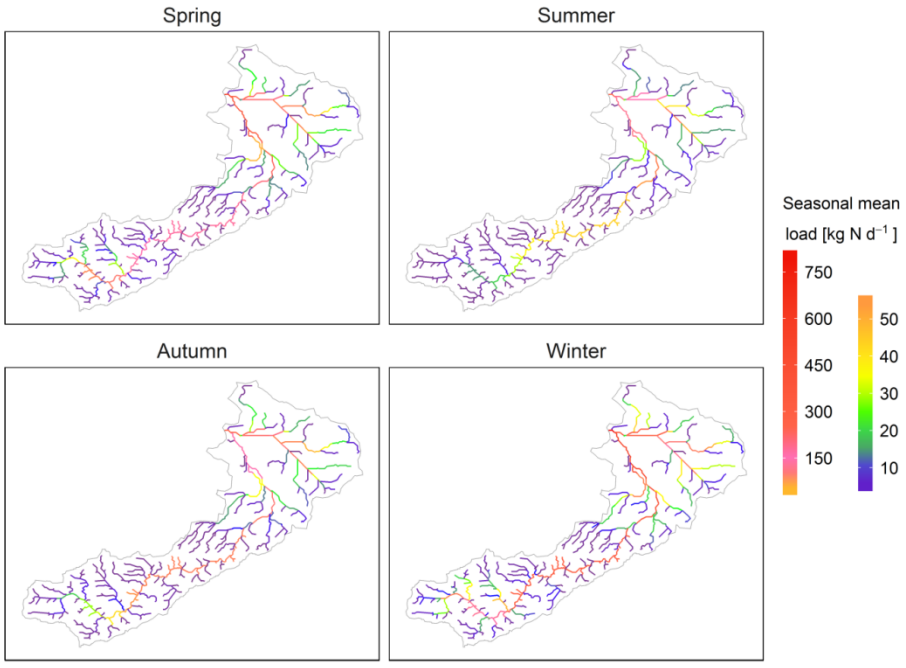

Figure S3.8. Seasonal mean NO_3^- load at the Selke river network.

Chapter 4: Sensitivity analysis of fully distributed model parameterization reveals insights into heterogeneous catchment responses for water quality modeling

Key points

- For the first time, sensitivity analysis of spatially distributed parameterization was conducted in catchment nitrate modeling
- Parameter sensitivity showed high spatial variability and correlated significantly with varying controlling factors at different locations
- Results revealed insights into heterogeneous nitrate behaviors and provided implications for future water quality model parameterization

4.1. Abstract

Spatially distributed parameterization is preferable in capturing heterogeneity of catchment properties and in allowing a better model representation of catchment responses. In hydrological modeling, sensitivity analysis is recommended to address the high-dimensional parametric problems. However, less has been focused on water quality modeling, presumably due to the lack of suitable fully distributed models. Based on the new mesoscale hydrological-nitrate model (mHM-Nitrate), we investigated for the first time the spatially distributed parameter sensitivity of the nitrate model and correlated the sensitivity indices with multiple catchment factors. The study was conducted in the highly heterogeneous Selke catchment, Germany. Three nested catchments were defined based on the heterogeneous catchment responses (gauged by three nested stations). Results showed that parameters of soil denitrification, in-stream denitrification and in-stream assimilatory uptake were the most sensitive parameters throughout the catchment, while they all showed high spatial variability, which also varied when different gauging stations were considered. Spearman rank correlation indicated that the sensitivity of soil denitrification was controlled mainly by the relative limitations between terrestrial hydrological transport capacity and soil nitrate availability; the sensitivity of in-stream processes was predominated by spatial variability within the river network (e.g., proximity to the gauging station), rather than the local biogeochemical factors. Based on the insights gained from the spatial sensitivity and correlation analyses, we suggested that an appropriate monitoring scheme is important in reflecting actual catchment responses, and a cautious statistical correlation is informative in benefiting future parameter regionalization of water quality models.

4.2. Introduction

Non-point source pollution due to intensive agricultural activities has become one of the major causes blamed for water quality deterioration (EEA, 2005). Catchment water quality models have been widely accepted in formulizing the current understanding of catchment functioning, and further guiding mitigation measures to protect and improve our living environment (Rode et al., 2010; Wellen et al., 2015). In the context of specific process descriptions, the model applicability depends mainly on the spatial discretization of forcing data and the appropriateness of parameterization (Beven, 1993; Wagener et al., 2001; Clark et al., 2015). By allowing the forcing data to vary spatially, fully distributed models are particularly preferable in pursuing a better representation of the spatial variability of catchment properties. Meanwhile, such model structure offers high potential for spatially differentiated parameterization to better capture heterogeneous catchment responses. However, the cost of the largely increased complexity has also been well documented (Razavi & Gupta, 2016; Sheikholeslami et al., 2019), e.g., the complexity of high-dimensional, nonlinear parameter spaces. Such high model complexity inhibits identification of appropriate parameter values and diagnostic of model behaviors (Gupta et al., 2008; Pianosi et al., 2016). Efforts have been made to address the parametric difficulties in hydrological modeling through, e.g., parameter regionalization (Oudin et al., 2008; Samaniego et al., 2010) and spatially explicit configurations (Tang et al., 2007; Herman et al., 2013a, b). However, few studies have focused on the added water quality modeling.

Excessive nitrate export is one of the main reasons for water pollutions and eutrophication (Yu et al., 2019). Nitrate terrestrial leaching and in-stream transport are mostly driven by hydrological processes. In the process of adding on significant anthropogenic impacts, catchment nitrate behaviors show a higher degree of spatial heterogeneity than the hydrological basics (e.g., Yang et al. (2018)). Aiming to balance the process representation and the model complexity in process-based modeling (Rode et al., 2010), the conceptualization and parameterization of the processes are normally formulated in two parts: (1) the impacts of known factors are quantified through empirical equations, e.g., the temperature impacts on denitrification (Stanford et al., 1975); and (2) the impacts of biogeochemical reactions are reflected by model parameters (referred as reaction “rate”). These rates are usually assigned as land-cover/soil type dependent in catchment model developments, partially intending to be compatible with the hierarchical structure of semi-distributed models (i.e., catchment, subcatchments and basic calculating units) (Wade et al., 2002; Huang et al., 2009; Lindström et al., 2010). However, such parameterization scheme restricts the parameter only to land-cover or soil information, which likely underestimates the spatial heterogeneity and its relevance in nature (Clark et al., 2017).

Alternatively, fully distributed parameterization provides the opportunity to spatially link the reaction rates with multiple catchment factors, including meteorological forcing, catchment characteristics and modelled state variables and fluxes. However, the number of available models and their applications are still limited (see the review by Wellen et al. (2015)), especially in larger catchments (e.g., > 200 km^2). Recently, Yang et al. (2018) developed a fully distributed catchment nitrate model (i.e., the mHM-Nitrate model) based on the gridded implementations of the mesoscale Hydrological Model (mHM) (Samaniego et al., 2010; Kumar et al., 2013). The model balances the spatial representation and the model complexity using the multi-resolution structure and the multiscale parameter regionalization (MPR) technique (Samaniego et al., 2010). The model has been evaluated in terms of reproducing well heterogeneous flow and nitrate concentration and providing reliable detailed spatial information of flow and nitrate fluxes (Yang et al., 2018). In addition, the in-stream autotrophic assimilation has been regionalized and improved based on the high-frequency sensor data (Yang et al., 2019). The model is, therefore, a promising tool to further investigate the spatially distributed parameterization of the biogeochemical reactions and their links with multiple catchment information.

Sensitivity analysis (SA) has long been taken as a foundational diagnostic approach in revealing insights into the model responses regarding variations in *input factors*, including model parameters (Razavi & Gupta, 2015; Pianosi et al., 2016). It is still challenging to accurately estimate the sensitivity indices (Gupta & Razavi, 2018), especially for the spatially distributed configuration. Therefore, parameter ranking and screening are more interesting for the earth and environmental system modeling community (Sheikholeslami et al., 2019). They are commonly recommended to reduce the dimensionality by determining the (non-)informative parameters (e.g., Cuntz et al. (2015)) and to identify spatially differentiated model controls under varying conditions (e.g., the impacts of spatial distributions of event-scale precipitation (Tang et al., 2007; van Werkhoven et al., 2008b)). Meanwhile, consistent model performance could be achieved under parameter-/cell-based screening strategies (Tang et al., 2007). Fully spatiotemporal distribution of parameter sensitivity by Herman et al. (2013a) explicitly revealed that different processes dominated in different periods and at different locations of the catchment. However, most of the grid-based studies only qualitatively attribute the spatial variations of parameter sensitivity to the variations of catchment factors, while ignoring further information that can be derived from the quantitative correlation investigation. For instance, van Werkhoven et al. (2008a) demonstrated significant correlations between parameter sensitivity and catchment factors in 12 catchments, which further extended the number of identifiable parameters more than usually assumed.

In this study, we revise the parameterization scheme for the nitrate processes of the mHM-Nitrate model in a fully spatially distributed manner, i.e., each nitrate submodel parameter varies independently in each grid cell (for terrestrial parameters) or each stream reach (for stream parameters). By conducting the global parameter SA, spatial distributions of parameter sensitivity indices are obtained, revealing the relative importance of each nitrate process and its spatial variability. Further, the spatial sensitivity information is correlated with a wide range of catchment factors in each grid cell/stream reach, including meteorological forcing, catchment characteristics and modeled state variables and fluxes of flow and nitrate. We conduct our analysis in the highly heterogeneous Selke catchment (in terms of geographic characteristics, meteorological conditions and impacts of human activities), where three nested gauging stations are deployed to capture the heterogeneous catchment responses (Yang et al., 2018). The objectives of this study are (1) to analyze the full-spatial variability of parameter sensitivity in the domain of process-based catchment water quality modeling, (2) to determine the most influential catchment factors for sensitive nitrate processes and the spatial variation of such correlations, and (3) to reveal insights into nitrate responses of heterogeneous meteor-hydrological and anthropogenic conditions at catchment scale. The anticipant insights can provide implications on future parameter regionalization of catchment water quality modeling.

4.3. Methodology

4.3.1. Morris method

The method of Morris (1991), also called Elementary Effect (EE) test, is a multi-starts perturbation sensitivity analysis method (Pianosi et al., 2016). Based on the one-at-a-time (OAT) method, an individual trajectory is created by perturbing each parameter p_i by a variation Δ_i. The number of perturbations of each trajectory is equal to the number of parameters ($n, i = 1,2, \cdots n$). Elementary effect of the i^{th} parameter (EE_i) is, therefore, estimated as follows:

$$EE_i = \frac{f(X|_{p_i+\Delta_i}) - f(X|_{p_i})}{\Delta_i}, \tag{4.1}$$

where $f(X)$ denotes the evaluation metrics used for sensitivity analysis. Here we used two metrics: the Root-Mean-Squared-Error (RMSE) and the Kling-Gupta Efficiency (KGE) (Gupta et al., 2009). Starting from multiple points within the feasible parameter space, multiple trajectories (r) are generated to compute the sensitivity indices, i.e., the mean of EEs (μ_i^*) denoting the global sensitivity of each parameter, and the standard deviation of EEs (σ_i) denoting the interaction with other parameters. Eq.(4.2) gives the calculations of these indices suggested by Campolongo et al. (2007):

$$\mu_i^* = \frac{1}{r}\sum_{j=1}^{r}\left|EE_i^j\right|, \sigma_i = \sqrt{\frac{1}{r-1}\sum_{j=1}^{r}\left(EE_i^j - \mu_i^*\right)^2}, \quad (4.2)$$

where EE_i^j denotes EE_i of the j^{th} trajectory.

Sampling strategies differ mainly in the starting-point sampling and the trajectory generation. A proper sampling strategy can efficiently improve the accuracy of the sensitivity estimates (Pianosi et al., 2016). Aiming to balance the sampling efficiency and coverage within the feasible space, we used the Latin-Hypercube sampling method (van Griensven et al., 2006) to generate the starting points and Δ_i. Instead of sequential trajectory, we used the radial-based OAT design (Campolongo et al., 2011) to generate the trajectories. This approach takes Δ_i for each p_i all from the starting point of each trajectory, which has been proofed to be more efficient (Campolongo et al., 2011). The SA was performed using the SAFE (Sensitivity Analysis For Everybody) tool by Pianosi et al. (2015).

Morris method requires $n + 1$ model runs for each trajectory and $r \times (n + 1)$ runs for computing the global sensitivity indices. The computation requirement of Morris method is far lower than the majority of other all-at-a-time based methods (Pianosi et al., 2016). This advantages its utility for SA of spatially distributed parameterization, which is characterized as a high-dimensional, time-consuming problem. The method is also particularly suitable and efficient for the purposes of ranking and screening (Herman et al., 2013b; Pianosi et al., 2016).

4.3.2. Spearman rank correlation

Based on the sensitivity results, we further correlated the parameter indices with catchment factors using the Spearman rank correlation. The Spearman rank correlation can be taken as a non-parametric version of the Pearson correlation, and is normally performed when the assumptions of the Pearson correlation (i.e., normality and linearity) cannot be fulfilled. It measures the strength and direction of the monotonic relationship between rankings of two variables, which are assumed to be independent. The monotonic relationship is not strictly an assumption, but a measure to determine if there is a monotonic component associated between the two variables. The Spearman coefficient (ρ) is calculated to assess the correlation strength and direction:

$$\rho = 1 - \frac{6\sum d}{N(N^2-1)} \quad (4.3)$$

where N denotes the number of activated grid cells in this study; and d denotes the ranking distance. The positive ρ value denotes positive correlation, and vice versa.

4.3.3. The catchment hydrological nitrate model - mHM-Nitrate

The mHM-Nitrate model is a fully distributed, process-based catchment nitrate model (Yang et al., 2018). The model is developed based on the grid-based mesoscale Hydrological Model (mHM) platform (Samaniego et al., 2010; Kumar et al., 2013). Nitrate process descriptions are mainly introduced from the Hydrological Predictions of the Environment (HYPE) model (Lindström et al., 2010). The mHM-Nitrate model simulates state variables and fluxes of flow and nitrate in both terrestrial and in-stream phases at a daily step. In the terrestrial phase, along with hydrological processes, the nitrate submodel includes atmospheric deposition, fertilizer and manure supply, plant/crop uptake, denitrification, infiltration to different soil layers, percolation to deep groundwater and export to surface water. Physical and biochemical transformations between four nitrogen forms (i.e., dissolved inorganic nitrogen, dissolved organic nitrogen, active and inactive solid organic nitrogen) are considered for each soil layer and the pool sizes are updated for each time step. Total terrestrial exports of nitrate-N ($N-NO_3^-$) are calculated from four runoff components (i.e., direct runoff from impervious area, fast interflow, slow interflow and baseflow) and corresponding $N-NO_3^-$ concentrations therein. The exports from each grid cell are connected with neighboring cells according to the main flow direction, which formulates the modeled river network. A complete set of in-stream flow routing and nitrate processes (i.e., denitrification, assimilatory uptake and remineralization) is computed for each stream reach. Detailed model descriptions of mHM and mHM-Nitrate are given by Samaniego et al. (2010) and Yang et al. (2018), respectively.

Nitrate submodel parameters are parsimoniously introduced, representing individual or combined biogeochemical transformation(s) (**Table 4.1**). The model descriptions of soil denitrification, soil mineralization, soil degradation, soil dissolution and in-stream denitrification processes remain the same as the original mHM-Nitrate model (Yang et al., 2018). These transformations are conceptualized considering the impacts of the well-known physical factors, the availability of source nitrogen forms and the biogeochemical reaction rate. The pool sizes of nitrogen forms are updated for each simulation time step considering both physical flux exchanges and biogeochemical transformations. The impacts of well-known factors (e.g., soil or water temperature) are estimated using widely accepted empirical equations. The reaction rates are taken as model parameters listed in **Table 4.1**. These parameters have not yet been regionalized presumably due to the spatiotemporal complexity of the transformations and the limited direct observations for individual process. Therefore, as a normal procedure in water quality modeling, they are assigned as land-use dependent in the original mHM-Nitrate model.

The in-stream assimilatory uptake process has recently been refined based on a new regionalization approach proposed by Yang et al. (2019), where the autotrophic nitrate uptake is regionalized using global radiation (representing light availability above stream canopy), and leaf area index (representing the shading effect of riparian vegetation) data. Both types of data are normalized respectively to generate the time series of above-canopy light coefficients ($f_{GR,t}$) and the shading coefficients ($f_{LAI,t}$). The overall near-surface light coefficients ($f_{L,t} \in [0,1]$) are calculated as $f_{L,t} = f_{GR,t} \cdot \left(1 - f_{LAI}^{i}\right)$. The potential autotrophic uptake rate ($U_{a,max}, mg\ N\ m^{-2}d^{-1}$) is then introduced, as a model parameter, to calculate the actual autotrophic uptake rate (i.e., $U_{a,max} \cdot f_{L,t}$). The introduced parameter $U_{a,max}$ is a regionally transferable parameter. The rational and transferability of the approach have been validated in the agricultural and forested streams of the study catchment (the Selke catchment), where continuous daily autotrophic uptake data are available based on the high-frequency sensor monitoring. Based on the dataset, the parameter value for the Selke catchment is also obtained ($U_{a,max}$= 283 $mg\ N\ m^{-2}d^{-1}$). The approach has also been integrated into the mHM-Nitrate model for the networked uptake estimation, assuming stream riparian vegetation is similar as the surrounding land use (Yang et al., 2019). Therefore, we adopted the new approach in this study. Notably, part of the autotrophically assimilated nitrate can be re-mineralized and returned back to stream waters. Therefore, the parameter *npprt* was introduced and analyzed to represent the net assimilatory uptake rate (**Table 4.1**). Detailed descriptions of the transformations and parameterizations were provided in **Supporting Information** and references therein.

Table 4.1. Brief parameter descriptions of the nitrate submodel in the mHM-Nitrate model.

Parameter	Description	Biogeochemical transformation
denis	Rate of soil denitrification (d^{-1})	Permanent removal of nitrate in soil phase by denitrification process
minlr	Rate of soil mineralization (d^{-1})	From the dissolved and the active part of solid organic nitrogen pools to the nitrate pool in soil moisture by mineralization process
degdr	Rate of soil degradation (d^{-1})	From the inactive part of solid organic nitrogen pool to the active part of soil organic nitrogen pool by degradation process
dislr	Rate of soil dissolution (d^{-1})	From the active part of solid organic nitrogen pool to the dissolved organic pool in soil moisture by dissolution process
deniw	Rate of in-stream denitrification ($kg\ m^{-2}d^{-1}$)	Permanent removal of nitrate in stream water by denitrification process

npprt	Rate of in-stream net assimilatory uptake ($kg\ m^{-2}d^{-1}$)	Net removal of nitrate in the stream water due to assimilatory uptake and remineralization processes

The mHM-Nitrate model has a flexible structure, which balances the spatial representation and model complexity. The mHM platform integrates a multiscale parameter regionalization (MPR) technique (Samaniego et al., 2010): hydrological parameters are firstly related to geographic characteristics using a set of transfer functions at the basic geographic data level; then, the regionalized hydrological parameters are upscaled to the modeling level in the second step of MPR. Catchment characteristics (e.g., land-use proportions) and model inputs (e.g., meteorological forcing) are also scaled to the modeling level. Hydrological submodel parameters introduced in those transfer functions are taken as transferable and quasi scale-invariant (Kumar et al., 2013) and their sensitivities are well documented in Cuntz et al. (2015). Therefore, we exclusively focused on the nitrate submodel parameters.

4.4.4. Study site and model setup

The study was conducted in the Selke catchment (456 km^2, **Figure 4.1a**), a subcatchment of the Bode catchment in central Germany (The TERENO Harz/Central German lowland observatory (Wollschläger et al., 2016)). The catchment has strong physiographic gradients from upper mountainous areas to lowland areas: elevation decreases from 605 to 53 m, annual mean temperature increases from ca. 8 to ca. 10 ℃ and annual precipitation decreases from 790 to 450 mm (the overall mean of 660 mm). Agricultural lands dominate the lowland areas, whereas forests are predominant land-use type in the upper mountains, with considerable agricultural lands in the upper plateau (**Figure 4.1b**). Cambisols and chernozems are the main soil types in the upper and lower parts of the catchment, respectively; and shallow schist/claystone and deep tertiary sediments formulate the geological conditions, respectively (see details in Yang et al. (2018)). The shallow impermeable schist leads a preference of flashier flow path in the upper area, whereas flow path in the lowland area is deeper due to the permeable sedimentary materials (Jiang et al., 2014; Dupas et al., 2017).

Due to such high heterogeneity, three nested gauging stations (i.e., Silberhütte (SILB), Meisdorf (MEIS) and Hausneindorf (HAUS)) are located along the main stem of the Selke River (**Figure 4.1a**), monitoring discharge (Q) and $N-NO_3^-$ concentration behaviors and their longitudinal changes. Areas above station SILB (SILB catchment, 99 km^2) are predominated by forest (60%), with considerable arable lands (25%). Station MEIS locates at the exit of forested areas. Within areas above station MEIS (MEIS catchment,

184 km^2), the share of forest increased up to 72%. The area between station MEIS and the outlet HAUS is occupied mainly by arable land (almost 80%) and urban area. During high-flow conditions (e.g., $Q > 2\ m^3 s^{-1}$, the 3rd Quartile at HAUS), flow generates mostly from the upper mountains (Q at station MEIS accounts for 80 ± 15% of that at station HAUS). During low-flow periods ($Q < 0.65\ m^3 s^{-1}$, the 1st Quartile), upper and lower subareas contribute equivalently to the outlet discharge (62 ± 20% from the area above station MEIS). The region has long been intensively cultivated. The rotation sequence of four main crops (winter white, sugar beet, spring barley and rapeseed) was considered in all arable lands. Fertilizer and manure were applied in the middle-late spring, and the total amount ranges from 130-190 $kg\ N\ ha^{-1} yr^{-1}$ depending on specific crop type. Due to the long-term agricultural activities, $N - NO_3^-$ concentration in lowland soil water reaches up to higher than 25 $mg\ l^{-1}$. Although similar amount of fertilizer applies in the upper arable lands, the flashier flow path prevents nutrients accumulating in soil water and deeper groundwater (Dupas et al., 2017). Therefore, the ranges and seasonal patterns of $N - NO_3^-$ concentration at stations SILB and MEIS are similar (mean ± SD = 1.37 ± 1.08 and 1.60 ± 1.00 $mg\ l^{-1}$, respectively) but different from those at the outlet HAUS (3.61 ± 1.09 $mg\ l^{-1}$).

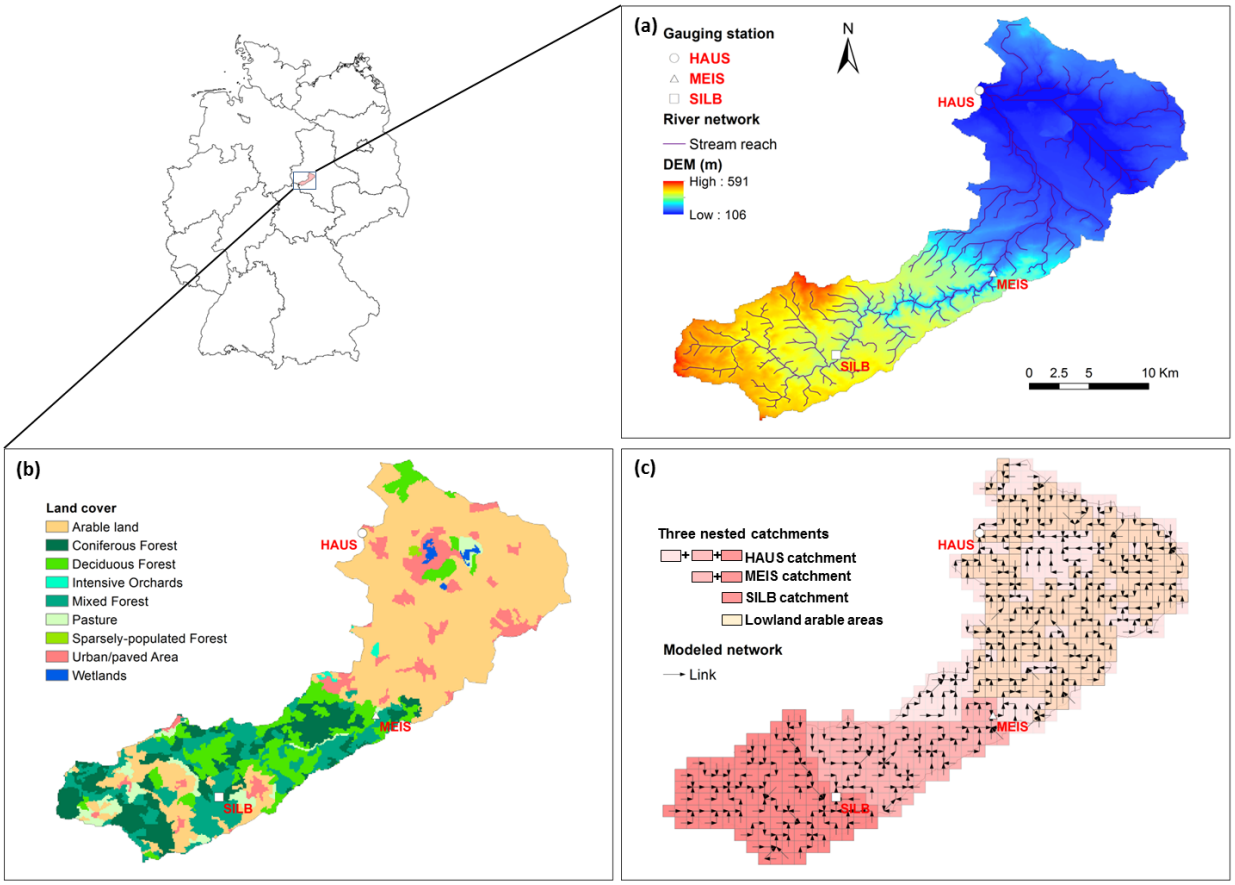

Figure 4.1. The Selke catchment, central Germany: (a) the locations of the nested gauging stations (i.e., Hausneindorf (HAUS), Meisdorf (MEIS) and Silberhütte (SILB)), river network and Digital Elevation Model (DEM); (b) the land cover types; and (c) the discretization and network connection of the mHM-Nitrate model and territories of the three nested catchments. Here we defined the nested catchment as the downstream catchment including the area of the upper one(s). Note that HAUS catchment represents the whole territory of the Selke catchment, and the lowland arable areas (the yellow-colored grid cells) represent areas in the lower part where areal proportion of arable land $>$ 0.70.

Daily simulation of the mHM-Nitrate model was set up in the Selke catchment using a 1 km^2 cell size for both terrestrial and in-stream phases. **Figure 4.1c** showed the model discretization of the Selke catchment (533 grid cells in total) and the grid cell connections (i.e., model river network, 532 stream reaches). Note that the area of the border grid cells can be < 1 km^2, depending on the actual area that belongs to the catchment. Basic data at geographic level were all resampled to 100 m resolution, and meteorological data from DWD (German Weather Service) were interpolated to 1 km^2 resolution. For details on data sources and model boundary conditions, please refer to Yang et al. (2018). Continuous daily discharge and $N-NO_3^-$ concentration in the period 2011-2015 were collected from LHW (the State Agency for Flood Protection and Water Management of Saxony-Anhalt, Germany) and the TERENO Project coordinated by Helmholtz Centre for Environmental Research – UFZ. The data at the three gauging stations were used to validate the mHM-Nitrate model performance and to calculate the evaluation metrics.

4.4. Computational design

Following the multi-objective calibration strategy by Yang et al. (2018), we firstly re-calibrated the mHM-Nitrate model against the daily observations of both discharge and nitrate concentration (2011-2015) at the three gauging stations. At this stage, nitrate submodel parameters remained as land-use dependent. The purpose of this step was to obtain hydrological and $N-NO_3^-$ simulations, in terms of (1) discharge and $N-NO_3^-$ concentrations at each stream reach, and (2) state variables and fluxes of both flow and $N-NO_3^-$ in each grid cell. Secondly, we revised the six nitrate submmodel parameters (**Table 4.1**) as grid cell/stream reach dependent. Therefore, we considered in total 3,196 parameters (533 × 4 = 2,132 and 532 × 2 = 1,064 parameters for the four terrestrial parameters and two stream parameters, respectively).

Given the large number of parameters, the computational load would increase sharply depending on the number of trajectories (r) of the Morris method. Pianosi et al. (2016) suggested 10-100 trajectories

would be sufficient (i.e., model runs are 10-100 times of total parameter number). Herman et al. (2013b) compared the Morris performances in hydrological modeling using different number of r and further referred them to a baseline performance of the Sobol' method (Sobol', 2001). They demonstrated that the performance of the low-sample Morris experiment is comparable with the baseline performance. In this study, we used relatively large number of trajectories (r = 80, resulting in the total number of model runs as 255,760) to ensure the robustness of the sensitivity results.

The sensitivity indices were calculated based on RMSE and KGE over the whole period (2011-2015). Since $N-NO_3^-$ responses differed largely at the three stations, we calculated parameter sensitivity indices for the three nested catchments (i.e., the SILB catchment, the MEIS catchment and the HAUS catchment, **Figure 4.1c**) based on the $N-NO_3^-$ concentration observations at station SILB, MEIS and HAUS, respectively. The HAUS catchment, covering the entire Selke catchment, was used to emphasize that the further calculations only used observations at the outlet station HAUS. The Spearman rank correlation between sensitivity indices and catchment factors was then performed for each of the nested catchment. Additionally, the correlations were also calculated exclusively for the lowland arable areas (i.e., areal proportion of arable land > 0.70, **Figure 4.1c**) in the domain of the HAUS catchment.

4.5. Results

The mHM-Nitrate model performed well in simulating both discharge and $N-NO_3^-$ concentration (**Supporting Information Figure S4.1**). Nash-Sutcliffe efficiency coefficients were ca. 0.80 and above 0.43 for discharge and $N-NO_3^-$ concentration simulations, respectively, at the three stations. Due to similar model setup and boundary conditions, results were in line with those provided by Yang et al. (2018), where detailed discussion of the model performance and rationality are provided. Catchment factors for each grid cell and each stream reach were, therefore, calculated and provided in **Supporting Information Data S4.1**, with selected factors provided in **Figure 4.2**.

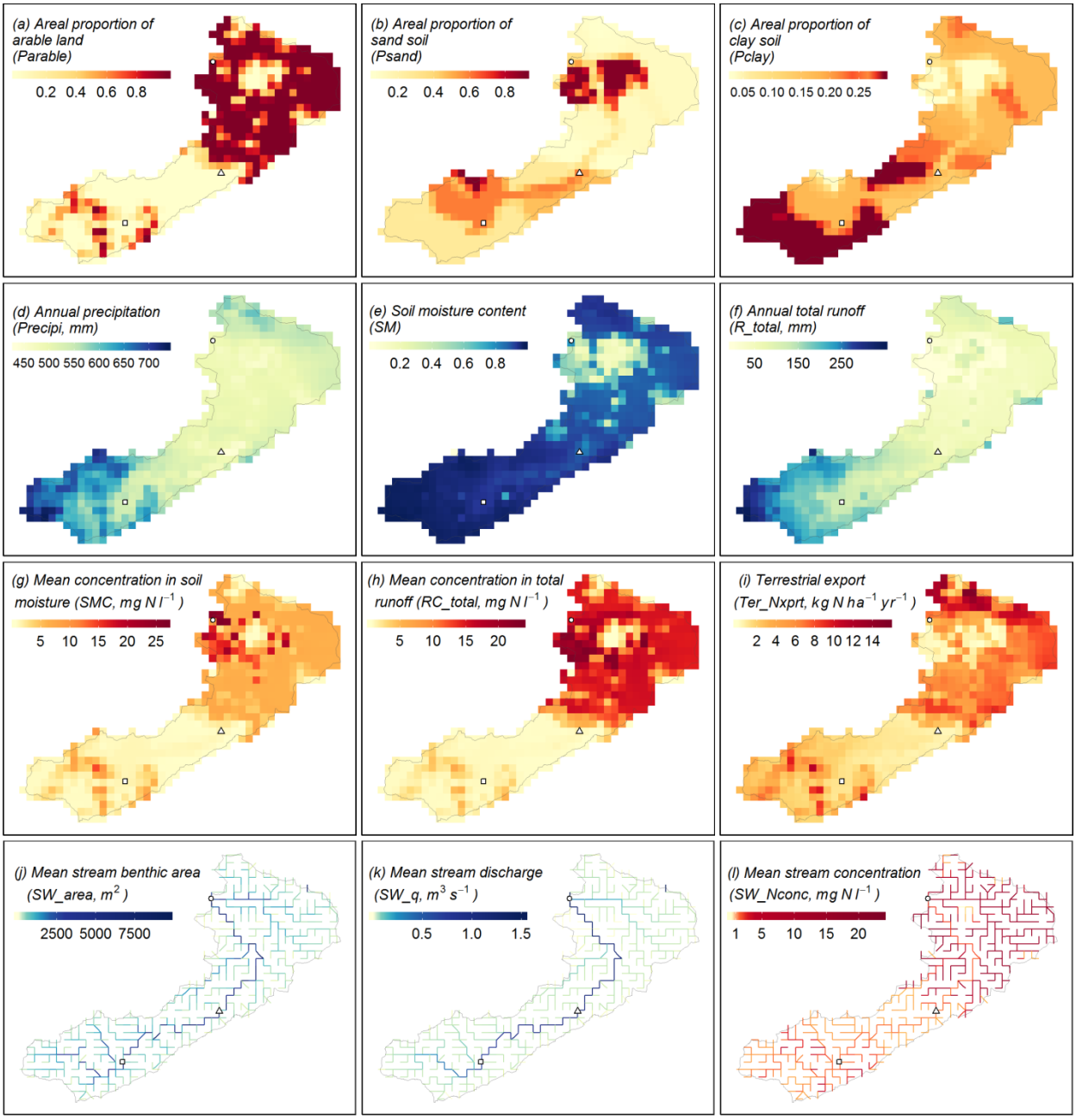

Figure 4.2. Spatial distributions of selected catchment factors, which are strongly supportive for the discussion. The title of each subplot instructed the brief meaning, abbreviation and unit of the presenting factor. Detailed explanations were given in **Appendix** (**Table A4.1**). For values of the complete set of catchment factors, please refer to **Supporting Information Data S4.1**.

4.5.1. Overall sensitivity ranking

Given the potential influence from the selection of evaluation metrics (Wagener et al., 2009), we calculated the sensitivity indices based on both RMSE and KGE, which mathematically biases more

weight during high-value period and balances different components of time series, respectively. Results showed that parameter sensitivity rankings were consistent with each other (Pearson $R^2 > 0.97$, $p < 0.01$, Supporting Information **Figure S4.2**). Therefore, from here on our analysis focused exclusively on the RMSE-based indices. The convergence of the sensitivity index μ^* was further examined using an increasing sample size. All parameters showed convergent trends as the sample size increases; the top 50 sensitive parameters converged mostly within the range of [0, 1.00e-2] after 150,000 model runs (Supporting Information **Figure S4.3**).

For each catchment, parameter sensitivity ranking was demonstrated by plotting μ_i^* versus σ_i (**Figure 4.3**). The more to the right-up section the point, the more sensitive and interactive the parameter becomes. In general, the sensitive zone (i.e., right-up section of the plot) was occupied by parameters *denis*, *deniw* and *npprt*, indicating that soil denitrification, in-stream denitrification and in-stream assimilatory uptake processes, respectively, were the most influential processes for nitrate dynamics throughout the nested three catchments. Parameter *minlr* was located in the middle section, indicating relatively moderate sensitivity of soil mineralization process. Parameters *degdr* and *dislr* were consistently located in the left-low section of each subplot, indicating transformations within soil organic nitrogen forms were not important for nitrate dynamics. Stream parameters were mostly located lower than terrestrial parameters, reflecting that in-stream processes were less interactive than terrestrial processes. Parameter *deniw* was mostly located more right and higher than parameter *npprt*, indicating that in-stream denitrification was relatively more sensitive and less independent, respectively, than in-stream assimilatory uptake.

The μ^* values showed large variations within and between the six groups of parameters (note the log scales in **Figure 4.3** and statistic values shown in **Table 4.2**). The μ^* means of the most sensitive parameters (e.g., denitrification parameters *denis* and *deniw*) were three to four orders of magnitude higher than those of insensitive parameters (e.g., organic N transformation parameters *degdr* and *dislr*). The μ^* values of parameter *denis* were intensively crowded in the sensitive zones for the three nested catchments, and the coefficient of variations (CVs) were relatively low compared to those of other parameters. Stream parameters *deniw* and *npprt* spanned from the upper-right sections to the lower-left sections, with highest CV values, indicating a generally high degree of heterogeneity of in-stream processes throughout the river network. In the HAUS catchment, parameters of in-stream denitrification (*deniw*) became the most sensitive parameters, and the relative importance of the in-stream processes increased compared to that of terrestrial processes (**Figure 4.3c**). CVs of all parameters increased when

moving from the upper-most SILB catchment to the HAUS catchment (**Table 4.2**), indicating an increased spatial variability.

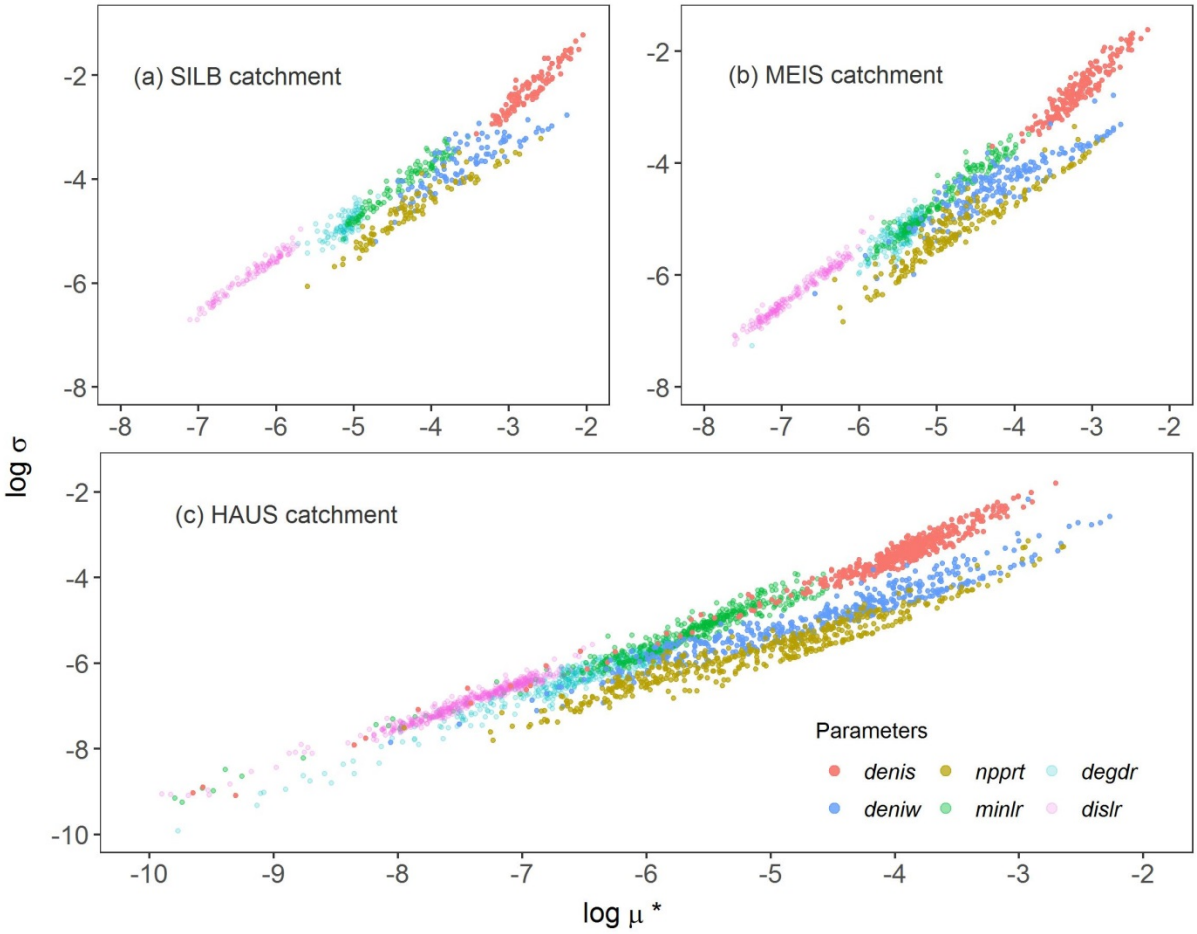

Figure 4.3. Morris sensitivity ranking of the nitrate submodel parameters for the (a) SILB, (b) MEIS and (c) HAUS catchments. The parameters are colored and divided into six groups. Each point represents one of the six parameters in one activated grid cell or one activated stream reach. Terrestrial parameters *denis*, *minlr*, *degdr* and *dislr* are soil denitrification rate, soil mineralization rate, soil degradation rate and soil dissolution rate, respectively. Stream parameters *deniw* and *nppprt* are in-stream denitrification rate and in-stream net assimilatory uptake rate, respectively. Detailed descriptions of the parameters were given in **Table 4.1** and **Supporting Information Text S4.1**. Note that we omitted the grid cells/stream reaches that have extremely low μ_i^* values (i.e., ≤ 10e-10).

Table 4.2. Statistics of the mean Elementary Effects (μ^*) of each parameter in the three nested catchments.SD denotes Standard Deviation and CV denotes Coefficient of Variation.

Parameter	SILB			MEIS			HAUS		
	mean	SD	CV	mean	SD	CV	mean	SD	CV
denis	2.50e-3	2.00e-3	8.02e-1	9.17e-4	8.25e-4	9.01e-1	1.80e-4	2.61e-4	1.45e+0
deniw	5.46e-4	8.55e-4	1.57e+0	2.26e-4	4.23e-4	1.87e+0	1.54e-4	4.71e-4	3.06e+0
npprt	1.72e-4	3.53e-4	2.05e+0	9.00e-5	2.08e-4	2.32e+0	6.43e-5	2.17e-4	3.39e+0
minlr	6.68e-5	5.70e-5	8.53e-1	2.31e-5	2.63e-5	1.14e+0	4.31e-6	5.21e-6	1.21e+0
degdr	8.23e-6	2.85e-6	3.47e-1	3.70e-6	1.51e-6	4.07e-1	5.02e-7	4.37e-7	8.70e-1
dislr	6.77e-7	4.78e-7	7.05e-1	2.49e-7	2.41e-7	9.66e-1	5.73e-8	5.11e-8	8.92e-1

4.5.2. Spatial distributions of the parameter sensitivity

In addition to the consistency in the sensitive and insensitive categorization, the sensitive parameters showed high spatial variability and the spatial patterns differed among the three nested catchments. Therefore, detailed spatial distributions of the four most sensitive parameters (i.e., *denis*, *deniw, npprt* and *minlr*) were further analyzed and compared.

In the upper-most SILB catchment, the scaled μ^* values of parameter *denis* were relatively high compared to those of other parameters (**Figure 4.4a**). The highest values were derived in the grid cells that are coincidently characterized as the arable-dominant area (defined as areal proportion of arable land, *Parable*, $>$ 0.70, **Figure 4.2a**) and the wet area (defined as annual precipitation, *Precipi*, $>$ 660 mm**,** **Figure 4.2d**). Moreover, the sensitivity of the forest/pasture cells within the wet area (i.e., the mountainous boundary areas) was equivalent to that of the arable-dominant cells outside of the wet area (i.e., the central arable areas, **Figure 4.4a**). The μ^* values of *minlr* were homogeneously low (**Figure 4.4b**). Therefore, the soil mineralization process was taken as homogeneously insensitive for $N-NO_3^-$ concentration. The sensitivities of the stream parameters *deniw* and *npprt* showed large spatial variability (**Figures 4.4c** and **d**). Parameters of higher-order reaches were generally more sensitive than those of headwater reaches (i.e., 1st and 2nd orders). Unlike the smooth increase of sensitivity in parameter *npprt*, parameter *deniw* showed extraordinarily higher sensitivity for few individual downstream reaches (**Figure 4.4c**). These reaches were receiving water from arable-dominant grid cells with high terrestrial $N-NO_3^-$ exports (*Ter_Nxprt* = 8.28 ± 1.64 (mean ± SD), $kg\ N\ ha^{-1}\ yr^{-1}$, **Figure 4.2i**).

The in-between area of station SILB and station MEIS was occupied mainly by natural forests (ca. 87% of the area), where *Ter_Nxprt* was very low (1.29 ± 0.73 $kg\ N\ ha^{-1}\ yr^{-1}$). Consequently, the $N-NO_3^-$ load at station MEIS was mostly contributed from the upper area belonging to the SILB catchment. Therefore, the spatial sensitivity pattern of parameter *denis* was generally maintained from the upper SILB catchment to the MEIS catchments (**Figure S4.2a**). Sensitivity of stream parameters *deniw* and *npprt*

generally followed the same spatial pattern as in the SILB catchment, resulting in higher μ^* values in the downstream higher-order reaches (**Figures S4.2c** and **d**).

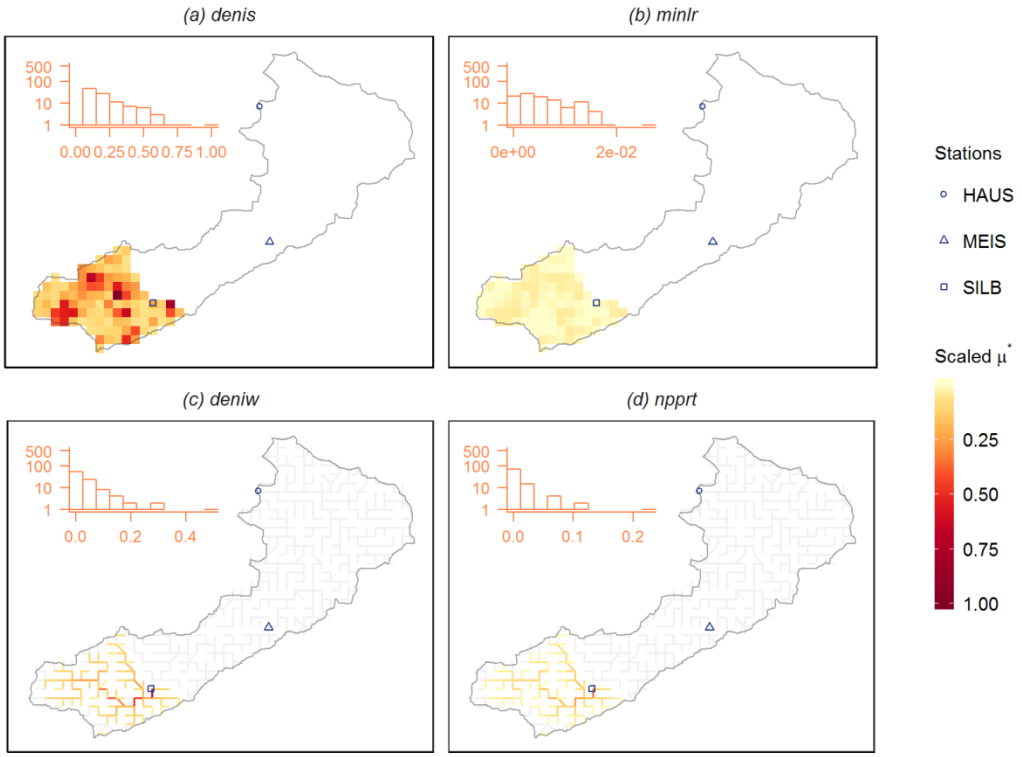

Figure 4.4. Spatial distributions of parameter sensitivity in the upper-most SILB catchment (grid size 1 km^2). The μ^* (absolute mean of EEs) values are scaled into the range of [0, 1] for the four most sensitive parameters (a) *denis*-soil denitrification rate, (b) *minlr*-soil mineralization rate, (c) *deniw*-in-stream denitrification rate and (d) *npprt*-in-stream net assimilatory uptake rate. The inserted histogram plot represents the distribution of the scaled μ^* values for each parameter. The y-axis denotes the frequency of grid cells/stream reaches and has been log-transformed. Deactivated grid cells and stream reaches are excluded and shown in gray lines, respectively.

For the HAUS catchment, however, the spatial sensitivity patterns and relative importance of each parameter varied largely (**Figure 4.5**). The μ^* values of parameter *denis* scattered throughout the catchment (**Figure 4.5a**): the spatial pattern of the upper grid cells was similar to that observed in the upper catchments, but the relative importance reduced; the values of the lowland grid cells spanned at a larger range, including the highest ones for the whole catchment. Parameter *minlr* showed similar low sensitivity and spatial homogeneity (**Figure 4.5b**). Therefore, the soil mineralization process was excluded in further analysis in this study. The μ^* values of both stream parameters *deniw* and *npprt*

were significantly higher in the lowland reaches than in the reaches upstream of station MEIS (ANOVA test, $p < 0.01$) (**Figures 4.5c** and **d**).Within each subarea, higher-order reaches were generally more sensitive than headwater reaches. Among all parameters, the highest μ^* values were derived from parameter *deniw* in the downstream reaches closing to the outlet station HAUS (**Figure 4.5c**).

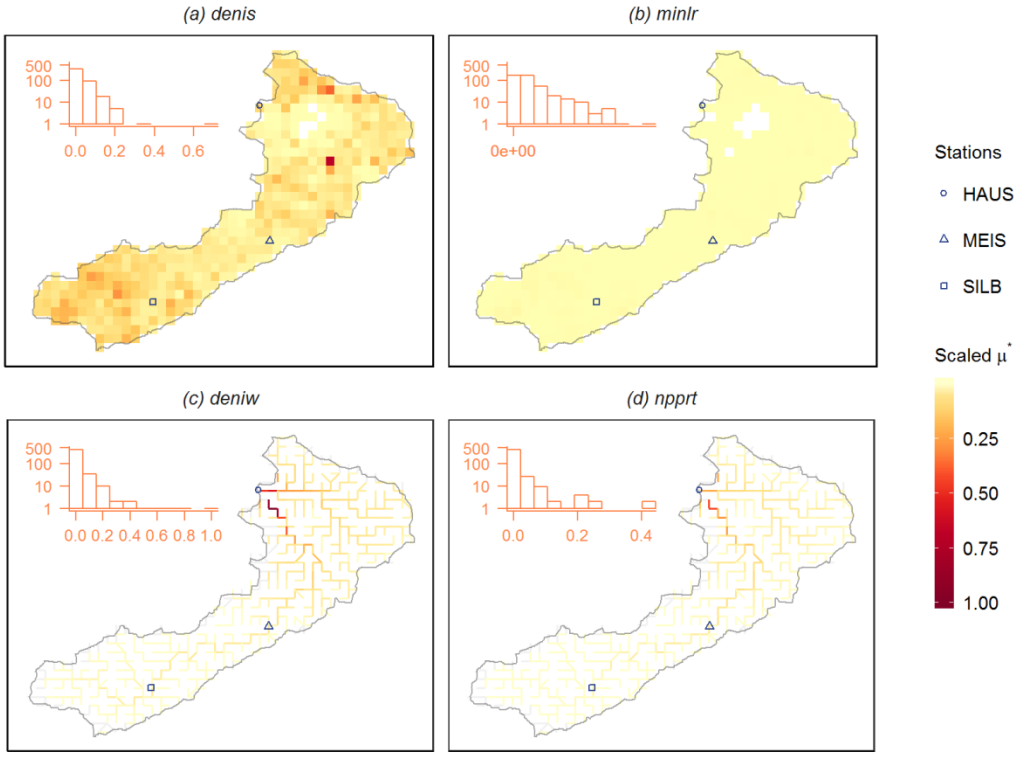

Figure 4.5. Spatial distributions of parameter sensitivity indices in the HAUS catchment (grid size 1 km^2). The μ^* values are scaled into the range of [0, 1] for the four most sensitive parameters (a) *denis*-soil denitrification rate, (b) *minlr*-soil mineralization rate, (c) *deniw*-in-stream denitrification rate and (d) *npprt*-in-stream net assimilatory uptake rate.

4.5.3. Correlations between parameter sensitivity and catchment factors

The correlations were conducted using the Spearman rank correlation for the three nested catchments and exclusively for the lowland arable areas (**Table 4.3**). In the SILB catchment, Spearman coefficients showed that the sensitivity of parameter *denis* was correlated highly, positively with terrestrial $N - NO_3^-$ state variables and fluxes ($\rho \geq 0.77$), but non-significantly with terrestrial flow state variables and fluxes ($p > 0.01$). It was also correlated significantly with areal proportion of arable land (*Parable*, ρ = 0.65) and annual precipitation (*Precipi*, ρ = 0.39). The sensitivities of stream parameters *deniw* and *npprt* were both correlated highly with stream discharge (*SW_q*) and stream benthic area (*SW_area*), i.e., $\rho \geq$

0.75 and 0.88 , respectively, but non-significantly with stream $N-NO_3^-$ concentration (*SW_Nconc*, $p >$ 0.01). Both stream parameter sensitivities also showed slight negative correlations with terrestrial flow state variables and fluxes and non-significant correlations with terrestrial $N-NO_3^-$ state variables and fluxes.

Compared to the results in the SILB catchment, the sensitivity of parameter *denis* in the MEIS catchment were also correlated highly with terrestrial $N-NO_3^-$ state variables and fluxes ($\rho \geq 0.56$), while the correlation with *Precipi* strengthened (ρ = 0.63) and correlations with flow state variables and fluxes became significant (ρ = 0.37 - 0.51, $p < 0.01$, **Table 4.3**). The sensitivities of stream parameters *deniw* and *npprt* were highly correlated with *SW_q* and *SW_area* ($\rho \geq 0.73$ and 0.82, respectively), while the correlation of parameter *deniw* with *SW_Nconc* became significant (ρ = 0.46, $p < 0.01$). The sensitivity of parameter *deniw* was slightly correlated with terrestrial $N-NO_3^-$ state variables (ρ = ca. 0.24), and the sensitivity of parameter *npprt* was negatively correlated with terrestrial flow state variables and fluxes (ρ mostly equals to -0.50).

For the HAUS catchment, the sensitivity of parameter *denis* was correlated highly with annual precipitation (*Precipi*, ρ = 0.64) and significantly with most flow state variables and fluxes in a weaker manner (ρ =0.43 - 0.60, **Table 4.3**). The correlation with terrestrial $N-NO_3^-$ export (*Ter_Nxprt*) was still positive, but with reduced strength compared to that in the upper catchments (ρ = 0.41 vs. ca. 0.80, respectively). Moreover, the high correlation with *Parable* was eliminated (ρ = 0.15). Correlations of stream parameters *deniw* and *npprt* differed largely compared to the upper catchments (**Table 4.3**). Results showed that their sensitivities correlated with *SW_Nconc* (ρ = ca. 0.50) in a higher degree than with *SW_q* and *SW_area* (ρ = ca. 0.35 and ca. 0.47, respectively). Moreover, the sensitivities were correlated with terrestrial $N-NO_3^-$ state variables ($\rho > 0.55$), whereas negatively with terrestrial flow statues and fluxes ($|\rho| > 0.65$).

Interestingly, correlations exclusively within the lowland arable areas differed compared to the whole HAUS catchment (**Table 4.3**). The correlation coefficient of parameter *denis* with *Precipi* decreased (ρ = 0.40), but the correlations with flow state variables and fluxes remained relatively high ($\rho > 0.54$). The correlation with Parable remained weak (ρ = 0.26), while that with soil properties became relevant (ρ = 0.40 and -0.46 for clay and sand proportions, respectively). Sensitivities of both stream parameters were highly positively correlated with *SW_q* and *SW_area* ($\rho \geq 0.69$ and 0.79, respectively) and negatively correlated with *SW_Nconc* (ρ = -0.40).

Table 4.3. The Spearman rank correlation coefficients (ρ) between spatial sensitivity of nitrate submodel parameters and catchment factors in three nested catchments and the lowland arable areas. The bold and italic gray-colored values denote highly significant (i.e., $|\rho| \geq 0.60$) and non-significant (i.e., p value < 0.01) correlations, respectively. Detailed instructions and original values of the factors were given in **Appendix** (**Table A4.1**) and **Supporting Information Data S4.1**, respectively.

Property	SILB			MEIS			HAUS			Lowland arable areas		
	denis	*deniw*	*npprt*	*denis*	*deniw*	*npprt*	*denis*	*deniw*	*npprt*	*denis*	*deniw*	*npprt*
Parable	**0.65**	*0.09*	*-0.01*	**0.62**	*0.12*	*-0.12*	0.15	0.59	0.52	0.26	*-0.03*	*-0.12*
Pclay	*-0.06*	*-0.04*	*-0.12*	0.27	*0.07*	*-0.15*	0.38	-0.46	-0.49	0.40	-0.21	-0.25
Psand	*0.08*	*-0.02*	*0.06*	*-0.17*	*0.02*	*0.15*	-0.22	*-0.18*	*-0.16*	-0.46	0.35	0.40
T	*0.04*	0.33	0.51	-0.46	*0.17*	0.51	-0.46	**0.72**	**0.75**	-0.40	0.43	0.43
ET	-0.42	*-0.10*	*-0.03*	-0.43	*-0.07*	*0.13*	*0.07*	*-0.14*	*-0.10*	*0.06*	*0.01*	*-0.04*
Precipi	0.39	*-0.17*	-0.41	**0.63**	*-0.14*	-0.50	**0.64**	-0.48	-0.58	0.40	-0.29	-0.29
SM	*0.13*	*-0.26*	-0.47	0.51	*-0.21*	-0.53	**0.60**	**-0.67**	**-0.72**	0.57	-0.31	-0.36
R_total	*0.04*	-0.30	-0.52	0.49	*-0.18*	-0.51	0.43	**-0.69**	**-0.73**	0.54	-0.30	-0.34
R_slow	*-0.12*	-0.33	-0.50	0.38	-0.23	-0.51	0.57	**-0.67**	**-0.71**	0.59	-0.28	-0.33
R_base	*0.22*	*-0.24*	-0.35	0.37	*-0.11*	-0.34	0.54	**-0.65**	**-0.68**	0.58	-0.17	-0.21
SMC	**0.78**	*0.14*	*0.06*	**0.70**	0.23	*-0.04*	*0.06*	**0.63**	0.56	*-0.08*	0.28	0.25
RC_total	**0.81**	*0.11*	*-0.01*	**0.73**	0.24	*-0.05*	*-0.01*	**0.69**	**0.63**	-0.25	0.29	0.27
RC_slow	**0.78**	*0.14*	*0.06*	**0.69**	0.24	*-0.04*	*0.06*	**0.63**	0.55	*-0.08*	0.27	0.25
RC_base	**0.77**	*0.15*	*0.06*	0.56	0.27	*0.11*	*-0.02*	**0.66**	**0.62**	0.30	*0.04*	*-0.04*
Ter_Nxprt	**0.78**	*-0.02*	*-0.17*	**0.79**	*0.04*	-0.33	0.41	0.34	0.25	0.58	-0.20	-0.25
SW_q	--	**0.84**	**0.75**	--	**0.85**	**0.73**	--	0.37	0.35	--	**0.73**	**0.69**
SW_Nconc	--	*0.18*	*0.11*	--	0.46	*0.19*	--	0.54	0.50	--	-0.40	-0.40
SW_area	--	**0.89**	**0.88**	--	**0.88**	**0.82**	--	0.47	0.48		**0.79**	**0.85**

4.6. Discussion

The Selke catchment is characterized by high variations in meteor-hydrological and nitrate dynamics, resulting from the highly heterogeneous catchment conditions. These variations are well captured by the three nested gauging stations (i.e., station SILB, MEIS and the outlet HAUS), and the observed stream $N - NO_3^-$ concentrations are more distinct than the observed stream discharge among three stations (Jiang et al., 2014; Yang et al., 2018). Therefore, sensitivity analysis of spatially distributed nitrate submodel parameterization is informative, and also necessary, to identify the most influential processes and their driving factors at different conditions. In this study, sensitivity results demonstrated that soil denitrification, in-stream denitrification and in-stream assimilatory uptake were the most sensitive processes for nitrate dynamics throughout the nested catchments, while their spatial patterns and corresponding controling catchment factors varied largely when moving from the upper-most SILB catchment to the whole HAUS catchment.

4.6.1. Soil denitrification

For all nested catchments, soil denitrification rate was identified as one of the most sensitive parameters with high spatial variability. The sensitivity indices were most correlated with terrestrial $N-NO_3^-$ exports (i.e., the load, $kg\ N\ ha^{-1}\ yr^{-1}$), which integrates the overall transports of flow and $N-NO_3^-$ from the terrestrial phase. However, the controlling factors of the soil denitrification differed spatially within the Selke catchment, presumably due to the high spatial variabilities of meteor-hydrological conditions and anthropogenic impacts. In the SILB catchment, the spatial sensitivity pattern generally followed the distribution of the areal proportion of arable land (e.g., **Figures 4.4a** and **2a**, respectively); the sensitivity indices were highly positively correlated with terrestrial $N-NO_3^-$ state variables and fluxes (Table 3). The soil moisture content and runoff generation were homogeneously high within the SILB catchment (**Figures 4.2e** and **f**, respectively), while much higher $N-NO_3^-$ supplies were observed in the arable lands (25% of the total area) compared to the rest pristine forest and pasture areas. This resulted in an overall soil $N-NO_3^-$ limitation in the upper part of the Selke catchment. In contrast, within the lowland arable areas, the sensitivity distribution followed the distributions of soil moisture content and runoff generation (**Figures 4.4a** and **2e**, respectively); flow state variables and fluxes became highly correlated (Table 3). Due to long-term agricultural activities, soil $N-NO_3^-$ was homogenously sufficient in arable lands (**Figure 4.2g**), while the soil moisture content and the subsequent runoff generation (**Figures 4.2e and f**, respectively) varied largely due to the heterogeneous soil properties (areal proportions of sand and clay shown as **Figures 4.2b** and **c**, respectively). Therefore, hydrological transport limitation is likely pronounced in the lowland part of the catchment. Overall, the sensitivity of soil denitrification depends on the relative limitations between the soil $N-NO_3^-$ availability and the hydrological transport capacity.

Compared to soil $N-NO_3^-$ availability, hydrological transport capacity likely has a stronger influence on the sensitivity of soil denitrification. In the SILB catchment, the highest sensitivity was derived in grid cells where sufficient soil $N-NO_3^-$ sources (i.e., in the arable-dominant cells) encountered with the most active hydrological dynamics (i.e., in the wet area); the forest-/ pasture-dominant cells in the wet area had similar sensitivity to the arable-dominant cells outside of this area, although the former cells had much lower soil $N-NO_3^-$ sources. In turn, some grid cells in the lowland arable areas showed extreme limitations on hydrological transport capacity. This further caused very low sensitivity of soil denitrification, although mean soil $N-NO_3^-$ concentration was up to higher than 20 $mg\ l^{-1}$ (**Figure 4.2g**). Mechanistically, the variations in flow fluxes are usually orders of magnitude higher than the variations in $N-NO_3^-$ concentrations; meanwhile, soil redox conditions in wetter areas favor the

activity of denitrifiers, which further promotes the sensitivity of soil denitrification. Therefore, higher hydrological transport capacity likely compensates, to a certain degree, the limitation on soil $N-NO_3^-$ availability, but not vice versa.

4.6.2. In-stream denitrification and assimilatory uptake

Compared to the terrestrial processes, in-stream processes showed a higher degree of spatial heterogeneity, and their general importance likely increased with increasing catchment size. Both in-stream denitrification and assimilatory uptake showed generally higher sensitivities in downstream, higher-order reaches. This effect of proximity to evaluation location was confirmed by the high correlations between the parameter sensitivities and stream discharge and stream benthic area (Table 3). First, processes happened in downstream reaches close to the evaluation station would have a stronger influence on $N-NO_3^-$ concentration (Tang et al., 2007; Wagener et al., 2009). Second, stream benthic area would increase as flow accumulating to higher-order reaches (**Figure 4.2j**), which likely increases the opportunity for nitrate to be denitrified and/or to be assimilated by periphyton. The in-stream processes were positively and negatively correlated with stream $N-NO_3^-$ concentration in the forested MEIS catchment and the lowland arable areas, respectively (Table 3). The observed correlations with stream $N-NO_3^-$ concentrations are likely caused by the large concentration gradients between the main stem of the Selke River and the tributaries (forest and agricultural tributaries in the MEIS and HAUS catchments, respectively (**Figure 4.2l**). Moreover, the correlations were nonsignificant in the SILB catchment, although the concentrations varied largely due to the more scattered mixture of forests and arable lands. Overall, in-stream processes at river network scale are predominated by the proximity to evaluation location and unlikely influenced by the stream $N-NO_3^-$ concentration. The high degree of spatial variability plausibly surpasses the local biogeochemical factors in controlling the fate of nitrogen at catchment scale (Gomez-Velez et al., 2015).

In water quality modeling, it is difficult to distinguish in-stream $N-NO_3^-$ removals from the highly confounded denitrification and assimilatory uptake processes (Rode et al., 2016b). In this study, the sensitivity indices of both process parameters did highly correlate with each other (Pearson's $\gamma > 0.90$), indicating potential "equifinality" effects. Nevertheless, from the process understanding perspective, increased $N-NO_3^-$ concentration can likely stimulate in-stream denitrification (Beaulieu et al., 2011). While for in-stream assimilatory uptake, light availability is the predominant factor as nutrients are usually not limiting in most anthropogenically impacted rivers (Yang et al., 2019). In this study, we adopted these state-of-the-art understandings of the processes(**Supporting Information Eq. S4.9-S4.13**),

and such different process descriptions were somehow reflected in the sensitivity distributions. For instance, the sensitivity of parameter *npprt* increased in a more gentle way than that of parameter *deniw* moving to the downstream, higher-order reaches. This implicated that research efforts in process understanding would help in addressing the complexity of model parameterization and, therefore, should be embedded in model development activities.

4.6.3. Implications and future work

Catchment functioning of hydrology and nutrient dynamics varies under different catchment and anthropogenic conditions. Parameters are introduced in the model development to tolerate such variations, while maintaining the main describing equations (Beven, 1995). Parameter sensitivity analysis in specific catchment indicates relative importance of different processes on catchment response; catchment response relies on the information provided by the gauging network. Therefore, an appropriate monitoring scheme, that can truly reflect heterogeneous catchment responses, is critical for parameter sensitivity analysis in the first place. Insights into the catchment functioning can be gained only if sensitivity analysis is conducted based on adequate information (e.g., referred as the choice of model response by Gupta and Razavi (2018)). In the Selke catchment, the distinct stream $N-NO_3^-$ concentration dynamics in the upper and lower parts are well captured by the three nested stations. Parameter sensitivity derived from the corresponding nested catchments showed large differences in terms of spatial distributions (**Figures 4.4** and 4.**5**). The "hot spots" of soil denitrification in the upper part of the catchment could not be sufficiently reflected when only using the $N-NO_3^-$ dynamic information at the outlet. Likewise, the relative importance and spatial variability of in-stream processes in the upper stream reaches attenuated largely when only using the data at the outlet. Therefore, we suggest that multi-site sensitivity evaluation is needed to make the most of the information provided by the monitoring scheme and to obtain the actual spatial distribution of parameter sensitivity, as shown in **Figure 4.6** (the sensitivity indices were calculated based on data at all three stations).

In addition to advancing process understanding, correlating parameter sensitivity with catchment factors also provides insights into the heterogeneous nitrate behaviors at catchment scale. In this study, the sensitivity of soil denitrification process was limited by soil $N-NO_3^-$ availability (indicated by, e.g., areal proportion of arable lands) and hydrological transport capacity (indicated by, e.g., soil moisture content) in upper forests and lower arable lands, respectively. Moreover, higher hydrological transport capacity could likely compensate the deficit in soil $N-NO_3^-$ availability based on the physical and microbial mechanisms. In-stream denitrification and assimilatory uptake processes at network scale

were mainly controlled by the spatial variability (indicated by e.g., the proximity to evaluation stations), rather than the local biogeochemical factors (e.g., the stream $N - NO_3^-$ concentration). Consciously, one should also be aware that the statistical correlations might be misleading. For instance, soil denitrification appeared to be exclusively correlated with meteor-hydrological properties for the HAUS catchment (**Table 4.3**). This is mainly due to the high meteor-hydrological gradients moving from the upper to the lowland areas, e.g., annual total runoff (*R_total*) decreased from 206.9 ± 46.8 to 44.5 ± 21.9 mm (**Figure 4.2f**). Such high gradients plausibly override the actual influential factors identified when investigating separately in the SILB catchment and the lowland arable areas.

The insights can offer new prospects for future process conceptualization and model parameterization. Current parameterization schemes for water quality models are normally based on broadly defined landscape information (e.g., land-use/soil types), which likely underestimates the actual heterogeneity in nature (Clark et al., 2017). Based on parameter sensitivity analysis in the context of fully distributed parameterization, the identified controlling factors could lead to a better modeling representation of processes in terms of their heterogeneity and relevance. For instance, soil denitrification rate is not only influenced by land use, but also the hydrological connectivity. The latter factor is likely more influential than the former, but is overlooked by most current models. The Spearman rank correlation is, however, theoretically weak in directly guiding quantitative relationship for new regionalization approaches. Similar analysis need to be conducted in more catchments across different regions. Then, robust spatial relationships between parameters and controlling factors could be obtained; with this, advanced process conceptualization and quantitative parameter regionalization could be potentially formulated and validated.

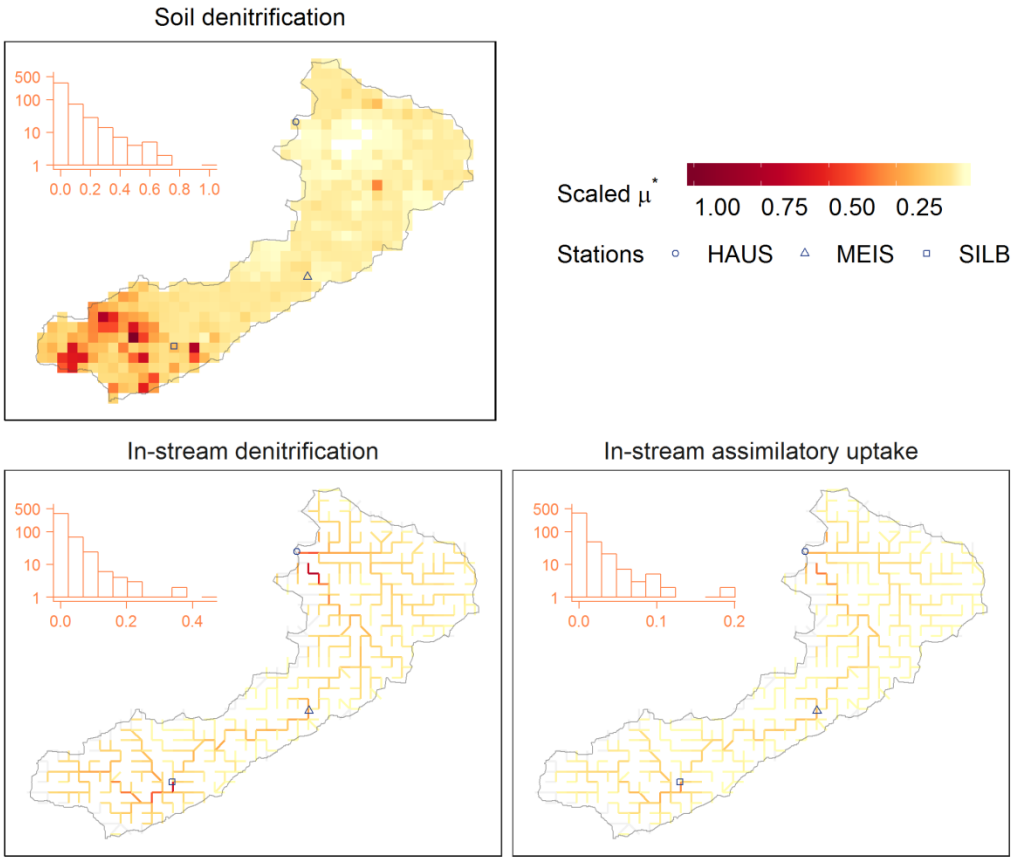

Figure 4.6. Combined spatial distributions of parameter sensitivity indices using the measured data from all three gauging stations (grid size 1 km^2). The μ^* values are scaled into the range of [0, 1]. Only the sensitive soil denitrification, in-stream denitrification and in-stream assimilatory uptake processes are presented. The inserted histogram plot represents the distribution of the scaled μ^* values for each parameter.

To the authors' knowledge, this study for the first time explicitly investigated the parameter sensitivity of fully distributed parameterization for water quality models. Therefore, several interesting issues are worth to be further investigated. First, biogeochemical processes are characterized as with strong seasonality. Temporal variability of parameter sensitivity in water quality models can be highly pronounced, but has rarely been investigated (but see Haas et al. (2015)). Moreover, the combined spatiotemporal SA, like Herman et al. (2013a) for hydrological modeling, is still missing in water quality modeling. Second, the correlations between parameter sensitivity and catchment property should be tested in a wide range of regions with varying climatic and anthropogenic impacts, until sound relationships can be obtained for further parameterization research. In addition, we are also aware of the methodological limitations of this study that should be further addressed, including preliminary

mapping for better parameter ranges (Bai et al., 2009), the selection of model response (Wagener et al., 2009; Gupta & Razavi, 2018) and a more comprehensive analysis of the robustness of the computational design (Sarrazin et al., 2016; Sheikholeslami et al., 2019).

4.7. Conclusions

Based on the fully distributed mHM-Nitrate model, we explicitly investigated the spatially distributed sensitivity of the nitrate submodel parameters. Parameters of soil denitrification, in-stream denitrification and in-stream assimilatory uptake were identified as the most sensitive parameters throughout the nested Selke catchment, while they all showed high spatial variabilities. Moreover, the sensitivity ranking and spatial distribution varied among the three nested catchments (gauged by the nested SILB, MEIS and HAUS stations, respectively). Spearman rank correlations confirmed that the parameter sensitivity was predominated by variable catchment factors at different locations, presumably due to the high heterogeneity of geographical, meteor-hydrological and anthropogenic conditions within the Selke catchment. Insights into catchment nitrate behaviors were derived from the spatial sensitivity and correlation analyses. The importance of soil denitrification process depended on the relative limitations between soil nitrate availability and hydrological transport capacity. The latter could likely compensate for the former, but not vice versa. Compared to the terrestrial processes, the relative importance of the in-stream processes increased with increasing catchment size; meanwhile, their spatial distribution throughout the river network was predominated by spatial variability (e.g., the proximity to evaluation station), rather than local biogeochemical factors (e.g., the stream $N-NO_3^-$ concentration).

These insights are informative in advancing our understanding of the heterogeneous catchment nitrate behaviors. However, sensitivity results rely largely on the information provided by gauging networks. Therefore, we recommend that (1) an appropriate monitoring scheme, which can truly reflect heterogeneous catchment responses, is important in the first place; and (2) sensitivity evaluation should make most use of the gauging information to achieve a better representation of the spatial heterogeneity of processes. As a step further, the correlations between parameter sensitivity and catchment factors can reveal varying controlling factors of important processes within the catchment/river network. Therefore, the statistical correlation, with cautious selection of catchment factors, can guide future model parameterization to achieve a better spatial representation of process heterogeneity and relevance.

Acknowledgement

Xiaoqiang Yang is funded by the Chinese Scholarship Council (CSC). We would like to thank the Editor Martyn Clark, the Associate Editor Julian Mai, and three anonymous Reviewers for their constructive comments, which helped to improve the manuscript significantly. We thank the German Weather Service (DWD), Federal Institute for Geosciences and Natrual Resources (BGR) and State Agency for Flood Protection and Water Management of Saxony-Anhalt (LHW) for providing the data used for setting up the model. The daily nitrate observations are obtained from the TERENO (Terrestrial Environment Observatories) project coordinated by Helmholtz Centre for Environmental Research – UFZ. The data used are presented in the tables, figures and supplements.

4.8. Appendix

Table A4.1. Abbreviations and physical meanings of the catchment factors used in this study. The last column notes the original information from the model implementation perspective (please refer to the source codes of mHM (https://git.ufz.de/mhm/mhm) and mHM-Nitrate (https://git.ufz.de/yangx/mHM-Nitrate) for the variable names). Note. *"*mean width"* is calculated based on the mean discharge and the empirical equation by Rode et al. (2016a) (see also Supporting Information Text S4.1).

Property category	Property	physical meaning	Note
Geographic and geological properties	*Parable*	The areal proportion of arable land ($\in [0,1]$)	Land-use input
	Pclay	The areal proportion of clay soil ($\in [0,1]$)	Soil type and soil property inputs
	Psand	The areal proportion of sand soil ($\in [0,1]$)	Soil type and soil property inputs
Meteorological properties	*T*	annual mean of mean daily air temperature (℃)	Meteorological input
	ET	annual evapotranspiration (mm)	Meteorological input
	Precipi	annual precipitation (mm)	Meteorological input
Hydrological state variables and fluxes	*SM*	annual mean soil moisture content ($\in [0,1]$) in the 3rd soil layer (50-200 cm)	mHM state variable: "*L1_soilMoist*"
	R_total	annual total runoff (mm)	mHM flux: "*L1_total_runoff*"
	R_slow	annual runoff component of slow interflow (mm)	mHM flux: "*L1_slowRunoff*"
	R_base	annual runoff component of baseflow (mm)	mHM flux: "*L1_baseflow*"

$N-NO_3^-$ state variables and fluxes	*SMC*	Mean $N-NO_3^-$ concentration in soil moisture of the 3rd soil layer ($mg\ l^{-1}$)	mHM-Nitrate state variable: "*L1_csoilMoist*"
	RC_total	Mean $N-NO_3^-$ concentration in total runoff ($mg\ l^{-1}$)	mHM-Nitrate state variable: "*L1_ctotal_runoff*"
	RC_slow	Mean $N-NO_3^-$ concentration in slow interflow ($mg\ l^{-1}$)	mHM-Nitrate state variable: "*L1_cslowRunoff*"
	RC_base	Mean $N-NO_3^-$ concentration in baseflow ($mg\ l^{-1}$)	mHM-Nitrate state variable: "*L1_cbaseflow*"
	Ter_Nxprt	Mean annual terrestrial $N-NO_3^-$ export load ($kg\ N\ ha^{-1}\ yr^{-1}$)	mHM-Nitrate flux: "*L1_total_runoff*" × "*L1_ctotal_runoff*" × 0.01
In-stream factors	*SW_q*	annual mean stream discharge ($m^3\ s^{-1}$)	mHM output: "*L11_qMod*"
	SW_Nconc	annual mean stream $N-NO_3^-$ concentration ($mg\ l^{-1}$)	mHM-Nitrate output: "*L11_concMod*"
	SW_area	The mean stream benthic area (m^2)	mHM-Nitrate state variable: "*L11_length*" × *mean width**

4.9. References

Bai, Y., Wagener, T., & Reed, P. (2009), A top-down framework for watershed model evaluation and selection under uncertainty, *Environmental Modelling & Software*, *24*(8), 901-916. https://doi.org/10.1016/j.envsoft.2008.12.012

Beaulieu, J. J., Tank, J. L., Hamilton, S. K., Wollheim, W. M., Hall, R. O., Mulholland, P. J., Peterson, B. J., Ashkenas, L. R., Cooper, L. W., Dahm, C. N., Dodds, W. K., Grimm, N. B., Johnson, S. L., McDowell, W. H., Poole, G. C., Valett, H. M., Arango, C. P., Bernot, M. J., Burgin, A. J., Crenshaw, C. L., Helton, A. M., Johnson, L. T., Brien, J. M., Potter, J. D., Sheibley, R. W., Sobota, D. J., & Thomas, S. M. (2011), Nitrous oxide emission from denitrification in stream and river networks, *Proceedings of the National Academy of Sciences*, *108*(1), 214. https://doi.org/10.1073/pnas.1011464108

Beven, K. (1993), Prophecy, reality and uncertainty in distributed hydrological modelling, *Advances in Water Resources*, *16*(1), 41-51. https://doi.org/10.1016/0309-1708(93)90028-E

Beven, K. (1995), Linking parameters across scales: Subgrid parameterizations and scale dependent hydrological models, *Hydrological Processes*, *9*(5-6), 507-525. https://doi.org/10.1002/hyp.3360090504

Campolongo, F., Cariboni, J., & Saltelli, A. (2007), An effective screening design for sensitivity analysis of large models, *Environmental Modelling & Software*, *22*(10), 1509-1518. https://doi.org/10.1016/j.envsoft.2006.10.004

Campolongo, F., Saltelli, A., & Cariboni, J. (2011), From screening to quantitative sensitivity analysis. A unified approach, *Computer Physics Communications*, *182*(4), 978-988. https://doi.org/10.1016/j.cpc.2010.12.039

Clark, M. P., Bierkens, M. F. P., Samaniego, L., Woods, R. A., Uijlenhoet, R., Bennett, K. E., Pauwels, V. R. N., Cai, X., Wood, A. W., & Peters-Lidard, C. D. (2017), The evolution of process-based hydrologic models: historical challenges and the collective quest for physical realism, *Hydrol. Earth Syst. Sci.*, *21*(7), 3427-3440. https://doi.org/10.5194/hess-21-3427-2017

Clark, M. P., Nijssen, B., Lundquist, J. D., Kavetski, D., Rupp, D. E., Woods, R. A., Freer, J. E., Gutmann, E. D., Wood, A. W., Brekke, L. D., Arnold, J. R., Gochis, D. J., & Rasmussen, R. M. (2015), A unified approach for process-based hydrologic modeling: 1. Modeling concept, *Water Resources Research*, *51*(4), 2498-2514. https://doi.org/10.1002/2015WR017198

Cuntz, M., Mai, J., Zink, M., Thober, S., Kumar, R., Schäfer, D., Schrön, M., Craven, J., Rakovec, O., Spieler, D., Prykhodko, V., Dalmasso, G., Musuuza, J., Langenberg, B., Attinger, S., & Samaniego, L. (2015), Computationally inexpensive identification of noninformative model parameters by sequential screening, *Water Resources Research*, *51*(8). https://doi.org/10.1002/2015WR016907

Dupas, R., Musolff, A., Jawitz, J. W., Rao, P. S. C., Jäger, C. G., Fleckenstein, J. H., Rode, M., & Borchardt, D. (2017), Carbon and nutrient export regimes from headwater catchments to downstream reaches, *Biogeosciences*, *14*(18), 4391-4407. https://doi.org/10.5194/bg-14-4391-2017

EEA (2005), Source apportionment of nitrogen and phosphorus inputs into the aquatic environment, *Rep. No 7/2005*, European Environment Agency, Copenhagen, Denmark.

Gomez-Velez, J. D., Harvey, J. W., Cardenas, M. B., & Kiel, B. (2015), Denitrification in the Mississippi River network controlled by flow through river bedforms, *Nature Geoscience*, *8*, 941. https://doi.org/10.1038/ngeo2567

Gupta, H. V., & Razavi, S. (2018), Revisiting the Basis of Sensitivity Analysis for Dynamical Earth System Models, *Water Resources Research*, *54*(11), 8692-8717. https://doi.org/10.1029/2018WR022668

Gupta, H. V., Wagener, T., & Liu, Y. (2008), Reconciling theory with observations: elements of a diagnostic approach to model evaluation, *Hydrological Processes*, *22*(18), 3802-3813. https://doi.org/10.1002/hyp.6989

Gupta, H. V., Kling, H., Yilmaz, K. K., & Martinez, G. F. (2009), Decomposition of the mean squared error and NSE performance criteria: Implications for improving hydrological modelling, *Journal of Hydrology*, *377*(1), 80-91. https://doi.org/10.1016/j.jhydrol.2009.08.003

Haas, M. B., Guse, B., Pfannerstill, M., & Fohrer, N. (2015), Detection of dominant nitrate processes in ecohydrological modeling with temporal parameter sensitivity analysis, *Ecological Modelling*, *314*, 62-72. https://doi.org/10.1016/j.ecolmodel.2015.07.009

Herman, J. D., Kollat, J. B., Reed, P. M., & Wagener, T. (2013a), From maps to movies: high-resolution time-varying sensitivity analysis for spatially distributed watershed models, *Hydrol. Earth Syst. Sci.*, *17*(12), 5109-5125. https://doi.org/10.5194/hess-17-5109-2013

Herman, J. D., Kollat, J. B., Reed, P. M., & Wagener, T. (2013b), Technical Note: Method of Morris effectively reduces the computational demands of global sensitivity analysis for distributed watershed models, *Hydrology Earth System Sciences*, *17*(7), 2893-2903. https://doi.org/10.5194/hess-17-2893-2013

Huang, S., Hesse, C., Krysanova, V., & Hattermann, F. (2009), From meso- to macro-scale dynamic water quality modelling for the assessment of land use change scenarios, *Ecological Modelling*, *220*(19), 2543-2558. https://doi.org/10.1016/j.ecolmodel.2009.06.043

Jiang, S., Jomaa, S., & Rode, M. (2014), Modelling inorganic nitrogen leaching in nested mesoscale catchments in central Germany, *Ecohydrology*, *7*(5), 1345-1362. https://doi.org/10.1002/eco.1462

Kumar, R., Samaniego, L., & Attinger, S. (2013), Implications of distributed hydrologic model parameterization on water fluxes at multiple scales and locations, *Water Resources Research*, *49*(1). https://doi.org/10.1029/2012WR012195

Lindström, G., Pers, C., Rosberg, J., Strömqvist, J., & Arheimer, B. (2010), Development and testing of the HYPE (Hydrological Predictions for the Environment) water quality model for different spatial scales, *Hydrology research*, *41*(3-4), 295-319. https://doi.org/10.2166/nh.2010.007

Morris, M. D. (1991), Factorial sampling plans for preliminary computational experiments, *Technometrics*, *33*(2), 161-174. https://doi.org/10.2307/1269043

Oudin, L., Andréassian, V., Perrin, C., Michel, C., & Le Moine, N. (2008), Spatial proximity, physical similarity, regression and ungaged catchments: A comparison of regionalization approaches based on 913 French catchments, *Water Resources Research*, *44*(3). https://doi.org/10.1029/2007WR006240

Pianosi, F., Sarrazin, F., & Wagener, T. (2015), A matlab toolbox for global sensitivity analysis, *Environmental Modelling & Software*, *70*, 80-85. https://doi.org/10.1016/j.envsoft.2015.04.009

Pianosi, F., Beven, K., Freer, J., Hall, J. W., Rougier, J., Stephenson, D. B., & Wagener, T. (2016), Sensitivity analysis of environmental models: A systematic review with practical workflow, *Environmental Modelling & Software*, *79*, 214-232. https://doi.org/10.1016/j.envsoft.2016.02.008

Razavi, S., & Gupta, H. V. (2015), What do we mean by sensitivity analysis? The need for comprehensive characterization of “global” sensitivity in Earth and Environmental systems models, *Water Resources Research*, *51*(5), 3070-3092. https://doi.org/10.1002/2014WR016527

Razavi, S., & Gupta, H. V. (2016), A new framework for comprehensive, robust, and efficient global sensitivity analysis: 1. Theory, *Water Resources Research*, *52*(1), 423-439. https://doi.org/10.1002/2015WR017558

Rode, M., Halbedel née Angelstein, S., Anis, M. R., Borchardt, D., & Weitere, M. (2016a), Continuous In-Stream Assimilatory Nitrate Uptake from High-Frequency Sensor Measurements, *Environmental Science & Technology*, *50*(11), 5685-5694. https://doi.org/10.1021/acs.est.6b00943

Rode, M., Arhonditsis, G., Balin, D., Kebede, T., Krysanova, V., van Griensven, A., & van der Zee, S. E. A. T. M. (2010), New challenges in integrated water quality modelling, *Hydrological Processes*, *24*(24), 3447-3461. https://doi.org/10.1002/hyp.7766

Rode, M., Wade, A. J., Cohen, M. J., Hensley, R. T., Bowes, M. J., Kirchner, J. W., Arhonditsis, G. B., Jordan, P., Kronvang, B., Halliday, S. J., Skeffington, R. A., Rozemeijer, J. C., Aubert, A. H., Rinke, K., & Jomaa, S. (2016b), Sensors in the Stream: The High-Frequency Wave of the Present, *Environmental Science & Technology*, *50*(19), 10297-10307. https://doi.org/10.1021/acs.est.6b02155

Samaniego, L., Kumar, R., & Attinger, S. (2010), Multiscale parameter regionalization of a grid-based hydrologic model at the mesoscale, *Water Resources Research*, *46*(5). https://doi.org/10.1029/2008WR007327

Sarrazin, F., Pianosi, F., & Wagener, T. (2016), Global Sensitivity Analysis of environmental models: Convergence and validation, *Environmental Modelling & Software*, *79*, 135-152. https://doi.org/10.1016/j.envsoft.2016.02.005

Sheikholeslami, R., Razavi, S., Gupta, H. V., Becker, W., & Haghnegahdar, A. (2019), Global sensitivity analysis for high-dimensional problems: How to objectively group factors and measure robustness and convergence while reducing computational cost, *Environmental Modelling & Software*, *111*, 282-299. https://doi.org/10.1016/j.envsoft.2018.09.002

Sobol', I. M. (2001), Global sensitivity indices for nonlinear mathematical models and their Monte Carlo estimates, *Mathematics and Computers in Simulation*, *55*(1), 271-280. https://doi.org/10.1016/S0378-4754(00)00270-6

Stanford, G., Dzienia, S., & Vander Pol, R. A. (1975), Effect of Temperature on Denitrification Rate in Soils1, *Soil Science Society of America Journal*, *39*, 867-870. https://doi.org/10.2136/sssaj1975.03615995003900050024x

Tang, Y., Reed, P., van Werkhoven, K., & Wagener, T. (2007), Advancing the identification and evaluation of distributed rainfall-runoff models using global sensitivity analysis, *Water Resources Research*, *43*(6). https://doi.org/10.1029/2006WR005813

van Griensven, A., Meixner, T., Grunwald, S., Bishop, T., Diluzio, M., & Srinivasan, R. (2006), A global sensitivity analysis tool for the parameters of multi-variable catchment models, *Journal of Hydrology*, *324*(1), 10-23. https://doi.org/10.1016/j.jhydrol.2005.09.008

van Werkhoven, K., Wagener, T., Reed, P., & Tang, Y. (2008a), Characterization of watershed model behavior across a hydroclimatic gradient, *Water Resources Research*, *44*(1). https://doi.org/10.1029/2007WR006271

van Werkhoven, K., Wagener, T., Reed, P., & Tang, Y. (2008b), Rainfall characteristics define the value of streamflow observations for distributed watershed model identification, *Geophysical Research Letters*, *35*(11). https://doi.org/10.1029/2008GL034162

Wade, A. J., Durand, P., Beaujouan, V., Wessel, W. W., Raat, K. J., Whitehead, P. G., Butterfield, D., Rankinen, K., & Lepisto, A. (2002), A nitrogen model for European catchments: INCA, new model structure and equations, *Hydrology and Earth System Sciences*, *6*(3), 559-582. https://doi.org/10.5194/hess-6-559-2002

Wagener, T., van Werkhoven, K., Reed, P., & Tang, Y. (2009), Multiobjective sensitivity analysis to understand the information content in streamflow observations for distributed watershed modeling, *Water Resources Research*, *45*(2). https://doi.org/10.1029/2008WR007347

Wagener, T., Boyle, D. P., Lees, M. J., Wheater, H. S., Gupta, H. V., & Sorooshian, S. (2001), A framework for development and application of hydrological models, *Hydrol. Earth Syst. Sci.*, *5*(1), 13-26. https://doi.org/10.5194/hess-5-13-2001

Wellen, C., Kamran-Disfani, A.-R., & Arhonditsis, G. B. (2015), Evaluation of the Current State of Distributed Watershed Nutrient Water Quality Modeling, *Environmental Science and Technology*, *49*(6), 3278-3290. https://doi.org/10.1021/es5049557

Wollschläger, U., Attinger, S., Borchardt, D., Brauns, M., Cuntz, M., Dietrich, P., Fleckenstein, J. H., Friese, K., Friesen, J., Harpke, A., Hildebrandt, A., Jäckel, G., Kamjunke, N., Knöller, K., Kögler, S., Kolditz, O., Krieg, R., Kumar, R., Lausch, A., Liess, M., Marx, A., Merz, R., Mueller, C., Musolff, A., Norf, H., Oswald, S. E., Rebmann, C., Reinstorf, F., Rode, M., Rink, K., Rinke, K., Samaniego, L., Vieweg, M., Vogel, H.-J., Weitere, M., Werban, U., Zink, M., & Zacharias, S. (2016), The Bode hydrological observatory: a platform for integrated, interdisciplinary hydro-ecological research within the TERENO Harz/Central German Lowland Observatory, *Environmental Earth Sciences*, *76*(1), 29. https://doi.org/10.1007/s12665-016-6327-5

Yang, X., Jomaa, S., Büttner, O., & Rode, M. (2019), Autotrophic nitrate uptake in river networks: A modeling approach using continuous high-frequency data, *Water Research*, *157*, 258-268. https://doi.org/10.1016/j.watres.2019.02.059

Yang, X., Jomaa, S., Zink, M., Fleckenstein, J. H., Borchardt, D., & Rode, M. (2018), A new fully distributed model of nitrate transport and removal at catchment scale, *Water Resources Research*, *54*(8), 5856-5877. https://doi.org/10.1029/2017WR022380

Yu, C., Huang, X., Chen, H., Godfray, H. C. J., Wright, J. S., Hall, J., Gong, P., Ni, S., Qiao, S., Huang, G., Xiao, Y., Zhang, J., Feng, Z., Ju, X., Ciais, P., Stenseth, N. C., Hessen, D. O., Sun, Z., Yu, L., Cai, W., Fu, H., Huang, X., Zhang, C., Liu, H., & Taylor, J. (2019), Managing nitrogen to restore water quality in China, *Nature*. https://doi.org/10.1038/s41586-019-1001-1

4.10. Supplementary Materials

Text S4.1. Descriptions of the nitrogen transformations in the mHM-Nitrate model (Lindström et al., 2010; Yang et al., 2018). The parameter ranges were adopted from Jiang et al. (2014) and Yang et al. (2018) where the Selke catchment is used for the HYPE model and the mHM-Nitrate model.

(1) Empirical equations for impacts of well-known factors

(i) Impact of soil temperature ($soil\_temp$, ℃):

$$f_{soil\_temp} = \begin{cases} 0, & soil\_temp < 0 \\ 2^{(soil\_temp-20)/10}, & 0 < soil\_temp < 5 \\ \frac{soil\_temp}{5} \cdot 2^{(soil\_temp-20)/10}, & soil\_temp > 5 \end{cases} \quad \text{(S4.1)}$$

Soil temperature is calculated from the soil temperature in previous time step, air temperature (air_temp) and deep soil temperature (fixed as 5 ℃) and aggregated as:

$$soil\_temp = (1 - weight - 0.001) \cdot soil\_temp + weight \cdot air\_temp + 0.001 \cdot 5 \quad \text{(S4.2)}$$

where $weight = \frac{1}{30+10 \cdot snowdepth}$ and the $snowdepth$ is the snow depth that is updated at each time step of the model simulation.

(ii) Impact of soil moisture (SM):

$$f_{sm} = \begin{cases} 0, & SM < 0.3 \\ (\frac{\frac{SM}{SM\_SAT} - 0.3}{1 - 0.3})^{2.5}, & 0.3 < SM < 1 \end{cases} \quad \text{(S4.3)}$$

where SM_SAT denotes the saturated soil moisture content.

(iii) Impact of nitrate concentration in soil water (SMC):

$$f_{smc} = \frac{SMC}{SMC + 1.0} \quad \text{(S4.4)}$$

For more information on those empirical equations, please refer to the source code of mHM-Nitrate (https://git.ufz.de/yangx/mHM-Nitrate) or the HYPE model description document (http://www.smhi.net/hype/wiki/doku.php?id=start:hype_model_description, last accessed on September 1st 2019).

(2) Soil denitrification (Parameter *denis,* d^{-1})

This transformation describes the denitrification process in all soil layers. Soil denitrification ($DENI, mg\ N\ m^2\ d^{-1}$) is a sink of nitrate, depending on the denitrification rate (*denis* as a model parameter) and the pool size of nitrate in the soil water (DIN) and the impacts of soil temperature (f_{soil_temp}), soil moisture (f_{sm}) and nitrate concentration (f_{smc}) which are estimated based on above empirical equations.

$$DENI = denis \cdot f_{soil\_temp} \cdot f_{sm} \cdot f_{smc} \cdot DIN \quad \text{(S4.5)}$$

The range of parameter *denis* is given as [1.00e-8, 1.00e+0].

(3) Soil mineralization (Parameter *minlr,* d^{-1})

This transformation describes the overall soil mineralization of the labile organic nitrogen (dissoved and active solid organic pools, DON and SON_A, respectively) to DIN. The soil mineralization ($MINL, mg\ N\ m^2\ d^{-1}$) is calculated based on the mineralization rate (*minlr*), the pool size of the organic nitrogen forms and the impacts of soil temperature (f_{soil_temp}) and soil moisture (f_{sm}).

$$\begin{aligned} MINL1 &= minlr \cdot f_{soil\_temp} \cdot f_{sm} \cdot SON_A \\ MINL2 &= minlr \cdot f_{soil\_temp} \cdot f_{sm} \cdot DON \end{aligned} \quad \text{(S4.6)}$$

The range of parameter *minlr* is given as [1.00e-4, 1.00e+0].

(4) Soil dissolution rate (Parameter *dislr,* d^{-1})

This transformation describes the organic nitrogen dissolution from SON_A to DON. The soil dissolution ($DISL, mg\ N\ m^2\ d^{-1}$) depends on the dissolution rate (*dislr*), the pool size of SON_A and the impacts of soil temperature (f_{soil_temp}) and soil moisture (f_{sm}).

$$DISL = dislr \cdot f_{soil\_temp} \cdot f_{sm} \cdot \mathrm{SON}_A \quad \text{(S4.7)}$$

The range of parameter *dislr* is give as [1.00e-3, 2.00e+2].

(5) Soil degradation rate (Parameter *degdr,* d^{-1})

This transformation describes the soil organic nitrogen degradation from the inactive form (SON_I) to the active form (SON_A). The soil degradation ($DEGD, mg\ N\ m^2\ d^{-1}$) depends on the degradation rate (*degdr*), the pool size of SON_I and the impacts of soil temperature (f_{soil_temp}) and soil moisture (f_{sm}).

$$DEGD = degdr \cdot f_{soil\_temp} \cdot f_{sm} \cdot SON_I \quad \text{(S4.8)}$$

The range of parameter *degdr* is give as [1.00e-5, 5.00e-5].

(6) In-stream denitrification (Parameter *deniw,* $mg\ N\ m^{-2}d^{-1}$)

This transformation describes the denitrification process in the in-stream phase. The in-stream denitrification ($DENIw, mg\ N\ d^{-1}$) depends on the stream denitrification rate (*deniw*), water temperature ($water\_temp$), stream $N - NO_3^-$ concentration (N_conc) and the stream benthic area (SW_area, m^2).

$$DENIw = deniw \cdot f_{water\_temp} \cdot f_{N_{conc}} \cdot SW\_area \quad \text{(S4.9)}$$

Where the impacts of water temperature (f_{water_temp}) and nitrate concentration (f_{N_conc}), have the same empirical formulations as those in the soil phase, respectively. The $water\_temp$ is calculated as 20-day's moving average of air temperature.

The stream benthic area SW_area:

$$SW\_area = width \times length \quad \text{(S4.10)}$$

where $width = 5.4 \cdot Q^{0.5}$ (Rode et al., 2016a) and $length$ is obtained from the digital elevation model (DEM) used in the mHM-Nitrate.

The range of parameter *deniw* is given as [1.00e-8, 5.00e-2].

(7) In-stream net assimilatory uptake (Parameter *npprt,* $mg\ N\ m^{-2}d^{-1}$)

This transformation describes the net in-stream assimilatory uptake (i.e., the net effect of in-stream autotrophic assimilatory uptake and in-stream remineralization).

The autotrophic assimilatory uptake ($UPTKauto, mg\ N\ d^{-1}$) is estimated based on a new regionalization approach by Yang et al. (2019b) as:

$$UPTKauto = U_{a,max} \cdot f_L \cdot SW\_area \quad \text{(S4.11)}$$

where $U_{a,max}$ denotes the potential autotrophic nitrate uptake rate; and f_L denotes the stream surface light coefficient quantified as:

$$f_L = f_{GR} \cdot (1 - f_{LAI}) \tag{S4.12}$$

where f_{GR} denotes the impact of above-canopy light availability (represented by global radiation, GR), and f_{LAI} denotes the impact of riparian shading (represented by leaf area index, LAI). The f_{GR} and f_{LAI} (both $\in [0,1]$) are normalized from the moving-averaged daily GR data and daily mean LAI data, respectively. The regionalization approach is parsimoniously designed with several assumptions. At river network scale, the stream riparian vegetation is assumed as the same as the surrounding land use. Therefore, for each stream reach, the overall f_{LAI} is calculated by the occurrence of land use types and weighted by their areal proportions ($f_{LAI} = \sum_{i=1}^{n} \alpha_i \cdot f_{LAI}^i$, where $\alpha_i$and f_{LAI}^idenote the areal proportion and normalized LAI of land-use type i, respectively; n denotes the number of total land-use types).

Part of the assimilated nitrogen will be re-mineralized and returned back to stream water as nitrate (i.e, the in-stream remineralization process). It is very difficult to quantify this process due to the limited process understanding. Therefore, the net uptake ($UPTKnet, mg\ N\ d^{-1}$) is assumed as a fraction of $UPTKauto$, and calculated as:

$$UPTKnet = \alpha \cdot U_{a,max} \cdot f_{GR} \cdot (1 - f_{LAI}) \cdot SW\_area \tag{S4.13}$$

where the fraction $\alpha \epsilon (0,1]$. In this study, we introduced the net assimilatory uptake rate ($nppr t = \alpha \cdot U_{a,max}, mg\ N\ m^{-2} d^{-1}$) as the model parameter. The value of $U_{a,max}$ has been quantified in the Selke catchment (283 $mg\ N\ m^{-2} d^{-1}$) based on the available continuous autotrophic data (Yang et al., 2019b). Here we directly adopted this value and set the range of α as [1.00e-4, 1.00e+0], resulting in the range of parameter $nppr t$ as [1.00e-3, 2.83e+2].

Table S4.1. The mHM model parameters and their calibrated values in the Selke catchment. Majority of the parameters is introduced from the transfer functions, which are included in the regionalization approach (i.e., the MPR technique, Samaniego et al. (2010)). Please refer to the reference for detailed description. *Note.* (1) *retentionCoefficient is the coefficient of a simple linear retention-delay method used in this study for the flow routing calculation; (2) °According to Samaniego et al. (2010), parameters of baseflow generation have not been regionalized yet ("GeoParam"), and therefore, are assigned as geological unit dependent.

mHM parameter	Range	Optimal value
CanopyInterceptionFactor	[1.49e-1, 4.00e-1]	1.51e-1
SnowTresholdTemperature	[-2.00e+0, 2.00e+0]	3.38e-1
degreeDayFactor_forest	[1.00e-4, 4.00e+0]	1.44e+0
degreeDayFactor_impervious	[0.00e+0, 1.00e+0]	2.44e-3
degreeDayFactor_pervious	[0.00e+0, 2.00e+0]	1.20e+0
increaseDegreeDayFactorByPrecip	[1.00e-1, 9.00e-1]	8.99e-1
maxDegreeDayFactor_forest	[0.00e+0, 8.00e+0]	1.31e+0
maxDegreeDayFactor_impervious	[0.00e+0, 8.00e+0]	6.82e-3
maxDegreeDayFactor_pervious	[0.00e+0, 8.00e+0]	1.34e+0

orgMatterContent_forest	[0.00e+0, 2.00e+1]	1.53e+1
orgMatterContent_impervious	[0.00e+0, 1.00e+0]	9.99e-1
orgMatterContent_pervious	[0.00e+0, 4.00e+0]	3.99e+0
PTF_lower66_5_constant	[6.46e-1, 9.51e-1]	9.50e-1
PTF_lower66_5_clay	[1.00e-4, 2.90e-3]	4.15e-4
PTF_lower66_5_Db	[-3.73e-1, -1.87e-1]	-2.91e-1
PTF_higher66_5_constant	[5.36e-1,1.12e+0]	9.21e-1
PTF_higher66_5_clay	[-5.50e-3, 4.90e-3]	-5.48e-3
PTF_higher66_5_Db	[-5.51e-1, -9.13e-2]	-9.14e-2
PTF_Ks_constant	[-1.20e+0, -2.85e-1]	-9.03e-1
PTF_Ks_sand	[6.00e-3, 2.60e-2]	8.58e-3
PTF_Ks_clay	[3.00e-3, 1.30e-2]	3.34e-3
PTF_Ks_curveSlope	[1.00e+0, 1.50e+2]	6.23e+1
rootFractionCoefficient_forest	[9.00e-1, 1.00e+0]	9.62e-1
rootFractionCoefficient_impervious	[9.00e-1, 9.50e-1]	9.59e-1
rootFractionCoefficient_pervious	[1.00e-3, 9.00e-2]	5.08e-3
infiltrationShapeFactor	[1.00e+0, 4.00e+0]	2.94e+0
imperviousStorageCapacity	[0.00e+0, 5.00e+0]	4.99e+0
minCorrectionFactorPET	[7.00e-1, 1.30e+0]	1.02e+0
maxCorrectionFactorPET	[0.00e+0, 2.00e-1]	7.15e-2
aspectTresholdPET	[1.60e+2, 2.00e+2]	160e+2
interflowStorageCapacityFactor	[7.50e+1, 2.00e+2]	7.51e+1
interflowRecession_slope	[0.00e+0, 1.00e+1]	4.29e+0
fastInterflowRecession_forest	[1.00e+0, 3.00e+0]	1.00e+0
slowInterflowRecession_Ks	[1.00e+0, 3.00e+1]	1.42e+1
exponentSlowInterflow	[5.00e-2, 3.00e-1]	1.20e-1
rechargeCoefficient	[0.00e+0, 5.00e+1]	4.41e+1
rechargeFactor_karstic	[-5.00e+0, 5.00e+0]	1.18e+0
*retentionCoefficient	[1.00e-2, 1.00e+0]	9.51e-1
°GeoParam1_SalianSed	[1.00e+0, 1.00e+3]	2.05e+1
°GeoParam3_HoloceneSed	[1.00e+0, 1.00e+3]	3.79e+2
°GeoParam4_UCretaceousSed	[1.00e+0, 1.00e+3]	1.21e+0
°GeoParam5_DevonianWacke	[1.00e+0, 1.00e+3]	2.60e+1
°GeoParam10_MississippianWacke	[1.00e+0, 1.00e+3]	9.98e+2
°GeoParam11_EoceneClasticSed	[1.00e+0, 1.00e+3]	2.03e+2
°GeoParam12_OlenekianCalsticSed	[1.00e+0, 1.00e+3]	2.10e+2
°GeoParam104_AnisianCarbonSed	[1.00e+0, 1.00e+3]	7.50e+2
°GeoParam111_CarboniferousSed	[1.00e+0, 1.00e+3]	4.44e+0
°GeoParam112_TriassicSed	[1.00e+0, 1.00e+3]	3.21e+2

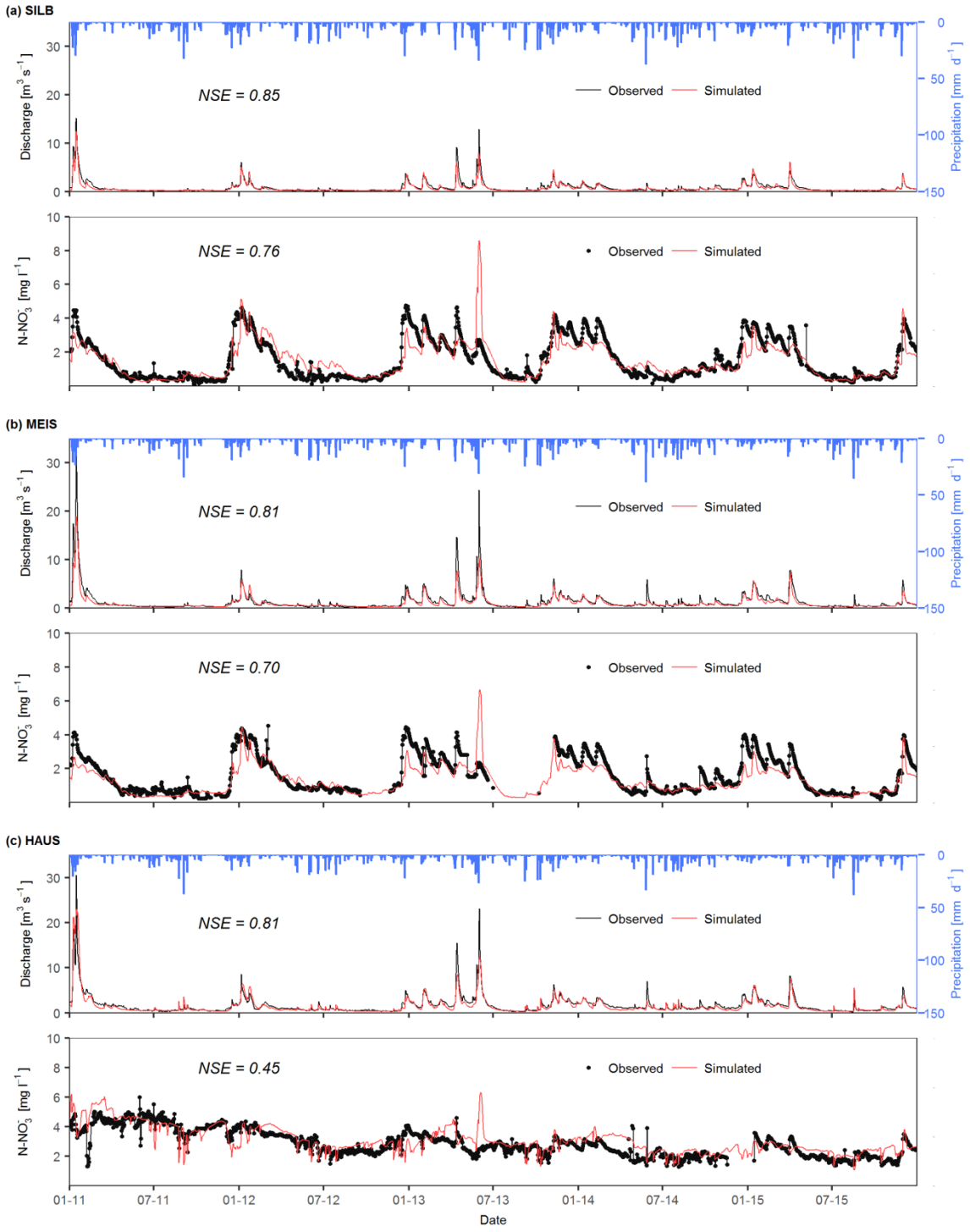

Figure S4.1. The mHM-Nitrate model daily simulations (2011-2015) of discharge and $N - NO_3^-$ concentration at the three nested gauging stations (i.e., (a) SILB, (b) MEIS, and (c)HAUS, representing station Silberhütte, Meisdorf, and Hausneindorf, respectively). NSE stands for Nash-Sutcliffe efficiency coefficient. For detailed discussions on the model performance, please refer to Yang et al. (2018).

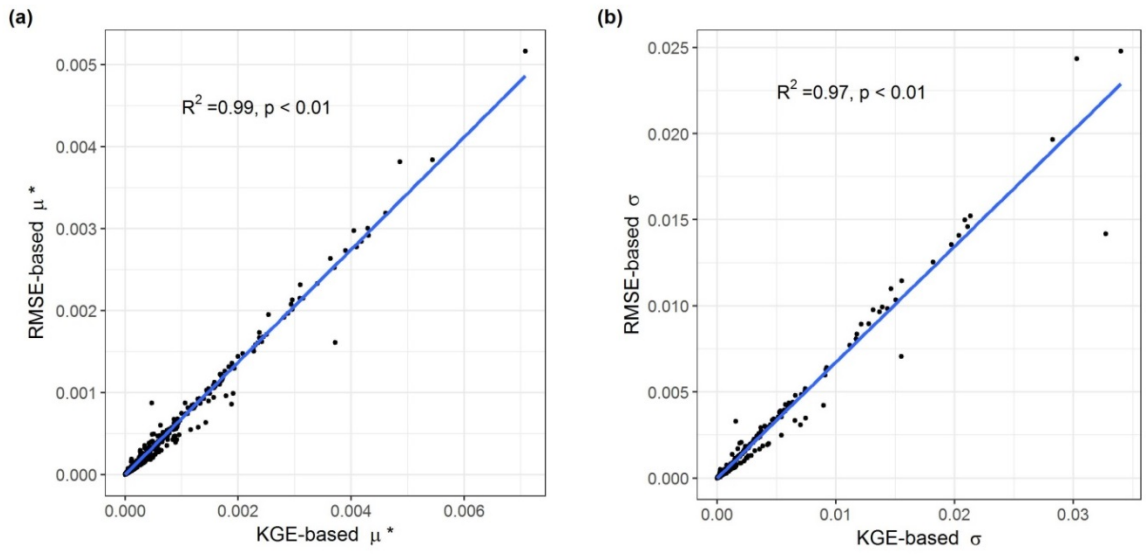

Figure S4.2. The consistency of the sensitivity indices based on different evaluation metrics, i.e., the RMSE (Root-Mean-Squared-Error) and the KGE (Kling-Gupta Efficiency(Gupta et al., 2009)). Plot (a) and (b) show the linear correlations of μ^* and σ, respectively, between the RMSE and the KGE. For each subplot, each dot represents one parameter of the total 3196 parameters. The sensitivity indices were calculated based on $N - NO_3^-$ concentration observations at all three gauging stations.

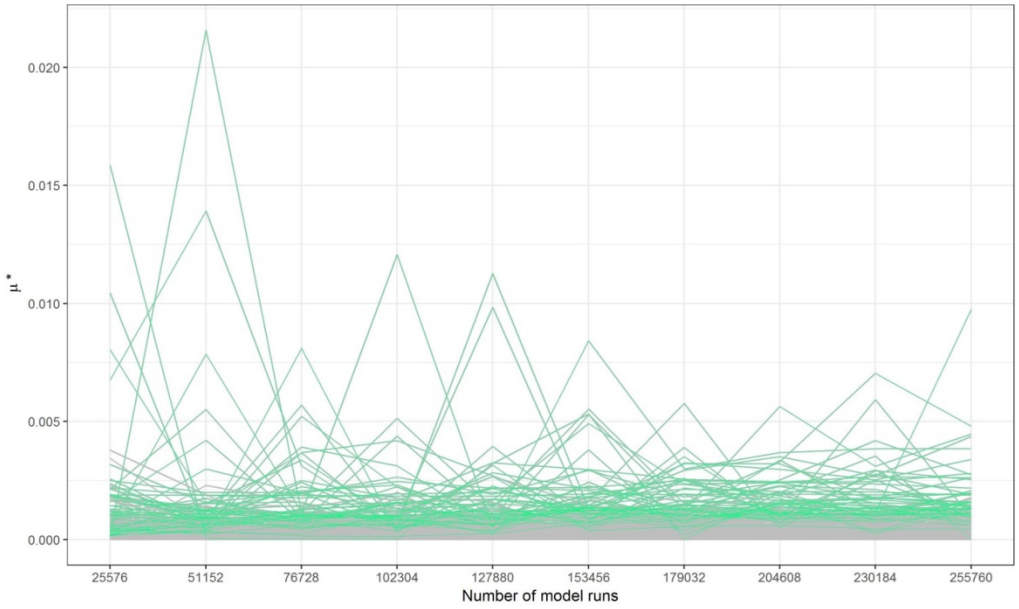

Figure S4.3. The convergence of the sensitivity index μ^* (i.e., the absolute mean of EE). Each line in the plot represents one of the 3196 parameters considered in this study. The blue lines highlight the convergences of the top 50 sensitive parameters.

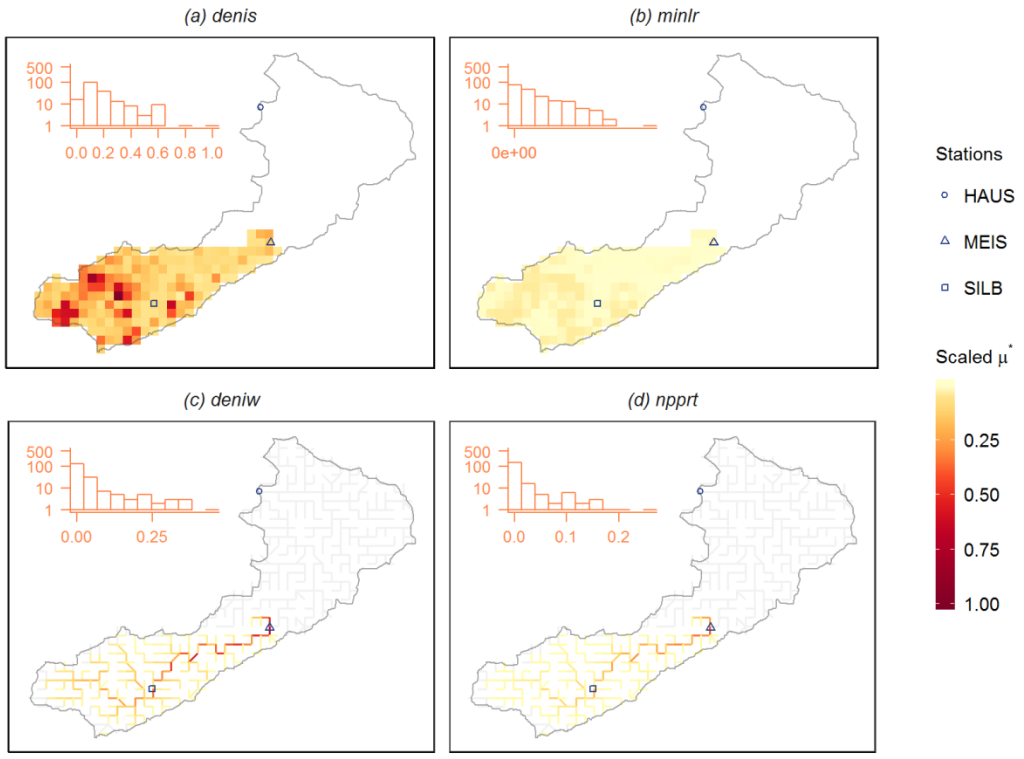

Figure S4.4. Spatial distributions of parameter sensitivity indices in the MEIS subcatchment (grid size 1 km^2). The μ^* (absolute mean of EEs) values are scaled into the range of [0, 1]. Only the most sensitive parameters (a) *denis*, (b) *minlr*, (c) *deniw* and (d) *npprt*, representing the soil denitrification, soil mineralization, in-stream denitrification and in-stream assimilatory uptake processes, respectively, are presented. The inserted histogram plot represents the distribution of the scaled μ^* values for each parameter. The y-axis denotes the number of grid cells/stream reaches and has been log-transformed. Deactivated grid cells are excluded, while deactivated stream reaches are shown in gray lines.

Data S4.1. The whole dataset of catchment factors.

(Please find this data in https://git.ufz.de/yangx/sensitivity-analysis, last accessed on 01.09.2020)

Chapter 5: Discussion

In this dissertation, a new fully distributed catchment nitrate model (mHM-Nitrate) is developed to balance accurate spatial representation and manageable model complexity (Chapter 2). Based on continuous high-frequency nitrate data, in-stream autotrophic nitrate uptake at monitoring reaches can be directly calculated. Driving by this newly available information, a parsimonious regionalization approach of the assimilatory nitrate uptake process is proposed using widely accessible information, i.e., global radiation and leaf area index. Integrating the new mHM-Nitrate model and the new regionalization approach enables such reach-scale advances to be upscaled to the river network scale (Chapter 3). In being compatible with the grid-based catchment discretization, the fully distributed parameterization is further analyzed through sensitivity analysis. Sensitive parameters and their controlling factors (i.e., catchment factors including meteorological forcing, catchment characteristics and modelled state variables and fluxes) are demonstrated explicitly at a full spatial range (Chapter 4). In this section, new insights into, and future perspectives of spatiotemporal nitrate dynamics at catchment and river network scale are discussed.

5.1. Benefits from the fully distributed modeling and parameterization

Considering current challenges of water environmental protection, the mHM-Nitrate model is developed to serve as a scientific evaluation tool for catchment scientists, as well as a practical decision-supporting tool for catchment managers and related stakeholders (Yang et al., 2018). The process-based descriptions of nitrate dynamics (mainly adopted from the HYPE model by Lindström et al. (2010)) are fully integrated into the grid-based, multiscale Hydrological Model platform (i.e., the mHM model by Samaniego et al. (2010)). The implementation scheme of mHM-Nitrate provides essential technical advantages as follows:

- Spatial discretization structure: Based on mHM, the resolution of modeling grid cells can be specified separately from that of the basic geographic inputs. The modeling grid cell can, therefore, be taken as a combination of the subcatchment and the homogeneous unit of the semi-distributed modeling. Such multi-resolution implementation balances the model complexity, meanwhile reserves flow and nitrate information for specific locations.
- Model parameterization: Adopting the MPR technique, model parameters are firstly determined at the geographic level either by regionalization functions or simply by category assignment, and then upscaled to the modeling level according to the areal share of each category. This

implementation largely simplifies the parameterization and maintains a certain degree of spatial variation between modeling grid cells. Moreover, the model parameters are likely robust and independent from the modeling resolution (Kumar et al., 2013).

- Consideration of anthropogenic impacts: An additional map of crop rotation type is implemented in mHM–Nitrate to consider the spatial variations of crops and the corresponding external fertilizer applied. This new feature also facilitates a more straightforward scenario analysis in assessing the effects of spatially differentiated mitigation measures. Moreover, the model allows time series point source as input to be added at the stream reach where WWTPs are located.

Table 5.1 lists comparisons between the mHM-Nitrate model and the HYPE model in several modeling aspects (the similarity marks are roughly assigned). Both models are quite similar in terms of hydrological and nitrate process descriptions and input data requirements (including meteorological forcing, geographic data and basic farming information). Therefore, they are expected to have similar performance in terms of reproducing discharge and nitrate observations at gauging stations. For instance, the HYPE model also performed well at the three gauging stations of the Selke catchment (Jiang et al., 2014; Jiang et al., 2015). While, above technical advantages do stand out the new mHM-Nitrate model in the following aspects:

- In addition to a good performance at gauging station, mHM-Nitrate provides detailed information of flow and nitrate fluxes in each grid cell/stream reach. The comprehensive evaluation in the Selke catchment demonstrates that such information is reliable (Chapter 2 (Yang et al., 2018)). The “hot-spot” and “hot-moment” of nitrate non-point source pollution can be explicitly identified from the spatial and temporal simulation of nitrate dynamics. As a step further, the effects of different mitigation measures can be evaluated by the model, so that more costly measures can be targeted in the critical locations at the right time.
- All parameter values are firstly determined by catchment properties (land-use, soil types and properties, etc.) at the basic geographic data level, and then upscaled to the modeling level. Such parameterization scheme acts as a suitable platform to upscale advanced process understandings, which are normally gained at field or reach scale, to catchment or river network scale (see, e.g., Chapter 3 (Yang et al., 2019b)).
- Basic information of catchment properties is also upscaled to the modeling level. This enables direct analysis and correlations between parameters and catchment factors by spatially

distributed parameter configuration. Insights into the spatial variability of parameter sensitivity and their controlling factors can be gained (see, e.g., Chapter 4 (Yang et al., 2019a)).

Table 5.1. A brief comparison between the mHM-Nitrate model and the HYPE model (the more colored star marks indicates the higher degree of similarity).

Category		mHM-Nitrate (Yang et al., 2018)	HYPE (Lindström et al., 2010)	Similarity
Model structure	Catchment discretization	Fully distributed (grid-based)	Semi-distributed	☆☆☆☆☆
	Hierarchical structure	multiple levels (i.e., basic geographic data level, meteorological data level and modeling levels)	catchment, subcatchment, soil and land-use class (SLC)	☆☆☆☆☆
	Hydrological submodel	mHM (based on the HBV model)	The modified HBV model	★★★★☆
	Substances	Nitrate	IN, TN, PP, SP, TP, DOC, Sediment	★★☆☆☆
	Water quality submodel	Mainly adopted from HYPE and INCA-N(Wade et al., 2002)	HBV-NP (Andersson et al., 2005)	★★★★☆
	River network	Grid cells are linked according to the main flow direction	Subcatchments are linked by geographic connections	☆☆☆☆☆
Model parameterization		Regionalization approach by Samaniego et al. (2010) and Yang et al. (2019b); geological unit or land-use dependent parameters	General, regional, soil type or land-use dependent parameters	★★☆☆☆
Data requirement	Meteorological inputs	Precipitation, temperature and data for different methods of evapotranspiration	Precipitation, temperature and data for different methods of evapotranspiration	★★★★★
	Geographic inputs	DEM, land-use type, soil type, soil properties, geological unit, etc.	DEM, land-use map, soil map, etc.	★★★★☆
Anthropogenic inputs	Agricultural activities	For each crop: fertilizer/manure amount, applied dates, farming dates (sowing, harvesting), nutrient potential uptake function, etc. Crop rotation: YES	For each crop: fertilizer/manure amount, applied dates, farming dates (sowing, harvesting), nutrient potential uptake function, etc. Crop rotation: YES	★★★★★
	Water management	Not yet	Tile drainage, irrigation, lakes/reservoirs, water extraction	☆☆☆☆☆
	Point source input	The exact location of WWTP, time-varying discharge and concentration from point source	Point source assigned to the corresponding subcatchment, constant discharge, multiple constant concentrations for different periods	★☆☆☆☆
Time step		Daily (hourly is also technically possible)	Daily	★★★★★

5.2. Benefits from long-term grab sampling and continuous high-frequency monitoring

Due to the development of sensor techniques, high-frequency sensor monitoring has been increasingly deployed in many catchments across different climatic and environmental regions. This has raised comparative discussions between the two monitoring strategies, i.e., traditional regular grab sampling and high-frequency sensor deployment. In this dissertation, data from both strategies are used, and complementary in different aspects of nitrate dynamics and modeling.

At regional scale, long-term, regularly sampled time series data can reflect the trend reversals of environmental or ecological status due to climatic and social-economic changes (Reusch et al., 2018). At catchment scale, nitrate transport from agricultural uplands to receiving waters may take years to decades (Wriedt & Rode, 2006). Traditional long-term grab sampling data (e.g., biweekly or monthly) are, therefore, essential to assess the long-term nitrate trend and the effects of agricultural practices and measures on surface water nitrate concentration levels (Dupas et al., 2016). Nearly 20-year's biweekly data are used in this dissertation to achieve a comprehensive validation of the mHM-Nitrate model, given the large inter-annual variations in point-source impacts and spatiotemporal distributions of meteorological forcing.

In contrast, high-frequency sensor monitoring offers tremendous opportunities for process understandings by upgrade the monitoring resolution to the time scales of biogeochemical processes (Dupas et al., 2016; Rode et al., 2016b). Specifically for in-stream autotrophic nitrate uptake, daily uptake rate ($U_{a-NO_3^-}$) can be directly obtained from the diel cycles of stream metabolism and nitrate concentration (Heffernan & Cohen, 2010; Dupas et al., 2016). The $U_{a-NO_3^-}$ dataset presented in this dissertation (i.e., the daily values obtained from continuous 5-year sensor deployments in a forested and an agricultural stream) provides the unique opportunity to identify the controlling factors, and further, to validate the regionalization approach of the process.

It has been argued that high-frequency monitoring is equivalent to regular grab sampling in terms of, e.g., general model calibrations (Jiang et al., 2019) and nutrient fluxes estimates (Wollheim et al., 2017). Similarly in this dissertation, the mHM-Nitrate model is calibrated using biweekly observations at three gauging stations, but it reasonably well reproduces short-term nitrate dynamics (e.g., fluctuations during high concentration periods at forest stations) that are observed in the daily observations. However, from another perspective, the simulated short-term dynamics can only be validated through additional higher frequency observations. Moreover, higher frequency data is informative in inferring the changes

of flow pathways during flood events (Dupas et al., 2016; Miller et al., 2016) and capturing the actual range of nitrate dynamics in complex large catchment (Carey et al., 2014). Overall, the high-frequency sensor data and the long-term grab sampling data complement each other in allowing comprehensive analysis and modeling of nitrate dynamics under the changing environment.

5.3. Future work

The newly proposed methodologies (i.e., the newly developed model, the approach based on the new data and the spatially distributed parameterization) contribute to advancing the state-of-the-art in modeling and analyzing catchment nitrate dynamics. Unavoidably, there are several constraints within the scope of this dissertation, which are also worthwhile for future research:

- Model further applications and development. The development of the mHM-Nitrate model is intended to provide a general modeling platform that is applicable for regions with different conditions. Further model applications could go to (i) applying the model to larger catchments (e.g., the Bode catchment, to which the Selke catchment belongs, with the size of 3000 km^2), and (ii) applying the model to different regions with different climatic and anthropogenic conditions. Moreover, the model can be a promising paradigm for other water quality compounds (e.g., phosphorus, organic carbon, sediment, etc.) to achieving a comprehensive "water quality model".
- Model further usage. The new model is oriented to address real-world environmental problems. Its grid-based structure is of particular suitable for current demands on spatially differentiated mitigation measures. Therefore, it is worthwhile to use the model to assess the effects of land-use change or mitigation scenarios on surface water nitrate levels.
- Benefiting further from high-frequency data. In stream nitrate processes (denitrification, assimilatory uptake and remineralization) are highly convoluted with each other. By digging deep into the increasing high-frequency dataset and with the help of new sensor-based experimental design, these processes can potentially be separated (see, e.g., Heffernan and Cohen (2010), Kunz et al. (2017) and Jarvie et al. (2018)). The regionalization and upscaling procedure for autotrophic nitrate uptake presented here can, therefore, act as a paradigm for other processes.
- Interdisciplinary efforts on in-stream uptake. The regionalization approach presented here is parsimoniously designed but captures reasonably well the ranges and seasonal patterns under different conditions. However, considerable simplifications and assumptions are introduced.

Interdisciplinary efforts from hydrology, hydraulics, limnology and aquatic ecology are needed for a comprehensive assessment of the process dynamics.

- Thoughtful parameter analysis. For fully distributed modeling, the complexity of model parameterization is one of the most challenging issues. This study demonstrates that mathematic analysis tools are helpful in reducing the dimensionality of parameter space (using sensitivity analysis) and in assessing the uncertainty of parameter determination (using uncertainty analysis). However, more thoughtful parametric analyses that make the most of the techniques are recommended, e.g., the time-varying, spatially distributed sensitivity analysis (Herman et al., 2013b; Schrön et al., 2017) and distinguishing various sources of uncertainty (Ajami et al., 2007).

Chapter 6: Summary

This study presents a new process-based catchment nitrate model (the mHM-Nitrate model) with the emphasis on providing detailed spatial information of nitrate concentrations and fluxes (Chapter 2). Based on the multiscale design of the hydrological mHM model, all model inputs (i.e., geographic information and meteorological forcing) are dis-/aggregated to the modeling grid cells, of which the spatial resolution can be specified according to the objectives of the user. Such catchment discretization, therefore, largely reduces the model complexity and meanwhile maintains sufficient spatial representation. The mHM-Nitrate model has been thoughtfully evaluated in the highly heterogeneous Selke catchment (456 km^2) in terms of (i) calibration and validation using the 20-year's long-term discharge and biweekly nitrate observations, (ii) reasonably capture event-scale nitrate temporal dynamics using daily observations, (iii) robust performance by conducting sensitivity and uncertainty analyses, and (iv) providing detailed spatial distributions of nitrate terrestrial balance and in-stream fluxes, which are in reliable range as compared to values in literature.

In addition to the spatial discretization, advancing physical understandings of the nitrate biogeochemical transformations and further formulating it into the model are essential for model development. The emerging high-frequency sensor monitoring enables direct measuring at the time scales of biogeochemical processes. Therefore, new insights into the process understanding can be derived from the new data. Chapter 3, specifically, focuses on the in-stream autotrophic nitrate uptake process. Continuous five-year's daily uptake rates ($U_{a-NO_3^-}$) are obtained based on the high-frequency sensor deployments in a forested and an agricultural stream. Based on this new information, a parsimonious approach of regionalizing $U_{a-NO_3^-}$ is proposed using the catchment-wide accessible global radiation and leaf area index data and validated in the two study streams. Moreover, the approach is further integrated into the mHM-Nitrate model. Due to aforementioned technical advantages, the mHM-Nitrate model is considered as an outstanding platform to upscale the reach-scale advanced understanding to the whole river network; in turn, the approach helps refine the model description of the in-stream uptake process.

Catchment functioning varies under different natural and anthropogenic conditions. Model parameters are generally introduced to tolerate such variations and to maintain the main process descriptions. Therefore, parameterization is one of the main challenges for current process-based modeling (Clark et al., 2017). To further assess the spatial variability of catchment nitrate dynamics, the fully distributed

parameterization is investigated through parameter sensitivity analysis (Chapter 4). All nitrate submodel parameters are configured as grid cell/stream reach dependent, resulting in more than 3000 parameters for the testing Selke catchment. The most sensitive nitrate processes is identical (i.e., soil denitrification, in-stream denitrification and in-stream uptake), but their parameter sensitivities all show high spatial variabilities. Using the Spearman rank correlation, controlling factors of parameter sensitivity vary significantly throughout the catchment/river network. Moreover, the spatial distributions of parameter sensitivity and the corresponding controlling factors are also influenced by the gauging information being used for sensitivity evaluation. The insights gained from this sensitivity analysis are informative in guiding future parameter regionalization of catchment nitrate models.

References

Ajami, N. K., Duan, Q., & Sorooshian, S. (2007), An integrated hydrologic Bayesian multimodel combination framework: Confronting input, parameter, and model structural uncertainty in hydrologic prediction, *Water Resources Research*, *43*(1). https://doi.org/10.1029/2005wr004745

Alexander, R. B., Böhlke, J. K., Boyer, E. W., David, M. B., Harvey, J. W., Mulholland, P. J., Seitzinger, S. P., Tobias, C. R., Tonitto, C., & Wollheim, W. M. (2009), Dynamic modeling of nitrogen losses in river networks unravels the coupled effects of hydrological and biogeochemical processes, *Biogeochemistry*, *93*(1), 91-116. https://doi.org/10.1007/s10533-008-9274-8

Allen, R. G., Pereira, L. S., Raes, D., & Smith, M. (1998), *Crop evapotranspiration - Guidelines for computing crop water requirements*, FAO - Food and Agriculture Organization of the United Nations, Rome, Italy.

Andersson, L., Rosberg, J., Pers, B. C., Olsson, J., & Arheimer, B. (2005), Estimating catchment nutrient flow with the HBV-NP model: sensitivity to input data, *AMBIO*, *34*(7), 521-532. https://doi.org/10.1579/0044-7447-34.7.521

Arnold, J. G., Srinivasan, R., Muttiah, R. S., & Williams, J. R. (1998), Large area hydrologic modeling and assessment part I: Model development *Journal of the American Water Resources Association*, *34*(1), 73-89. https://doi.org/10.1111/j.1752-1688.1998.tb05961.x

Arnold, J. G., Allen, P. M., Volk, M., Williams, J. R., & Bosch, D. D. (2010), Assessment of different representations of spatial variability on SWAT model performance, *Trans. ASABE*, *53*(5), 1433-1443. https://doi.org/10.13031/2013.34913

Bergström, A. K., & Jansson, M. (2006), Atmospheric nitrogen deposition has caused nitrogen enrichment and eutrophication of lakes in the northern hemisphere, *Global Change Biology*, *12*(4), 635-643. https://doi.org/10.1111/j.1365-2486.2006.01129.x

Bergström, S. (1976), Development and application of a conceptual runoff model for Scandinavian catchments, *Rep. RH 07*, SMHI, Norrköping, Sweden.

Bergström, S. (1995), The HBV model, in *Computer Models of Watershed Hydrology*, edited by V. P. Singh, pp. 443-476, Water Resour. Publ., Highlands Ranch, Colorado, USA.

Bernhardt, E. S., Likens, G. E., Hall, R. O., Buso, D. C., Fisher, S. G., Burton, T. M., Meyer, J. L., McDowell, W. H., Mayer, M. S., Bowden, W. B., Findlay, S. E. G., Macneale, K. H., Stelzer, R. S., & Lowe, W. H. (2005), Can't See the Forest for the Stream? In-stream Processing and Terrestrial Nitrogen Exports, *BioScience*, *55*(3), 219-230. https://doi.org/10.1641/0006-3568(2005)055[0219:ACSTFF]2.0.CO;2

Beven, K. (1989), Changing ideas in hydrology — The case of physically-based models, *Journal of Hydrology*, *105*(1), 157-172. https://doi.org/10.1016/0022-1694(89)90101-7

Beven, K. (2000), Uniqueness of place and process representations in hydrological modelling, *Hydrol. Earth Syst. Sci.*, *4*(2), 203-213. https://doi.org/10.5194/hess-4-203-2000

Beven, K. (2001), How far can we go in distributed hydrological modelling?, *Hydrol. Earth Syst. Sci.*, *5*(1), 1-12. https://doi.org/10.5194/hess-5-1-2001

Bicknell, B. R., Imhoff, J. C., Kittle, J. L., Jr., Donigian, A. S., Jr., & Johanson, R. C. (1997), *Hydrological Simulation Program--Fortran, User's manual for version 11: U.S. Environmental Protection Agency*, National Exposure Research Laboratory, Athens, Georgia.

Bieger, K., Arnold, J. G., Rathjens, H., White, M. J., Bosch, D. D., Allen, P. M., Volk, M., & Srinivasan, R. (2017), Introduction to SWAT+, A Completely Restructured Version of the Soil and Water Assessment Tool, *Journal of the American Water Resources Association*, *53*(1), 115-130. https://doi.org/10.1111/1752-1688.12482

Borah, D. K., & Bera, M. (2003), WATERSHED-SCALE HYDROLOGIC AND NONPOINT-SOURCE POLLUTION MODELS: REVIEW OF MATHEMATICAL BASES, *Transactions of the ASAE*, *46*(6), 1553-1566. https://doi.org/10.13031/2013.15644

Bott, T. L., Montgomery, D. S., Newbold, J. D., Arscott, D. B., Dow, C. L., Aufdenkampe, A. K., Jackson, J. K., & Kaplan, L. A. (2006), Ecosystem metabolism in streams of the Catskill Mountains (Delaware and Hudson River watersheds) and Lower Hudson Valley, *Journal of the North American Benthological Society*, *25*(4), 1018-1044. https://doi.org/10.1899/0887-3593(2006)025[1018:Emisot]2.0.Co;2

Bowes, M. J., Jarvie, H. P., Halliday, S. J., Skeffington, R. A., Wade, A. J., Loewenthal, M., Gozzard, E., Newman, J. R., & Palmer-Felgate, E. J. (2015), Characterising phosphorus and nitrate inputs to a rural river using high-frequency concentration–flow relationships, *Science of The Total Environment*, *511*, 608-620. https://doi.org/10.1016/j.scitotenv.2014.12.086

Bronstert, A., & Bárdossy, A. (1999), The role of spatial variability of soil moisture for modelling surface runoff generation at the small catchment scale, *Hydrol. Earth Syst. Sci.*, *3*(4), 505-516. https://doi.org/10.5194/hess-3-505-1999

Burnash, R. J. C. (1995), The NEW River Forecast System - catchment modeling, in *Computer Models of Watershed Hydrology*, edited by V. P. Singh, pp. 311 - 366, Water Resour. Publ., Highlands Ranch, Colorado, USA.

Burnash, R. J. C., Ferrell, R. L., & McGuire, R. A. (1973), A generalized streamflow simulation system, Jt. Fed.-State River Forecast Center, Sacramento, CA.

Carey, R. O., Wollheim, W. M., Mulukutla, G. K., & Mineau, M. M. (2014), Characterizing Storm-Event Nitrate Fluxes in a Fifth Order Suburbanizing Watershed Using In Situ Sensors, *Environmental Science & Technology*, *48*(14), 7756-7765. https://doi.org/10.1021/es500252j

Chaubey, I., Cotter, A. S., Costello, T. A., & Soerens, T. S. (2005), Effect of DEM data resolution on SWAT output uncertainty, *Hydrological Processes*, *19*(3), 621-628. https://doi.org/10.1002/hyp.5607

Clark, M. P., Bierkens, M. F. P., Samaniego, L., Woods, R. A., Uijlenhoet, R., Bennett, K. E., Pauwels, V. R. N., Cai, X., Wood, A. W., & Peters-Lidard, C. D. (2017), The evolution of process-based hydrologic models: historical challenges and the collective quest for physical realism, *Hydrol. Earth Syst. Sci.*, *21*(7), 3427-3440. https://doi.org/10.5194/hess-21-3427-2017

Collins, A. L., Stutter, M., & Kronvang, B. (2014), Mitigating diffuse pollution from agriculture: International approaches and experience, *Science of The Total Environment*, *468-469*, 1173-1177. https://doi.org/10.1016/j.scitotenv.2013.11.001

Covino, T., McGlynn, B., & Baker, M. (2010), Separating physical and biological nutrient retention and quantifying uptake kinetics from ambient to saturation in successive mountain stream reaches, *Journal of Geophysical Research: Biogeosciences*, *115*(G4), n/a-n/a. https://doi.org/10.1029/2009JG001263

Davis, K. F., Chiarelli, D. D., Rulli, M. C., Chhatre, A., Richter, B., Singh, D., & DeFries, R. (2018), Alternative cereals can improve water use and nutrient supply in India, *Science Advances*, *4*(7), eaao1108. https://doi.org/10.1126/sciadv.aao1108

Dodds, W. K., & Smith, V. H. (2016), Nitrogen, phosphorus, and eutrophication in streams, *Inland Waters*, *6*(2), 155-164. https://doi.org/10.5268/IW-6.2.909

Doyle, M. W. (2005), Incorporating hydrologic variability into nutrient spiraling, *Journal of Geophysical Research: Biogeosciences*, *110*(G1). https://doi.org/10.1029/2005jg000015

Dupas, R., Jomaa, S., Musolff, A., Borchardt, D., & Rode, M. (2016), Disentangling the influence of hydroclimatic patterns and agricultural management on river nitrate dynamics from sub-hourly to decadal time scales, *Science of The Total Environment*, *571*, 791-800. https://doi.org/10.1016/j.scitotenv.2016.07.053

Dupas, R., Musolff, A., Jawitz, J. W., Rao, P. S. C., Jäger, C. G., Fleckenstein, J. H., Rode, M., & Borchardt, D. (2017), Carbon and nutrient export regimes from headwater catchments to downstream reaches, *Biogeosciences*, *14*(18), 4391-4407. https://doi.org/10.5194/bg-14-4391-2017

EEA (2005), Source apportionment of nitrogen and phosphorus inputs into the aquatic environment, *Rep. No 7/2005*, European Environment Agency, Copenhagen, Denmark.

EEA (2012), European waters - current status and future challenges - a synthesis, *Rep. No 9/2012*, European Environment Agency, Copenhagen, Denmark.

EEA (2018), European waters -- Assessment of status and pressures 2018, *Rep. No 7/2018*, European Environment Agency, Copenhagen, Denmark.

Ensign, S. H., & Doyle, M. W. (2006), Nutrient spiraling in streams and river networks, *Journal of Geophysical Research: Biogeosciences*, *111*(G4). https://doi.org/10.1029/2005JG000114

Fatichi, S., Vivoni, E. R., Ogden, F. L., Ivanov, V. Y., Mirus, B., Gochis, D., Downer, C. W., Camporese, M., Davison, J. H., Ebel, B., Jones, N., Kim, J., Mascaro, G., Niswonger, R., Restrepo, P., Rigon, R., Shen, C., Sulis, M., & Tarboton, D. (2016), An overview of current applications, challenges, and future trends in distributed process-based models in hydrology, *Journal of Hydrology*, *537*, 45-60. https://doi.org/10.1016/j.jhydrol.2016.03.026

Futter, M. N., Erlandsson, M. A., Butterfield, D., Whitehead, P. G., Oni, S. K., & Wade, A. J. (2014), PERSiST: a flexible rainfall-runoff modelling toolkit for use with the INCA family of models, *Hydrol. Earth Syst. Sci.*, *18*(2), 855-873. https://doi.org/10.5194/hess-18-855-2014

Gomez-Velez, J. D., & Harvey, J. W. (2014), A hydrogeomorphic river network model predicts where and why hyporheic exchange is important in large basins, *Geophysical Research Letters*, *41*(18), 6403-6412. https://doi.org/10.1002/2014gl061099

Gomez-Velez, J. D., Harvey, J. W., Cardenas, M. B., & Kiel, B. (2015), Denitrification in the Mississippi River network controlled by flow through river bedforms, *Nature Geoscience*, *8*, 941. https://doi.org/10.1038/ngeo2567

Grant, S. B., Azizian, M., Cook, P., Boano, F., & Rippy, M. A. (2018), Factoring stream turbulence into global assessments of nitrogen pollution, *Science*, *359*(6381), 1266-1269. https://doi.org/10.1126/science.aap8074

Güntner, A., & Bronstert, A. (2004), Representation of landscape variability and lateral redistribution processes for large-scale hydrological modelling in semi-arid areas, *Journal of Hydrology*, *297*(1), 136-161. https://doi.org/10.1016/j.jhydrol.2004.04.008

Gupta, H. V., & Razavi, S. (2018), Revisiting the Basis of Sensitivity Analysis for Dynamical Earth System Models, *Water Resources Research*, *54*(11), 8692-8717. https://doi.org/10.1029/2018WR022668

Gupta, H. V., Kling, H., Yilmaz, K. K., & Martinez, G. F. (2009), Decomposition of the mean squared error and NSE performance criteria: Implications for improving hydrological modelling, *Journal of Hydrology*, *377*(1), 80-91. https://doi.org/10.1016/j.jhydrol.2009.08.003

Hall, R. O., & Tank, J. L. (2003), Ecosystem metabolism controls nitrogen uptake in streams in Grand Teton National Park, Wyoming, *Limnology and Oceanography*, *48*(3), 1120-1128. https://doi.org/doi:10.4319/lo.2003.48.3.1120

Hall, R. O., Baker, M. A., Rosi-Marshall, E. J., Tank, J. L., & Newbold, J. D. (2013), Solute-specific scaling of inorganic nitrogen and phosphorus uptake in streams, *Biogeosciences*, *10*(11), 7323-7331. https://doi.org/10.5194/bg-10-7323-2013

Hall, R. O., Tank, J. L., Baker, M. A., Rosi-Marshall, E. J., & Hotchkiss, E. R. (2016), Metabolism, Gas Exchange, and Carbon Spiraling in Rivers, *Ecosystems*, *19*(1), 73-86. https://doi.org/10.1007/s10021-015-9918-1

Hansen, A. L., Gunderman, D., He, X., & Refsgaard, J. C. (2014), Uncertainty assessment of spatially distributed nitrate reduction potential in groundwater using multiple geological realizations, *Journal of Hydrology*, *519*, 225-237. https://doi.org/10.1016/j.jhydrol.2014.07.013

Heffernan, J. B., & Cohen, M. J. (2010), Direct and indirect coupling of primary production and diel nitrate dynamics in a subtropical spring-fed river, *Limnology and Oceanography*, *55*(2), 677-688. https://doi.org/10.4319/lo.2010.55.2.0677

Helton, A. M., Poole, G. C., Meyer, J. L., Wollheim, W. M., Peterson, B. J., Mulholland, P. J., Bernhardt, E. S., Stanford, J. A., Arango, C., Ashkenas, L. R., Cooper, L. W., Dodds, W. K., Gregory, S. V., Hall, R. O., Hamilton, S. K., Johnson, S. L., McDowell, W. H., Potter, J. D., Tank, J. L., Thomas, S. M., Valett, H. M., Webster, J. R., & Zeglin, L. (2011), Thinking outside the channel: modeling nitrogen cycling in networked river ecosystems, *Frontiers in Ecology and the Environment*, *9*(4), 229-238. https://doi.org/10.1890/080211

Herman, J. D., Kollat, J. B., Reed, P. M., & Wagener, T. (2013a), Technical Note: Method of Morris effectively reduces the computational demands of global sensitivity analysis for distributed watershed models, *Hydrology Earth System Sciences*, *17*(7), 2893-2903. https://doi.org/10.5194/hess-17-2893-2013

Herman, J. D., Kollat, J. B., Reed, P. M., & Wagener, T. (2013b), From maps to movies: high-resolution time-varying sensitivity analysis for spatially distributed watershed models, *Hydrol. Earth Syst. Sci.*, *17*(12), 5109-5125. https://doi.org/10.5194/hess-17-5109-2013

Hoellein, T. J., Tank, J. L., Rosi-Marshall, E. J., Entrekin, S. A., & Lamberti, G. A. (2007), Controls on spatial and temporal variation of nutrient uptake in three Michigan headwater streams, *Limnology and Oceanography*, *52*(5), 1964-1977. https://doi.org/10.4319/lo.2007.52.5.1964

Jarvie, H. P., Sharpley, A. N., Kresse, T., Hays, P. D., Williams, R. J., King, S. M., & Berry, L. G. (2018), Coupling High-Frequency Stream Metabolism and Nutrient Monitoring to Explore Biogeochemical Controls on Downstream Nitrate Delivery, *Environmental Science & Technology*, *52*(23), 13708-13717. https://doi.org/10.1021/acs.est.8b03074

Jiang, S., Jomaa, S., & Rode, M. (2014), Modelling inorganic nitrogen leaching in nested mesoscale catchments in central Germany, *Ecohydrology*, *7*(5), 1345-1362. https://doi.org/10.1002/eco.1462

Jiang, S., Jomaa, S., Büttner, O., Meon, G., & Rode, M. (2015), Multi-site identification of a distributed hydrological nitrogen model using Bayesian uncertainty analysis, *Journal of Hydrology*, *529*, 940-950. https://doi.org/10.1016/j.jhydrol.2015.09.009

Jiang, S. Y., Zhang, Q., Werner, A. D., Wellen, C., Jomaa, S., Zhu, Q. D., Büttner, O., Meon, G., & Rode, M. (2019), Effects of stream nitrate data frequency on watershed model performance and prediction uncertainty, *Journal of Hydrology*, *569*, 22-36. https://doi.org/10.1016/j.jhydrol.2018.11.049

Krysanova, V., Müller-Wohlfeil, D.-I., & Becker, A. (1998), Development and test of a spatially distributed hydrological/water quality model for mesoscale watersheds, *Ecological Modelling*, *106*(2–3), 261-289. https://doi.org/10.1016/S0304-3800(97)00204-4

Kumar, R., Samaniego, L., & Attinger, S. (2013), Implications of distributed hydrologic model parameterization on water fluxes at multiple scales and locations, *Water Resources Research*, *49*(1). https://doi.org/10.1029/2012WR012195

Kunz, J. V., Annable, M. D., Rao, S., Rode, M., & Borchardt, D. (2017), Hyporheic Passive Flux Meters Reveal Inverse Vertical Zonation and High Seasonality of Nitrogen Processing in an Anthropogenically Modified Stream (Holtemme, Germany), *Water Resources Research*, *53*(12), 10155-10172. https://doi.org/10.1002/2017WR020709

Lindström, G., Pers, C., Rosberg, J., Strömqvist, J., & Arheimer, B. (2010), Development and testing of the HYPE (Hydrological Predictions for the Environment) water quality model for different spatial scales, *Hydrology research*, *41*(3-4), 295-319. https://doi.org/10.2166/nh.2010.007

Mellander, P.-E., Jordan, P., Melland, A. R., Murphy, P. N. C., Wall, D. P., Mechan, S., Meehan, R., Kelly, C., Shine, O., & Shortle, G. (2013), Quantification of Phosphorus Transport from a Karstic Agricultural Watershed to Emerging Spring Water, *Environmental Science & Technology*, *47*(12), 6111-6119. https://doi.org/10.1021/es304909y

Merz, R., & Blöschl, G. (2004), Regionalisation of catchment model parameters, *Journal of Hydrology*, *287*(1), 95-123. https://doi.org/10.1016/j.jhydrol.2003.09.028

Meybeck, M. (1982), Carbon, nitrogen, and phosphorus transport by world rivers, *Am. J. Sci*, *282*(4), 401-450. https://doi.org/10.2475/ajs.282.4.401

Miller, M. P., Tesoriero, A. J., Capel, P. D., Pellerin, B. A., Hyer, K. E., & Burns, D. A. (2016), Quantifying watershed-scale groundwater loading and in-stream fate of nitrate using high-frequency water quality data, *Water Resources Research*, *52*(1), 330-347. https://doi.org/10.1002/2015WR017753

Morris, M. D. (1991), Factorial sampling plans for preliminary computational experiments, *Technometrics*, *33*(2), 161-174. https://doi.org/10.2307/1269043

Mulholland, P. J., Tank, J. L., Webster, J. R., Bowden, W. B., Dodds, W. K., Gregory, S. V., Grimm, N. B., Hamilton, S. K., Johnson, S. L., Martí, E., McDowell, W. H., Merriam, J. L., Meyer, J. L., Peterson, B. J., Valett, H. M., & Wollheim, W. M. (2002), Can uptake length in streams be determined by nutrient addition experiments? Results from an interbiome comparison study, *Journal of the North American Benthological Society*, *21*(4), 544-560. https://doi.org/10.2307/1468429

Mulholland, P. J., Helton, A. M., Poole, G. C., Hall, R. O., Hamilton, S. K., Peterson, B. J., Tank, J. L., Ashkenas, L. R., Cooper, L. W., Dahm, C. N., Dodds, W. K., Findlay, S. E. G., Gregory, S. V., Grimm, N. B., Johnson, S. L., McDowell, W. H., Meyer, J. L., Valett, H. M., Webster, J. R., Arango, C. P., Beaulieu, J. J., Bernot, M. J., Burgin, A. J., Crenshaw, C. L., Johnson, L. T., Niederlehner, B. R., O'Brien, J. M., Potter, J. D., Sheibley, R. W., Sobota, D. J., & Thomas, S. M. (2008), Stream denitrification across biomes and its response to anthropogenic nitrate loading, *Nature*, *452*, 202-205. https://doi.org/10.1038/nature06686

Newbold, J. D., Elwood, J. W., O'Neill, R. V., & Winkle, W. V. (1981), Measuring Nutrient Spiralling in Streams, *Canadian Journal of Fisheries and Aquatic Sciences*, *38*(7), 860-863. https://doi.org/10.1139/f81-114

Newbold, J. D., Elwood, J. W., O'Neill, R. V., & Sheldon, A. L. (1983), Phosphorus Dynamics in a Woodland Stream Ecosystem: A Study of Nutrient Spiralling, *Ecology*, *64*(5), 1249-1265. https://doi.org/10.2307/1937833

Odum, H. T. (1956), Primary Production in Flowing Waters, *Limnology and Oceanography*, *1*(2), 102-117. https://doi.org/10.4319/lo.1956.1.2.0102

Oudin, L., Andréassian, V., Perrin, C., Michel, C., & Le Moine, N. (2008), Spatial proximity, physical similarity, regression and ungaged catchments: A comparison of regionalization approaches based on 913 French catchments, *Water Resources Research*, *44*(3). https://doi.org/10.1029/2007WR006240

Phillips, S., Focazio, M. J., & Bachman, L. J. (1999), Discharge, nitrate load, and residence time of ground water in the Chesapeake Bay watershed, *Report Rep. 150-99*.

Pianosi, F., Beven, K., Freer, J., Hall, J. W., Rougier, J., Stephenson, D. B., & Wagener, T. (2016), Sensitivity analysis of environmental models: A systematic review with practical workflow, *Environmental Modelling & Software*, *79*, 214-232. https://doi.org/10.1016/j.envsoft.2016.02.008

Rathjens, H., Oppelt, N., Bosch, D. D., Arnold, J. G., & Volk, M. (2015), Development of a grid-based version of the SWAT landscape model, *Hydrological Processes*, *29*(6), 900-914. https://doi.org/10.1002/hyp.10197

Refsgaard, J. C. (1997), Parameterisation, calibration and validation of distributed hydrological models, *Journal of Hydrology*, *198*(1), 69-97. https://doi.org/10.1016/S0022-1694(96)03329-X

Refsgaard, J. C., Højberg, A. L., He, X., Hansen, A. L., Rasmussen, S. H., & Stisen, S. (2016), Where are the limits of model predictive capabilities?, *Hydrological Processes*, *30*(26), 4956-4965. https://doi.org/10.1002/hyp.11029

Refsgaard, J. C., Hansen, A. L., Højberg, A. L., Olesen, J. E., Hashemi, F., Wachniew, P., Wörman, A., Bartosova, A., Stelljes, N., & Chubarenko, B. (2019), Spatially differentiated regulation: Can it save the Baltic Sea from excessive N-loads?, *Ambio*. https://doi.org/10.1007/s13280-019-01195-w

Refsgaard, J. C., Auken, E., Bamberg, C. A., Christensen, B. S. B., Clausen, T., Dalgaard, E., Effersø, F., Ernstsen, V., Gertz, F., Hansen, A. L., He, X., Jacobsen, B. H., Jensen, K. H., Jørgensen, F., Jørgensen, L. F., Koch, J., Nilsson, B., Petersen, C., De Schepper, G., Schamper, C., Sørensen, K. I., Therrien, R., Thirup, C., & Viezzoli, A. (2014), Nitrate reduction in geologically heterogeneous catchments — A framework for assessing the scale of predictive capability of hydrological models, *Science of The Total Environment*, *468-469*, 1278-1288. https://doi.org/10.1016/j.scitotenv.2013.07.042

Reusch, T. B. H., Dierking, J., Andersson, H. C., Bonsdorff, E., Carstensen, J., Casini, M., Czajkowski, M., Hasler, B., Hinsby, K., Hyytiäinen, K., Johannesson, K., Jomaa, S., Jormalainen, V., Kuosa, H., Kurland, S., Laikre, L., MacKenzie, B. R., Margonski, P., Melzner, F., Oesterwind, D., Ojaveer, H., Refsgaard, J. C., Sandström, A., Schwarz, G., Tonderski, K., Winder, M., & Zandersen, M. (2018), The Baltic Sea as a time machine for the future coastal ocean, *Science Advances*, *4*(5), eaar8195. https://doi.org/10.1126/sciadv.aar8195

Roberts, B. J., & Mulholland, P. J. (2007), In-stream biotic control on nutrient biogeochemistry in a forested stream, West Fork of Walker Branch, *Journal of Geophysical Research: Biogeosciences*, *112*(G4). https://doi.org/10.1029/2007JG000422

Roberts, B. J., Mulholland, P. J., & Hill, W. R. (2007), Multiple Scales of Temporal Variability in Ecosystem Metabolism Rates: Results from 2 Years of Continuous Monitoring in a Forested Headwater Stream, *Ecosystems*, *10*(4), 588-606. https://doi.org/10.1007/s10021-007-9059-2

Rode, M., Thiel, E., Franko, U., Wenk, G., & Hesser, F. (2009), Impact of selected agricultural management options on the reduction of nitrogen loads in three representative meso scale catchments in Central Germany, *Science of The Total Environment*, *407*(11), 3459-3472. https://doi.org/10.1016/j.scitotenv.2009.01.053

Rode, M., Halbedel née Angelstein, S., Anis, M. R., Borchardt, D., & Weitere, M. (2016a), Continuous In-Stream Assimilatory Nitrate Uptake from High-Frequency Sensor Measurements, *Environmental Science & Technology*, *50*(11), 5685-5694. https://doi.org/10.1021/acs.est.6b00943

Rode, M., Arhonditsis, G., Balin, D., Kebede, T., Krysanova, V., van Griensven, A., & van der Zee, S. E. A. T. M. (2010), New challenges in integrated water quality modelling, *Hydrological Processes*, *24*(24), 3447-3461. https://doi.org/10.1002/hyp.7766

Rode, M., Wade, A. J., Cohen, M. J., Hensley, R. T., Bowes, M. J., Kirchner, J. W., Arhonditsis, G. B., Jordan, P., Kronvang, B., Halliday, S. J., Skeffington, R. A., Rozemeijer, J. C., Aubert, A. H., Rinke, K., & Jomaa, S. (2016b), Sensors in the Stream: The High-Frequency Wave of the Present, *Environmental Science & Technology*, *50*(19), 10297-10307. https://doi.org/10.1021/acs.est.6b02155

Samaniego, L., Kumar, R., & Attinger, S. (2010), Multiscale parameter regionalization of a grid-based hydrologic model at the mesoscale, *Water Resources Research*, *46*(5). https://doi.org/10.1029/2008WR007327

Schlesinger, W. H. (2009), On the fate of anthropogenic nitrogen, *Proceedings of the National Academy of Sciences*, *106*(1), 203-208. https://doi.org/10.1073/pnas.0810193105

Schrön, M., Köhli, M., Scheiffele, L., Iwema, J., Bogena, H. R., Lv, L., Martini, E., Baroni, G., Rosolem, R., Weimar, J., Mai, J., Cuntz, M., Rebmann, C., Oswald, S. E., Dietrich, P., Schmidt, U., & Zacharias, S. (2017), Improving calibration and validation of cosmic-ray neutron sensors in the light of spatial sensitivity, *Hydrol. Earth Syst. Sci.*, *21*(10), 5009-5030. https://doi.org/10.5194/hess-21-5009-2017

Seitzinger, S. P., Styles, R. V., Boyer, E. W., Alexander, R. B., Billen, G., Howarth, R. W., Mayer, B., & van Breemen, N. (2002), Nitrogen retention in rivers: model development and application to watersheds in the northeastern U.S.A, *Biogeochemistry*, *57*(1), 199-237. https://doi.org/10.1023/a:1015745629794

Sheikholeslami, R., Razavi, S., Gupta, H. V., Becker, W., & Haghnegahdar, A. (2019), Global sensitivity analysis for high-dimensional problems: How to objectively group factors and measure robustness and convergence while reducing computational cost, *Environmental Modelling & Software*, *111*, 282-299. https://doi.org/10.1016/j.envsoft.2018.09.002

Shrestha, R., Tachikawa, Y., & Takara, K. (2006), Input data resolution analysis for distributed hydrological modeling, *Journal of Hydrology*, *319*(1), 36-50. https://doi.org/10.1016/j.jhydrol.2005.04.025

Smith, R. A., Alexander, R. B., & Wolman, M. G. (1987), Water-Quality Trends in the Nation's Rivers, *Science*, *235*(4796), 1607-1615. https://doi.org/10.1126/science.235.4796.1607

Sobol', I. M. (2001), Global sensitivity indices for nonlinear mathematical models and their Monte Carlo estimates, *Mathematics and Computers in Simulation*, *55*(1), 271-280. https://doi.org/10.1016/S0378-4754(00)00270-6

Song, X., Zhang, J., Zhan, C., Xuan, Y., Ye, M., & Xu, C. (2015), Global sensitivity analysis in hydrological modeling: Review of concepts, methods, theoretical framework, and applications, *Journal of Hydrology*, *523*, 739-757. https://doi.org/10.1016/j.jhydrol.2015.02.013

Stream Solute Workshop (1990), Concepts and Methods for Assessing Solute Dynamics in Stream Ecosystems, *Journal of the North American Benthological Society*, *9*(2), 95-119. https://doi.org/10.2307/1467445

Stutter, M. I., Chardon, W. J., & Kronvang, B. (2012), Riparian Buffer Strips as a Multifunctional Management Tool in Agricultural Landscapes: Introduction, *Journal of Environmental Quality*, *41*, 297-303. https://doi.org/10.2134/jeq2011.0439

Tang, Y., Reed, P., van Werkhoven, K., & Wagener, T. (2007), Advancing the identification and evaluation of distributed rainfall-runoff models using global sensitivity analysis, *Water Resources Research*, *43*(6). https://doi.org/10.1029/2006WR005813

Tank, J. L., Rosi-Marshall, E. J., Baker, M. A., & Hall, R. O. (2008), Are rivers just big streams? A pulse method to quantify nitrogen demand in a large river, *Ecology*, *89*(10), 2935-2945. https://doi.org/10.1890/07-1315.1

Tank, J. L., Martí, E., Riis, T., von Schiller, D., Reisinger, A. J., Dodds, W. K., Whiles, M. R., Ashkenas, L. R., Bowden, W. B., Collins, S. M., Crenshaw, C. L., Crowl, T. A., Griffiths, N. A., Grimm, N. B., Hamilton, S. K., Johnson, S. L., McDowell, W. H., Norman, B. M., Rosi, E. J., Simon, K. S., Thomas, S. A., & Webster, J. R. (2017), Partitioning assimilatory nitrogen uptake in streams: an analysis of stable isotope tracer additions across continents, *Ecological Monographs*, n/a-n/a. https://doi.org/10.1002/ecm.1280

Thober, S., Cuntz, M., Kelbling, M., Kumar, R., Mai, J., & amaniego, L. (2019), The multiscale routing model mRM v1.0: simple river routing at resolutions from 1 to 50 km, *Geosci. Model Dev.*, *12*, 2501–2521. https://doi.org/10.5194/gmd-12-2501-2019

Tockner, K., Pusch, M., Borchardt, D., & Lorang, M. S. (2010), Multiple stressors in coupled river–floodplain ecosystems, *Freshwater Biology*, *55*(s1), 135-151. https://doi.org/10.1111/j.1365-2427.2009.02371.x

Trauth, N., Schmidt, C., Vieweg, M., Oswald, S. E., & Fleckenstein, J. H. (2015), Hydraulic controls of in-stream gravel bar hyporheic exchange and reactions, *Water Resources Research*, *51*(4), 2243-2263. https://doi.org/10.1002/2014wr015857

Tsivoglou, E. C., & Neal, L. A. (1976), Tracer Measurement of Reaeration: III. Predicting the Reaeration Capacity of Inland Streams, *Journal (Water Pollution Control Federation)*, *48*(12), 2669-2689. http://www.jstor.org/stable/25040082

van Werkhoven, K., Wagener, T., Reed, P., & Tang, Y. (2008a), Rainfall characteristics define the value of streamflow observations for distributed watershed model identification, *Geophysical Research Letters*, *35*(11). https://doi.org/10.1029/2008GL034162

van Werkhoven, K., Wagener, T., Reed, P., & Tang, Y. (2008b), Characterization of watershed model behavior across a hydroclimatic gradient, *Water Resources Research*, *44*(1). https://doi.org/10.1029/2007WR006271

Wade, A. J., Durand, P., Beaujouan, V., Wessel, W. W., Raat, K. J., Whitehead, P. G., Butterfield, D., Rankinen, K., & Lepisto, A. (2002), A nitrogen model for European catchments: INCA, new model structure and equations, *Hydrology and Earth System Sciences*, *6*(3), 559-582. https://doi.org/10.5194/hess-6-559-2002

Wagener, T., & Wheater, H. S. (2006), Parameter estimation and regionalization for continuous rainfall-runoff models including uncertainty, *Journal of Hydrology*, *320*(1), 132-154. https://doi.org/10.1016/j.jhydrol.2005.07.015

Wagener, T., van Werkhoven, K., Reed, P., & Tang, Y. (2009), Multiobjective sensitivity analysis to understand the information content in streamflow observations for distributed watershed modeling, *Water Resources Research*, *45*(2). https://doi.org/10.1029/2008WR007347

Webster, J. R. (1975), Analysis of potassium and calcium dynamics in stream ecosystems on three Southern Appalachian watersheds of contrasing vegetation, Ph.D. dissertation, University of Georgia. Athens, USA.

Webster, J. R., Mulholland, P. J., Tank, J. L., Valett, H. M., Dodds, W. K., Peterson, B. J., Bowden, W. B., Dahm, C. N., Findlay, S., Gregory, S. V., Grimm, N. B., Hamilton, S. K., Johnson, S. L., Martí, E., Mcdowell, W. H., Meyer, J. L., Morrall, D. D., Thomas, S. A., & Wollheim, W. M. (2003), Factors affecting ammonium uptake in streams – an inter-biome perspective, *Freshwater Biology*, *48*(8), 1329-1352. https://doi.org/10.1046/j.1365-2427.2003.01094.x

Wellen, C., Kamran-Disfani, A.-R., & Arhonditsis, G. B. (2015), Evaluation of the Current State of Distributed Watershed Nutrient Water Quality Modeling, *Environmental Science and Technology*, *49*(6), 3278-3290. https://doi.org/10.1021/es5049557

Whitehead, P. G., Wilson, E. J., & Butterfield, D. (1998), A semi-distributed Integrated Nitrogen model for multiple source assessment in Catchments (INCA): Part I — model structure and process equations, *Science of The Total Environment*, *210–211*, 547-558. https://doi.org/10.1016/S0048-9697(98)00037-0

Wohl, E. (2017), The significance of small streams, *Frontiers of Earth Science*, *11*(3), 447-456. https://doi.org/10.1007/s11707-017-0647-y

Wollheim, W. M., Mulukutla, G. K., Cook, C., & Carey, R. O. (2017), Aquatic Nitrate Retention at River Network Scales Across Flow Conditions Determined Using Nested In Situ Sensors, *Water Resources Research*, *53*(11), 9740-9756. https://doi.org/10.1002/2017WR020644

Wollheim, W. M., Vörösmarty, C. J., Peterson, B. J., Seitzinger, S. P., & Hopkinson, C. S. (2006), Relationship between river size and nutrient removal, *Geophysical Research Letters*, *33*(6). https://doi.org/10.1029/2006gl025845

Wollheim, W. M., Peterson, B. J., Thomas, S. M., Hopkinson, C. H., & Vörösmarty, C. J. (2008), Dynamics of N removal over annual time periods in a suburban river network, *Journal of Geophysical Research: Biogeosciences*, *113*(G3). https://doi.org/10.1029/2007JG000660

Wollschläger, U., Attinger, S., Borchardt, D., Brauns, M., Cuntz, M., Dietrich, P., Fleckenstein, J. H., Friese, K., Friesen, J., Harpke, A., Hildebrandt, A., Jäckel, G., Kamjunke, N., Knöller, K., Kögler, S., Kolditz, O., Krieg, R., Kumar, R., Lausch, A., Liess, M., Marx, A., Merz, R., Mueller, C., Musolff, A., Norf, H., Oswald, S. E., Rebmann, C., Reinstorf, F., Rode, M., Rink, K., Rinke, K., Samaniego, L., Vieweg, M., Vogel, H.-J., Weitere, M., Werban, U., Zink, M., & Zacharias, S. (2016), The Bode hydrological observatory: a platform for integrated, interdisciplinary hydro-ecological research within the TERENO Harz/Central German Lowland Observatory, *Environmental Earth Sciences*, *76*(1), 29. https://doi.org/10.1007/s12665-016-6327-5

Wriedt, G., & Rode, M. (2006), Modelling nitrate transport and turnover in a lowland catchment system, *Journal of Hydrology*, *328*(1–2), 157-176. https://doi.org/10.1016/j.jhydrol.2005.12.017

Yang, J. (2011), Convergence and uncertainty analyses in Monte-Carlo based sensitivity analysis, *Environmental Modelling & Software*, *26*(4), 444-457. https://doi.org/10.1016/j.envsoft.2010.10.007

Yang, X., Jomaa, S., & Rode, M. (2019a), Spatially distributed sensitivity analysis reveals insights into heterogeneous responses of catchment water quality modeling, *Water Resources Research*, *Under Review* (# 2019WR025575).

Yang, X., Jomaa, S., Büttner, O., & Rode, M. (2019b), Autotrophic nitrate uptake in river networks: A modeling approach using continuous high-frequency data, *Water Research*, *157*, 258-268. https://doi.org/10.1016/j.watres.2019.02.059

Yang, X., Jomaa, S., Zink, M., Fleckenstein, J. H., Borchardt, D., & Rode, M. (2018), A new fully distributed model of nitrate transport and removal at catchment scale, *Water Resources Research*, *54*(8), 5856-5877. https://doi.org/10.1029/2017WR022380

Ye, S., Covino, T. P., Sivapalan, M., Basu, N. B., Li, H. Y., & Wang, S. W. (2012), Dissolved nutrient retention dynamics in river networks: A modeling investigation of transient flows and scale effects, *Water Resources Research*, *48*(6). https://doi.org/doi:10.1029/2011WR010508

Ye, S., Reisinger, A. J., Tank, J. L., Baker, M. A., Hall Jr., R. O., Rosi, E. J., & Sivapalan, M. (2017), Scaling Dissolved Nutrient Removal in River Networks: A Comparative Modeling Investigation, *Water Resources Research*, *53*(11), 9623-9641. https://doi.org/10.1002/2017WR020858

Young, R., Onstad, C., Bosch, D., & Anderson, W. (1989), AGNPS: A nonpoint-source pollution model for evaluating agricultural watersheds, *Journal of soil and water conservation*, *44*(2), 168-173.

Yu, C., Huang, X., Chen, H., Godfray, H. C. J., Wright, J. S., Hall, J., Gong, P., Ni, S., Qiao, S., Huang, G., Xiao, Y., Zhang, J., Feng, Z., Ju, X., Ciais, P., Stenseth, N. C., Hessen, D. O., Sun, Z., Yu, L., Cai, W., Fu, H., Huang, X., Zhang, C., Liu, H., & Taylor, J. (2019), Managing nitrogen to restore water quality in China, *Nature*. https://doi.org/10.1038/s41586-019-1001-1

Zhao, R. J. (1992), The Xinanjiang model applied in China, *Journal of Hydrology*, *135*(1), 371-381. https://doi.org/10.1016/0022-1694(92)90096-E

Zhao, R. J., Zhang, Y. L., Fang, L. R., Liu, X. R., & Zhang, Q. S. (1980), The Xinanjiang Model in *Hydrological Forecasting Proceedings Oxford Symposium*, edited, pp. 351-356, IASH.